ON THE THERMAL INTERACTION OF BUILDING STRUCTURE AND HEATING AND VENTILATING SYSTEM

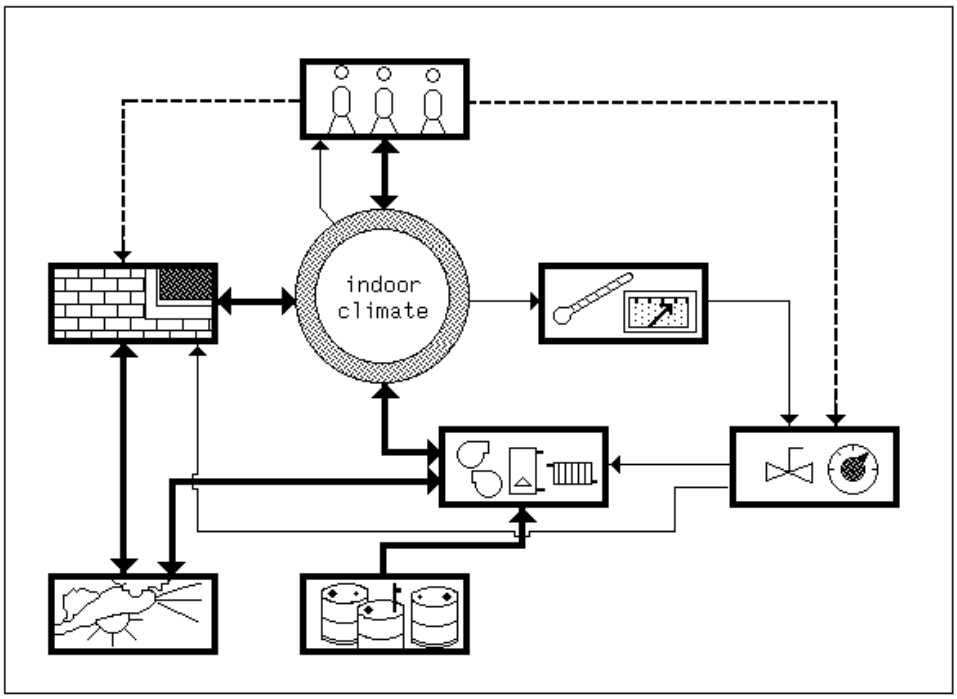

Jan L.M. Hensen

ON THE THERMAL INTERACTION OF BUILDING STRUCTURE AND HEATING AND VENTILATING SYSTEM

PROEFSCHRIFT

ter verkrijging van de graad van doctor
aan de Technische Universiteit Eindhoven,
op gezag van de Rector Magnificus,
prof.dr.J.H. van Lint, voor een commissie
aangewezen door het College van Dekanen
in het openbaar te verdedigen op
vrijdag 7 juni 1991 te 16.00 uur

door

JOANNES LAURENTIUS MARIA HENSEN

geboren te Tilburg

Dit proefschrift is goedgekeurd
door de promotoren

prof.dr.J.A. Clarke (University of Strathclyde, Glasgow)
prof.ir.J. Vorenkamp

CIP-DATA KONINKLIJKE BIBLIOTHEEK, DEN HAAG

Hensen, Joannes Laurentius Maria

On the thermal interaction of building structure and heating and ventilating system /
Joannes Laurentius Maria Hensen. - Eindhoven : Technische Universiteit Eindhoven
Thesis Eindhoven. - With ref. - With summary in Dutch.
ISBN 90-386-0081-X bound
Subject headings: energy simulation / building performance analysis.

© 1991 by J.L.M. Hensen

Aan mijn ouders

PREFACE

According to the 1987 report "Our Common Future" by a special United Nations commission chaired by Mrs.G.H. Brundtland, the industrialised countries will eventually have to lower their energy consumption by 50%. This objective is translated in the 1989 Dutch long term (1990 - 2010) strategic plan on environmental protection ("Nationaal Milieubeleidsplan") into a specific goal for the building sector which demands a 25% reduction of the fuel consumption for space heating in commercial buildings and houses by the year 2000.

In The Netherlands some 45 10^9 *HFL*/*a* - ie 50% of the gross national investment - is related to building activities. So building is not a minor industrial activity.
When we look at the costs of a new building, some 30% up to 50% is related to the systems in case of commercial buildings, and 5% up to 10% in case of domestic buildings.

Hence, both with respect to environmental impact and economics, the ability to make sensible and well based decisions regarding the choice of heating and ventilating systems, is of the utmost importance.

With current computers, performance analysis by simulation of complex building and plant configuration became available for most of the research community. This will soon be the case for every concerned engineer. However, to be able to do so requires a strong investment on the modelling of the thermal interaction of building structure and heating and ventilating system. This dissertation sets out to be a basic contribution in this area.

This work could not have been completed without the support and help of many people and institutions, for which I am very grateful.

I am especially grateful to prof.ir.J. Vorenkamp for enabling me to carry out the present work and for his encouragement over the years. I am sincerely and deeply indebted to Professor Joe Clarke who conveyed his enthusiasm for computer simulation to me, and who has given me guidance and support in so many ways.

I would like to thank prof.ir.R.W.J. Kouffeld and prof.J. Lebrun who - as core members of the award committee - reviewed and commented the drafts for this dissertation. To the other members of the committee prof.dr.ir.M.F.Th. Bax, prof.ir.J. Wisse, prof.ir.K. te Velde, prof.dr.ir.A.A. van Steenhoven, and ir.H.J. Nicolaas, I would also like to express my gratitude.

While realizing that the following list must be incomplete, I would like to thank in no particular order:
- Marga Croes, Marieke van der Laan, Frank Lambregts, Paul Triepels, who - as students - contributed to this work,
- Wim van de Ven and Louis Dings for their technical assistance and much more,

- Marieke van der Laan and Cor Pernot for profoundly proofreading the manuscript and for numerous other kinds of helpful actions,
- Paul Hoen and Jean Dick for their friendship and support over the years,
- my positive colleagues in FAGO, who provided a very much appreciated environment to work in,
- all members of ESRU and ABACUS for creating a marvelous atmosphere in which it was a pleasure (PDB !) and a honour to be a guest during several visits,
- NOVEM (Netherlands Agency for Energy and the Environment), the British Council, and Eindhoven University of Technology for supplying additional funds which enabled these visits,
- George Walton and James Axley who willingly shared their theoretical approach to building air flow modelling and with whom I had some stimulating discussions, and
- my family and friends for their encouragement and for accepting neglection of social contacts on my part.

Finally, I sincerely want to thank my parents who gave me the opportunity to study and to whom I would like to dedicate this work.

Jan Hensen, June 1991

Table of Contents

Preface vii
List of symbols xiii

1. INTRODUCTION 1.1
1.1. THE NEED FOR AN INTEGRAL APPROACH 1.1
1.2. THE BUILDING AS AN INTEGRATED DYNAMIC SYSTEM 1.2
1.3. OBJECTIVE AND OUTLINE OF THE PRESENT WORK 1.4
References 1.5

2. THE OBJECTIVE FUNCTIONS 2.1
2.1. THERMAL COMFORT AND OPTIMUM FUEL CONSUMPTION 2.1
2.2. ASSESSING THERMAL COMFORT 2.1
2.3. THE HUMAN DYNAMIC THERMOREGULATORY SYSTEM 2.2
2.4. REVIEW OF EXPERIMENTS ON TRANSIENT CONDITIONS 2.5
2.4.1. Results for Cyclical Temperature Changes 2.6
2.4.2. Results for Other Changes 2.8
2.5. CONCLUSIONS 2.11
References 2.12

3. BUILDING ENERGY SIMULATION 3.1
3.1. INTRODUCTION 3.1
3.2. THE CABD CONTEXT 3.1
3.3. STATE OF THE ART 3.5
3.4. THE ESP^{R} SIMULATION ENVIRONMENT 3.6
3.4.1. Background and History 3.7
3.4.2. Status at Project Commencement 3.9
3.4.3. Development Areas 3.12
References 3.13

4. FLUID FLOW SIMULATION 4.1
4.1. INTRODUCTION 4.1
4.2. PROBLEM DESCRIPTION 4.2
4.3. CALCULATION PROCESS 4.6
4.3.1. Wind Pressure 4.7
4.3.2. Buoyancy Driven Flow 4.10
4.3.3. Simultaneous Fluid Flow Network Solution 4.12
4.3.4. Results Handling 4.16
4.4. AVAILABLE FLUID FLOW COMPONENT TYPES 4.17
4.4.1. Power Law Flow Component (type 10, 15, 17) 4.18
4.4.2. Quadratic Law Flow Component (type 20, 25) 4.20
4.4.3. Constant Flow Rate Component (type 30, 35) 4.20
4.4.4. Common Orifice Flow Component (type 40) 4.21
4.4.5. Laminar Pipe Flow Component (type 50) 4.21
4.4.6. Specific Air Flow Components 4.22
4.4.6.1. Specific air flow opening (type 110) 4.22
4.4.6.2. Specific air flow crack (type 120) 4.22
4.4.6.3. Specific air flow door (type 130) 4.22

4.4.7. General Flow Conduit Component (type 210) 4.23
4.4.8. Conduit & Junction with Flow Ratio Dependent Dynamic Losses 4.25
4.4.8.1. Conduit ending in converging 3-leg junction (type 220) 4.27
4.4.8.2. Conduit starting in diverging 3-leg junction (type 230) 4.28
4.4.8.3. Conduit ending in converging 4-leg junction (type 240) 4.29
4.4.8.4. Conduit starting in diverging 4-leg junction (type 250) 4.30
4.4.9. General Flow Inducer Component (type 310) 4.31
4.4.10. General Flow Corrector Component (type 410) 4.33
4.4.11. Flow Corrector with Polynomial Local Loss Factor (type 420) 4.38
4.4.12. Ideal (Frictionless) Flow Controller (type 450) 4.38
4.5. COUPLING OF FLUID FLOW SIMULATION AND ESP^{R} 4.39
References 4.41

5. PLANT SIMULATION 5.1
5.1. INTRODUCTION 5.1
5.2. PROBLEM DESCRIPTION 5.3
5.3. CALCULATION PROCESS 5.6
5.3.1. Modular-Simultaneous Approach to Plant Simulation 5.6
5.3.2. Basic Plant Component Model 5.6
5.3.3. Establishing the Plant Matrices 5.11
5.3.4. Interaction with mfs 5.15
5.3.5. Simultaneous Solution of the Plant Matrices 5.15
5.3.6. Results Handling 5.16
5.4. AVAILABLE PLANT COMPONENT MODELS 5.18
5.4.1. Flow Merge (component type 10, 230) 5.21
5.4.2. Flow Inducer (component type 30, 240) 5.21
5.4.3. Air Heating Coil; single node (component type 50, 110) 5.22
5.4.4. Air Heating Coil; multi node (component type 410) 5.25
5.4.5. Flow Conduit (component type 60, 220) 5.28
5.4.6. Boiler; single node & flux control (component type 200) 5.31
5.4.7. Boiler; two node & on/off control (component type 250) 5.31
5.4.8. Boiler; two node & aquastat control (component type 260) 5.35
5.4.9. Radiator (component type 210, 270) 5.38
5.4.10. Plate Heat Exchanger (component type 120) 5.42
5.4.11. Thermostatic Radiator Valve (component type 500) 5.45
5.4.12. Mechanical Room Thermostat (component type 510) 5.47
5.4.13. Imaginary Mass-less Temperature Source (component type 900) 5.49
5.5. AVAILABLE PLANT CONTROL FEATURES 5.49
5.6. COUPLING OF BUILDING AND PLANT 5.53
References 5.56

6. VERIFICATION AND VALIDATION 6.1
6.1. INTRODUCTION 6.1
6.2. METHODOLOGY 6.2
6.2.1. Theory and Code Examination 6.3
6.2.2. Analytical Verification 6.4
6.2.3. Inter-Model Comparison 6.5
6.2.4. Empirical Validation 6.8
6.2.5. Parametric Sensitivity Analysis 6.12
6.3. FUTURE WORK 6.14
References 6.14

7. APPLICATION 7.1
7.1. INTRODUCTION 7.1
7.2. RESULTS RECOVERY 7.1
7.2.1. Fluid Flow Simulation Results 7.2

7.2.2. Plant Simulation Results 7.4
7.2.3. Using UNIX Tools 7.4
7.3. CASE STUDIES: MODELLING ORIENTATED CONTEXT 7.6
7.3.1. Numerical Approximation of Energy Balance Equation 7.7
7.3.2. Iteration vs Time Step Reduction 7.9
7.4. CASE STUDIES: BUILDING ENGINEERING CONTEXT 7.10
7.4.1. Air Flow through Shopping Arcade 7.11
7.4.2. Environmental Assessment of Hospital Spaces 7.13
7.4.3. Influence of Acceleration Heating on Room Thermostat Behaviour 7.16
References 7.21

8. CONCLUSIONS AND FUTURE OUTLOOK 8.1
8.1. INTRODUCTION 8.1
8.2. CONCLUSIONS 8.1
8.3. FUTURE WORK 8.2
8.3.1. Theory 8.2
8.3.2. User Interface 8.3
8.3.3. Software Structure 8.3
8.3.4. Application 8.3
8.3.5. Technology Transfer 8.4
References 8.4

Summary xvii
Samenvatting xix
Curriculum Vitae xxi

LIST OF SYMBOLS

English Letter Symbols

a	weighting factor, –
a	terrain dependent constant
a	flow constant, m^3/s or kg/s
a	flow coefficient, $Pa/m^3/s$ or $Pa/kg/s$
a	polynomial fit coefficient
A	area, m^2
b	flow coefficient, $Pa/(m^3/s)^2$ or $Pa/(kg/s)^2$
$\overline{c}$	mass weighted average specific heat, $J/kg \cdot K$
c_p	specific heat at constant pressure, $J/kg \cdot K$
d	infinite small difference
C	local loss factor, –
C_d	discharge facor, –
C_p	surface pressure coefficient, –
C	pressure correction, Pa
C	fluid capacity rate, W/K
CPH	cycles per hour, h^{-1}
d	displacement length, m
D	diameter, m
E	electric power consumption, W
f	friction factor, –
F	fuel firing rate, m_3/s or kg/s
g	acceleration due to gravity, m/s^2
h	relative height, m
h	heat transfer coefficient, W/m^2K
H	fuel heating value, J/m^3 or J/kg
H	height, m
H	valve/damper position, m
I_{cl}	clothing thermal resistance, clo (1 clo = 0.155 m^2K/W)
k	wall material roughness, m
k	thermal conductance, W/K
K	terrain dependent constant
K	number of connections
L	length, m
L	relative heat loss, –
$\dot{m}$	mass flow rate, kg/s
M	metabolic rate, met (1 met = 58 W/m^2)
M	mass, kg
N	number of ...,
N	Nusselt number ($h\,D/\lambda$), –
p	static pressure, Pa
P	total pressure, Pa

PS	pressure difference due to stack effect, Pa
$\dot{q}$	volume flow rate, m^3/s
r	ratio of successive pressure corrections, –
r	radius, m
R	mass flow residual, kg/s
R	mass diversion ratio, –
R	gas constant, J/kgK
R	thermal resistance, m^2K/W
Re	Reynolds number ($\rho\, v\, D/\, \mu$), –
RH	relative humidity, –
S	control signal, SU
SU	sensed units
t	time, s
U	heat transfer coefficient, W/m^2K
U	wind speed, m/s
UA	overall heat transfer coefficient, W/K
v	velocity, m/s
W	width, m
z_0	roughness length, m

Greek Letter Symbols

α	terrain dependent constant,
α	angle
β	angle
∂	infinite small difference
Δ	finite difference
ε	absolute wall material roughness, m
ε	effectiveness, –
η	efficiency, –
γ	terrain dependent constant,
λ	thermal conductivity, W/mK
μ	dynamic viscosity, $kg/m \cdot s$
ν	kinematic viscosity, m^2/s
θ	temperature, $°C$
Θ	temperature, K
ϕ	heat flux, W
ρ	density, kg/m^3

Subscripts

0	nominal
a	air
a	ambient
c	condensation
d	direction
dew	dew point
e	environment
f	face or frontal
f	fuel
h	hydraulic

h	heat transfer
i	internal or inside
i	inlet
l	local
L	laminar
lg	logarthmic
ln	linear
m	mean
m	measured
m	metal
mrt	mean radiant
o	operative
o	outdoors
ptp	peak-to-peak
r	reference or rated
s	(cross)section
s	solid
s	supply
sb	stand-by
	set point
T	turbulent
TU	transfer units
v	valve
v	vapour
w	water
x	exit or exhaust
z	height

Superscripts

*	previous time step or known value
+	positive values only

CHAPTER ONE

INTRODUCTION

1.1. THE NEED FOR AN INTEGRAL APPROACH

The dynamic thermal interaction, under the influence of occupant behaviour and outdoor climate, between building and heating / cooling and ventilating system is still difficult to predict. In practice this often results in non-optimal, malfunctioning, or even "wrong" building / system combinations.

This is not an over-statement as can be demonstrated with examples from our own experience (Hensen 1986, 1987). This concerned predictions and measurements related to an extensive real scale experiment with several types of low-energy houses. With respect to reduction of heat-loss by transmission and natural ventilation through building structural measures, the experiment is regarded as very successful. Without going into any further details, another one of the main conclusions was however that there is definitively a need - and room - for improvement on the plant side and with respect to building / system thermal interaction.
There are also several other examples from practice. It was found for instance, that the real seasonal efficiency of high efficiency boilers is in practice markedly lower than was expected from experimental results collected in a laboratory environment. The reason being that return water temperatures are actually higher than anticipated (ie often above flue gas condensation temperature). Another example is that of premature boiler aging which is regularly encountered in multi-family housing. This damage seems to be caused by large temperature stress which occurs frequently during heating-up periods (ie when the boiler operates at full power and return water temperatures are at its lowest).

These are merely a few examples drawn from a large class of problems for which the complete "system" consisting of building structure, occupants, HVAC plant, and prevailing climate must be evaluated simultaneously and as a whole. Other topics belonging to the same problem domain and which definitively also need this integral approach are (in no particular order): Sick Building Syndrome, Building Energy Management Systems, application of passive solar energy, HVAC system and control development and testing, integrated systems (eg floor heating, ice rink, swimming pool), and unusual building / system combinations which may occur for instance when a historical building finds a new destination (eg a church being converted into a multi-purpose centre) or in case of relatively new developments like atria.

Several reasons may be identified to illustrate why the above mentioned problems and the need for an integral approach have become more important during the last decades. When emphasizing domestic applications:

- reduction of space heating demand; for example, the average natural gas consumption for domestic space heating in The Netherlands has dropped from about 3500 m^3/a in 1973 to approximately 1700 m^3/a in 1989. The average heating system capacity in newly built

Dutch houses was lowered by a factor three during the same period. The installed capacity used to be much lower for domestic hot water than for space heating. At present, the ratio between heating capacity for hot water and for space heating is between two and four. Due to these effects, the heating system has become much more sensitive to both external and internal thermal disturbances.

- energy conscious behaviour; for instance nighttime temperature setback is only effective / comfortable when preheating periods are short. This implies that the system must have enough additional heating capacity to allow for these short preheating periods. This implies at the same time that the system will almost always operate at low to very low loads (on average over the heating season, say 15% of full load). Another form of energy conscious behaviour is to shut-off parts of the system (e.g. in unused rooms). In that case too the operation of the heating system (e.g. the flow rates) will be strongly different from the design conditions. Questions that arise then are: what will be the effect on system efficiency, fuel consumption and comfort and what are the (structural) consequences for the system.

- higher comfort levels; for example individual room control also makes higher demands upon the building / system tuning. The same questions as before can be asked and again the answer can only be found through an integral approach of building and system.

Up to now the building design process is more or less sequential; first the building is designed and subsequently the heating / cooling / ventilating system. The dynamic thermal interaction is usually left out of consideration completely. Thermal comfort requirements are commonly reduced to required air-temperature, neglecting other important thermophysiological environmental parameters like radiant temperature and air velocity. For system design, usually only extreme internal and ambient conditions are considered.
It is obvious that this cannot be the right approach for either thermal comfort or for energy consumption.

So it is clear that there is definitively need for tools which enable an integral approach of the building and its plant system as a whole.

1.2. THE BUILDING AS AN INTEGRATED, DYNAMIC SYSTEM

One could argue that the main objective of a building is to provide an environment which is acceptable to the building users. Whether or not the indoor climate is acceptable, depends mainly on the tasks which have to be performed in case of commercial buildings, whereas in domestic buildings acceptability is more related to user expectation.
As illustrated in Figure 1.1 (modified after Lammers 1978), a building's indoor climate is determined by a number of sources acting via various heat and mass transfer paths. The main sources may be identified as:
- outdoor climate of which - in the present context - the main variables are: air temperature, radiant temperature, humidity, solar radiation, wind speed, and wind direction
- occupants who cause casual heat gains by their metabolism, usage of various household or office appliances, lighting, etc.
- auxiliary system which may perform heating, cooling, and / or ventilating duties.

These sources act upon the indoor climate via various heat and mass transfer processes:
- conduction through the building envelope and partition walls

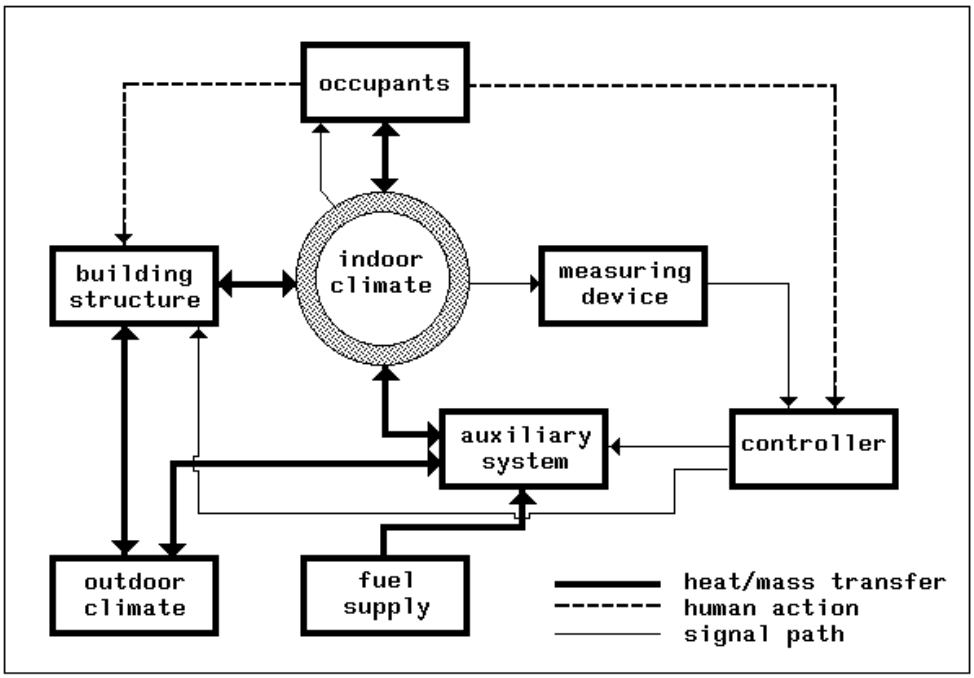

Figure 1.1 Diagrammatic representation of building and plant

- radiation in the form of solar transmission through transparent parts of the building envelope, and in the form of long wave radiation exchange between surfaces
- convection causing heat exchange between surfaces and the air, and for instance heat exchange inside plant components
- air flow through the building envelope, inside the building, and within the heating, cooling, and / or ventilating system
- flow of fluids encapsulated within the plant system.

The indoor climate may be controlled by the occupants basically via two mechanisms:
- altering the building envelope or inner partitions by for example opening doors, windows, or vents, or by closing curtains, lowering blinds, etc.
- scheduling or adjusting the set point of some controller device which may act upon the auxiliary system or upon the building by automating tasks exemplified above.

Within the overall configuration as sketched in Figure 1.1, several sub-systems may be identified each with their own dynamic thermal characteristics:
- the occupants, who may be regarded as very complicated dynamic systems themselves as will be evidenced in Chapter 2
- the building structure which incorporates elements with relatively large time constants, although some building related elements may have fairly small time constants (eg the enclosed air volume, furniture, etc.)
- the auxiliary system which embodies components having time constants varying by several orders of magnitude (eg from a few seconds up to many hours in case of for instance a hot

water storage tank).

The cycle periods of the exitations acting upon the system are also highly diverse. They range from something in the order of seconds for the plant, via say minutes in case of the occupants, to hours, days and year for the outdoor climate.

From the above it will be apparent that we are indeed addressing a very complicated dynamic system.

1.3. OBJECTIVE AND OUTLINE OF THE PRESENT WORK

Having identified the need for tools which enable an integral approach of the complex dynamic system incorporating the building and its HVAC system, we are now able to state the objective of the present work: development / enhancement of building performance evaluation tools which treat the building and plant as an integrated, dynamic system.

In this respect the present work is a follow-up of previous work at Eindhoven University of Technology, which focussed on the relation between building design and energy consumption (Bruggen 1978), building design and thermal comfort (Lammers 1978), and energy consumption and indoor environment in houses (Hoen 1987). hoen

There may be several alternative ways to achieve the objective identified above. However, one of the most powerful tools currently available for the analysis and design of complex systems, is computer simulation. As Aburdene (1988) points out:

> *"Simulation is the process of developing a simplified model of a complex system and using the model to analyze and predict the behavior of the original system. Why simulate? The key reasons are that real-life systems are often difficult or impossible to analyze in all their complexity, and it is usually unnecessary to do so anyway. By carefully extracting from the real system the elements relevant to the stated requirements and ignoring the relatively insignificant ones (which is not as easy as it sounds), it is generally possible to develop a model that can be used to predict the behavior of the real system accurately."*

The *stated requirements* with respect to the objective of the present work - ie thermal comfort and minimum fuel consumption - are elaborated in Chapter 2.

In view of the hectic developments in the area of information technology, it is impossible to make predictions regarding future building performance evaluation tools. There is no doubt however that their appearance will be quite different and that the power and features on offer will be much larger than at present (see eg Augenbroe and Laret 1989). In practice this means that it is not yet clear what kind of form the evaluation tools should take. Because of this unclearness and to link up with established and recently initiated international research (intelligent knowledge based systems, energy kernel systems (see eg Augenbroe and Winkelmann 1990, Buhl et al. 1991, Clarke and Maver 1991), the best strategy seems to start from an established platform and to focus on enhancement of knowledge concerning computer simulation of building and heating system. This is elaborated further in Chapter 3.

Chapter 3 also identifies those parts of this existing platform which needed further development in view of the subject of the present work. The results of these developments

are described in Chapter 4, which describes the work regarding fluid flow simulation, and in Chapter 5 which concerns plant simulation.

In order to be able to use the simulations with confidence, verification and validation is absolutely necessary. This is the subject of Chapter 6.

Then Chapter 7 addresses some user aspects regarding simulation results recovery, and exemplifies the need for the tools presented in this thesis by showing their application both in a modelling orientated context and in a building engineering context.

Finally Chapter 8 describes conclusions which may be drawn from the present work, and indicates possible directions for future research.

References

M.F. Aburdene 1988. *Computer simulation of dynamic systems,* Wm. C. Brown Publishers, Dubuque, IA.

G. Augenbroe and F. Winkelmann 1990. ‘‘Integration of simulation into building design: the need for a joint approach,’’ in *Proc. ASME Int. Solar Energy Conf. on Design Tools for Passive Solar and Building Energy Conservation held in Miami, 1990.*

G.L.M. Augenbroe and L. Laret 1989. ‘‘COMBINE (Computer Models for the Building Industry in Europe) Pilot study report,’’ Information package for the DG XII programme "JOULE", Commission of the European Communities DG XVII, Brussels.

R.J.A. van der Bruggen 1978. ‘‘Energy consumption for heating and cooling in relation to building design,’’ Doctoral dissertation Eindhoven University of Technology (FAGO).

F. Buhl, E. Erdem, J-M. Nataf, F.C. Winkelmann, M.A. Moshier, and E.F. Sowell 1991. ‘‘The U.S. EKS: advances in the SPANK-based Energy Kernel System,’’ in *Proc. 3rd Int. Conf. on System Simulation in Buildings, Dec 1990,* pp. 107-150, University of Liege. Lawrence Berkeley Laboratory report LBL-29419

J.A. Clarke and T.W. Maver 1991. ‘‘Advanced design tools for energy conscious building design: development and dissemination,’’ *Building and Environment*, vol. 26, no. 1, pp. 25-34.

J.L.M. Hensen and P.J.J. Hoen 1986. ‘‘Energieproeftuin: a real scale experiment with low-energy dwellings in The Netherlands,’’ in *Proc. Int. Climatic Architecture Congress*, Louvain-la-Neuve (B).

J.L.M. Hensen 1987. ‘‘Energieproeftuin: results of an experiment on low-energy housing in The Netherlands,’’ in *Proc. European Conference on Architecture*, Munich.

P.J.J. Hoen 1987. ‘‘Energy consumption and indoor environment in residences,’’ Doctoral dissertation Eindhoven University of Technology (FAGO).

J.T.H. Lammers 1978. ‘‘Human factors, energy conservation and design practice,’’ Doctoral dissertation Eindhoven University of Technology (FAGO).

CHAPTER TWO

THE OBJECTIVE FUNCTIONS

2.1. THERMAL COMFORT AND OPTIMUM FUEL CONSUMPTION

One could argue that the most important objective of a building is to provide us with a comfortable indoor climate. It is only human that we want to achieve this as economically as possible. So here we have two equally important objective functions.

The optimum with respect to fuel consumption depends on many aspects including economical and environmental impact issues. Because the building is an integrated, dynamic system, it is difficult to establish an optimum for any objective function influenced by this dynamic behaviour. Optimisation of just a part of a system, "never" yields the optimum for the system as a whole. So one thing is certain, in order to establish optimum fuel consumption, we first need to be able to approach the overall system integrally. As this is precisely the goal of the present work, it is inevitable that we have to leave research on optimum fuel consumption for the future.

Without going into this matter any further, it will be apparent that - no matter what - we will need assessment criteria with respect to thermal comfort. Establishment of these criteria is the subject of the remainder of this chapter.

2.2. ASSESSING THERMAL COMFORT

Thermal comfort is generally defined as that condition of mind which expresses satisfaction with the thermal environment (e.g. in ISO 1984). Dissatisfaction may be caused by the body as a whole being too warm or cold, or by unwanted heating or cooling of a particular part of the body (local discomfort).

From earlier research (as reported and reviewed in e.g. Fanger 1972, McIntyre 1980, Gagge 1986) we know that thermal comfort is strongly related to the thermal balance of the body. This balance is influenced by:

- environmental parameters like: air temperature (θ_a) and mean radiant temperature (θ_{mrt})†, relative air velocity (v) and relative humidity (RH)
- individual parameters like: activity level or metabolic rate (M) (units: 1 met = 58 W/m^2) and clothing thermal resistance (I_{cl}) (units: 1 clo = 0.155 m^2K/W)

Extensive investigations and experiments involving numerous subjects have resulted in methods for predicting the degree of thermal discomfort of people exposed to a still thermal

† θ_a is often combined with θ_{mrt} to form operative temperature ($\theta_o = a\theta_a + (1-a)\theta_{mrt}$ where $a < 1$)

environment. The most well known and widely accepted methods are (1) Fanger's "Comfort Equation" and his practical concepts of "Predicted Mean Vote" and "Predicted Percentage of Dissatisfied" (Fanger 1972) and (2) the J.B. Pierce two-node model of human thermoregulation (Gagge 1973, 1986). With these methods several thermal comfort standards (e.g. Fanger 1980, ASHRAE 1981, ISO 1984, Jokl 1987) have been established during the past decade. These standards specify environmental parameter ranges (ie comfort zones) in which a large percentage of occupants (generally at least 80%) with given individual parameters will regard the environment as acceptable[‡]. Most work related to thermal comfort has concentrated on steady-state conditions. This is expressed by the fact that only one of the above standards (ASHRAE 1981) also specifies limits for changing environmental parameters (for θ_o only).

Because of the thermal interaction between building structure, occupancy, climate and HVAC system, pure steady-state conditions are rarely encountered in practice. For example, Madsen (1987) found indoor temperature fluctuations between 0.5 K and 3.9 K (during 24 hours with a constant set point) which depended on the combination of heating and control system. Sometimes it may even be advantageous to allow the environmental conditions to change. This was demonstrated in a field experiment (Hensen 1987) where it was found that decreasing the acceleration heating of the room thermostat in a dwelling resulted in a lower fuel consumption. This led however to considerably increased indoor temperature fluctuations, but it was not clear at the time whether or not these fluctuations would be acceptable to the occupants.

This is the background for reviewing literature on thermal comfort in transient conditions. The main results of this study, for which Croes (1988) made initial contributions, are already published (Hensen 1990).
We know that temperature is the most important environmental parameter with respect to thermal comfort, so this study focusses mainly on the effects of changes in temperature and mainly in homes, offices, etc.
In Section 2.3 the human thermoregulatory system is discussed so as to show the interaction between people, building and HVAC system. Our present understanding of human thermoregulatory mechanisms however is not sufficient for us to predict with confidence the human response to time-varying stimuli and recourse must be had to controlled tests. The results of such work on cyclic varying temperatures are present in Section 2.4.1. and on other types of changes in the following section. Finally in Section 2.5 some conclusions towards assessment criteria are made.

2.3. THE HUMAN DYNAMIC THERMOREGULATORY SYSTEM

The human body produces heat (principally by metabolism (ie oxidation of food elements)), exchanges heat with the environment (mainly by radiation and convection) and loses heat by evaporation of body fluids. During normal rest and exercise these processes result in average vital organ temperatures near $37°C$. The body's temperature control system tries to maintain these temperatures when thermal disturbances occur. According to Hensel (1981),

---

‡ For example, ISO (1984) recommends for light, mainly sedentary activity during winter conditions (heating period): *"a) The operative temperature shall be between 20 and 24°C (ie 22 ± 2°C). b) ...";* and during summer conditions (cooling period): *"a) The operative temperature shall be between 23 and 26°C (ie 24.5 ± 1.5°C). b) ...";*

who studied a vast amount of literature on the subject, the human thermoregulatory system is more complicated and incorporates more control principles than any actual technical control system. It behaves mathematically in a highly non-linear manner and contains multiple sensors, multiple feedback loops and multiple outputs.

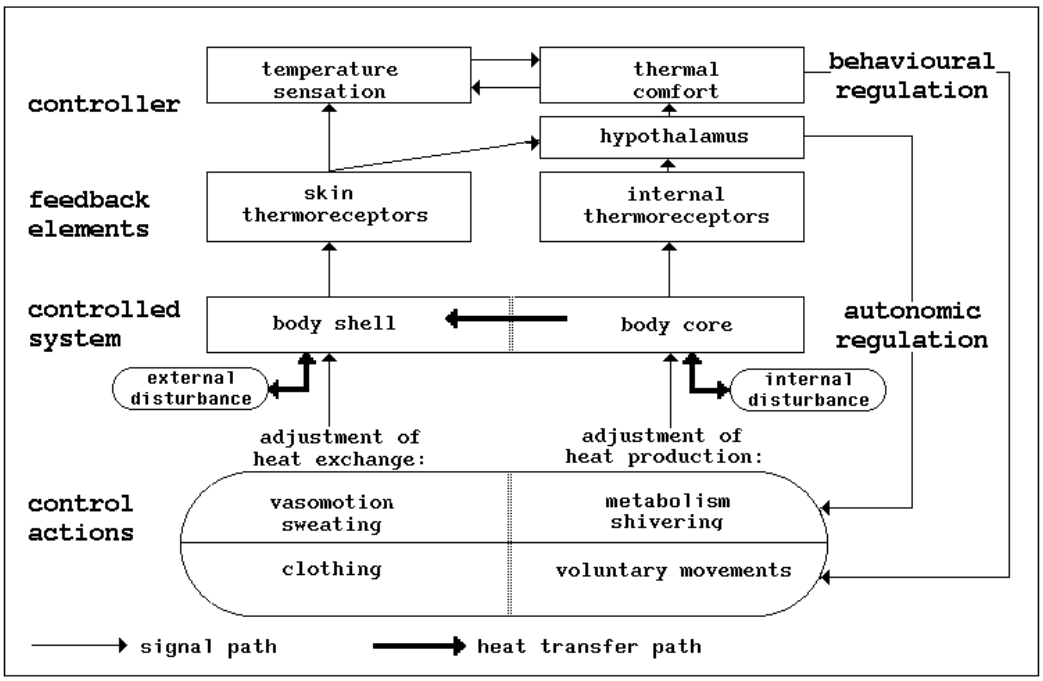

Figure 2.1 Diagram of autonomic and behavioural human temperature regulation (modified from Hensel 1981).

Figure 2.1 shows some basic features of the human thermoregulatory system. The controlled variable is an integrated value of internal temperatures (ie near the central nervous system and other deep body temperatures) and skin temperatures. The controlled system is influenced by internal (e.g. internal heat generation by exercise) and external (e.g. originating from environmental heat or cold) thermal disturbances. External thermal disturbances are rapidly detected by thermoreceptors in the skin. This enables the thermoregulatory system to act before the disturbances reach the body core. Important in this respect is that the thermoreceptors in the skin respond to temperature as well as to the rate of change of temperature. According to Madsen (1984) the latter is actually done by sensing heat flow variations through the skin.

Autonomic thermoregulation is controlled by the hypothalamus. There are different autonomic control actions such as adjustment of: heat production (e.g. by shivering), internal thermal resistance (by vasomotion; ie control of skin blood flow), external thermal resistance (e.g. by control of respiratory dry heat loss), water secretion and evaporation (e.g. by sweating and respiratory evaporative heat loss). The associated temperatures for these autonomic control actions need not necessarily be identical nor constant or dependent on each other.

Besides autonomic thermoregulation there is also behavioural thermoregulation with control actions such as active movement and adjustment of clothing. According to Hensel (1981), behavioural thermoregulation is associated with conscious temperature sensation as well as with thermal comfort or discomfort. The difference between temperature sensation and thermal comfort is that temperature sensation is a rational experience that can be described as being directed towards an objective world in terms of "cold" and "warm". Thermal comfort on the other hand is an emotional experience which can be characterised in terms of "pleasant" and "unpleasant". As McIntyre (1980) points out, the meaning of words like "pleasant" and "comfortable" do not have an absolute value, but will be relative to experience and expectation.

Hensel (1981) found that temperature sensations (especially local cold sensations) depend mainly on the activity of thermoreceptors in the skin whereas thermal comfort or discomfort reflects a general state of the thermoregulatory system (though this does not imply that changes in thermal comfort are always slower than changes in thermal sensation, as will be seen later on). The condition of thermal comfort is therefore sometimes defined as a state in which there are no driving impulses to correct the environment by behaviour (after Benzinger 1979). This is a more objective definition than the ISO definition.

According to McIntyre (1980), it is conventional to treat overall thermal discomfort (a subjective condition) in terms of thermal sensation (an objective quantity). This may be justifiable in case of steady-state conditions however probably not when transient conditions have to be judged. The difference between thermal comfort and temperature sensation during changing environmental conditions was clearly demonstrated by experiments of Gagge et al. (1967). They exposed subjects for one hour to neutral thermal conditions ($29°C$), then a step change to a much colder ($17.5°C$) or warmer ($48°C$) environment for a two hour exposure, which was followed by a step change back to neutral conditions. On entering the cold conditions there were immediate reports of cold sensations and discomfort. On returning to the neutral environment discomfort almost immediately disappeared, while temperature sensations lagged considerably behind the comfort reports and did not return to neutral for all subjects during the one hour postexposure period. The transient exposures to the hot environment showed much the same responses. On entering the hot conditions there were immediate reports on warm sensations and discomfort. On reentering the neutral conditions discomfort disappeared rapidly however more slowly than in the case of the cold to neutral step. The temperature sensations showed an overshoot with some initial reports of slightly cool.

In the past much work has been done aimed at finding practical methods for predicting the effects of a particular thermal environment in terms of comfort or discomfort. Reviews and summaries of this were made by Hardy (1970), Fanger (1972), Benzinger (1979), McIntyre (1980) and ASHRAE (1985). From these references it is clear that there is much evidence (from steady-state experiments) for cold discomfort being strongly related to mean skin temperature and that warmth discomfort is strongly related to skin wettedness caused by sweat secretion. These relations are the basis for methods like Fanger's (1972) Comfort Equation and the work of Gagge et al. (1973, 1986). In a recent evaluation by Doherty and Arens (1988) it was shown that these models are accurate for humans involved in near-sedentary activity and steady-state conditions.

From the fact that the skin thermoreceptors not only sense temperature but also the rate of change of temperature and that thermal comfort depends on an integrated value of central

and peripheral temperatures, it may be concluded that skin temperature alone is unlikely to be an adequate index for cold discomfort in transient conditions. Because sweat secretion reflects the general state of the thermoregulatory system, skin wettedness is probably a more adequate predictive index for warmth discomfort in transient conditions than mean skin temperature is for cold discomfort. No experimental proof of this has been found however. From these observations one may conclude that the above mentioned essentially steady-state methods are probably not adequate for predictions regarding thermal comfort in transient conditions.

A number of models for simulation of the dynamic behaviour of the human thermoregulatory system have been developed in the past. A well known example is the model of Stolwijk (1970) which was later expanded by Gordon (1974). In this model the human body is divided into a large number of segments (originally 24 and in Gordon's version 140) linked together via the appropriate blood flows. Each segment represents volume, density, heat capacitance, heat conductance, metabolism and blood flow of a certain part of the body. The temperature and rate of change of temperature of each segment is available as an input into the control system, and any effector output from the control system can be applied to any part of the controlled system.
The main application field for this kind of model is research on body temperature regulation itself. No model has been developed which also predicts whether a particular thermal environment is thermally uncomfortable and to what degree. It may be possible to link a model of this kind with the present knowledge on temperature sensation and thermal comfort, so as to enable comfort predictions to be made for transient conditions. This is however beyond the scope of the present study.

From the above discussion it follows that at present there is no other source except results of thermal comfort experiments to assess the acceptability of changing environmental conditions.

2.4. REVIEW OF EXPERIMENTS ON TRANSIENT CONDITIONS

A large number of experiments have been conducted on the human response to the thermal environment. Concerning the objectives of the experiments, distinction can be made between investigations on the thermoregulatory system on the one hand and the establishment of thermally comfortable or acceptable conditions on the other hand. The latter type of experiments are of primary interest in the present study.
Although most work has been concentrated on steady-state conditions, some experiments have examined transient conditions. In principle any of the human heat balance variables (θ_a and θ_{mrt} or θ_o, v, RH, M and I_{cl}) may change in time. However in most cases, changing ambient temperatures has been of interest. Changes can be categorised as:
- cyclic: triangular or sinusoidal changes in the transient variable (e.g. resulting from the deadband of the HVAC control system), characterised by mean value, peak to peak amplitude and fluctuation period or frequency†
- ramps or drifts: monotonic, steady changes with time. Ramps refer to actively controlled changes and drifts to passive changes (as one might encounter in a building with no active

† With triangular changes, peak to peak amplitude $\Delta\theta_{ptp}$, cycle frequency CPH and rate of change of temperature $\delta\theta/\delta t$ are related according to: $\delta\theta/\delta t = 2.CPH.\Delta\theta_{ptp}\ K/h$

temperature control). These changes are characterised by starting value, amplitude and rate of change
- steps, such as one experiences in going from one thermal environment to another. Step changes are described by starting value, direction and amplitude.

The following section describes the results of the most important thermal comfort experiments with cyclic temperature changes since these are of primary interest in the present context. The next section describes results of some other related experiments. All results relate to environmental conditions in or near the comfort zone for sedentary or slightly active persons wearing normal indoor clothing.

2.4.1. Results for Cyclic Temperature Changes

Sprague and McNall (1970) conducted experiments aimed at providing data, obtained under controlled conditions, as a basis for confirming or modifying existing specifications on fluctuating thermal conditions. Before, these specifications were largely based on field experience. Their first series of tests were designed to study the effect of fluctuating dry bulb temperature on the thermal sensation of sedentary persons (N = 192; college age; M = 1.2 met; I_{cl} = 0.6 clo; θ_{mrt} = 25.6$°C$; RH = 45%; v < 0.15 m/s). The dry bulb temperature varied according to a triangular wave form with average fluctuation rates in the range 1.7 to 10.9 K/h and peak to peak amplitudes ranging from 0.6 K to 3.3 K, resulting in 1.0 to 2.0 $cycles/hour$. All tests started from the middle of the comfort zone (mean dry bulb temperature was 25.6$°C$). Although it is not clear how acceptability was defined the authors concluded that no serious occupancy complaints should occur due to dry bulb temperature fluctuations if $\Delta\theta_{ptp}{}^2 \cdot CPH < 4.6\ K^2/h$ in which $\Delta\theta_{ptp}$ is the peak to peak amplitude of the temperature fluctuation and CPH is the cycle frequency (cycles/h). This expression, which was only validated inside the comfort zone and for two fluctuation rates, suggests that $\Delta\theta_{ptp}$ could be large for slow fluctuations and that $\Delta\theta_{ptp}$ would have to be small when fluctuations are rapid. This result seems strange; when the human body is regarded as one or more thermal capacitances, one would expect opposite results (ie an increase of acceptable $\Delta\theta_{ptp}$ with increasing fluctuation rate). Therefore, results like this must be related to the thermoregulation control mechanisms and indicate that the rate of change of temperature is very important.
The authors specifically state that their expression does not apply to systems, where the mean radiant temperature fluctuates, since the effect of varying radiant temperatures was not investigated. However, assuming (according to (ASHRAE 1981, ISO 1984)) that, at air speeds of 0.4 m/s or less, the operative temperature is simply the arithmetic mean of dry bulb temperature and mean radiant temperature, the relation between maximum acceptable peak to peak amplitude and cycle rate of operative temperature can be assumed to be $\Delta\theta_{ptp}{}^2 \cdot CPH < 1.2\ K^2/h.$

Following these results the acceptable peak-to-peak temperature amplitude decreases with increasing fluctuation rates. This seems to be contradicted by work of Wyon et al. (1971) who performed experiments in which the amplitude of the temperature swings was under the subjects' control. They found that subjects tolerated greater amplitudes when the temperature changed more rapidly. In their view this was due to purely physical reasons, as rapid changes of ambient temperature cause skin temperature, and hence thermal sensation, to lag further behind in time and this effectively reduced the sensed temperature fluctuations. It was also found that subjects tolerated greater amplitudes when performing mental work

than when resting. McIntyre and Griffiths (1974) later pointed out that due to a much smaller rate of change of the mean radiant temperature, when compared with the air temperature, and unusual acceptability criteria (spontaneous dial voting when the temperature was too hot or too cold) the tolerated range in operative temperature was actually smaller than normally found in steady-state conditions.
Later experiments of Wyon et al. (1973) were designed to investigate the effects on comfort and performance of predetermined ambient temperature swings under more normal working conditions. The subjects (N = 16; student age; M = 1.2 met; I_{cl} = 0.6 clo; v < 0.1 m/s) were exposed to sinusoidal swings around the average preferred ambient temperatures with peak to peak amplitudes in the range 2 to 8 K and periods ranging from 32 to 8 minutes (ie 1.9 to 7.5 $cycles/hour$), resulting in fluctuation rates between 15 K/h and 60 K/h. Certain complications resulted in considerable damping (up to 75%) of the amplitude of the temperature swings below head level. Also the actual amplitudes of the mean radiant temperatures were lower than half of the intended amplitudes. The authors state that for these reasons the experiments are probably best regarded as an investigation of air temperature swings at head height. From the results they concluded: *"Large temperature swings ..... cause increased discomfort"* and *"Large ambient temperature swings appear to have a stimulating effect that is to be preferred to the apparently opposite effect of small temperature swings, but a constant, optimally comfortable temperature, where this can be achieved, would still seem to be preferable to either"*. To be able to compare these results with the other references, Wyons raw data was examined. This revealed that 80% of the votes were in the comfort zone for all swings with intended peak to peak amplitudes of 4 K or less. As indicated above this actually suggests maximum acceptable peak to peak amplitudes of operative temperature fluctuation for the whole body in the range 1 to 2 K

Experiments with large ambient temperature swings were also conducted by Nevins et al. (1975). The subjects (N = 18; different ages; M = 1.2 met; I_{cl} = 0.6 clo; RH = 50%; v = 0.25 m/s) were exposed to ambient temperature ($\theta_a = \theta_{mrt}$) swings with a peak to peak amplitude of 10 K and an average fluctuation rate of 19 K/h (0.9 $cycles/hour$). The mean ambient temperature was 25$^\circ C$. From the results it was concluded that the preferred ambient temperatures for comfort agreed well with the results of earlier steady-state experiments (on which for instance (ASHRAE 1974) is based) and that there was no clear evidence of an increased or decreased range of acceptable ambient temperatures due to fluctuation. An examination of Nevins' raw data however suggests a maximum acceptable peak to peak amplitude of about 2.8 K. This is a little less than the width of the comfort zone for steady-state conditions. It should be noted that when unacceptable temperatures are left out, a rate of temperature change of 19 K/h. would have resulted in a fluctuation frequency of about 3.4 $cycles/hour$ or alternatively 0.9 $cycles/hour$ would have resulted in an average rate of change of 5 K/h.

Rohles et al. (1980) conducted a series of experiments in which the subjects (N = 804; college age; M = 1.2 met; I_{cl} = 0.6 clo; RH = 50%) were exposed to cyclic changes around various basal temperatures (17.8 to 29.4$^\circ C$) with different amplitudes (1.1 K to 5.6 K) at rates ranging from 1.1 K/h to 4.4 K/h (0.3 to 1.5 $cycles/hour$). The results showed that if (steady-state) temperature conditions for comfort are met, the thermal environment will be acceptable, for near-sedentary activity while wearing summer clothing, if the rate of change does not exceed 3.3 K/h and the peak to peak amplitude is equal to or less than 3.3 K (which is approximately the same as the width of the steady-state comfort zone). The discussion following the presentation of the results revealed some criticism which was acknowledged by the authors. Apparently, their acceptability criteria were less course than

usual. Due to the heat capacity of the building fabric, the mean radiant temperature swings were damped and delayed when the air temperature cycled. For this reasons the acceptable maximum rate of change and peak to peak amplitude of operative temperature will probably be lower than the values mentioned above.

There are a number of difficulties which should be noted when comparing the results of the above mentioned experiments:
- the results are in fact subjective responses of a highly complex system of which we most probably do not yet know all the processes involved to the extent necessary for controlling all relevant parameters during experiments
- usage of different semantic voting scales, both in type (ie directed towards acceptance (with words like acceptable and unacceptable), comfort, sensation or mixed) and appearance (e.g. 2 , 7 or 9 point, and discrete or continuous)
- differences in acceptability criteria (e.g. comfort interval on a 7 point semantic comfort scale defined as centre-point ± 1.0 vote as opposed to centre-point ± 0.5 votes) which is sometimes unavoidable because of the scale differences
- differences in conditions: subjects resting or performing mental work, fluctuating dry bulb temperature or fluctuating operative temperature
- differences in subjects; our knowledge of the distribution of thermoregulatory efficiency (and thus the time factor in discomfort) among individuals is still very limited and this can easily lead to sample errors

Regardless of these differences all results seem to indicate that with cyclic fluctuating ambient temperatures the bandwidth of acceptable temperatures decreases with increasing fluctuation frequency. This bandwidth seems to be at its maximum in steady-state conditions. This can be seen in Figure 2.2 which comprises the major results of the experiments and indicates which fluctuation frequencies were investigated.
The results suggest that there is a certain amplitude threshold (at about 1 K) below which the influence of fluctuation frequency is negligible. At frequencies below approximately 1.5 $cycles/hour$ the maximum acceptable peak to peak amplitude increases with decreasing frequency until the steady-state comfort bandwidth is reached.

As shown in Figure 2.2 the results seem to be quite adequately described by ASHRAE's standard 55-1981 which states with regard to cycling temperature: *"If the peak variation in operative temperature exceeds 1.1* K *the rate of temperature change shall not exceed 2.2* K/h. *There are no restrictions on the rate of temperature change if the peak to peak is 1.1* K *or less".* The maximum rate of temperature change of about 2.2 K/h can be regarded as conservative when compared with the experimental results.

2.4.2. Results for Other Changes

Comfort experiments involving temperature drifts or ramps are reported by McIntyre and Griffiths (1974), Berglund and Gonzalez (1978, 1978a), Berglund (1979) and Rohles et al. (1985). From the results it may be concluded that slow temperature changes up to about 0.5 K/h have no influence on the width of the comfort zone as established under steady-state conditions.
McIntyre and Griffiths (1974) report no difference between temperature changes of 0.5 K/h, 1.0 K/h and 1.5 K/h nor steady-state with respect to permissible deviations from neutral temperature.
Berglund and Gonzalez (1978) found however that with faster rates of temperature change

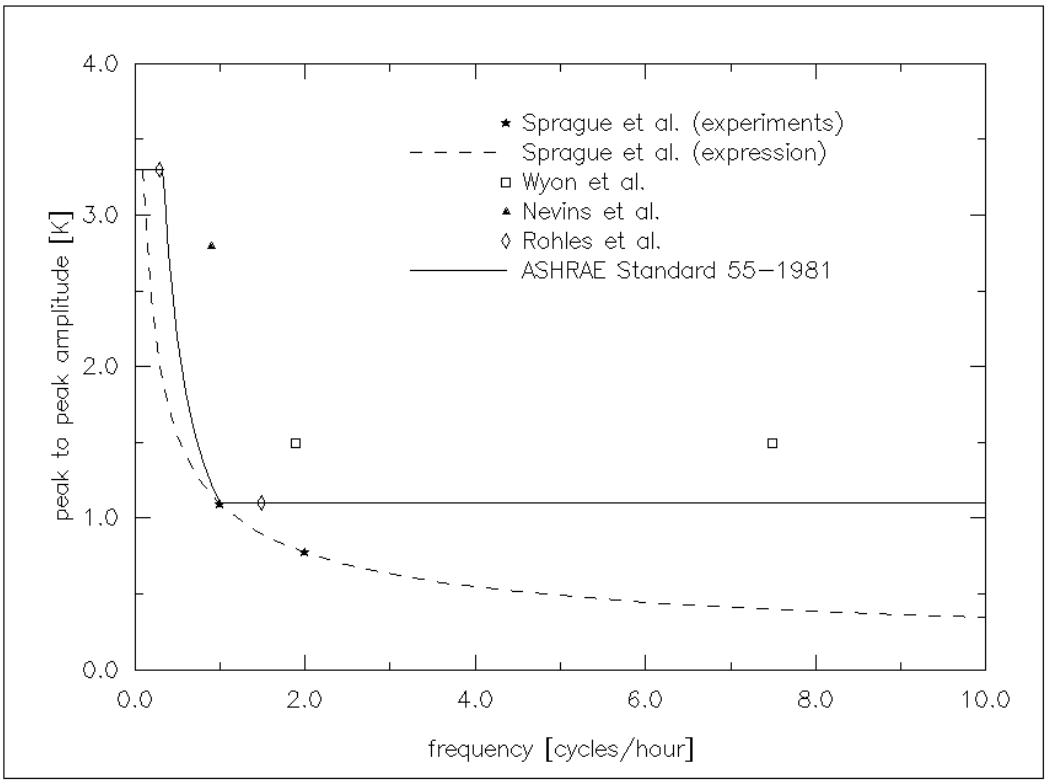

Figure 2.2 Maximum acceptable peak to peak amplitudes of cyclic fluctuating operative temperature as a function of cycle frequency for near-sedentary activity while wearing summer clothing (derived from Sprague 1970[1], Wyon 1973[1], Nevins 1975, Rohles 1980, ASHRAE 1981[2]).
1) Operative temperatures estimated from given dry bulb temperatures (see text).
2) Value at 0.0 $cycles/hour$ indicates width of steady-state comfort band

(ie 1.0 K/h and 1.5 K/h) the permissible deviation from neutral temperature was larger than was the case for the 0.5 K/h temperature change. This difference was more pronounced for subjects wearing summer clothing (0.5 clo) than for those wearing warmer clothing (0.7 or 0.9 clo). It should be mentioned however that these authors used an unusual assessment of acceptability. Instead of the more common procedure of deriving acceptability indirectly from comfort votes, a direct two point acceptability question was used. This resulted in a considerably wider ambient temperature zone where the acceptability of the subjects was 80% or higher when compared to the usual comfort zones. Also the acceptable zone was shifted somewhat to the warm side, implying that a slightly warm environment is more acceptable than a slightly cool one.
From their eight-hour-long experiments Berglund and Gonzalez (1978a) concluded that a temperature ramp of 0.6 K/h between 23$^{\circ}C$ and 27$^{\circ}C$ was thermally acceptable to more than 80% of the subjects (wearing summer clothing). This would imply an increased comfort zone. The section on temperature drifts or ramps in the ASHRAE standard (1981) states that *"slow rates of operative temperature change (approximately 0.6 K/h) during the occupied period are acceptable provided the temperature during a drift or ramp does not extend*

beyond the comfort zone by more than 0.6 K and for longer than one hour". This statement is most probably based on these results. As indicated above the results are however based on a different acceptability assessment from the usual ones. Furthermore, as Benzinger (1979) points out, the results may have been influenced by the fact that the human thermoregulatory set point is higher in the afternoon than in the morning; that is, our tolerance for heat increases during the day. In view of this, the ASHRAE standard (1981) should probably be restricted to acceptable changes during daytime and in upward direction only.

From Nevins' (1975) experiments with cyclic changes with average fluctuation rates of 19 K/h it was concluded that there was no clear evidence of increased or decreased comfort zones due to fluctuation of ambient temperature. As pointed out by McIntyre and Griffiths (1974), the results of the experiments with about the same average fluctuation rate by Wyon et al. (1971) on the other hand do seem to provide evidence of decreased acceptable ranges due to fluctuation.

From experiments in the 1950's by Hensel (also reported in Hensel 1981) it became clear that when the human skin is exposed to changing temperatures the difference between neutral temperature and the temperature at which warm or cold sensations occur (ie thermal sensation threshold) decreases inversely with the rate at which the temperature is changed. This thermal sensation threshold depends also on the temperature to which the skin is adapted when the change starts, on the direction of change, on the exposed part of the body and on the area being exposed. The latter two factors have a considerable influence on the intensity of temperature sensation as well. Although it cannot be proved, these aspects may very well be partly the cause of the contradictory results and conclusions of the experiments discussed above.
The fact that there is a threshold for thermal sensations, and that this threshold is affected by the rate of temperature change, makes it likely that the same is true for thermal comfort. This would be in support of Figure 2.2.

Contradictory results are also found with respect to sex differences. Wyon et al. (1972), using high-school pupils, found significant differences between the responses of male and female subjects when exposed to changes in ambient temperature (about 4 K/h). Males in general feel hotter and react faster than females. Nevins et al. (1975), using college age males and young and older female office workers, reported that the females had significantly higher warmth sensitivity than the male group.
An explanation for these and previously mentioned contradictions may be related to the choice of subjects (ie sampling error). This can be deduced from the conclusion of Stolwijk (1979) who, after reviewing a considerable amount of research in this area, states: *"Differences in effectiveness of the thermoregulatory system in different individuals will result in different dynamic comfort responses to changing thermal environments: people with efficient thermoregulation will experience thermal discomfort sooner than those with less effective thermoregulatory systems. Our knowledge of the distribution of thermoregulatory efficiency among people is still very limited."*

The effect of the level of clothing insulation and activity on the human thermal sensitivity during temperature changes was investigated by McIntyre and Gonzalez (1976). They exposed young college males who were either rather heavily clothed (1.1 clo) or almost nude and who were either resting (1.1 met) or bicycling (2.3 met) to a 6 K step change in air temperature. The temperatures were so chosen that the subjects started warmer than neutral and finished cooler than neutral. The experiments took place in June and were partly

replicated in August (after summer heat acclimatization) to see whether there are seasonal changes in thermal sensitivity. From the results it was concluded that in general the change in whole body thermal sensation was affected by clothing, exercise and season. For resting subjects thermal sensitivity was not affected by clothing insulation or season. However the change in skin temperature following a change in air temperature was greater when unclothed than clothed. From this the authors concluded that change in mean skin temperature is therefore not an adequate predictor of thermal sensation. For unclothed subjects thermal sensitivity was greater when resting than when exercising. The responses of clothed, exercising subjects interacted with season (e.g. they felt cooler in August).
As indicated earlier, the effect of greater sensitivity during rest than when performing mental work was also found with the cyclic temperature change experiments by Wyon et al. (1971). That clothing insulation does not seem to have an effect on thermal sensitivity may be explained by the fact that in general various thermally sensitive parts of the body (e.g. hand, neck, hands) are uncovered.

Probably because of the minor influence of moderate humidities on thermal comfort and thermal sensation, there are only few experiments reported which investigate the effect of changing humidity. Four studies, those by Gonzalez and Gagge (1973), Nevins et al. (1975), Gonzalez and Berglund (1979) and Stolwijk (1979) all indicate that when operative temperature is inside or near the comfort zone, fluctuations in relative humidity from 20% to 60% do not have an appreciable effect on the thermal comfort of sedentary or slightly active, normally clothed persons. Relative humidity becomes more important when conditions become warmer and thermoregulation depends more on evaporative heat loss.

Regarding changing air velocities no references have been found except of course those dealing with the effect of air turbulence on sensation of draught. Velocity fluctuations due to turbulence are in general much faster (ranging from 0.01 Hz to 10 Hz) than ambient temperature fluctuations which generally can be measured in units of cycles per hour. Fanger et al. (1988) concluded that an air flow with high turbulence causes more complaints of draught than air flow with low turbulence at the same mean velocity. As possible reasons for this were mentioned the relation between convective heat transfer and turbulence and the relation between the heat flux (or rate of temperature change) as sensed by the skin thermoreceptors and turbulence.

Finally it is repeated that care must be taken in applying the above results. In general many contradictory results have been found. These were most pronounced with respect to rate of temperature change, sex difference and age difference. The possible reasons have already been indicated in the previous section.

2.5. CONCLUSIONS

Our theoretical knowledge concerning thermal comfort in transient conditions is still limited. At present, results of thermal comfort experiments seem to be the only source of information on the thermal acceptability of changing environmental conditions.
The present study is restricted to conditions characteristic for homes, offices, etc. The following assessment criteria are supplementary to the steady-state comfort criteria which are usually associated with those conditions; ie sedentary or slightly active persons, wearing normal indoor clothing in an environment with low air movement ($< 0.15\ m/s$) at 50% relative humidity.

The experimental results related to **cyclic** fluctuation of ambient temperatures are, although perhaps a little conservative, quite adequately described by ASHRAE's standard 55-1981 which states with regard to cyclic changes: *"If the peak variation in operative temperature exceeds 1.1 K the rate of temperature change shall not exceed 2.2 K/h. There are no restrictions on the rate of temperature change if the peak to peak is 1.1 K or less".*

With respect to temperature **drifts** or **ramps**, there is good experimental evidence that at rates of operative temperature change below 0.5 K/h, the environment is experienced as in steady-state conditions. At rates between 0.5 K/h and 1.5 K/h there is, apart from experiments with uncommon acceptability assessment procedures, no clear evidence of increased or decreased comfort zones due to transient conditions. The paragraph in ASHRAE's standard 55-1981 states that *"slow rates of operative temperature change (approximately 0.6 K/h) during the occupied period are acceptable provided the temperature during a drift or ramp does not extend beyond the comfort zone by more than 0.6 K and for longer than one hour",* but this should probably be restricted to acceptable changes during daytime and in upward direction only. No evidence was found why the limit for cyclic changes (ie if the rate of temperature change exceeds 2.2 K/h the peak variation shall not exceed 1.1 K) should not be valid for temperature drifts and ramps as well.

From several experiments it was found that **clothing insulation** has a negligible effect on thermal sensitivity during temperature changes. This implies that the limits stated above are valid for summer as well as winter conditions.
Regarding **activity level** a greater sensitivity was generally found during rest than when performing mental work. From this it follows that the above limits may be regarded as conservative in case of light sedentary activity in offices, homes, etc.

Provided that the operative temperature is inside the comfort zone, **humidity** fluctuations, as long as the relative humidity is in the range from 20% to 70%, do not seem to have an appreciable effect.
Regarding changing **air velocity**, no references were found except those dealing with the effect of increased draught complaints when air turbulence is higher.

References

ASHRAE 1974. ''Thermal comfort conditions for human occupancy,'' ASHRAE Standard 55-1974, American Society of Heating, Refrigerating and Air-Conditioning Engineers, New York.

ASHRAE 1981. ''Thermal environmental conditions for human occupancy,'' ANSI/ASHRAE Standard 55-1981, American Society of Heating, Refrigerating and Air-Conditioning Engineers, Atlanta, GA.

ASHRAE 1985. *Handbook of Fundamentals,* American Society of Heating, Refrigerating and Air-Conditioning Engineers, Atlanta, GA.

T.H. Benzinger 1979. ''The physiological basis for thermal comfort,'' in *Indoor Climate*, ed. P.O. Fanger and O. Valbjorn, pp. 441-476, Danish Building Research Institute, Copenhagen.

L.G. Berglund and R.R. Gonzalez 1978. ''Application of acceptable temperature drifts to built environments as a mode of energy conservation,'' in *ASHRAE Transactions*, vol. 84:1, pp. 110-121, Atlanta, GA.

L.G. Berglund and R.R. Gonzalez 1978. ‘‘Occupant acceptability of eight-hour-long temperature ramps in the summer at low and high humidities,’’ in *ASHRAE Transactions*, vol. 84:2, pp. 278-284, Atlanta, GA.

L.G. Berglund 1979. ‘‘Occupant acceptance of temperature drifts,’’ in *Indoor Climate*, pp. 507-525, Copenhagen.

M.E.J. Croes 1988. ‘‘De invloed van de omgevingsparameters op de thermische behaaglijkheid,’’ FAGO afstudeerrapport, Eindhoven University of Technology, Eindhoven.

T.J. Doherty and E. Arens 1988. ‘‘Evaluation of the physiological bases of thermal comfort models,’’ in *ASHRAE Transactions*, vol. 94:1, Atlanta, GA. (preprint)

P.O. Fanger 1972. *Thermal comfort. Analysis and applications in environmental engineering*, McGraw-Hill, New York.

P.O. Fanger 1980. ‘‘Proposed Nordic standard for ventilation and thermal comfort,’’ in *Proc. Int. Conf. On Building Energy Managment*, Povoa De Varzim (P).

P.O. Fanger, A.K. Melikov, H. Hanzawa, and J. Ring 1988. ‘‘Air turbulence and sensation of draught,’’ *Energy and Buildings*, vol. 12, 1, pp. 21-39.

A.P. Gagge, J.A.J. Stolwijk, and J.D. Hardy 1967. ‘‘Comfort and thermal sensations and associated responses at various ambient temperatures,’’ *Environmental Research*, no. 1, pp. 1-20.

A.P. Gagge 1973. ‘‘Rational temperature indices of man’s thermal environment and their use with a 2-node model of his temperature regulation,’’ *Federation Proceedings*, vol. 32, no. 5, pp. 1572-1582, Federation of American Societies for Experimental Biology.

A.P. Gagge, A.P. Fobelets, and L.G. Berglund 1986. ‘‘A standard predictive index of human response to the thermal environment,’’ in *ASHRAE Transactions*, vol. 92:2B, pp. 709-731, Atlanta, GA.

R.R. Gonzalez and A.P. Gagge 1973. ‘‘Magnitude estimates of thermal discomfort during transients of humidity and operative temperature and their relation to the new ASHRAE Effective Temperature (ET*),’’ in *ASHRAE Transactions*, vol. 79:1, pp. 88-96, Atlanta, GA.

R.R. Gonzalez and L.G. Berglund 1979. ‘‘Efficacy of temperature and humidity ramps in energy conservation,’’ *ASHRAE Journal*, vol. 6, pp. 34-41.

R.G. Gordon 1974. ‘‘The response of a human temperature regulatory system model in the cold,’’ PhD thesis University of California, Santa Barbara, CA.

J.D. Hardy 1970. ‘‘Thermal comfort: skin temperature and physiological thermoregulation,’’ in *Physiological and behavioral temperature regulation*, ed. Hardy, J.D., A.P. Gagge and J.A.J. Stolwijk, pp. 856-873, Thomas Books, Springfield, IL.

H. Hensel 1981. *Thermoreception and temperature regulation*, Academic Press, London. (Monographs of the physiological society ; nr. 38)

J.L.M. Hensen, L.C.H. Dings, and W.J.A. van de Ven 1987. ‘‘Meetproject Someren,’’ rapport FAGO 87.08.K., Technische Universiteit Eindhoven, Eindhoven.

J.L.M. Hensen 1990. ‘‘Literature review on thermal comfort in transient conditions,’’ *Building and Environment*, vol. 25, no. 4, pp. 309-316.

ISO 1984. ‘‘Moderate thermal environments - determination of the PMV and PPD indices and specification of the conditions for thermal comfort,’’ International Standard ISO 7730, International Organisation for Standardization.

M.V. Jokl 1987. ‘‘A new "COMECON" standard for thermal comfort within residential and civic buildings,’’ in *Indoor Air ’87*, vol. 3, pp. 457-460, Berlin.

T.L. Madsen 1984. ‘‘Why low air velocities may cause thermal discomfort?,’’ in *Proc. 3rd Int. Conference on Indoor Air Quality and Climate*, pp. 331-336, Stockholm.

T.L. Madsen 1987. ‘‘Measurement and control of thermal comfort in passive solar systems,’’ in *Proc. 3rd Int. Congress on Building Energy Managment ICBEM87*, vol. IV, pp. 489-496, Lausanne.

D.A. McIntyre and I.D. Griffiths 1974. ‘‘Changing temperatures and comfort,’’ *Building Services Engineer*, vol. 42, 8, pp. 120-122.

D.A. McIntyre and R.R. Gonzalez 1976. ‘‘Man’s thermal sensitivity during temperature changes at two levels of clothing insulation and activity,’’ in *ASHRAE Transactions*, vol. 82:2, pp. 219-233, Atlanta, GA.

D.A. McIntyre 1980. *Indoor climate*, Applied Science Publishers Ltd, London.

R.G. Nevins, R.R. Gonzalez, Y. Nishi, and A.P. Gagge 1975. ‘‘Effect of changes in ambient temperature and level of humidity on comfort and thermal sensations,’’ in *ASHRAE Transactions*, vol. 81:2, pp. 169-182, Atlanta, GA.

F.H. Rohles, G.A. Milliken, D.E. Skipton, and I. Krstic 1980. ‘‘Thermal comfort during cyclical temperature fluctuations,’’ in *ASHRAE Transactions*, vol. 86:2, pp. 125-140, Atlanta, GA.

F.H. Rohles, J.E. Laviana, R. Wei, and R. Wruck 1985. ‘‘The human response to temperature drifts in a simulated office environment,’’ in *ASHRAE Transactions*, vol. 91:1A, pp. 116-123, Atlanta, GA.

C.H. Sprague and P.E. McNall jr 1970. ‘‘The effects of fluctuating temperature and relative humidity on the thermal sensation (thermal comfort) of sedentary subjects,’’ in *ASHRAE Transactions*, vol. 76:1, pp. 146-156, Atlanta, GA.

J.A.J. Stolwijk 1970. ‘‘Mathematical model of thermoregulation,’’ in *Physiological and behavioral temperature regulation*, ed. Hardy, J.D., A.P. Gagge and J.A.J. Stolwijk, pp. 703-721, Thomas Books, Springfield, IL.

J.A.J. Stolwijk 1979. ‘‘Physiological responses and thermal comfort in changing environmental temperature and humidity,’’ in *Indoor Climate*, pp. 491-506, Copenhagen.

D.P. Wyon, N.O. Bruun, S. Olesen, P. Kjerulf-Jensen, and P.O. Fanger 1971. ‘‘Factors affecting the subjective tolerance of ambient temperature swings,’’ in *Proc. 5th Int. Congress for Heating, Ventilating and Air Conditioning*, vol. 1, pp. 87-107, Copenhagen.

D.P. Wyon, I. Andersen, and G.R. Lundqvist 1972. ‘‘Spontaneous magnitude estimation of thermal discomfort during changes in the ambient %A temperature,’’ *Journal of Hygiene*, vol. 70, pp. 203-221.

D.P. Wyon, T. Asgeirsdottir, P. Kjerulf-Jensen, and P.O. Fanger 1973. ‘‘The effects of ambient temperature swings on comfort, performance and behaviour,’’ *Arch. Sci.*

Physiol., vol. 27, pp. A441-A458.

CHAPTER THREE

BUILDING ENERGY SIMULATION

3.1. INTRODUCTION

As identified in Chapter 1, the objective of the present work is development / enhancement of building performance evaluation tools which treat the building and plant as an integrated, dynamic system.
One of the techniques which may be employed to achieve this, is modelling and simulation. Modelling is the art of developing a model which faithfully represents a complex system. Simulation is the process of using the model to analyze and predict the behaviour of the real system. Simulation may be based on a physical model (to scale or real size), some (eg electric) analogon, or a numerical model. Computer simulation may use analog, hybrid, or digital techniques.
The present work uses the most popular technique of today: digital computer modelling and simulation.

Modelling and simulation have become indispensable engineering techniques in the fields of design (eg of buildings, plant configurations, and on the component level) and operation (system control, understanding, and interaction). The main reasons for this are that modelling and simulation offer vast advantages - over for example experimentation - with respect to:
- economy; in an increasing number of cases, simulation is faster, better and cheaper than experimentation,
- prediction; allows analysis of a (model of a) system which does not yet exist, and
- education; models are easily adapted, inexpensive to operate, able to simulate adverse conditions and may also serve as an aid in communication.

It should be noted though that simulation and experimentation are complementary: experimentation to discover new unknown phenomena or for validation purposes, and simulation to understand interactions of the known components of a system.

In the current context, modelling and simulation is thus used for predictions to help solve real world problems regarding buildings and the HVAC systems which service them. The building in question may be an existing structure, a proposed modification of an existing structure, or a new design.
This chapter will continue with sections on respectively the context of building energy simulation, the state-of-the-art, the simulation platform from which the present work started, and finishes by identifying the parts of that environment which are addressed in the present work.

3.2. THE CABD CONTEXT

Since the early 1960's, the use of computers in the field of building design - ie CAD (Computer Aided Design) which was only later specified to CABD (Computer Aided Building Design) - has been increasing steadily (Rooney and Steadman 1987). Although,

according to Gero (1983), its potential has and is taking longer to realise than was first thought. This statement is still true, judging from comparison of Gero's predictions for the then immediate future of 1983 with the actual situation at present (see eg Ratford 1991). Having mentioned this, CAD in the field of building design has received more and more attention, both from research and commercial communities. Due to economic factors, the draughting function has received the most - commercial - attention and is now becoming well established in building design practices.

The design process itself is very complicated, as may be concluded from the vast amount of work aimed at establishing models of the process of design. As Butera (1990) points out, the architectural design process may even be approached using principles from the so-called "deterministic chaos" theory. The complexity and the diversity of parameters to be taken into account leave large opportunities to chance in identifying the design optimum. The optimum may be regarded as a "strange attractor" in this context.
Due to its complexity, general software to aid in the design process, is much less developed and received much less attention than draughting and design process management tools. In recent years promising research activities have been - or are about to be - initiated aimed at relieving this deficiency. These studies often involve pluri-disciplinary research teams and employ very sophisticated research techniques (eg Dubois 1990, and Clarke and Duffy et al. 1991).

There is however one activity throughout the design process which has received much attention: building performance appraisal. Powerful, computer-based models were created to assess cost, performance and visual impact issues in design: from life-cycle cost estimates at the design proposal stage, through realistic visualisations of the design, to comprehensive evaluations of building energy and environmental performance. A demand for systems which possess both draughting and appraisal functions is however steadily growing. In response, appraisal programs were appended to draughting packages, thus creating what we may call early CABD (Computer Aided Building Design) systems.

As elaborated by Clarke (1989), CABD, and the sub-systems which it comprises, are affected by continuous changes in: power and cost of hardware, quality of software, elegance and effectiveness of human-computer interfaces (HCI), and user interface management systems (UIMS), and in (computer aided) software engineering (CASE) methods with which a greater degree of sub-system integration is possible. Table 3.1 (Clarke 1989), which is self-explanatory, summarizes several of the important issues in this respect.

When this table is compared with the actual situation at present, it seems that we are already in the short-term or perhaps even mid-term columns as far as the technology is concerned. This is due to recent technological and economical developments: ie relatively inexpensive, high performance, graphics workstations, strong reduction of data storage costs, and emergence of early expert systems (see eg MacRandal 1988). To further illustrate this: at the start of present work (late 1986) a high-resolution, bit-mapped, graphics workstation, offering a performance of 1.5 Mips (million instructions per second) and 70 Mbyte data storage, was purchased for approximately 20 kECU (≈ fl 50000). Now, 4.5 years later, two new workstations have been ordered one of which is only half the price and offers a 15 Mips performance, and another which still costs 20 kECU but offers 28 Mips performance and 1 Gbyte of storage capacity, instead.
As another exemplification of fast developing technology consider the following quote from Hartman (1988), which in addition illustrates usage of worldwide networking as may be

Table 3.1 Issues underlying CABD evolution (Clarke 1989)

Issue	**Time Scale**			
	Immediate (now)	Short-term (now-5 years)	Mid-term (5-10 years)	Long-term (10^{+} years)
Technology	• Micros • Drafting • Early performance prediction	• Supermicros • Partial CAD integration • Early expert systems	• Networking (worldwide) • Expert systems • Full CAD integration	• Computer ubiquity • Artificial Intelligence • Natural language • Full IKBS
Applications	• Drafting • Information technology • Performance prediction	• 'Accredited' performance prediction • 3-D Visualisation • Regulations	• Performance specification • Solids modelling • Integrated functions	• Participation • Client-orientated CABD • Post occupancy applications
Education and training	• Applications exploration • Hardware familiarisation	• In-depth postgraduate training	• Advanced undergraduate & mid-career training	• Full computer assisted design systems
Research	• Application knowledge • Validation • System evaluation	• Human-orientated CAD • UIMS, Shells Environments & Knowledge Bases	• Systems for computer-naive designers • Implementation of advanced m/c environments	• Non-traditional communication • Design optimisation
Impact	• Expensive & time consuming • Job shifts	• Skills shortage	• De-skilling • Breakdown of professional boundaries	• De-professionalisation
Net result				• Improved product performance

deducted from the reference:

> *Technology which seems unearthly and ethereal today will be reality and commonplace tomorrow. Fiberoptics and electronic imaging will allow us instant access to networks and information systems throughout the world. CD-ROM, WORM, and huge optical disks will provide mass storage capabilities with speedy searching and retrieval. Animation, simulation, video and voice input and output, and supercomputer power will be focused on the desktop. And while computer processing will become decentralized as workstations continue to proliferate, networks and shared systems will weave strength into our interdependence. Not technology for technology's sake, but more people performing more computing and incorporating computers in new and innovative ways in the pursuit of excellence in teaching and research.*

With respect to applications ,in 1991, we still seem to be in the "immediate" column, except perhaps for 3-D visualisation which appears to be the next commercial goal (ie following draughting). The same is true for education and training, where as yet, only few educational institutions offer in-depth postgraduate training.
Regardless of technological developments, CABD will not become commonplace unless

there is a high standard of user training. Although, as pointed out by Clarke (1989), it could be that ultimately user training becomes less important due to high level assistance by the computer. This does not imply however, that setting-up of education and training schemes is not of the utmost importance now.

With respect to research, up to now the majority of activity is directed towards proving the system and towards the acquisition of application knowledge. In the field of building energy simulation for example, a number of projects concerned with model validation have been or are being carried out (see Chapter 6), and indeed the present work may also be regarded as directed towards application knowledge acquisition.
Currently there are indications that the building energy simulation research activity is broadening in its scope (see eg Augenbroe and Laret 1989, and Clarke and Maver 1991). More effort is being expended on human-orientated CABD, through expert systems, HCI research and the like (eg Clarke and Rutherford et al. 1989). There is also a greater tendency to approach the problems underlying CABD in a multi-disciplinary, inter-institutional manner (e.g. Clarke and Hirsch et al. 1986, Clarke and Irving et al. 1988, and Augenbroe and Winkelmann 1990). This is also reflected in the recent formation of building analysis clubs: International Building Performance Simulation Association (IBPSA) based in the United States, Building Environmental Performance Analysis Club (BEPAC) in the United Kingdom and Building Analysis Groups (BAG) in the Benelux.

Clarke (1988) points out that CABD is not a remedy for all difficulties. At worst it is an automation of much of the mechanics of design. At best it allows an evaluation of the relationships inherent in a given design hypothesis. At present, the application of CABD is expensive, in terms of required human resource, and time consuming. In the near future the profession will probably experience a skills shortage. In the longer term however, with further advances in technology, application knowledge and education and training, CABD might bring important changes in the design process, involving de-skilling and the breakdown of professional boundaries. CABD could well become the common denominator of all parties involved in the design process, through some future IIBDS (Integrated Intelligent Building Design System). This will lower or even remove inter-professional barriers and improve the quality of the end product, the building.

As indicated, CABD is an evolutionary process which is characterised by several strong interrelations between quite different issues. For example, the level of application of energy simulation is as much a function of education and training as it is of hardware and HCI. Of course, CABD must also be regarded in the light of other technological and other developments which are taking place around us. That is, CABD will certainly become integrated in the "office of the future" which might offer multi-media personal work environments, incorporating integrated CAD/CAE (Computer Aided Engineering) features. One important issue not yet mentioned above is that of politics. There seams to be trends towards requiring that specified conditions must be achieved during the operation of buildings as well as in the design of buildings (as in ASHRAE’s 1989 standard on ventilation and air quality, and towards setting up "responsibilty chains", ultimately making a design team liable for the performance of the end product (as implied in for instance ASHRAE’s (1989) guideline for commissioning of HVAC systems). It could well be that if these trends are followed and accepted by the building industry, such issues will become major catalysts in the evolution of CABD.
Building energy simulation must be placed within this evolutionary context. Contemporary energy models are an important improvement compared with the traditional methods they

replace. However, there are still several important developments which must be undertaken before valid, easy to use models can be delivered to the design profession. The current research project seeks to be a part of this evolution.

3.3. STATE OF THE ART

As indicated in the introduction to this chapter, modelling and simulation have become popular engineering tools since they permit us to predict the behaviour of a system before the conditions we are interested in occur, and indeed even without the system actually existing. In fact, modelling and simulation are the only techniques available that allow us to analyze arbitrarily non-linear systems accurately and under varying experimental conditions.

Simulation is used in many areas of science and engineering. It is used in different senses to study a variety of systems which may be classified as: continuous vs discrete, deterministic vs stochastic, or dynamic vs steady-state. From Section 1.2, it is clear that building energy simulation addresses very complicated, highly interacting, continuous, deterministic, dynamic systems.

Table 3.2 The evolution of building energy models (Clarke 1988)

1st generation	Handbook orientated		Indicative
	Analytical in formulation	<----	Application limited
	As simplified as possible	|	Difficult to use
	Piecemeal in approach	|	|
2nd generation	Dynamics important	Feedback loop	|
	Still analytical	|	|
	Still piecemeal	>----	Increasing integrity
	Suitable for low-order problems	|	vis-å-vis the real
	with time invariance	|	world
3rd generation	Field problem approach	|	|
(current generation)	requiring numerical methods	|	|
	Integrated view of energy	|	|
	sub-system	|	|
	Suitable for high-order problems	>----	Leading to
	with time variation	|	|
	Heat and mass transfer considered	|	|
	Better user interface and partial CABD	|	|
	integration	|	V
Next generation	Full CABD integration	|	Predictive
	More advanced numerical methods	Feedback loop	Generalized
	Intelligent knowledge-based	>-----	Easy to use
	Object-orientated software		
	architecture		

Building energy modelling and simulation is part of an evolutionary process in the field of building design tools. Table 3.2 (from Clarke 1988) summarizes one view of the evolution of these design tools, from the traditional via the present day simulation approach to the 4th generation tools by the late 90s.
For more information regarding current advances in building energy simulation the reader is referred to reviews by Winkelmann (1988) and by Wiltshire and Wright (1988).

In terms of Table 3.2, the present work must be regarded as a 3rd generation approach, which also tries to make some links towards the next generation models.
Early work in 3rd generation approaches, focussed on the relation between building design and energy consumption (eg Clarke 1977, Bruggen 1978), or between building design and thermal comfort (eg Lammers 1978). In this and in later work (eg Hoen 1987), the auxiliary system was still more or less regarded as a given boundary condition instead of as a variable. These workers emphasized the building side of the overall problem domain, while others (eg McLean 1982, Murray 1984, Tang 1985, Lebrun 1988) focussed more on the plant side.
In the former approach the influence of the plant system is more or less neglected by over-simplification of the plant. In that approach it is common practice to base the estimation of energy consumption on some presumed, imposed indoor air temperature profile. In the latter approach the complex building energy flow paths are usually grossly simplified, and the building (or each building zone) is commonly regarded as just another component which in this case imposes a thermal load on the plant.
Although justifiable at that time, it is now felt that neither approach is preferable for the majority of problems which are affected by the thermal interaction of building structure and auxiliary system.

In recent times an increased interest in coupled problems may be observed. This is often still limited to coupled air flow and heat transfer problems (eg Kohonen and Ojanen 1985, McLean 1986, Axley and Grot 1990).
Here we want to make a further step and start from the principle that both building and plant have to be approached on equal levels of complexity and detail while taking into account all major fluid flow and heat transfer couplings.

For the present work, we had the choice of starting from scratch (as the precursory work indicated above, had become obsolete due to computer science department policies) or to start from what already existed in the international research community. The latter option was chosen.
Then there was the choice of starting from a plant orientated simulation environment like TRNSYS (SEL 1988) and HVACSIM$^+$ (Clark 1985), and enhancing this towards the building side of the overall problem, or alternatively, working the other way around, and start from an established building energy simulation environment and enhance this on the plant simulation side of the overall problem domain.
Here we opted for the latter approach, one reason being that this coincides better with the building engineering background of our unit.

3.4. THE ESP^R SIMULATION ENVIRONMENT

The decision to work with the *ESP^R* (Environmental Systems Performance, Research version) energy simulation environment, was based on (among others) the following arguments:
- it is clearly a research orientated environment, with the objective to simulate the real world as rigorously as possible to a level which is dictated by international research efforts/ results on the matter in question. Step-by-step it will be enhanced/ improved. It seeks to incorporate the latest state-of-the-art techniques to a feasible level, which means that the specific technique must be more or less generally applicable and there must be a certain amount of international consensus about the technique.
- sets out to take fully into account all building & plant energy flows and their inter-connections. It also offers the possibility to assess building & plant performance in terms of

thermal comfort. Thus it is specifically suited to do research on subjects in which inter-weaving of energy and mass flows plays an important role.
- source code is available and well accessible, because the system is highly modular in nature and offers important features like inbuild trace facilities.
- the system is well documented: it is heavily commented within the code itself, there is an extensive manual which is updated on a regular basis (Clarke and Hand et al. 1991), and there is also comprehensive background material available (eg Clarke 1985).
- the system is used by various international research groups (see next section).
- the system has been - and still is - the subject of various international validation programmes (see Chapter 6).
- the system offers extensive graphics facilities.
- because it runs in a UNIX† operating system environment, all other UNIX utilities (for software engineering, numerical techniques, documentation, data retrieval, data reduction, data analysis, etc) are "automatically" available to anyone using the system.

It should be noted though - and this is clearly not meant in any negative sense - that because of its research orientated and evolving nature, the *ESP*^{R} energy simulation environment is not as slick as one would demand of for instance a commercial package. Instead the system expects - and deserves - a pro-active approach of the user.

Starting from such an established and internationally recognised platform offers vast advantages for any individual research group. The most important ones are:
- economical; due to the complexity involved and the sheer size of the software to result, it is practically impossible for any (small) research unit to develop and maintain such a system as an independent product,
- academical:
  - as an individual group it is not necessary to have expertise in all areas,
  - areas not addressed within a specific research project will still be state-of-the-art,
  - results transfer to the international research community is implicit and therefore very efficient,
- practical; as more people are using the system, any bugs or flaws are likely to surface - and be solved - sooner.

This chapter will now continue with a description of *ESP*^{R}'s background and history, its current status, and by identifying areas where further development is necessary.

3.4.1. Background and History

The numerical engine of *ESP* was researched between 1974 and 1977 when the various techniques for modelling energy flow - response functions in time and frequency domain and numerical methods - were investigated and compared (Clarke 1977). This lead to a prototype model which used state-space equations and a numerical processing scheme to represent all building heat flux exchanges and dynamic interactions. Central to the model is its customised matrix equation processor which is designed to accommodate variable time-stepping, complex distributed control and the treatment of 'stiff' systems in which time constants can vary by more than an order of magnitude. Within a simulation, a special numerical technique ensures that all flow-paths evolve simultaneously to fully preserve the important spatial and temporal relationships.

† UNIX is a trademark of Bell Laboratories.

Between 1977 and 1982 *ESP* was extensively re-worked to allow simultaneous multi-zone processing and to create the infrastructure to support complementary program modules covering data input, graphical results display and interrogation, climate and construction database management; the computation of shading, solar beam tracking, view factors and window spectral behaviour; and facilities for comfort assessment, condensation checks, and the like.
Two other tasks were undertaken during this period: (1) model testing against hypothetical buildings (IEA 1980) and real buildings (Clarke and Forrest 1981, IEA 1984); and (2) the program was installed in a large multi-disciplinary design practice where its application to a number of live design projects was passively observed (Maver and Ellis 1982).
These activities lead to further theoretical and user-interface refinements so that a robust and (for its time) user-friendly system was beginning to emerge. The predictive accuracy, while not proven, was in diminishing doubt and, documentation was extensive and wide ranging.

Between 1982 and 1985 the system underwent its second major retrofit when air flow modelling (based on work by Cockroft 1979), and plant simulation (based on work by McLean 1982, and Tang 1985) was added.

The next step was to port the model to a UNIX operating system environment, running on high-performance, bit-mapped, graphics workstations. This operating system is widely regarded by computer scientists as the best environment for writing and maintaining sophisticated software. Its main strenghts (after MacRandal 1988) being: (1) hardware independence and standardization, (2) multitasking capability, (3) hierarchal file system, (3) extensive range of utilities, (4) powerful command shells, (5) i/o redirection and piping facilities, and (5) based on a software development philosophy[†]. Through this move, we may now truly speak of an energy simulation environment because all UNIX tools (numerical, documentation (for instance the typesetter used for formatting this dissertation), data retrieval, reduction, and analysis, on-line manuals, etc) and various (public domain) 3rd party products (graphics for exploratory results analysis, graphical editors (for instance the one used for editing the figures in this dissertation, etc) become available to the user at will.

By 1985 then, the *ESP* system was equipped to perform comprehensive energy and mass balance simulations for combined building and plant systems when constrained to conform to distributed control action. The system was non-building type specific and was able to handle any plant system as long as mathematical models of the constituent components were pre-installed in the required form.
It was during this period that *ESP* was selected as the European reference model in the field of passive solar architecture (CEC 1986). The system's validity was further tested in now completed validation projects (Bloomfield 1987, Lebrun and Liebecq 1988), and in the still ongoing EEC passive solar project PASSYS (Gicquel and Cools 1986, CEC 1989) in which various centres throughout Europe are rigorously testing the system against test cell experiments.

In the same period a number of organisations began to use the model commercially. And since early 1988, a separate version of the system is being commercialised by a private

---

[†] Also according to MacRandal (1988), paradoxically, UNIX's main weakness is its power. From the point of the novice, the terse command syntax and the lack of feedback (essential for UNIX commands to be usable from other programs), coupled with the expert orientated documentation, makes the whole system rather opaque to the novice.

company, ABACUS Simulations Limited.
The present work, starts from *ESP*^{R} which refers to the research version of the system, and which is controlled by ESRU (Energy Simulation Research Unit) at the University of Strathclyde. Several research groups are now working with the system. For example, in North America the model is established at Lawrence Berkeley Laboratory, at the National Institute of Standards and Technology (formerly: National Bureau of Standards) and at the Northwest Pacific Laboratory. And in Europe, it is operational at lead research centres in each of the EC member states.

3.4.2. Status at Project Commencement

Figure 3.1 shows the modular structure of the system and its status as described in (Clarke 1985). The system is able to address different problem configurations - from a single zone entity to a full multi-zone structure; from the 'no plant' case to combined building and plant networks; and from an energy only analysis to combined energy and mass balance. The user has full control of the simulation process and is given the software tools to progressively increase the simulation rigour as the design evolves.

ESP system figure here

Figure 3.1 The *ESP* system (Clarke 1985)

ESP^R has undergone major developments which is reflected in the fact that the main simulation engine now (1991) comes in three different versions (*bld* for building only simulation, *plt* for plant only simulation, and *bps* for combined building and plant simulation), and by for instance the new results handler *res* and radiant temperature prediction *mrt* modules. Notwithstanding that these modules are not incorporated in Figure 3.1., they will be referred to in the remainder of this dissertation.

What follows is a brief description of the system facilities at project commencement with respect to air flow modelling and plant simulation, as these are the primary subjects of the present work. For more comprehensive descriptions on all features of the system, the reader is referred to (Clarke 1985, Clarke and Hand et al. 1991).

As described by Clarke and McLean (1986), at project commencement the system offered an air flow simulation module called *air*. This module addresses building air flows as caused by boundary wind pressure and buoyancy forces acting on a distributed leakage scheme. Where internal temperature variations give rise to time dependent buoyancy forces, a version of *air* integrated in *sim* could be invoked. The technique of *air*, is to assign an arbitrary pressure to each of the "nodes" participating in a network and representing volumes of air. The flow along each connecting branch - representing either cracks, area openings, or doorways - is the determined from empirical equations relating air flow to pressure difference. The *air* algorithm uses a node-wise Newton-Raphson technique to iteratively adjust nodal pressures until the air mass balance equals zero at each node simultaneously. Without going into details, *air* has a convergence device to ensure this end result even for networks involving a mix of large and small flow paths.

ESP^R had been generalised so that it could simultaneously process any number of plant components so long as they form a closed loop network and so long as mathematical models of the constituent components are pre-installed in the required form. Table 3.3 identifies the plant component types on offer at project commencement. A plant components' database facility *pdb* was created to contain and manage these component models.
It should be noted, that although the foundation for plant simulation was present, at that point in time the plant simulation features were still very much in their development stage. Only limited prototype-like provisions were available and they were mostly only experimental.

Table 3.3 Plant component models (experimentally) on offer at project commencement (WCH: wet central heating)

Code	Nodes	Fluid	Description
10	1	air	mixing box with 1 external connection and parameterized outside air mass ratio
20	1	air	humidifier with controllable water supply rate
30	1	air	fan with controllable volume flow rate
40	1	air	cooling coil with controllable cooling duty
50	1	air	heating coil with controllable heating duty
60	1	air	duct
70	1	water	WCH boiler
80	1	water	WCH radiator
90	1	water	WCH pipe
100	1	water	WCH convergent flow tee-piece
110	1	water	WCH pump with controllable volume flow rate
120	1	water	WCH divergent flow tee-piece

The treatment of control had also been radically modified to allow the specification of any number of plant control loops to dictate plant component flux injection or flow rate control. As will be elaborated in Section 5.5 a building/plant control strategy is defined by several elements: sensor, actuator, controller type, and control law.
When referring to Table 5.4, at project commencement the sensor type "-1" was "only" able to measure the temperature of a plant component node, and sensor type "-4" was not

available at all. When referring to Table 5.5, an actuator of type "-1" was coupled to the component node, instead of to the control variable for the corresponding component type. When referring to Table 5.6, at project commencement "only" the controller types 0 to 6 were supported. Table 3.4 identifies the plant control laws which were on offer at project commencement.

Table 3.4 Plant control laws (experimentally) on offer at project commencement

Index	Description
0	The plant is to be switched off
1	Single node, counterflow air heating coil controller which acts to determine the coil heat addition. A basic proportional controller is incorporated to throttle the hot water volume flow rate as a function of the sensed control variable (temperature or enthalpy)
2	Single node, counterflow air cooling coil controller which acts to determine coil heat extraction. A basic proportional controller is incorporated to throttle the chilled water volume flow rate as a function of the sensed control variable (temperature or enthalpy)
3	Represents a controller with a basic proportional control action on heating or cooling flux as a function of the sensed control variable (temperature or enthalpy)
4	Represents a controller with a basic proportional control action on volume flow rate as a function of the sensed control variable (temperature or enthalpy)

The plant simulation model has been designed to handle both energy and two phase mass balances, by means of a three step matrix equation set-up and solution process. Thermodynamic couplings (eg flow dependent temperature differences, or temperature dependent flows) between the three matrix structures *within* a particular time step, are not yet considered. Plant simulation results comprise plant nodal temperatures, and working fluid mass flow rates. The plant simulation model does incorporate features to permit variable equation types depending on the time dependent relationship between component time constants and the computational time-step.

A complete building side simulation time increment (perhaps smaller than one hour) involves the evaluation of all building-side zones followed by the processing of the plant system equations. Since it is common practice to process plant matrices at a greater frequency than building matrices (because of the different time constants) two different solvers are employed, operating in tandem. The building-side solver (based on a matrix partitioning technique as described by Clarke 1985) is invoked once per user-specified time-step. As far as the building is concerned, plant connections are treated as excitations. At some user-specified sub-interval the plant matrix is established, this time with building connections treated as excitations, and solved by a sparse matrix method. The above implies that building and plant interaction incorporates time shifts. These may also occur, when building-side control is based on a plant-side originating signal or vise versa.

The total heat exchange of a plant component with its environment is comprised of a ’deliberate part’ and the component losses or parasitic heat exchange. For the deliberate part, at project commencement, only a "heat exchange via air flow"-connection between a plant (air) component and a building zone air point was possible. Although the component parasitic heat losses are evaluated when processing the plant energy matrix, there is no "energy feedback" into the building zones.

3.4.3. Development Areas

ESP^R objective is to simulate the real world as rigorously as possible to a level which is dictated by international research on the matter in question. The model seeks to incorporate the latest state-of-the-art techniques to a feasible level, which means that the specific technique must be more or less generally applicable and there must be a certain amount of international consensus about the technique. Hence, a technique like CFD (Computational Fluid Dynamics) is not yet incorporated.
Examples of techniques and provisions currently being researched and developed, and which will be be included in the near future are: extensions to allow for thermal bridge effects, and building material water vapour absorption / desorption, features for making the system more user friendly by the use of IKBS (Intelligent Knowledge Based Systems) techniques, and for making system development and maintenance more efficient by employing sophisticated CASE (Computer Aided Software Engineering) techniques. This will be elaborated further in Chapter 8.

As implied in the previous section, *ESP*^{R} was examined - at project commencement - to evaluate its facilities and capabilities in the area of simultaneous building and plant energy simulation. The outcome of this was that there was definitively a need to further develop its:

- fluid flow simulation capabilities. Although *air* was certainly state-of-the-art at the time it was developed, it was now found to be rather limited in terms of performance, and air flow component types on offer. Because *air* was clearly oriented towards simulation of building side heat exchange via inter-zone air flows and infiltration, *air* neither supports plant side air flow simulation nor simulation of any other working fluid.

- plant simulation capabilities. Although a number of plant simulation features were already incorporated in the system, most were still prototype-like in an early development stage, and mostly only experimentally active. So, the plant simulation side needed to become much more robust, and less terse for the user. Also there was definitively a need for additional - and more comprehensive - plant simulation features (eg ability to handle open loop networks), plant component models, plant control facilities, and plant results.

- integration of building and plant, heat and fluid flow. This obviously in order to enable an integral approach of the complex dynamic system incorporating the building and its HVAC system.

These developments, together with accompanying validation and application studies, were identified as goals for the present work. At certain points, for instance when deciding which specific plant or fluid flow component models to start with, the overall problem domain had to be restricted. It is obviously an impossible undertaking for one worker to cover the complete range of components as found in actual buildings. In the present work, emphasis was placed on domestic building and plant applications in cases where such a choice was necessary. The methodology itself however, is in no way whatsoever affected by this choice; ie the methodology is equally applicable to domestic and commercial buildings.
How the goals identified above, have been achieved, will be elaborated in the following chapters.

References

ASHRAE 1989. ‘‘Guideline for commissioning of HVAC systems,’’ ASHRAE Guideline 1-1989, American Society of Heating, Refrigerating and Air-Conditioning Engineers, Atlanta, GA.

ASHRAE 1989. ‘‘Ventilation for acceptable indoor air quality,’’ ASHRAE Standard 62-1989, American Society of Heating, Refrigerating and Air-Conditioning Engineers, Atlanta, GA.

G. Augenbroe and F. Winkelmann 1990. ‘‘Integration of simulation into building design: the need for a joint approach,’’ in *Proc. ASME Int. Solar Energy Conf. on Design Tools for Passive Solar and Building Energy Conservation held in Miami, 1990.*

G.L.M. Augenbroe and L. Laret 1989. ‘‘COMBINE (Computer Models for the Building Industry in Europe) Pilot study report,’’ Information package for the DG XII programme "JOULE", Commission of the European Communities DG XVII, Brussels.

J. Axley and R.A. Grot 1990. ‘‘Coupled airflow and thermal analysis for building system simulation by element assembly techniques,’’ in *Proc. Roomvent ’90*, Oslo.

D.P. Bloomfield 1987. ‘‘Work on the development of a model validation methodology,’’ Building Research Establishment report for SERC grant, Garston (UK).

R.J.A. van der Bruggen 1978. ‘‘Energy consumption for heating and cooling in relation to building design,’’ Doctoral dissertation Eindhoven University of Technology (FAGO).

F.M. Butera 1990. ‘‘Conflicts between physics and architecture in solar systems optimization,’’ in *Proc. 2nd European Conf. on Architecture held at Paris, Dec. 1989*, ed. T.C. Steemers and W. Palz, pp. 346-352, Kluwer Academic Publishers, Dordrecht (NL).

CEC 1986. *European passive solar handbook. Basic principles and concepts for passive solar architecture*, Commission of the European Communities DG XVII, Brussels. P. Achard and R. Gicquel (Eds.), Preliminary edition

CEC 1989. ‘‘The PASSYS Project Phase 1. Subgroup Model Validation and Development Final Report 1986-1989,’’ 033-89-PASSYS-MVD-FP-017, Commission of the European Communities, DG XII of Science, Research and Development, Brussels. S. Østergaard Jensen (Ed.)

D.R. Clark 1985. ‘‘HVACSIM+ Building systems and equipment simulation program: reference manual,’’ NBS report NBSIR 84-2996, U.S. Dept. of Commerce, Gaithersburg, MD.

J.A. Clarke 1977. ‘‘Environmental Systems Performance,’’ PhD thesis University of Strathclyde, Glasgow.

J.A. Clarke and I. Forrest 1981. ‘‘Validation of ESP against test houses,’’ University of Strathclyde ABACUS Occasional Paper, Glasgow.

J.A. Clarke 1985. *Energy simulation in building design*, Adam Hilger Ltd, Bristol (UK). (ISBN 0-85274-797-7)

J.A. Clarke and D.J. McLean 1986. ‘‘ESP: A building and plant energy simulation system,’’ ESP Manual version 5 / release 3, University of Strathclyde, Glasgow.

J.A. Clarke, J. Hirsch, F. Winkelmann, F. Buhl, and E. Erdem 1986. ‘‘Planned developments in building energy simulation,’’ in *Proc. 5th Int. Symp. on Use of Computers for Environmental Engineering Related to Buildings*, pp. 482-491, Bath (UK).

J.A. Clarke 1988. ‘‘The Energy Kernel System,’’ *Energy and Buildings*, vol. 10, no. 3, pp. 259-266.

J.A. Clarke, A.D. Irving, S. Lockley, and D. MacRandal 1988. ‘‘An object-orientated approach to building performance modelling,’’ in *Proc. USER 1 working conference at Ostend*, pp. 144-151, Ghent.

J.A. Clarke 1989. ‘‘Building energy simulation: the state-of-the-art,’’ *Solar and Wind Technology*, vol. 6, no. 4, pp. 345-355.

J.A. Clarke, J.H. Rutherford, and D. MacRandal 1989. ‘‘An intelligent front-end for computer-aided building design,’’ in *Proc. 3rd European Simulation Congress, Sept. 1989, Edinburgh*, pp. 362-368, Society for Computer Simulation International, Ghent (B).

J.A. Clarke and T.W. Maver 1991. ‘‘Advanced design tools for energy conscious building design: development and dissemination,’’ *Building and Environment*, vol. 26, no. 1, pp. 25-34.

J.A. Clarke, A. Duffy, B. Lees, J. Lewis, D. MacRandal, and T.W. Maver1991. , *Elicitation of the knowledge underlying design conceptualisation*, Glasgow.

J.A. Clarke, J.W. Hand, P. Strachan, J.L.M. Hensen, and C.E.E. Pernot 1991. ‘‘ESP^{R} A building and plant energy simulation research environment,’’ Energy Simulation Research Unit, ESRU Manual U91/2, University of Strathclyde, Glasgow.

J.P. Cockroft 1979. ‘‘Heat transfer and air flow in buildings,’’ PhD thesis University of Glasgow.

A-M. Dubois 1990. ‘‘Presentation of CIBAO: a new approach for integrated computer-aided design systems for the building activities,’’ in *Proc. 2nd European Conf. On Architecture, Paris*, pp. 507-510, Dordrecht.

J.S. Gero 1983. ‘‘Computer-aided architectural design - past, present and future,’’ *Architectural Science Review*, vol. 26, no. 3, pp. 2-5.

R. Gicquel and C. Cools 1986. *Programme PASSYS: status report*, Ecole des Mines, Sophia Antipolis (F).

A. Hartman 1988. ‘‘Plus ca change ..... "Comment" from the Tulane computing services newsletter,’’ in *Articles database of CCNEWS, the Electronic Forum for Campus Computing Newsletter Editors*, EDUCOM, BITNET.

P.J.J. Hoen 1987. ‘‘Energy consumption and indoor environment in residences,’’ Doctoral dissertation Eindhoven University of Technology (FAGO).

IEA 1980. ‘‘Comparison of load determination methodologies for building analysis programmes,’’ Energy conservation in buildings & community systems programme; Annex I, International Energy Agency. Distribution: Air Infiltration and Ventilation Centre, Coventry (UK)

IEA 1984. ‘‘Glasgow commercial building monitoring project; final report,’’ Energy conservation in buildings & community systems programme; Annex IV, International Energy Agency. Operating agent: Building Research Establishment, Garston (UK)

R. Kohonen and T. Ojanen 1985. ‘‘Coupled convection and conduction in two dimensional building structures,’’ in *Proc. 4th Int. Conf. On Numerical Methods in Thermal Problems Part I*, Swansea.

J.T.H. Lammers 1978. ‘‘Human factors, energy conservation and design practice,’’ Doctoral dissertation Eindhoven University of Technology (FAGO).

J. Lebrun and G. Liebecq 1988. ‘‘System Simulation Synthesis Report,’’ Energy conservation in buildings & community systems programme; Final report Annex X, International Energy Agency. Operating agent: University of Liège, J. Lebrun, report AN10 881020-RF

D. MacRandal 1988. ‘‘Some trends in computing: the implications for simulation,’’ *Energy and Buildings*, vol. 10, no. 3, pp. 249-258.

T.W. Maver and J. Ellis 1982. ‘‘Implementation of an energy model within a multidisciplinary practice,’’ in *Proceedings CAD82*.

D.J. McLean 1982. ‘‘The simulation of solar energy systems,’’ PhD thesis University of Strathclyde, Glasgow.

D.J. McLean 1986. ‘‘Simultaneous dynamic simulation of air flow and energy in buildings,’’ in *Proc. 5th Int. Symp. on Use of Computers for Environmental Engineering Related to Buildings*, pp. 181-190, Bath (UK).

M.A.P. Murray 1984. ‘‘Component based performance simulation of HVAC systems,’’ PhD thesis Loughborough University of Technology.

A. Radford 1991. ‘‘Editorial: developments in computer-aided design,’’ *Building and Environment*, vol. 26, 1, pp. 25-34.

J. Rooney and P. Steadman 1987. *Principles of computer-aided design*, Pitman, London. (Open University set book)

SEL 1988. ‘‘TRNSYS, a transient system simulation program,’’ Engineering Experiment Station Report 38-12, University of Wisconsin-Madison, Solar Energy Laboratory, Madison, WI. Manual for version 12.2 and later

D. Tang 1985. ‘‘Modelling of heating and air-conditioning system,’’ PhD thesis University of Strathclyde, Glasgow.

T.J. Wiltshire and A.J. Wright 1988. ‘‘Advances in building energy simulation in the UK - the Science and Engineering Research Council’s programme,’’ *Energy and Buildings*, vol. 10, no. 3, pp. 175-183.

F. Winkelmann 1988. ‘‘Advances in building energy simulation in North America,’’ *Energy and Buildings*, vol. 10, no. 3, pp. 161-173.

CHAPTER FOUR

FLUID FLOW SIMULATION

4.1. INTRODUCTION

Fluid flow can be encountered in several areas of combined building and plant simulation:
- air flow through cracks and various openings in the building envelop and interior walls (infiltration and natural ventilation)
- flow of air through the distribution network designed for satisfying thermal comfort and air quality demands
- flow of heating/cooling fluids within the plant system network
- convective fluid flow inside interior spaces or plant components

Knowledge on the magnitude of such flows is necessary for heat transfer analysis including load and energy calculations, thermal comfort assessment including plant control analysis and for contaminant and moisture dispersal analysis including ventilation and smoke control calculations. Although fluid flow is thus an important aspect of combined building and plant simulation, its analysis has considerably lagged behind the modelling of other building features. The main reasons for this seem to be the lack of sufficient data and computational difficulties.
Recently more emphasis has been put on fluid flow simulation. Two main areas of approach and interest can be distinguished:

- computational fluid dynamics (CFD) modelling, which is based on the solution of conservation equations for mass, momentum and thermal energy on all grid points of a two or three dimensional grid inside or around the object under investigation (flow field method). A well known example of a CFD-model is PHOENICS (Spalding 1981). In theory it is possible to simulate any thermo-fluid phenomenon using CFD modelling. In practice there are however a number of limitations of which the amount of necessary computing resources is only one (Chen 1988). This means that CFD models are primarily used for steady-state problems. Examples in the field of building energy simulation are the prediction of temperature and velocity fields inside large or technically complex enclosures like atria and television studios (Markatos 1984) and the prediction of the pressure field around a building (Häggkvist et al. 1989).

- mass balance/flow network approach (zonal method). This approach is based on the assumption that a building and or plant can be considered as being composed of a number of zones or nodes (e.g. rooms, plant components) which are linked by connections (e.g. openings, cracks, ducts, pipes). Furthermore it is assumed that there is a simple nonlinear relationship between the flow through a connection and the pressure difference across it. Conservation of mass for the flows into and out of each node leads to a set of simultaneous nonlinear equations which has to be solved.
  The number of nodes/equations - and subsequently the calculation times - involved is much smaller than in the case of CFD modelling. Given our contemporary computing power the network approach can already be used in combined transient building and plant

modelling.

The latter technique can be used equally well for building side air flow modelling as well as for plant system fluid flow modelling or for a combined fluid flow modelling problem. It is the network approach then which is used in the newly developed fluid mass flow modelling module of *ESP*^{R}.
The network approach also facilitates a more or less independent development of flow component models, excitation models, and solution method. The computer program modules obviously mirror the theoretical. Input and output modules were added to create a useful simulation tool. The various models provide a toolkit for the analyst to consider a practically infinite variety of building and plant configurations. In this way, a general fluid mass flow network simulation computer program, was developed from earlier air flow analysis programs, *air* (Clarke and McLean 1986) and AIRNET (Walton 1989a, 1989b). The stand-alone version of this module is called *mfs*, and allows independent fluid flow studies of building and/or plant configurations which are predominantly pressure driven. *mfs* does include buoyancy effects, but against fixed nodal temperatures.
The core of *mfs* is also incorporated in *ESP*^{R}'s main building and plant energy simulation module *bps*. This enables *bps* to pursue mass flow simulation in tandem with the energy balance computations.

Modelling of fluid flow by the network approach requires:
- translation of the real world problem into a node and connections scheme
- determination of boundary conditions
- mathematical and numerical characterisation of the various fluid flow vs. pressure difference relationships
- solution of the resulting set of simultaneous (non-linear) equations

mfs is primarily concerned with the latter two aspects.

The computer program *mfs* is menu-driven in a fashion similar to the other *ESP*^{R} modules. It is written in FORTRAN 77 for usage in a UNIX environment (more specifically it is compiled with *f77* to run on a Sun workstation). Porting to other machine architectures and/or operating systems should not be too difficult. The program was set up in a highly modular way to facilitate easy maintenance and expansion.
Section 4.2. describes how a fluid flow problem may be described in terms of a mass flow network. Section 4.3. elaborates the calculation process, and in Section 4.4., the available fluid flow component types are described in detail. How *mfs* is incorporated in other *ESP*^{R} modules, is indicated in section 4.5.

4.2. PROBLEM DESCRIPTION

To apply the fluid flow problem to be considered to the simulation system, the user has to define the fluid flow network. Readers how are not yet interested in how this problem definition takes place, might want to skip the current section and continue with the next.
The nodes of a fluid flow network may represent rooms, connection points in a duct or in a pipe network, the outdoor environment, etc. Fluid flow components correspond to discrete fluid flow passages such as doorways, construction cracks, ducts, pipes, fans, pumps, etc. Figure 4.1 is a sketch of a part of a building consisting of two rooms, some connection between the rooms, a radiator heating system connected to one zone and an air heating system connected to the other zone. In this case the building and plant configuration contains at least two fluid flow networks (one for the air and one for the water). One possibility with

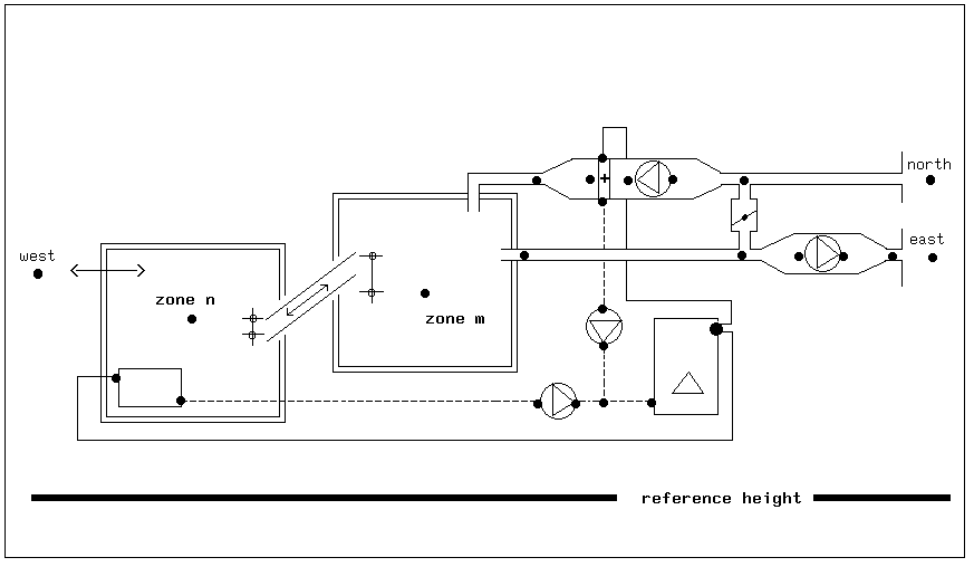

Figure 4.1 Schematic example building and plant configuration; the dots indicate a possibility for translation into a nodal scheme for fluid flow network solution

respect to the translation of this configuration into a nodal scheme is indicated by the dots.

A fluid flow network may consist of several sub-networks and is not restricted to one type of fluid. However, all nodes and components within a sub-network must be of the same fluid type.

Node data

Nodes are characterised by a name/identifier, fluid type, node type, height above datum, temperature, and up to two supplementary data items. At present only two fluid types are supported: air and water. This can easily be expanded. The possibilities with respect to node type are summarized in Table 4.1.

Table 4.1 Fluid flow network node types

	Type	Supplementary data
0	Internal; unknown pressure	None
1	Internal; known pressure	total pressure (Pa)
2	Boundary; known pressure	1) total pressure (Pa) 2) fluid temperature flag, indicating 0 = node temperature is constant 1 = node temperature equals outside air temperature
3	Boundary; wind pressure*	1) wind pressure coefficients index 2) surface azimuth (° clockwise from North)
* only available when fluid type is air		

The nodes of the network represent either internal or boundary pressures. The difference is that only internal nodes are subjected to the mass balance approach. Note that in the present context ’internal’ is not necessary equivalent to ’inside’ (say inside a building, ductwork, etc.) nor does ’boundary’ need to be equivalent to ’outside’! Usually the pressure at an internal node is unknown. However, in some cases it may be a known parameter (e.g. in case of an expansion vessel in a hydronic radiator system).† Obviously, pressures at boundary nodes must always be known; wind induced pressure is a special case. The defined network is then arrived at by connecting a number of internal and boundary nodes by branches which represent some resistance to inter-zone or intra-plant fluid flow. For the case of use by *bps*, the established fluid flow network need not match the multi-zone and plant component network referenced in the system configuration file to define the building and/or plant for energy simulation. At the time of system configuration file construction, it is necessary, if a fluid flow simulation is required, to define the mapping between building zones and plant components on the one hand and nodes defined as part of the fluid flow network on the other hand. This allows some flexibility in problem description since the energy and fluid flow systems are not constrained to the same boundary conditions. For example, it is possible to generate a partial building and plant model, of 5 building zones and 10 plant components say, for energy simulation purposes, and then to deploy a greater number of nodes, say 50, to represent an air flow network which accurately expresses the leakage distribution of the entire building and flow characteristics of the mechanical ventilation system. Some of the fluid flow nodes - 15 or less - will correspond to the building zones or plant components, the others are merely present to enhance the fluid flow predictions. Of course the schemes can be exactly matched if required. Within *bps* only the temperatures of matched zones or plant components will vary with time. All other nodes in the fluid flow network will retain, throughout a simulation, the temperatures assigned in the fluid flow network description file. As a special feature, it is possible to define the temperature of a node to be equal to the temperature of some other node in the network. By this mechanism, it is possible to map more then one fluid flow node to the same building or plant node. This feature is specifically useful in case of fluid flow nodes incorporated to handle flow controllers.

Each node is assigned a node reference height. This is used as part of the buoyancy calculations (which are dealt with later). The reference height defines the mean height of the associated building zone or plant component. The node reference height may be expressed relative to any arbitrary datum level, as long as this datum level is the same for all nodes in the network.

For each boundary node with wind induced pressure, a reference must be made to an appropriate pressure coefficient set as held in a pressure coefficients file. Any number of sets may reside in this file, with reference codes given simply as 1, 2, 3 and so on. It is the pressure coefficient, appropriate to the wind direction prevailing at any time, that dictates, as a function of the prevailing wind speed at roof height, the generated boundary (i.e. external surface) pressure. For wind induced pressure nodes, the azimuth is required to define the zone’s orientation relative to the building configuration. The required response is in degrees from north, clockwise positive, so that north is represented by 0, east by 90 and south by 180. In the case of an ‘up’ or ‘down’ zone, the azimuth has no meaning and may be set to zero.

---

† an interesting possibility is that this node type may be used in an air infiltration problem to mimic a pressurization test. In this way it is easy to compare the overall leakage characteristic with measured data

More information on the calculation of wind induced pressure and the concept of **wind speed reduction factor** can be found in Section 4.3.1.

Flow component data

Table 4.2 Fluid flow component types

Code	Type
10	Power law volume flow resistance element
15	Power law mass flow resistance element
17	Power law mass flow resistance element (diff. def.)
20	Quadratic law volume flow resistance element
25	Quadratic law mass flow resistance element
30	Constant volume flow rate element
35	Constant mass flow rate element
40	Common orifice flow element
50	Laminar pipe flow element
110	Specific air flow opening
120	Specific air flow crack
130	Specific air flow door
210	General flow conduit (duct or pipe)
220	Conduit ending in converging 3-leg junction & C = f(q/qc)
230	Conduit starting in diverging 3-leg junction & C = f(q/qc)
240	Conduit ending in converging 4-leg junction & C = f(q/qc)
250	Conduit starting in diverging 4-leg junction & C = f(q/qc)
310	General flow inducer (fan or pump)
410	General flow corrector (damper or valve)
420	Flow corrector with polynomial local loss factor
450	Ideal (frictionless) flow controller

A flow component is characterised by a name/identifier, type code (indicating duct/pipe, pump, crack, doorway, etc.), number of supplementary data items and number of additional linkage data items associated with that type of component, optionally a comment and the associated supplementary data. The comment is not read on input; it is supplied by *mfs*. When a certain flow component (including the associated supplementary data) is repeatedly present in the network, it only has to be defined once. The currently supported fluid flow component types are summarized in Table 4.2. Detailed information can be found in Section 4.4.

Connections data

The connections data defines the flow network. Each connection description consists of: (1) the name of the node on the positive side of the connection, (2) the height of the positive linkage point relative to the node on the positive side, (3) the name of the node on the negative side of the connection, (4) the height of the negative linkage point relative to the node on the negative side, (5) the name of the connecting flow component, and (6) up to two supplementary node names in case this information is needed for the flow component in question. More then one connection may exist between two nodes. The concept of a connection having a positive side and a negative side is used to keep track of the direction of fluid flow; i.e. the flow is positive when from positive side towards negative side. So, a connection joining node A to B is different from one joining B to A. For most fluid flow component types, uni-directional fluid flow will result (in either direction). However, some component types may show bi-directional fluid movement through a connection; e.g. in case of a doorway where due to the action of small density variations over the height, bi-directional flow may exist.

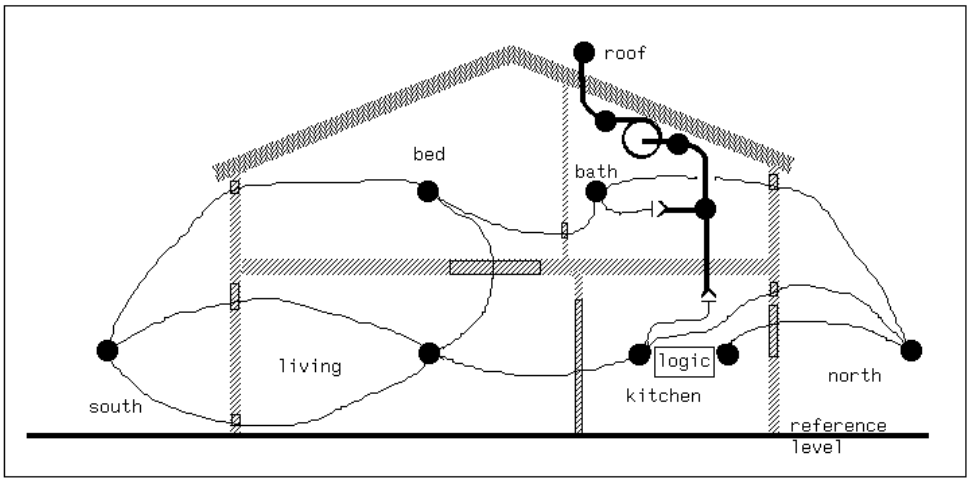

Figure 4.2 Diagrammatic representation of the fluid flow network described by Table 4.3.

As an example the description file of a fluid flow network - which is schematically drawn in Figure 4.2 - is shown in Table 4.3. It can be seen that the first record holds the number of nodes, components and connections respectively. It also holds a parameter called wind reduction factor. This factor is explained in the next section. It should be noted that all data-reads from this file are UNFORMATTED and that the comment records and the component description comment is not read by *mfs*. This means that if someone wants to alter the file with some text editor, there is no need to be concerned about formats. As may be seen from the table, *mfs* writes to the file in a FORMATTED fashion and supplies some comments.

4.3. CALCULATION PROCESS

With respect to fluid flow simulation, here we assume one-dimensional steady flow in a building and/or plant configuration which is subjected to certain boundary conditions regarding pressures and/or flows. This involves calculation of fluid flow through the connections of a nodal network. The nodes of the network represent either internal or boundary pressures; the connections represent fluid flow paths.
Information on potential fluid flows is given in terms of fluid type, node descriptions, flow component types, interconnections and boundary conditions. As elaborated in Section 4.2, in this way a nodal network (or perhaps several decoupled sub-networks) of connecting resistances is constructed. This may then be attached, at its boundaries, to known pressures or to pressure coefficient sets which represent the relationship between free-stream wind vectors and the zone surface pressures to result. This is elaborated in Section 4.3.1. The calculation of buoyancy driven flow (or stack effect) is described in Section 4.3.2. The subject of Section 4.3.3. is the simultaneous network solution, and finally Section 4.3.4. described how the simulation results are handled.

4.3.1. Wind Pressure

To be able to determine wind induced boundary pressures it is necessary to map the "free stream" wind velocity (as read from the climate file) onto the surface as a function of the wind’s vertical velocity profile and the sheltering effect of remote and local facade obstructions. The latter effect is usually accounted for by a dimensionless pressure

Table 4.3 Example of a fluid flow network description file

11	12	15	0.438	(nodes, components, connections, wind reduction)			
Node	**Fld.**	**Type**	**Height**	**Temperature**	**Data_1**	**Data_2**	
living	1	0	1.5000	21.000	0.	0.	
kitchen	1	0	1.5000	20.800	0.	0.	
w_ctl	1	0	1.5000	kitchen	0.	0.	
bed	1	0	4.5000	21.000	0.	0.	
bath	1	0	4.5000	21.000	0.	0.	
south	1	3	1.5000	0.	18.000	180.00	
north	1	3	1.5000	0.	18.000	0.	
roof	1	3	7.0000	0.	20.000	0.	
t_junc	1	0	5.0000	bath	0.	0.	
fan_in	1	0	6.0000	bath	0.	0.	
fan_ou	1	0	6.0000	bath	0.	0.	
Comp	**Type**	**C+**	**L+**	**Description**			
crack	120	3	0	Specific air flow crack	m = rho.f(W,L,dP)		
1.00	3.000E-03	5.000					
stairs	110	2	0	Specific air flow opening	m = rho.f(A,dP)		
1.000	1.000						
door	130	5	0	Specific air flow door	m = rho.f(W,H,dP)		
1.000	2.000	2.100	1.500	0.920			
window	40	3	0	Common orifice vol. flow rate comp. m = rho.f(Cd,A,rho,dP)			
1.000	1.000	0.650					
grl_ex	10	3	0	Power law vol. flow component	m = rho.a.dP^b		
1.000	0.020	0.700					
grl_in	10	3	0	Power law vol. flow component	m = rho.a.dP^b		
1.000	5.000	0.500					
fan	310	7	0	General flow inducer component	dP= a0+Sai(m/rho)^i		
1.000	0.	1.000E-01	125.000	0.	-12500.0	0.	
duct_1	220	13	1	Conduit ending in converging 3-leg junction & Ccp = f(q/qc)			
1.000	0.125	1.227E-02	2.500	1.500E-04	18.000	7.853E-03	
1.000E-02	0.	0.	1.500	-0.970	0.		
duct_2	220	13	1	Conduit ending in converging 3-leg junction & Ccp = f(q/qc)			
1.000	0.1250	1.227E-02	2.000	1.500E-04	36.00	7.853E-03	
-0.8000	2.970	-1.090	0.	0.	0.		
duct_3	210	6	0	General flow conduit component	m = rho.f(D,A,L,k,SCi)		
1.000	0.125	1.227E-02	1.500	1.500E-04	0.2500		
duct_4	210	6	0	General flow conduit component	m = rho.f(D,A,L,k,SCi)		
1.000	0.1250	1.227E-02	2.000	1.500E-04	2.900		
w_ctl	450	8	2	Ideal (frictionless) open/shut flow controller			
1.000	7.000	16.000	20.000	0.	2.000	20.000	0.
+Node	**dHght**	**-Node**	**dHght**	**Comp**	**Snod1**	**Snod2**	
living	0.000	kitche	0.000	door			
living	1.500	bed	-1.500	stairs			
bed	-1.000	bath	-1.000	grl_in			
south	-1.300	living	-1.300	crack			
south	1.300	living	1.300	grl_ex			
south	3.500	bed	0.500	grl_ex			
bath	0.500	north	3.500	crack			
kitche	1.200	north	1.200	crack			
kitche	0.000	w_ctl	0.000	w_ctl	kitche	north	
w_ctl	0.500	north	0.500	window			
kitche	0.500	t_junc	0.000	duct_1	bath		
bath	0.500	t_junc	0.000	duct_2	kitche		
t_junc	0.000	fan_in	0.000	duct_3			
fan_in	0.000	fan_ou	0.000	fan			
fan_ou	0.000	roof	0.000	duct_4			

coefficient:

$$C_{p,i,d} = \frac{P_i}{1/2\rho U_{rd}{}^2} \quad (-) \tag{4.1}$$

where $C_{p,i,d}$ is the pressure coefficient for a surface location i corresponding to wind from

direction d, P_i is the surface pressure due to wind (Pa), ρ is the air density (kg/m^3) and U_{rd} is the wind speed (m/s) at some reference level r and from direction d (expressed relative to the external surface normal vector). Since the strength of the wind close to the earth's surface is influenced by the roughness of the underlying terrain and the height above ground, a reference level for wind speed must be specified for use in the wind pressure calculation. The wind speed reference level is usually equal to the building height. The ratio between the local wind speed and the wind speed as read from the climate file, is called the wind speed reduction factor. This reduction factor accounts for any difference between measurement height and building height and for intervening terrain roughness. The reduction factor can be evaluated from some assumed wind speed profile. The wind speed profile depends on (upstream) terrain roughness and the vertical stability of the atmospheric boundary layer. The stability depends on the vertical heat flow through this boundary layer. Partly due to lack of information, in building engineering one usually assumes that there is no vertical heat flow, ie. a neutral atmospheric boundary layer.
Besides direct numerical input, *mfs* offers several user selectable wind profiles for evaluation of the wind speed reduction factor:

- power law wind profile (Liddament 1986); in this case the actual wind speed profile is approximated by an empirical exponential expression in which the coefficient and exponent account for terrain roughness differences between local site and measurement site:

$$\frac{U_l}{U_{10}} = K\ z_l{}^a \quad (-) \tag{4.2}$$

  where U_l is the local wind speed at a height z_l m above the ground (m/s), U_{10} the wind speed measured in open countryside (m/s) at a standard height of 10 m, and K, a are terrain dependent constants (see Table 4.4).

- logarithmic wind profile (Simiu & Scanlan 1986); it was found - both theoretically and experimental - that the wind speed is a logarithmic function of height:

$$\frac{U_l}{U_m} = \frac{U_{*,l}}{U_{*,m}} \left(\ln \frac{z_l - d_l}{z_{0,l}} / \ln \frac{z_m - d_m}{z_{0,m}} \right) \quad (-) \tag{4.3}$$

  where

$$\frac{U_{*,l}}{U_{*,m}} \approx \left(\frac{z_{0,l}}{z_{0,m}} \right)^{0.1} \quad (-) \tag{4.4}$$

  where U_m is the wind speed as measured at the meteo site (m/s) at a height of z_m m above the ground, U_* is the atmospheric friction speed (m/s), z_0 is the terrain dependent roughness length (m), and d is the terrain dependent displacement length (m) (see Table 4.4).

- LBL model wind profile (also reported in Liddament 1986); for reasons of completeness the Lawrence Berkeley Laboratory (LBL) air infiltration model wind profile - basically a power law profile - is also available:

$$\frac{U_l}{U_m} = \frac{\alpha\,(z/10)^{\gamma}}{\alpha_m\,(z_m/10)^{\gamma_m}} \quad (-) \tag{4.5}$$

  where α, γ are terrain dependent constants (see Table 4.4).

Table 4.4 Typical values for terrain dependent parameters (h = building height; source Liddament 1986)

Terrain	K	a	z_0	d	α	γ
Open flat country	0.68	0.17	0.03	0.0	1.00	0.15
Country with scattered wind breaks	0.52	0.20	0.1	0.0		
Rural			0.5	0.7 h	0.85	0.20
Urban	0.35	0.25	1.0	0.8 h	0.67	0.25
City	0.21	0.33	> 2.0	0.8 h	0.47	0.35

Compared with both the power law profile and the LBL wind profile, the logarithmic wind profile is to be preferred because it is based on physical laws rather than on a empirical formulation. It should be noted that all the wind profiles above are actually only valid for heights over $(20 * z_0 + d)$ and lower than $60 \cdots 100\ m$; ie. for a building height of 10 m in a rural area, the profiles are only valid for heights above $17\ m$, in an urban area above $28\ m$ and in a city area above $50\ m$. The layer below $(20 * z_0 + d)$ is often referred to as the urban canopy. Here the wind speed and direction is strongly influenced by individual obstacles, and can only be predicted through wind tunnel experiments or simulation with a CFD-model. If these are not available, it is advised to be **very cautious**, and to use - depending on the problem on hand - a high or low estimate of the wind speed reduction factor. For example, in case of an "energy consumption and infiltration problem" it is safer to use a high estimate of the wind speed reduction factor (eg. wind speed evaluated at a height of $(20 * z_0 + d)$). In case of for example an "air quality or overheating and ventilation problem" it is probably safer to use a low estimate (eg. wind speed evaluated at the actual building height).
To give a numerical example: assume a building with a height of $7.5\ m$ which is located in an urban area (say $z_0 = 1.0\ m$ and $d = 6\ m$; ie. the thickness of the urban canopy is approximately $26\ m$), and that the wind speed was measured at a height of $10\ m$ in an open flat country. If we make lower and upper estimates as indicated above, then the following local wind speed reduction factors at building height will result:

power law:	0.58	...	0.79	(-)
logarithmic law:	0.10	...	0.73	(-)
LBL profile:	0.62	...	0.85	(-)

The pressure coefficient, C_p , is an emperically derived parameter which is a function of the pattern of flow around the building. It varies according to wind direction and position of the building surface. It is also significantly affected by neighbouring obstructions with the result that similar buildings subjected to different surroundings may be expected to exhibit markedly different pressure coefficient patterns. Accurate evaluation of this parameter is one of the most difficult aspects of air infiltration modelling and, as yet, is not possible by theoretical means alone. For low buildings of up to typically 3 storeys, pressure coefficients may be expressed as an average value for each face of the building and for each compass direction. Typical design data based on published measurement results is presented in (Liddament 1986) and is available within ESP^R through a data file (**pressc.db1**) holding a collection of standard pressure coefficients sets. These sets can be used (with care) for low-rise buildings.

4.3.2. Buoyancy Driven Flow

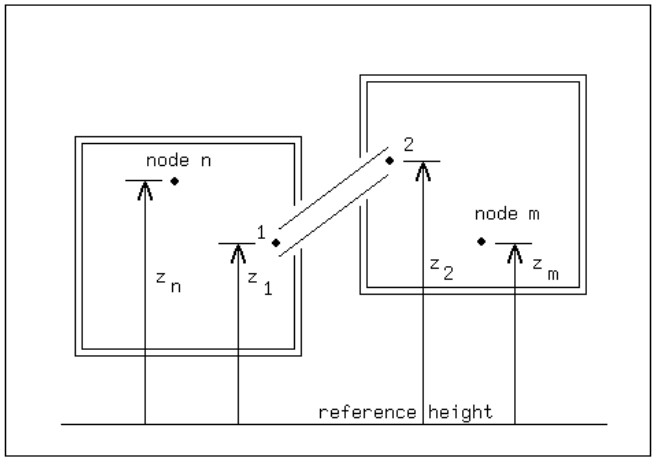

Figure 4.3 Schematic 2-volume configuration

The calculation of buoyancy driven flow (or stack effect) in *mfs* is similar to the approach by Walton (1989a, 1989b). This can be explained with Figure 4.3 which shows two volumes (e.g. a room) connected by some fluid flow component. It is assumed that each volume can be characterised by a single temperature and a single static pressure at some height relative to a common data plane. The inlet and outlet of the connecting component are at different heights relative to each other and relative to the nodes which represent the volumes. This complex arrangement is to show the entire calculation. Analysis of fluid flow through a component *i* is based on Bernoulli's equation for one-dimensional steady flow of an incompressible Newtonian fluid including a loss term:

$$\Delta P_i = (p_1 + \rho {V_1}^2/2) - (p_2 + \rho {V_2}^2/2) + \rho g(z_1 - z_2) \quad (Pa) \tag{4.6}$$

where ΔP_i is the sum of all friction and dynamic losses (Pa), p_1, p_2 are entry and exit static pressures (Pa), V_1, V_2 are entry and exit velocities (m/s), ρ is the density of the fluid flowing through the component (kg/m^3), g is the acceleration of gravity $(9.81\ m/s^2)$, and z_1, z_2 are entry and exit elevations (m).
ρ may be either ρ_n or ρ_m depending on the direction of flow. In *mfs* ρ is based on the most recently computed flow direction (this may cause some inaccuracy in case of alternating flow directions). The equation above defines a sign convention for the direction of flow: positive flow is from point 1 to point 2 (i.e. from node n to node m).
The equation can be simplified for use in the fluid flow algorithm by defining several related terms. Dynamic pressures are the $\rho V^2/2$ terms, and total pressure is defined to be the sum of static pressure and dynamic pressure; i.e. $P = p + \rho V^2/2$. If nodes n and m represent large volumes (e.g. a room), the dynamic pressures are effectively zero. If the nodes represent some point in a duct or pipe network, there will be a positive dynamic pressure. The pressures at the inlet and outlet of the flow component can be related to the node pressures by the hydrostatic law:

$$P_1 = P_n + \rho_n g(z_n - z_1) = P_n - \rho_n g h_1 \quad (Pa) \quad \text{where } h_1 = z_1 - z_n \quad (m) \tag{4.7}$$

and

$$P_2 = P_m + \rho_m g(z_m - z_2) = P_m - \rho_m g h_2 \quad (Pa) \quad \text{where } h_2 = z_2 - z_m \quad (m) \tag{4.8}$$

The relative heights, h_1 and h_2, are a convenient way of expressing the flow component inlet and outlet heights. For example, it is quite common for flow components in the building fabric to only differ with respect to inlet and outlet heights relative to the zone heights. On the other hand, if the flow component is part of a duct or pipe network, the relative heights will be zero. Bernoulli's equation can thus be reduced to:

$$\Delta P_i = P_n - P_m + \rho g(z_n + h_1 - z_m - h_2) - \rho_n g h_1 + \rho_m g h_2 \quad (Pa) \tag{4.9}$$

The terms $[\rho g(z_n + h_1 - z_m - h_2) - \rho_n g h_1 + \rho_m g h_2]$ can be collectively called the stack pressure, PS_i, acting on component i. For flow in the positive direction (ie $\rho = \rho_n$):

$$PS_i = \rho_n g(z_n - z_m) + h_2 g(\rho_m - \rho_n) \quad (Pa) \tag{4.10}$$

and for flow in the negative direction (ie $\rho = \rho_m$):

$$PS_i = \rho_m g(z_n - z_m) + h_1 g(\rho_m - \rho_n) \quad (Pa) \tag{4.11}$$

During tests it was found that this way of calculating the stack pressure, in some rare cases may lead to instable results when successive time steps are compared. When this was observed, the following conditions were present:

- an extensive network containing several internal nodes with "long" flow paths (ie. involving many other internal nodes) to boundary nodes
+ having connections which are very sensitive to small pressure disturbances (e.g. large openings)
+ in which the pressure differences primarily depend on stack effects; ie. buoyancy forces
+ and where the boundary pressures during successive time steps do not change at all or just change a little. If it were not for this condition (of which the user must be aware, by the way) the instability of the results would be hidden to the user and would not be perceived as a problem at all.

An actual example in which these conditions were met, was: a large mass flow network with relatively few boundary nodes representing building zones and air flow paths in a newly developed extensive city-centre mall including social facilities (Wisse & Pernot 1990; Pernot & Hensen 1990). The majority of flow components were either huge openings or large air flow doors. The mall consisted of several floor levels, each with a different air temperature, and the building was located in a dense urban area.

To be better equipped to handle such cases *mfs* offers an alternative stack pressure calculation model, which may be chosen by altering the user definable parameter: IPSMOD. In this alternative approach the stack pressure calculation is based on the average fluid density at the connected nodes:

$$PS_i = (g/2)\left[(\rho_n + \rho_m)(z_n - z_m) + (\rho_m - \rho_n)(h_1 + h_2)\right] \quad (Pa) \tag{4.12}$$

In case of a boundary node j with wind induced pressure, i.e. a outside surface air node, it is also necessary to make allowance for stack pressure effects. In *mfs* this is realised by calculating that node's total pressure from:

$$P_j = C_{p,j,d} 1/2\, \rho_o U_{rd}{}^2 - \rho_o g h_j \quad (Pa) \tag{4.13}$$

where P_j is the total pressure of boundary node j (Pa), $C_{p,j,d}$ is the pressure coefficient (-) for a surface location j corresponding to wind from direction d, U_{rd} is the wind speed (m/s)

at some reference level r and from direction d, ρ_o is the density of the outdoor air (kg/m^3), g is the acceleration of gravity ($9.81\ m/s^2$), and h_j is the height of node j (m).
Note that this effectively means that the outside air static pressure at height $h = 0$ is assumed implicitly to be equal zero.

4.3.3. Simultaneous Fluid Flow Network Solution

Each fluid flow component, i, relates the fluid mass flow rate, $\dot{m}_i$, through the component to the pressure drop, ΔP_i, across it. Conservation of mass at each internal node is equivalent to the mathematical statement that the sum of the mass flows equal zero at such a node. The flows are related nonlinearly to the pressures at the nodes (see Section 4.3.) thus requiring the iterative processing of a set of simultaneous nonlinear equations which are subjected to a given set of boundary conditions. The technique used by *mfs* to achieve the solution is to assign an arbitrary pressure to each internal node. The flow along each connection in the network is then determined from the appropriate equation as a function of the then prevailing pressure differences. The internal node mass flow residuals are then computed from:

$$R_i = \sum_{k=1}^{K_{i,i}} \dot{m}_k \quad (kg/s) \tag{4.14}$$

where R_i is node-i's mass flow residual for current iteration (kg/s), $\dot{m}_k$ is the mass flow rate along kth connection to node i (kg/s), and $K_{i,i}$ is the total number of connections linked to node i.
The nodal pressures are then iteratively corrected and the mass balance at each internal node is re-evaluated until some convergence criterion is met. The method which is used in *mfs*, is similar to the approach as suggested by Walton (1988a, 1989b). This approach was implemented and tested in an earlier version of ESP^R and shown to result in considerable speed improvements as evidenced in Table 4.5 (Clarke & Hensen 1988).

Table 4.5 Bench-mark results. All runs were performed on a SUN 3/50 and correspond to a one day (24 hour) simulation

Problem	**Original Solver**		**New Solver**		**24 hr**	**CPU**
	CPU Seconds	**Iterations** 1st hr - 24 hrs	**CPU** Seconds	**Iterations** 1st hr - 24 hrs	**Iteration** Ratio	**Ratio**
1. atria	3087	6363 - 152117	55	137 - 522	291	56
2. house 1	377	374 - 27863	17	29 - 459	60	21
3. house 2	48	146 - 2510	23.2	11 - 105	23	2
4. 2 zone	9	309 - 2376	3.6	16 - 287	8	2
5. 3 zone	3	27 - 358	2.5	4 - 90	3	1
6. Trombe	2168	14009 - 122754	50.2	29 - 474	258	43
		1st hr - 2nd hr		**1st hr - 2nd hr**	**1st - 2nd hr**	
7. large		13270 - 25318		24 - 1	552 - 25318	

It is based on a Newton-Raphson technique applied to the whole set of simultaneous nonlinear equations (see e.g. Conte and De Boor 1972). With this technique, a new estimate of the vector of all node pressures, **P**, is computed from the current estimate of pressures, $\mathbf{P}^*$, by:

$$\mathbf{P} = \mathbf{P}^* - \mathbf{C} \tag{4.15}$$

where the node pressure correction vector, **C**, is determined on the basis of a simultaneous solution of a Jacobian matrix which represents the nodal pressure corrections in terms of all branch flow partial derivatives. The pressure corrections vector **C** is given by:

$$\mathbf{C} = \mathbf{R}\ \mathbf{J}^{-1} \tag{4.16}$$

where **R** is the vector of nodal mass flow residuals and $\mathbf{J}^{-1}$ is the inverse of the square (i.e. N*N for a network of N nodes) Jacobian matrix whose diagonal elements are given by:

$$J_{n,n} = \sum_{k=1}^{K_{n,n}} \left(\frac{\partial \dot{m}}{\partial \Delta P} \right)_k \quad [kg/\,s\,Pa] \tag{4.17}$$

where $K_{n,n}$ is the total number of connections linked to node n, and ΔP_k is the pressure difference across the kth link.
The off-diagonal elements of **J** are given by:

$$J_{n,m} = \sum_{k=1}^{K_{n,m}} -\left(\frac{\partial \dot{m}}{\partial \Delta P} \right)_k \quad [kg/\,s\,Pa] \tag{4.18}$$

where $K_{n,m}$ is the number of connections between node n and node m. This means that - for internal nodes - the summation of the terms comprising each row of the Jacobian matrix are identically zero.

In the equations above, $\dot{m}_k$ and $[\partial \dot{m} / \partial \Delta P]_k$ are evaluated using the current estimate of pressure **P**. *mfs* contains a separate subroutine for each type of fluid flow component which returns the mass flow rate and the partial derivative for a given pressure difference input (see Section 4.4). For those flow component types where an analytical expression for the partial derivative is not known, a numerical approximation is used, ie.:

$$\frac{\partial \dot{m}}{\partial \Delta P} \approx \frac{\dot{m} - \dot{m}^*}{\Delta P - \Delta P^*} \quad [kg/\,s\,Pa] \tag{4.19}$$

where * denotes the value in the previous iteration step.

mfs currently supports two options with respect to solution of the matrix equation **J C** = **R** for the unknown pressure correction vector **C**:

- Gaussian elimination with back substitution; an efficient matrix solver is used to forward reduce the matrix **J** halfway, to a matrix whose components on the diagonal and above remain nontrivial. The solution vector **C** is then generated through back substitution of the known right hand side vector **R**.
- LU decomposition with implicit pivoting (also known as Crout's method with partial pivoting) and scaling; the implementation in use by *mfs* originates from (Press et al. 1986). In this case the matrix **J** is decomposed in a *lower triangular* matrix **L** and an *upper triangular* matrix **U**, such that **L U** = **J**. This decomposition is used to solve the linear set:

  $$\mathbf{J}\ \mathbf{C} = (\mathbf{L}\ \mathbf{U})\ \mathbf{C} = \mathbf{L}\ (\mathbf{U}\ \mathbf{C}) = \mathbf{R} \tag{4.20}$$

  by first solving (by forward substitution) for the vector **Y** such that **L Y** = **R** and then solving (by back substitution) **U C** = **Y**. The advantage is that both substitutions are quite trivial.
  Although for the problem on hand, pivoting may not be essential due to the diagonally dominant structure of the system of equations (Axley 1990, Walton 1990), the LU decomposition method as implemented, provided a numerically stable solution for a number of test cases for which the Gaussian elimination method was not able to do so. This may have been caused by the scaling feature of the implemented LU decomposition subroutine.

Both options are supported up to now, because choice of the matrix solver is still a subject of investigation. The matrix assembly process and the matrix equation solution process are highly modularized, which makes it easy to introduce yet another solution process. Sparse matrix methods could be used to reduce both the storage and execution time requirements. It should be noted that the degree of sparsity of the Jacobian matrix is dependent on the ordering of the nodes. Ordering can be improved by various algorithms or rules-of-thumb. This is not done at present.
In *mfs*, the nodes with known pressure are included in the system of equations. This gives an added flexibility in defining the fluid flow network at the cost of producing a non-symmetric and actually over-sized (constant pressure nodes don't need a pressure correction) set of equations. For known pressure nodes the **J C** = **R** matrix equation is processed so as to not change those nodal pressures. This actually means that the right hand side elements for known pressure nodes are set to zero. In some cases it is possible that an unknown pressure node's diagonal Jacobian element is equal to zero, e.g.: (1) when there is no flow through its connections, (2) when the partial derivatives of its connections are effectively zero. To avoid numerical problems when solving the matrix equation for these cases, the diagonal element is set to 1. and the right hand side element is set to zero (ie. don't change the pressure for the time being).

It should also be noted that it is quite easy to define a fluid flow network which has no unique solution. One requirement for solution is that at least one of the node pressures is known. A second requirement is that all nodes must be linked, through some path, to a known pressure node.

Conservation of mass at each internal node provides the convergence criterion. That is, if $\sum \dot{m}_k = 0$ for all internal nodes for the current system pressure estimate, the exact solution has been found. In practice, we are usually already quite satisfied when the internal node mass flow residuals are below a certain threshold. In this way the number of iterations can be reduced. *mfs* offers two user definable parameters to set this threshold:
- ERRMAX which is the largest percentage residual flow error allowed in any node. Iteration stops when:

$$\left(\frac{|\sum \dot{m}_k|}{\sum |\dot{m}_k|} \right)_{\max} \leq \frac{\text{ERRMAX}}{100} \quad (-) \tag{4.21}$$

- FLOMAX which is the largest absolute residual flow error allowed in any node. Iteration stops when:

$$(|\sum \dot{m}_k|)_{\max} \leq \text{FLOMAX} \quad (kg/s) \tag{4.22}$$

There is an additional stop criterion called MAXIT. This "safety" device defines the maximum number of iterations allowed during one time step.

In some cases, too large corrections for the successive values of node pressure may cause a numerical instability. Therefore, *mfs* offers a user definable parameter PMAX which sets the maximum absolute pressure correction applied to any node during the iteration process.

To be able to handle occasional instances of slow convergence due to oscillating pressure corrections on successive iterations, a method as suggested by Walton (1989a, 1989b) was adopted. Oscillating behaviour is indicated graphically in Figure 4.4 for the successive values of the pressure at a single node. In the case shown each successive pressure correction

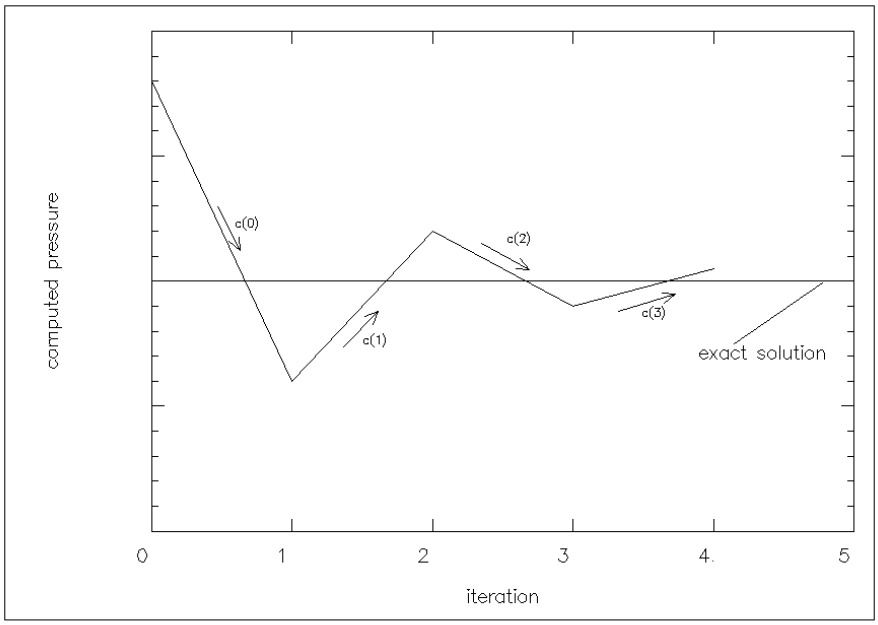

Figure 4.4 Example of successive computed values of the pressure and oscillating pressure corrections at a single node

is a constant ratio of the previous correction; ie. $C_i = -0.5\,C_i^*$ (where * denotes the previous iteration step value). In a number of tests the observed oscillating corrections came close to such a pattern. By assuming a constant ratio, it is simple to extrapolate the corrections to an assumed solution:

$$P_i = P_i^* - C_i/(1-r) \quad (Pa) \tag{4.23}$$

where r is the ratio of C_i for the current iteration to its value in the previous iteration. The factor $1/(1-r)$ is called a relaxation factor. The extrapolated value of node pressure can be used in the next iteration. If it is used in the next iteration, then r is not evaluated for that node in the following iteration but only in the one thereafter. In this way, r is only evaluated with unrelaxed pressure correction values. This process is similar to a Steffensen iteration (Conte and De Boor 1972) which is used with a fixed point iteration method for individual nonlinear equations. The iteration correction method presented above gives a variable and node dependent relaxation factor. When the solution is close to convergence, Newton-Raphson iteration converges quadratically. By limiting the application of relaxation factor above to cases where r is less than some value (a user definable parameter called STEFFR in *mfs*) such as -0.5, it will not interfere with the rapid convergence.
Only recently, evidence was encountered suggesting that in a number of cases simple under-relaxation would provide even better convergence acceleration than the Steffensen iteration (Walton 1990). Although it is quite easy to implement and test this thesis, this has not yet been done due to time constraints.

Some network simulation models incorporate a feature to compute an initial pressure starting vector from which the iterations will start. For instance AIRNET (Walton 1989a, 1989b) uses linear pressure-flow relations for this†. The main reasons for refraining from this in *mfs* are: 1) it is not possible to provide a linear pressure-flow relation for all envisaged flow component types, 2) after the initial start, the previous time step results probably provide

better iteration starting values than those resulting from linear pressure-flow relations (see eg Section 7.4.1.), and 3) this would impose an additional input burden upon the user.

In order for the user to be able to keep track of calculation progress, *mfs* supports a trace output facility. At present, the following trace output options are on offer:

-1 no trace output at all. This option is meant for - and the default - when mass flow simulation is performed by *bps*.
 0 no trace output, only indicate whether the solution of the set of simultaneous nonlinear equations was successful or whether it failed and how many iterations were performed. This is the default when mass flow simulation is performed by *mfs*.
 1 as 0 but also show pressure, residual and relative error of worst (relative) node for each iteration.
 2 as 1 but also show pressure and residual at all other nodes and mark the worst relative and absolute nodes for each iteration.
 3 as 2 but also give detailed information regarding the matrix equation solving process for each iteration. This information includes: (1) the Jacobian matrix with 'Newton-Raphson coefficients', (2) nodal mass flow residuals vector, (3) whether a diagonal element or right hand side element is reset, (4) the node pressure corrections vector, (5) the recalculated right hand side vector, (6) the relaxation factor if Steffensen's method is applied, and (7) the adjusted pressure correction if the pressure correction limit is exceeded

4.3.4. Results Handling

mfs writes its main results to a data file. These results include for each time step:
(1) date, time, climate data, number of iterations and a "flag" indicating whether the iteration process was successful (if yes OK = 1 else OK = 0)
(2) for each node in turn: node name, fluid type, node type, temperature ($°C$), height (m), pressure (Pa), mass flow residual (kg/s) and node coupled sum of absolute mass flow rates (kg/s)
(3) for each connection in turn: node and component names, component type, fluid type, total pressure difference across the connection (Pa), pressure difference due to stack effect (Pa) and one (usually) or two (in some cases, e.g. a door) mass flow rates (kg/s)

As an example, a small part of a fluid flow results file is shown in Table 4.6. In this particular case, the error tolerance parameters were equal to the default values: ERRMAX = 1.0 (%) ; FLOMAX = 0.00050 (kg/s). From the results it can be seen that the iteration process was successful and that in this case node **bed** is both the worst absolute node (residual is -0.00016 kg/s) and the worst relative node (0.4 %); in the 6th iteration, node **bed** was also the worst node with errors of 0.00123 (kg/s) and 3.3 (%) (this can not be seen from the final results; the trace facility must be used for this).

---

† According to Walton (1990) and Axley (1990), these are also necessary for low flow velocities so that a) flows are realistically modeled in the laminar flow regimes, and b) to avoid singular or nearly singular system Jacobians when employing Newton-Raphson solution strategies.
In *mfs* these problems are anticipated by a) the respective flow component types which are capable of modelling laminar flow, and b) the matrix solver as indicated above.

Table 4.6 Small part (one time step) of an *mfs* results file

Date: 9/ 1/1967 12.00 Dryb= -1.0 Wdir= 345. Wvel= 1.4 It= 7 OK=1

Node	**Fld**	**Type**	**Temp**	**Hght**	**Pressure**	**Residual**	**Sabs(Flw)**	
living	1	0	21.0	1.5	-23.150	0.51258E-06	0.42086	
kitche	1	0	20.8	1.5	-23.154	-0.52800E-07	0.40522	
w_ctl	1	0	20.8	1.5	-18.796	0.	0.	
bed	1	0	21.0	4.5	-57.997	-0.15738E-03	0.39116E-01	
bath	1	0	21.0	4.5	-57.997	0.46190E-07	0.48436E-01	
south	1	3	-1.0	1.5	-19.835	-0.45106E-01	0.45106E-01	
north	1	3	-1.0	1.5	-18.331	-0.12443E-01	0.12443E-01	
roof	1	3	-1.0	7.0	-88.818	0.57706E-01	0.57706E-01	
t_junc	1	0	21.0	5.0	-124.63	-0.71409E-06	0.11541	
fan_in	1	0	21.0	6.0	-141.52	0.64808E-06	0.11541	
fan_ou	1	0	21.0	6.0	-46.206	-0.17658E-06	0.11541	
From	**To**	**Comp**	**Typ**	**Fld**	**Pi-Pj**	**Pstack**	**Flw 1**	**Flw 2**
living	kitche	door	130	1.	0.39953E-02	0.	0.19456	-0.16930
living	bed	stairs	110	1.	34.847	-34.847	0.20067E-01	0.
bed	bath	grl_in	10	1.	0.11370E-04	0.	0.19963E-01	0.
south	living	crack	120	1.	3.9248	1.4580	0.10021E-01	0.
south	living	grl_ex	40	1.	3.9248	-1.4580	0.35434E-01	0.
south	bed	grl_ex	40	1.	38.772	-38.772	-0.23101E-03	0.
bath	north	crack	120	1.	-40.119	38.772	-0.42940E-02	0.
kitche	north	crack	120	1.	-5.2753	1.3363	-0.82791E-02	0.
kitche	w_ctl	w_ctl	450	1.	-4.7185	0.	0.	0.
w_ctl	north	window	40	1.	-0.55680	0.55680	0.	0.
kitche	t_junc	duct_1	220	1.	101.67	-40.682	0.33541E-01	0.
bath	t_junc	duct_2	220	1.	66.823	-5.8078	0.24256E-01	0.
t_junc	fan_in	duct_3	210	1.	16.905	-11.616	0.57797E-01	0.
fan_in	fan_ou	fan	310	1.	-95.216	0.	0.57797E-01	0.
fan_ou	roof	duct_4	210	1.	42.710	-11.616	0.57797E-01	0.

4.4. AVAILABLE FLUID FLOW COMPONENT TYPES

Flow within each fluid flow component is assumed to be governed by Bernoulli's equation for incompressible adiabatic steady† fluid flow. When expressed in terms of pressure and in its extended form - for flow through real systems - the Bernoulli relationship for fluid resistance between two sections of the flow component states:

$$\Delta P = (p_1 + \rho {v_1}^2/2) - (p_2 + \rho {v_2}^2/2) + \rho g(z_1 - z_2) \quad (Pa) \tag{4.24}$$

where ΔP is the total pressure drop between points 1 and 2 (Pa) (ie. sum of all friction and dynamic losses), p_1, p_2 is the static pressure at points 1 and 2(Pa), v_1, v_2 is the fluid velocity at points 1 and 2 (m/s), ρ is the density of fluid flowing through the component (kg/m^3), g is the acceleration of gravity (9.81 m/s^2), and z_1, z_2 is the elevation of points 1 and 2 (m).

The following parameters apply to the nodes: pressure, temperature (to compute density and viscosity), and height. The node height values are used to determine the stack effect. When the node represents a large volume, say a room, the fluid flow component may connect with the node at other than its reference height. The calculation of pressure difference due to stack effects PS (ie. the $\rho g(z_1 - z_2)$ term in the equation), was described in Section 4.3.1. before. Bernoulli's equation can be further simplified by combining several related terms. Dynamic pressures are the $\rho v^2/2$ terms, and total pressure is defined to be the sum of static pressure

† when time-steps much less than 1 sec are to be considered the acceleration term in Bernoulli's equation cannot be disregarded

and dynamic pressure; i.e. $P = p + \rho v^2/2$. If nodes n and m represent large volumes (e.g. a room), the dynamic pressures are effectively zero. If the nodes represent some point in a duct or pipe network, there will be a positive dynamic pressure. Bernoulli's equation thus reduces to:

$$\Delta P = P_n - P_m + PS_{nm} \quad (Pa) \tag{4.25}$$

where P_n, P_m is the total pressure at nodes n and m (Pa), and PS_{nm} is the pressure difference due to density and height differences across connection $n - m$ (Pa).

This equation defines a sign convention for the direction of flow: positive flow is from node n to node m. As will be seen in the following sections, the flow within each fluid flow component is described by a relation of the form $\dot{m} = f(\Delta P)$. The partial derivatives needed for the establishment of the Jacobian matrix (which represents the nodal pressure corrections in terms of all branch flow partial derivatives; see Section 4.3.3) are thus related by $\partial \dot{m} / \partial \Delta P_{nm} = -\partial \dot{m} / \partial \Delta P_{mn}$.

4.4.1. Power Law Flow Component (type 10, 15, 17)

These types of flow component use one of the following relationships between flow and pressure difference across the component:

$$(type\ 10) \quad \dot{m} = \rho\, a\, \Delta P^b \quad (kg/s) \tag{4.26a}$$

$$(type\ 15) \quad \dot{m} = a\, \Delta P^b \quad (kg/s) \tag{4.26b}$$

$$(type\ 17) \quad \dot{m} = a \sqrt{\rho}\, \Delta P^b \quad (kg/s) \tag{4.26c}$$

where $\dot{m}$ is the fluid mass flow rate through the component (kg/s), a is a flow coefficient, expressed in: $m^3/s \cdot Pa^b$ (type 10), $kg/s \cdot Pa^b$ (type 15), or $(kg\, m^3)^{1/2}/s \cdot Pa^b$ (type 17). ΔP is the total pressure loss across the component (Pa), and b is the flow exponent (-).

As can be seen, the difference between the three sub-types is only in the dimension of the flow coefficient a. Although in literature all three forms can be found, the first one is the most commonly encountered. The value of ρ depends on the type of fluid and on the direction of flow. If the flow is positive (ie. when $\Delta P \geq 0$) than the temperature of the node on the positive side is used to evaluate the fluid density. Likewise, for a negative flow the temperature of the node on the negative side of the connection is used. Theoretically, the value of the flow exponent b should lie between 0.5 (for fully turbulent flow) and 1.0 (for laminar flow). The power law relationship should, however, be considered a correlation rather than a physical law. It can conveniently be used to characterize openings for building air infiltration calculations, because the majority of building fabric leakage description data is available in this form (Liddament 1986). As an example, see Table 4.7. The power law relationship can also be used to describe flows through ducts and pipes, albeit to a lesser accuracy than by the technique as presented in Section 4.4.7. The primary advantage of the power law relationship for describing fluid flow components, is the simple calculation of the partial derivative needed for the Newton-Raphson approach:

$$\frac{\partial \dot{m}}{\partial \Delta P} = \frac{b\, \dot{m}}{\Delta P} \quad (kg/s \cdot Pa) \tag{4.27}$$

The problem with this equation is, however, that the derivative becomes undefined when the pressure drop (and the flow) approach zero. This is handled in *mfs* by switching to numerical

Table 4.7 Examples of building fabric air leakage data for usage with type 10 flow component (modified from Liddament 1986). Notes: (1) flow coefficient expressed in $10^{-3} m^3/s/Pa^b$, (2) mean values only, (3) **approximate data only**

Description	Unit of measure	Flow coefficient $10^{-3} m^3/s/Pa^b$	Flow exponent b –
Timber door, external, single side hung:			
- in timber, weatherstripped	L	0.96	0.64
- in timber, unweatherstripped	L	1.32	0.59
- in metal, unweatherstripped	L	0.038	0.66
Casement window, weatherstripped:			
- timber, side hung	L	0.03	0.66
- metal, side hung	L	0.27	0.66
- timber, top hung	L	0.42	0.57
- metal, top hung	L	0.32	0.6
- timber, central pivot vertical	L	0.03	0.78
- metal, central pivot vertical	L	0.07	0.66
Skylight, metal, unweatherstripped	L	0.18	0.55
Timber door/window frame in a:			
- masonry brick wall, caulked	L	0.0014	0.6
- timber wall, uncaulked	L	0.05	0.66
Exterior wall (including joints):			
- clay brick, unvented, cavity filled with granulated mineral wool, bare surface	A	0.024	0.81
- ditto but 3 coats plaster on inside surface	A	0.0034	1.0
- brick, ventilated cavity, glass fibre insulation, vapour barrier, wallboard inside	A	0.18	0.81
- multi-storey curtain wall	A	0.19	0.75
- timber frame and brick only	A	0.19	0.75
Miscellaneous:			
- open fireplace, brick chimney	C	17.0	0.5
- fireplace, damper closed	C	8.3	0.5
- mail slot	C	0.2	0.5
- flue vent through ceiling	C	3.0	0.66
Data expressed for:	L	each metre length of joint	
	A	each m^2 of surface	
	C	each component	

approximation of the partial derivative in case the pressure drop is smaller than a certain threshold (say $10^{-20}\ Pa$):

$$\frac{\partial \dot{m}}{\partial \Delta P} \approx \frac{\dot{m} - \dot{m}^*}{\Delta P - \Delta P^*} \quad (kg/s \cdot Pa) \tag{4.28}$$

where * denotes the value in the previous iteration step.

4.4.2. Quadratic Law Flow Component (type 20, 25)

According to some literature sources (e.g. Baker et al. 1987) air flow through building fabric infiltration openings is better described by a quadratic relationship between pressure difference across the component (ie. opening) and flow rate (in such a formulation the flow equation is divided in a laminar and a turbulent part). Therefore *mfs* offers the following fluid flow component types:

$$(type\ 20) \quad \Delta P = a\,\frac{\dot{m}}{\rho} + b\left(\frac{\dot{m}}{\rho}\right)^2 \quad (Pa) \tag{4.29a}$$

$$(type\ 25) \quad \Delta P = a\,\dot{m} + b\,\dot{m}^2 \quad (Pa) \tag{4.29b}$$

where a is a flow coefficient, expressed in: $Pa/(m^3/s)$ (type 20), or $Pa/(kg/s)$ (type 25). b is a flow coefficient, expressed in: $Pa/(m^3/s)^2$ (type 20), or $Pa/(kg/s)^2$ (type 25).

As can be seen, the difference between the two sub-types is only in the dimension of the flow coefficients. The first form is the most commonly encountered. If we define the "discriminant" $DSCR$ of the equation:

$$DSCR = \sqrt{a^2 + 4b|\Delta P|} \tag{4.30}$$

and we define an intermediate flow variable $FLWR$ by:

$$FLWR = \frac{-a + DSCR}{2\,b} \text{ if } a \neq 0 \text{ and } b \neq 0 \tag{4.31a}$$

$$FLWR = \frac{|\Delta P|}{a} \text{ if } a \neq 0 \text{ and } b = 0 \tag{4.31b}$$

$$FLWR = \sqrt{|\Delta P|/\,b} \text{ if } a = 0 \text{ and } b \neq 0 \tag{4.31c}$$

then the mass flow rate can be found from:

$$(type\ 20) \quad \dot{m} = \rho\ FLWR \quad (kg/s) \tag{4.32a}$$

$$(type\ 25) \quad \dot{m} = FLWR \quad (kg/s) \tag{4.32b}$$

where ρ depends on the type of fluid and both ρ and the sign of $\dot{m}$ depend on the direction of flow (ie. sign of ΔP). The same goes for the partial derivative which is found from:

$$(type\ 20) \quad \frac{\partial \dot{m}}{\partial \Delta P} = \frac{\rho}{DSCR} \quad (kg/s \cdot Pa) \tag{4.33a}$$

$$(type\ 25) \quad \frac{\partial \dot{m}}{\partial \Delta P} = \frac{1}{DSCR} \quad (kg/s \cdot Pa) \tag{4.33b}$$

In case the value of $DSCR$ is less than a certain threshold, *mfs* switches to numerical approximation of the partial derivative according to equation (4.28).

4.4.3. Constant Flow Rate Component (type 30, 35)

For many fluid flow network problem descriptions it is very convenient to have constant flow rate component types available. *mfs* offers:

$$(type\ 30) \quad \dot{m} = \rho a \quad (kg/s) \tag{4.34a}$$

$$(type\ 35) \quad \dot{m} = a \quad (kg/s) \tag{4.34b}$$

where a is a constant defining the flow rate in m^3/s (type 30), or kg/s (type 35).

The fluid density (ie. ρ) depends on the type of fluid and on the direction of flow; ie. is evaluated with the temperature of the sending node. Obviously, the partial derivative for a constant flow component type equals zero.

4.4.4. Common Orifice Flow Component (type 40)

A basic expression for turbulent flow through relatively large openings (e.g. a purposely provided vent in case of building air flow modelling or a restriction in a pipe in case of a hydronic network), is the common orifice flow equation. If expressed as mass flow rate this is given by:

$$\dot{m} = C_d A\sqrt{2\rho\Delta P} \quad (kg/s) \tag{4.35}$$

where C_d is the discharge factor (-), and A is the opening area (m^2).

Again, the fluid density depends on the direction of flow. The partial derivative for this fluid flow component is calculated from:

$$\frac{\partial\dot{m}}{\partial\Delta P} = \frac{.5\,\dot{m}}{\Delta P} \quad (kg/s \cdot Pa) \tag{4.36}$$

unless ΔP is too small, in which case *mfs* switches to the numerical approximation of equation (4.28).

4.4.5. Laminar Pipe Flow Component (type 50)

Another basic expression, but in this case for laminar flow through openings with relatively long flow paths (e.g. a narrow crack in the building fabric in case of building air flow modelling or fluid flow at low velocity in case of a hydronic network), is the laminar pipe flow equation. Expressed as mass flow rate this is given by:

$$\dot{m} = \frac{\rho\Delta P\pi r^4}{8\mu L} \quad (kg/s) \tag{4.37}$$

where r is the radius of opening (m), L is the length of the flow path (m), and μ is the fluid dynamic viscosity ($kg/m\ s$).

Both the fluid density ρ and the dynamic viscosity μ depend on the type of fluid and on the temperature of the sending node. The partial derivative is given by:

$$\frac{\partial\dot{m}}{\partial\Delta P} = \frac{\rho\pi r^4}{8\mu L} \quad (kg/s \cdot Pa) \tag{4.38}$$

During simulation this component checks if the flow is indeed laminar; if not a warning is issued. The warning is given if the Reynolds-number exceeds 2320. Expressed in mass flow rate and using the radius of the opening, the Reynolds-number may be calculated from:

$$\mathrm{Re} = \frac{2\,\dot{m}}{\mu\,\pi\,r} \quad (-) \tag{4.39}$$

4.4.6. Specific Air Flow Components

4.4.6.1. Specific air flow opening component (type 110)

For user convenience and reasons of compatibility with *air*, *mfs* offers a component called: air flow opening. This component is actually identical to a type 40 component with fluid type set to air and with discharge factor C_d equal to 0.65 (-)

4.4.6.2. Specific air flow crack component (type 120)

This is also a component which was introduced in *air* (see Clarke 1985). The relation between mass flow rate and pressure difference is given by:

$$\dot{m} = \rho\, k \Delta P^x \quad (kg/s) \tag{4.40}$$

where

$$x = 0.5 + 0.5 \exp(-500\, W) \quad (-) \tag{4.40a}$$

$$k = L\, 9.7\, (0.0092)^x / 1000 \quad (m^3/s \cdot Pa^x) \tag{4.40b}$$

where W is the crack width (m), and L is the crack length (m).

The value of ρ depends on the direction of air flow. The partial derivative is calculated from:

$$\frac{\partial \dot{m}}{\partial \Delta P} = \frac{x\, \dot{m}}{\Delta P} \quad (kg/s \cdot Pa) \tag{4.41}$$

unless ΔP is too small, in which case *mfs* switches to the numerical approximation of equation (4.28).

4.4.6.3. Specific air flow door component (type 130)

This is also a component as offered by *air* (see Clarke 1985).

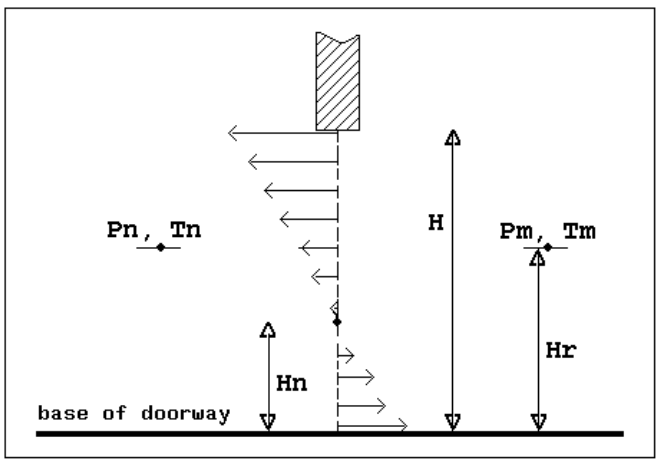

Figure 4.5 Bi-directional air flow across a doorway

With large vertical openings, such as doorways, it is unlikely that unidirectional flow can be

assumed. If a temperature difference exists across such an opening, then air flow can occur in both directions due to the action of small density variations over the door height causing a positive pressure at the bottom (or top) of the opening with a corresponding negative pressure difference at the top (or bottom). This situation is illustrated in Figure 4.5.

For this type of connection an expression by Cockroft (1979) is used:

$$\dot{m} = \rho(2/3)\,[C_d W\,H\,(2/\rho)^{1/2}\,(C_a{}^{3/2} - C_b{}^{3/2})/C_t] \quad (kg/s) \qquad (4.42)$$

where

$$C_a = (1 - r_{p)}\,C_t + (P_n - P_m) \quad (Pa) \qquad (4.42a)$$

$$C_b = (P_n - P_m) - r_p C_t \quad (Pa) \qquad (4.42b)$$

$$C_t = g\,P_o\,H/R \cdot (1/\Theta_m - 1/\Theta_n) \quad (Pa) \qquad (4.42c)$$

and C_d is the discharge factor (-), W is the opening width (m), H is the opening height (m), $r_p = H_r/H$ (-), g is the acceleration due to gravity (= 9.81 m/s^2), P_o is the atmospheric pressure (= 101325 Pa), R is the gas constant for dry air (= 287.1 J/kgK), Θ is the node temperature (K), and H_r is the reference height above base of doorway (m).

On evaluation this equation yields a sum of real and imaginary parts. The real part of the solution indicates the flow in the positive direction and the imaginary part indicates the flow in the other direction. The value which is used for the fluid density depends on the flow direction. The partial derivative is numerically approximated according to equation (4.28). In case the opening height is very small (< 0.01 m) or in case there is no or only a very small temperature difference (< 0.01 K) a door component is treated as an ordinary air flow opening (ie. type 110) because in those cases the buoyancy effects may be disregarded.

4.4.7. General Flow Conduit Component (type 210)

The irreversible transformation of mechanical energy into heat causes pressure losses in a fluid conduit (ie. a duct or a pipe). Two types of fluid losses exist:

(1) frictional losses; these are due to fluid viscosity and are a result of momentum exchange between molecules in laminar flow and between particles moving at different velocities in turbulent flow. Frictional losses occur along the entire length of the conduit.

(2) dynamic losses; these result from flow disturbances caused by fittings that change the fluid flow path's direction and/or area. Dynamic losses occur along the length of the conduit and cannot be separated from frictional losses. For ease of calculation, however, dynamic losses are assumed to be concentrated at a cross-section (local) and to exclude friction.

For fluid flow through a conduit (ie. a duct or a pipe) with (a) uniform cross-sectional area, (b) no pressure gain due to fan or pump, and (c) steady-state conditions, the sum of all friction and dynamic losses is found from:

$$\Delta P = fL\rho\overline{v}^2/2D_h + \Sigma C_i \rho\overline{v}^2/2 \quad (Pa) \qquad (4.43)$$

where f is the friction factor (-), L is the conduit length (m), D_h is the hydraulic diameter (= $4A/$ perimeter of the cross-section) (m), A is the cross-sectional area (m^2), O_s is the perimeter of the cross-section (m), $\overline{v}$ is the average velocity (m/s), and C_i is the local loss

factor due to fitting i (-).

The local loss factors, in the second right hand side term, represent dynamic losses resulting from flow disturbances caused by "fittings". In principle, local loss factors can be used for all those fittings or components which, from a fluid flow point of view, do not have to be modelled separately (this implies that the pressure loss for those components is assumed to be proportional to $\overline{v}^2$). Examples are:
- pipe and duct entries
- pipe and duct exits (except when there is a strong flow in the entered volume)
- elbows, bends and obstructions (sometimes Re-correction is needed though)
- converging or diverging transitions
- simple pipe and duct approximation in which a constant friction factor is assumed. In that case we set C_i equal to $f_{const} L/D$ and the length equal to zero, i.e. don't calculate friction loss.

Numerical values for the local loss factors may be found in various sources in literature (e.g. Miller 1978, ASHRAE 1985, ISSO 1986, etc.).

The first right hand side term in the equation above is also known as the Darcy-Weisbach equation for frictional losses of fluid flow through conduits. The friction factor in this term depends on the type of flow, which can be characterized by the Reynolds-number:

$$\mathrm{Re} = \overline{v}\, D_h/\nu \quad (-) \tag{4.44}$$

where ν is the kinematic viscosity (m^2/s).

In circular conduits the critical Reynolds-number is equal to 2320. At lower values the flow is laminar and at higher values the flow is turbulent. In the transition region ($2320 < \mathrm{Re} < 8000$) laminar flow can occur in case of smooth piping and hydrodynamically "well formed" entrances. The transition zone for laminar to turbulent flow moves toward lower Re-numbers when the pipe roughness increases; however never below $\mathrm{Re} = 2320$. This holds for fully developed flow. In technical systems however there are many bends, tee-pieces etc which may cause the flow to be turbulent even at $1000 < \mathrm{Re} < 2320$.

With respect to calculation of the friction factor, in (Hensen 1989), distinction was made between laminar flow through technically smooth (absolute wall roughness $k < 0.007\ mm$) and through technically rough conduits, and in case of turbulent flow between flow through technically smooth conduits ($\mathrm{Re} < 65\, D_h/k$), smooth to roughness flow transition region ($65\, D_h/k < \mathrm{Re} < 1300\, D_h/k$) and fully developed roughness flow ($\mathrm{Re} > 1300\, D_h/k$). *mfs* follows the approach as indicated in (ISSO 1986) which recognises only three regions.

For $\mathrm{Re} \leq 2300$ **laminar flow** is assumed, and the friction factor is calculated from:

$$f = 64/\mathrm{Re} \quad (-) \tag{4.45}$$

In the **transition region**, for $2300 < \mathrm{Re} < 3500$, the flow may be either laminar or turbulent depending on the degree of disturbance. The friction factor is found by linear interpolation:

$$f = \frac{f_L(3500 - \mathrm{Re}) + f_T(\mathrm{Re} - 2300)}{3500 - 2300} \quad (-) \tag{4.46}$$

where f_L is the friction factor for laminar flow at Re = 2300 (-), and f_T is the friction factor for turbulent flow at Re = 3500 (-).

For $\mathrm{Re} \geq 3500$ the flow is assumed to be **turbulent**, and the friction factor is calculated from an explicit approximation of the implicit Colebrook-White equation, which is sufficient accurate for most technical purposes:

$$f = 1/[2 \cdot \log(5.74/\mathrm{Re}^{0.901} + 0.27 \cdot k/D_h)]^2 \quad (-) \tag{4.47}$$

where k is the absolute wall material roughness (m).

The mass flow rate through a conduit can now be calculated from a "known" pressure difference by:

$$\dot{m} = A\sqrt{\frac{2\rho\Delta P}{fL/D + \Sigma C_i}} \quad (kg/s) \tag{4.48}$$

Because, effectively, we have an implicit formulation for $\overline{v}$, in case we want to calculate the frictional losses (ie. $L > 0$), the calculation of $\dot{m}$ needs some sort of iteration. *mfs* uses a fixed point iteration method with the following steps: (1) Re is calculated with $\overline{v}$ based on the most recent flow rate, (2) dependent on Re, a friction factor is established, (3) with this value a new flow rate is calculated which is compared with the one used in step 1, and (4) unless the difference is smaller than either error limit (ERRMAX, FLOMAX), the whole process is iteratively repeated.

In the equations above the fluid density and the fluid viscosity both depend on the direction of flow, ie. the temperature of the sending node. The partial derivative for this fluid flow component may be calculated from equation (4.36) unless ΔP is too small, in which case *mfs* switches to the numerical approximation of equation (4.28).

4.4.8. Conduit & Junction with Flow Ratio Dependent Dynamic Losses

As do all other fittings, flow junctions (tees, wyes, crosses, etc) cause frictional and dynamic losses. Actually, dynamic losses occur along a duct/pipe length and cannot be separated from frictional losses. For ease of calculation however, dynamic losses are assumed to be concentrated at a section (local) and to exclude friction.
Friction losses are generally accounted for by measuring pipe/duct lengths from the centerline of a junction or other component to that of the next; thus implicitly adding the junction friction loss to the friction loss of the adjacent pipe/duct section.
In case the dynamic local losses of a junction solely depend upon geometrical considerations they can be treated in a similar manner. However, although in general a local loss factor itself is not a function of the actual velocity,† they tend to be strongly related to the ratios of velocity or flow rate in the different parts of the junction; i.e. they depend on conditions

† this implies that the dynamic losses are proportional to $\overline{v}^2$. In reality, the dynamic local loss factor is only a constant in the fully developed turbulent flow region, i.e. $\mathrm{Re} \geq 10^5$. The local loss factors found in literature are usually restricted to this region. For lower values of Re there is hardly any reliable data available. For the time being, *mfs* does not discriminate between fully developed turbulent flow and otherwise.

elsewhere in the system network. The most common technique of describing dynamic local losses for junctions is by equations of the form:

$$\Delta P_{t,\,p} = C_{c,\,p}\,\frac{1}{2}\,\rho \overline{v}_c^{\,2} \quad (Pa) \tag{4.49}$$

where $\Delta P_{t,\,p}$ represent the total pressure losses through section p of the junction (Pa), $C_{c,\,p}$ is the dimensionless local loss factor for part p of the junction referenced to the velocity pressure at section c of the junction (usually this is a function of $\dot{q}_p/\dot{q}_c$ ($\overline{v}_p/\overline{v}_c$)), $\dot{q} = \dot{m}/\,\rho$ (m^3/s), subscript c indicates the common flow path, and subscript p indicates either straight (s) or branch (b) flow path.

Figure 4.6 Local loss factor for a converging wye (45°), round. Graph originates from ISSO (1986) (literature sources indicated are Idelchik 1986, ASHRAE 1985 and Miller 1971)
1 - branch flow path
2 - straight flow path
3 - common flow path

Values for $C_{c,\,p}$ can be found in several handbooks (e.g. Miller 1971, ASHRAE 1985, Idelchik 1986). Figure 4.6 is an example of such data. This figure also indicates that different literature sources not always yield identical values for certain fittings.
Through curve fitting on data encountered in literature or found from experiments, it is generally possible to derive, for each flow path's local loss factor, an approximate expression of the form:

$$C_{c,\,p} = a_0 + a_1\left(\frac{\dot{q}_p}{\dot{q}_c}\right) + a_2\left(\frac{\dot{q}_p}{\dot{q}_c}\right)^2 + a_3\left(\frac{\dot{q}_{p'}}{\dot{q}_c}\right) + a_4\left(\frac{\dot{q}_{p'}}{\dot{q}_c}\right)^2 + a_5\left(\frac{\dot{q}_p}{\dot{q}_c}\cdot\frac{\dot{q}_{p'}}{\dot{q}_c}\right) \tag{4.50}$$

where a_i are fit coefficients†, subscript p indicates either straight (s) or branch (b) flow path, and subscript p' then indicates branch (b) or straight (s) flow path, resp.

Thus, it would be possible to calculate the pressure drop across the different flow paths of the junction. However, there are some difficulties when a junction would be approached as just another type of flow component:
- for many junctions, $C_{c,\,p}$ becomes very small or even negative for certain values of $\dot{q}_p/\dot{q}_c$ (see e.g. Figure 4.6. This may easily lead to numerical difficulties when the flow rate through the different flow paths of the junction is to be calculated explicitly from the pressure difference across it.
- a junction flow component type does not blend well with the concept of a flow component type linking two separate nodes - which forms the basis of all other pressure/flow component types - because a junction obviously involves more than two nodes

The former problem is usually dealt with by avoiding explicit evaluation of the flow/pressure relationships at the junction component level. This may be done by adding the dynamic local loss factors to adjacent flow components instead. For this, and to handle the second difficulty, *mfs* offers some special flow conduit component types which allow assignment of the junction local loss factor $C_{c,\,s}$ or $C_{c,\,b}$ to the adjacent conduit. These special conduit components are explained in the following sections.

4.4.8.1. Conduit ending in converging 3-leg junction (type 220)

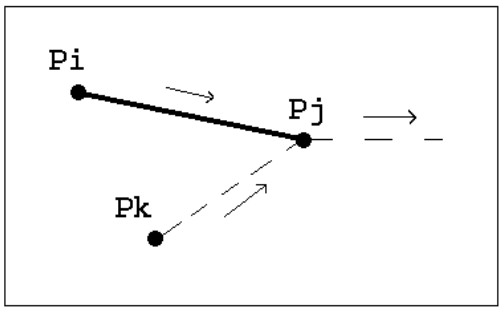

Figure 4.7 Conduit ending in converging 3-leg junction

This type of flow component is schematically drawn in Figure 4.7. The conduit type component links node i and node j but also comprises the dynamic local losses of either the "straight" or the branch flow path of the junction. The other entrance of the junction has to be represented by the conduit component linking node k with node j; so a type 220 component incorporates only one half of the junction. It is assumed that there is **only one connection** between node **i** and node **j**, and between node **k** and node **j** respectively. Furthermore the flow directions are assumed to be as indicated in the figure. If, during simulation, the flow is in the other direction, a warning message will be issued.

---

† note that the coefficients for describing $C_{c,\,s}$ differ from the fit coefficients which describe $C_{c,\,b}$. Note also that not necessary all $a_i \neq 0$

In addition to the parameters describing the flow/pressure relationship for the conduit itself (which have the same meaning as in case of a general flow conduit (see Section 4.4.7. on type 210)) the following component description data is needed:

a_0 to a_5	fit coefficients describing $C_{c,\,p} = f(\dot{q}_p/\dot{q}_c\ ,\ \dot{q}_{p'}/\dot{q}_c)$; subscript p refers to the junction section under consideration and subscript p' refers to the other entrance of the junction
A_c	cross-sectional area of the common flow path (m^2)

It should be noted that here $C_{c,\,p}$ is described as a function of $(\dot{q}_p/\dot{q}_c\ ,\ \dot{q}_{p'}/\dot{q}_{c)}$, while in literature one often finds $C_{c,\,p}$ described as function of $(\dot{q}_b/\dot{q}_{c)}$ (see eg. Figure 4.6) or as function of $(\overline{v}_b/\overline{v}_c)$. Obviously, it is then a trivial task to transform the coefficients to the form used in *mfs*.
Apart from the component parameters, it is also necessary to define node **k**. This is done by extending the linkage date for the connection in question (ie. from node i to node j) with the name of node k.

The algorithm now functions as follows:
(1) the local loss factor $C_{c,\,p}$ is evaluated based on the most recent calculated flow rates, with:

$$\dot{q}_p = \dot{m}_{i,\,j}/\rho_i \quad (m^3/s) \tag{4.51a}$$

$$\dot{q}_{p'} = \dot{m}_{k,\,j}/\rho_k \quad (m^3/s) \tag{4.51b}$$

$$\dot{q}_c = \dot{q}_p + \dot{q}_{p'} \quad (m^3/s) \tag{4.51c}$$

unless either $\dot{m}_{i,\,j} \leq 0$ or $\dot{m}_{k,\,j} < 0$, in which case (a) the local loss factor for this junction section is set to zero, (b) a warning message is issued, and (c) the algorithm proceeds with step (4).
(2) the local loss factor $C_{c,\,p}$ is now converted into the local loss factor $C_{i,\,j}$ referenced to the velocity pressure in section $i-j$ by:

$$C_{i,\,j} = C_{c,\,p}\,\frac{\rho_i}{\rho_c}\left(\frac{\dot{m}_c/\,A_c}{\dot{m}_{i,\,j}/\,A_{i,\,j}}\right)^2 \quad (-) \tag{4.52}$$

where

$$\dot{m}_c = \dot{m}_{i,\,j} + \dot{m}_{k,\,j} \quad (kg/s) \tag{4.52a}$$

$$\rho_c = \rho_j \quad (kg/m^3) \tag{4.52b}$$

(3) then the local loss factor $C_{i,\,j}$ is added to the sum of all other local loss factors ΣC_i of conduit $i-j$
(4) and now the algorithm can proceed as if it where a type 210 general flow conduit

4.4.8.2. Conduit starting in diverging 3-leg junction (type 230)

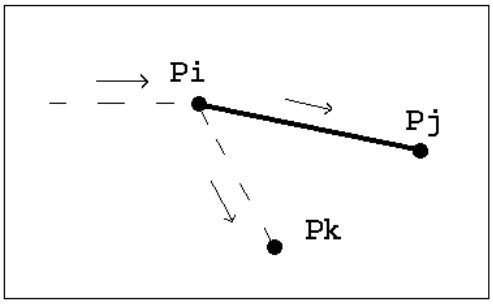

Figure 4.8 Conduit starting in diverging 3-leg junction

This type of flow component is schematically drawn in Figure 4.8. The conduit type component links node i and node j but also comprises the dynamic local losses of either the "straight" or the branch flow path of the junction. The other exit of the junction is represented by the conduit component linking node i with node k; so a type 230 component incorporates only one half of the junction. It is assumed that there is **only one connection** between node **i** and node **j**, and between node **i** and node **k** respectively. Furthermore the flow directions are assumed to be as indicated in the figure. If, during simulation, the flow is in the other direction, a warning message will be issued.

In addition to the parameters describing the flow/pressure relationship for the conduit itself (which have the same meaning as in case of a general flow conduit (see Section 4.4.7. (type 210))) the following component description data is needed:

a_0 to a_5	fit coefficients describing $C_{c,\,p} = f(\dot{q}_p/\dot{q}_c\ ,\ \dot{q}_{p'}/\dot{q}_c)$; subscript p refers to the junction section under consideration and subscript p' refers to the other exit of the junction
A_c	cross-sectional area of the common flow path (m^2)

For this component type, the same remarks and comments apply which were made for the type 220 component. Obviously, the calculation algorithm is also similar to that of a type 220 component. The only differences are:

$$\dot{q}_{p'} = \dot{m}_{i,\,k}/\rho_i \quad (m^3/s) \tag{4.53a}$$

$$\dot{m}_c = \dot{m}_{i,\,j} + \dot{m}_{i,\,k} \quad (kg/s) \tag{4.53b}$$

$$\rho_c = \rho_i \quad (kg/m^3) \tag{4.53c}$$

In case either $\dot{m}_{i,\,j} \leq 0$ or $\dot{m}_{i,\,k} < 0$, the local loss factor for this junction $C_{i,\,j}$ is set to zero.

4.4.8.3. Conduit ending in converging 4-leg junction (type 240)

This type of flow component is schematically drawn in Figure 4.9. The conduit type component links node i and node j but also comprises the dynamic local losses of either the

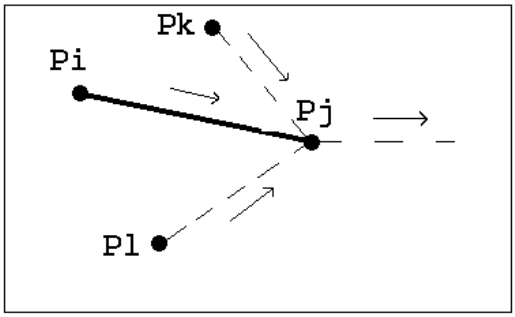

Figure 4.9 Conduit ending in converging 4-leg junction

"straight" or one of the branch flow paths of the junction. The other entrances of the junction will have to be represented by the conduit components linking node k with node j and node l with node j respectively; so a type 240 component incorporates only a part of the junction. It is assumed that there is **only one connection** between node **i** and node **j**, between node **k** and node **j** and between node **l** and node **j** respectively. Furthermore the flow directions are assumed to be as indicated in the figure. If, during simulation, the flow is in the other direction, a warning message will be issued.

The general formulation of the local loss factor $C_{c,\,p}$ for this type of flow component is:

$$C_{c,\,p} = a_0 + a_1\left(\frac{\dot{q}_p}{\dot{q}_c}\right) + a_2\left(\frac{\dot{q}_p}{\dot{q}_c}\right)^2 + a_3\left(\frac{\dot{q}_{p'}}{\dot{q}_c}\right) + a_4\left(\frac{\dot{q}_{p'}}{\dot{q}_c}\right)^2 + a_5\left(\frac{\dot{q}_p}{\dot{q}_c}\cdot\frac{\dot{q}_{p'}}{\dot{q}_c}\right) \quad (4.54)$$

$$+ a_6\left(\frac{\dot{q}_{p''}}{\dot{q}_c}\right) + a_7\left(\frac{\dot{q}_{p''}}{\dot{q}_c}\right)^2 + a_8\left(\frac{\dot{q}_p}{\dot{q}_c}\cdot\frac{\dot{q}_{p''}}{\dot{q}_c}\right) + a_9\left(\frac{\dot{q}_{p'}}{\dot{q}_c}\cdot\frac{\dot{q}_{p''}}{\dot{q}_c}\right) \quad (-)$$

In addition to the parameters describing the flow/pressure relationship for the conduit itself (which have the same meaning as in case of a general flow conduit (see Section 4.4.7. (type 210))) the following component description data is needed:

a_0 to a_9	fit coefficients describing $C_{c,\,p} = f(\dot{q}_p/\dot{q}_c\,,\,\dot{q}_{p'}/\dot{q}_c\,,\,\dot{q}_{p''}/\dot{q}_c)$; subscript p refers to the junction section under consideration, and subscripts p' and p'' refer to the other entrances of the junction. p' is defined by the first supplementary linkage data item, and p'' is defined by the second item
A_c	cross-sectional area of the common flow path (m^2)

For this component type, the same remarks and comments apply which were made for the type 220 component. Also, the calculation algorithm is quite similar to that of a type 220 component. The main differences are:

$$\dot{q}_{p'} = \dot{m}_{k,\,j}/\rho_k \quad (m^3/s) \qquad (4.55a)$$

$$\dot{q}_{p''} = \dot{m}_{l,\,j}/\rho_l \quad (m^3/s) \qquad (4.55b)$$

$$\rho_c = \rho_j \quad (kg/m^3) \tag{4.55c}$$

$$\dot{m}_c = \dot{m}_{i,j} + \dot{m}_{k,j} + \dot{m}_{l,j} \quad (kg/s) \tag{4.55d}$$

In case either $\dot{m}_{i,j} \leq 0$, $\dot{m}_{k,j} < 0$, or $\dot{m}_{l,j} < 0$, the local loss factor for this junction $C_{i,j}$ is set to zero.

4.4.8.4. Conduit starting in diverging 4-leg junction (type 250)

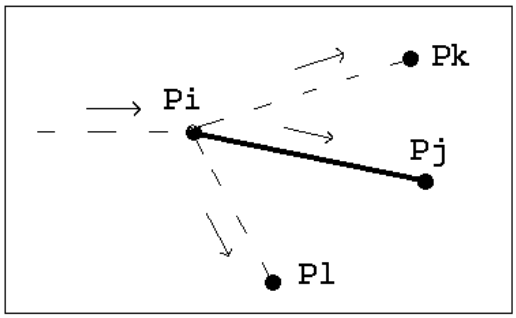

Figure 4.10 Conduit starting in diverging 4-leg junction

This type of flow component is schematically drawn in Figure 4.10. The conduit type component links node i and node j but also comprises the dynamic local losses of either the "straight" or one of the branch flow paths of the junction. The other exits of the junction will have to be represented by the conduit components linking node i with node k and node i with node l respectively; so a type 250 component incorporates only a part of the junction. It is assumed that there is **only one connection** between node **i** and node **j**, between node **i** and node **k** and between node **i** and node **l** respectively. Furthermore the flow directions are assumed to be as indicated in the figure. If, during simulation, the flow is in the other direction, a warning message will be issued.

In addition to the parameters describing the flow/pressure relationship for the conduit itself (which have the same meaning as in case of a general flow conduit (see Section 4.4.7. (type 210))) the following component description data is needed:

a_0 to a_9	fit coefficients describing $C_{c,p} = f(\dot{q}_p/\dot{q}_c\ ,\ \dot{q}_{p'}/\dot{q}_c\ ,\ \dot{q}_{p''}/\dot{q}_c)$; subscript p refers to the junction section under consideration, and subscripts p' and p'' refer to the other exits of the junction. p' is defined by the first supplementary linkage data item, and p'' is defined by the second item
A_c	cross-sectional area of the common flow path (m^2)

For this component type, the same remarks and comments apply which were made for the type 220 component. Also, the calculation algorithm is quite similar to that of a type 220 component. The main differences are:

$$\dot{q}_{p'} = \dot{m}_{i,k}/\rho_i \quad (m^3/s) \tag{4.56a}$$

$$\dot{q}_{p''} = \dot{m}_{i,l}/\rho_i \quad (m^3/s) \tag{4.56b}$$

$$\rho_c = \rho_i \quad (kg/m^3) \tag{4.56c}$$

$$\dot{m}_c = \dot{m}_{i,j} + \dot{m}_{i,k} + \dot{m}_{i,l} \quad (kg/s) \tag{4.56d}$$

In case either $\dot{m}_{i,j} \leq 0$, $\dot{m}_{i,k} < 0$, or $\dot{m}_{i,l} < 0$, the local loss factor for this junction $C_{i,j}$ is set to zero.

4.4.9. General Flow Inducer Component (type 310)

Due to practical reasons (ie. lack of detailed data) fan or pump performance modelling is usually based on an empirical instead of on an analytical approach. According to Wright and Hanby (1988), for system simulation studies an empirical model of fan performance based on experimentally determined fan performance data is most appropriate. There seems to be no reason why this would not be true for pumps as well. Fan or pump performance is usually characterized by a performance curve such as shown in Figure 4.11. This curve relates the total *pressure rise* to the volume flow rate for a given fan/pump speed and fluid density.

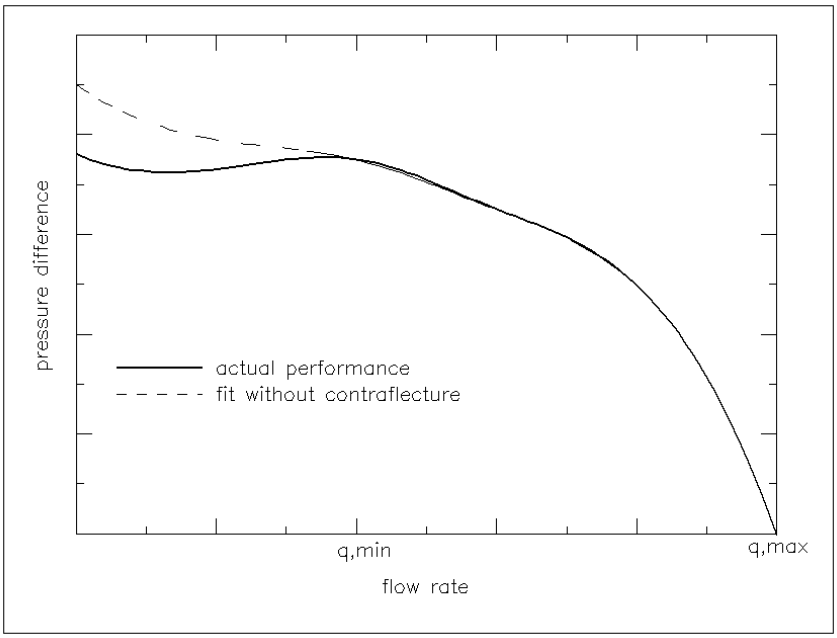

Figure 4.11 Schematic pump or fan performance curve

In principle there are a number of empirical fan or pump models possible. One of the simplest pressure - flow rate relationships incorporates only two empirical constants, but is nevertheless capable of giving an approximation to the general shape of the fan or pump characteristic:

$$\Delta P = P_{\max} - a\left(\frac{\dot{m}}{\rho}\right)^2 \quad (Pa) \tag{4.57}$$

where $P_{\max}$ (Pa) is the pressure rise at zero flow, and a is a fit coefficient $(Pa/(m^3/s)^2)$.

Other sources, e.g. ASHRAE (1975), suggest a more refined second-order polynomial of the form $\dot{m}(\Delta P)$. However, as suggested by Figure 4.11, the basic shape of the performance curve cannot be very well represented by a simple polynomial with ΔP as the independent variable (which would be preferable with respect to calculation of flow and partial derivative). Furthermore, as is also suggested by Figure 4.11, it is not uncommon for a performance curve to contain points of contraflecture, with up to three different flow rates possible at certain values of pump/fan pressure. This causes difficulty in solving for the flow rate and, more importantly, has points were the derivative $\partial\dot{m}/\partial\Delta P$ goes to infinity. In practice however, it is usually not recommended that the pump/fan operates in the region of the contraflecture points. Therefore, the flow characteristic may be modeled with a performance curve that does not include the contraflecture as long as it is checked that the pump/fan does not operate outside the flow region where the fan performance characteristic is valid.
In a type 310 general flow inducer component, a pump or fan performance curve is represented by a cubic polynomial:

$$\Delta P = a_0 + a_1\left(\frac{\dot{m}}{\rho}\right) + a_2\left(\frac{\dot{m}}{\rho}\right)^2 + a_3\left(\frac{\dot{m}}{\rho}\right)^3 \quad (Pa) \tag{4.58}$$

where

$$\dot{q}_{\min} \le \frac{\dot{m}}{\rho} \le \dot{q}_{\max} \quad (m^3/s) \tag{4.58a}$$

where ΔP is the total pressure rise across the component (Pa), a_i are fit coefficients ($Pa/(m^3/s)^i$), $\dot{q}_{\min}$ is the lower validity limit of the polynomial (m^3/s), and $\dot{q}_{\max}$ is the upper validity limit of the polynomial (m^3/s).

Note that the simple pressure/flow characteristic at the beginning of this section is a sub-set of the cubic polynomial. Also note that in case of a flow inducer ΔP stands for *pressure rise*, where ΔP stands for pressure drop with all other component types. If during the simulation the flow rate is outside the validity range, a warning is issued; the polynomial is still used however. The equation above requires an iterative approach to determine the mass flow rate for a given pressure difference. In this case, a fail-safe combination is used of bisection method (slow but safe) and Newton-Raphson method (simple and fast). In this hybrid approach a bisection step is taken whenever N-R would take the solution out of bounds, or whenever N-R does not reduce the size of the brackets (ie. bounds of bisection search interval which encloses the root) rapidly enough (see also Press et al. 1986). There is some difficulty in finding the initial brackets of the root. Here, we choose the interval $\dot{q}_{\min} - \dot{q}_{\max}$. If this interval does not contain the root, the size of the interval is increased with $(\dot{q}_{\max} - \dot{q}_{\min})$ in alternating positive and negative direction until the root is bracketed. If the root cannot be bracketed in MAXIT interval enlargement steps, this probably means that there is no root at all (eg. when current $\Delta P > P_{\max}$ in case of the parabolic fan performance characteristic above). In that case a warning message is issued and the flow rate is set to $\dot{q}_{\min}$ if current $\Delta P > \Delta P_{\dot{q}_{\min}}$, and the flow rate is set to $\dot{q}_{\max}$ if current $\Delta P < \Delta P_{\dot{q}_{\max}}$. In case of the former and if the parabolic fan performance characteristic is used, a new problem occurs if $\dot{q}_{\min}$ equals zero. Then the partial derivative $\partial\Delta P/\partial\dot{m}$ will also be zero at $\dot{q}_{\min}$, and the Newton-Raphson method will not lead to a solution. Situations like this, may be avoided by choosing $\dot{q}_{\min}$ and $\dot{q}_{\max}$ such that $\partial\Delta P/\partial\dot{m} \neq 0$ for all $\dot{q}_{\min} \le \dot{q} \le \dot{q}_{\max}$.
After the root has been bracketed, the iteration procedure begins. The termination criteria of

the iteration process are user-defined by ERRMAX and FLOMAX.
The value of the fluid density ρ, depends on the type of fluid and on the temperature of the originating node. The partial derivative, in terms of pressure rise, is calculated from:

$$\frac{\partial \dot{m}}{\partial \Delta P} = \frac{1}{\partial \Delta P / \partial \dot{m}} = \frac{1}{a_1/\rho + 2a_2\dot{m}/\rho^2 + 3a_3\dot{m}^2/\rho^3} \quad (kg/s/Pa) \qquad (4.59)$$

4.4.10. General Flow Corrector Component (type 410)

A flow corrector - or variable flow resistance - is the actuating part of a flow control loop or mechanism. Variable valves and dampers are examples of flow correctors. Fixed valves and dampers on the other hand can simply be described by local dynamic loss factors in a flow conduit (see Section 4.4.7.).

The performance of valves and dampers can be described by their inherent characteristic† which states the relation between the valve/damper position (i.e. valve stem displacement or damper blade angle) and the flow rate (usually relative to the fully-open flow rate) through the valve/damper at a constant pressure drop over the valve.
It is common practice to express the inherent characteristic of a valve in terms of: (1) volume flow rate k_v of a fluid with density ρ_0; (2) at a constant pressure drop ΔP_0; (3) as a function (usually either linear or logarithmic) of the valve/damper position H, and the parameters:

k_{vs}	volume flow rate (m^3/s) when fully-open (ie. $H/H_{100} = 100\%$) and ρ_0 and ΔP_0
k_{v0}/k_{vs}	theoretical (according to linear or logarithmic characteristic) volume flow rate (%) at $H/H_{100} = 0\%$ and ρ_0 and ΔP_0
k_{vr}/k_{vs}	lower validity limit (%) of the theoretical flow rate characteristic for ρ_0 and ΔP_0. When $k_v/k_{vs} \le k_{vr}/k_{vs}$ the characteristic is linearized towards the origin, ie. $k_v/k_{vs} = H/H_{100} = 0$, as indicated in Figure 4.12.

This concept is usually only used for valves, in which case ρ_0 is the density of water with a temperature between $5°C$ and $30°C$ (ie. approx. 1000 kg/m^3), and ΔP_0 is usually 100 kPa. There seems to be no objection though to use this concept also for describing the inherent characteristic of a damper provided the corresponding fluid density (ρ_0) and pressure drop (ΔP_0) are also input parameters.

The mass flow rate through the valve/damper can now be calculated from:

$$\dot{m} = \rho k_v \left(\frac{\Delta P \, \rho_0}{\Delta P_0 \, \rho} \right)^{1/2} \quad (kg/s) \qquad (4.60)$$

in which for a linear characteristic:

† The actual control efficiency of an installed valve/damper depends not only on the inherent characteristic but also on the valve/damper authority. This is the ratio between the pressure drop over the valve/damper and the pressure drop over that part of the network in which the flow is controlled by the valve/damper. In contrast to many other calculation methods, the valve/damper authority is in the present context not an input parameter but rather a result of the simulation.

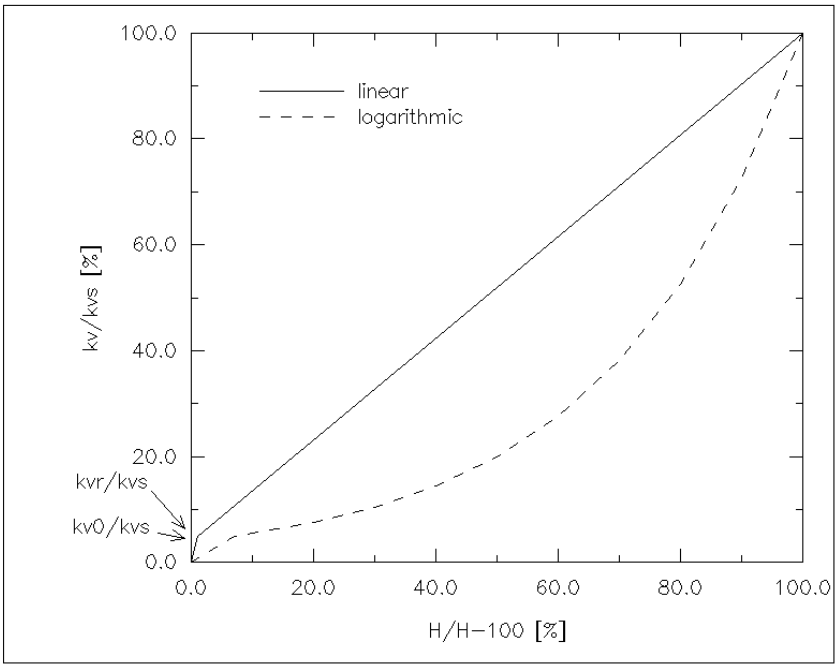

Figure 4.12 Relative volume flow rate k_v/k_{vs} through a valve/damper as a function of position H relative to fully-open position H_{100} at a constant pressure drop across the valve/damper; in this example k_{vr}/k_{vs} = 5 (%), k_{v0}/k_{vs} = 4 (%)

$$k_v = k_{v0} + n_{\ln} k_{vs} H/H_{100} \quad (m^3/s) \tag{4.60a}$$

$$n_{\ln} = 1 - k_{v0}/k_{vs} \quad (-) \tag{4.60b}$$

and for a logarithmic characteristic:

$$k_v = k_{v0} \exp(n_{lg} H/H_{100}) \quad (m^3/s) \tag{4.60c}$$

$$n_{lg} = \ln(k_{vs}/k_{v0}) \quad (-) \tag{4.60d}$$

In case $k_v < k_{vr}$, k_v is found by linear interpolation:

$$k_v = k_{vr} H/H_r \quad (m^3/s) \tag{4.60e}$$

where, in case of a linear valve/damper characteristic, H_r is found from:

$$H_r/H_{100} = (k_{vr} - k_{v0}) / (n_{\ln} k_{vs}) \quad (-) \tag{4.60f}$$

and in case of a logarithmic valve/damper characteristic, from:

$$H_r/H_{100} = \ln(k_{vr}/k_{v0}) / n_{lg} \quad (-) \tag{4.60g}$$

The value of the fluid density ρ, depends on the type of fluid and on the temperature of the originating node. The partial derivative for this fluid flow component is calculated from equation (4.36) unless ΔP is too small, in which case *mfs* switches to the numerical approximation of equation (4.28).

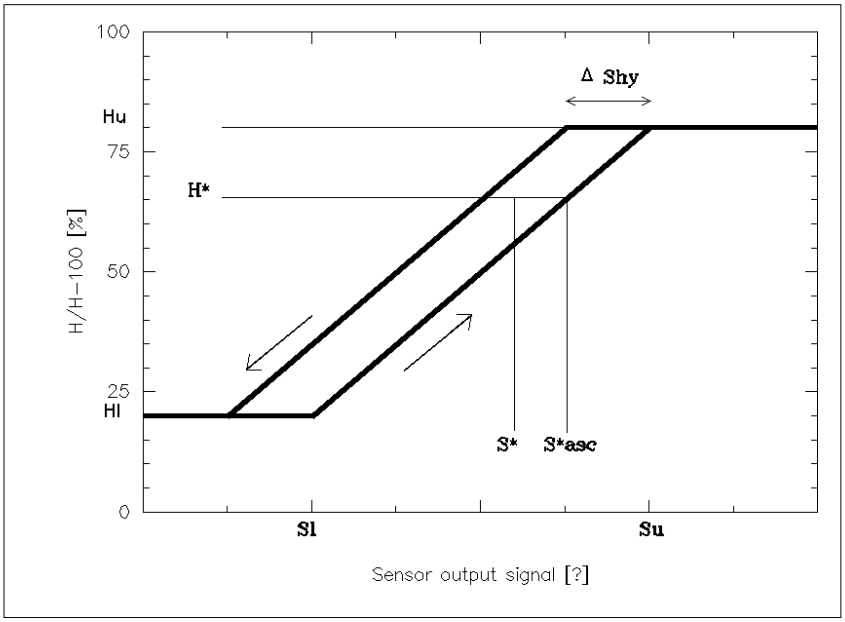

Figure 4.13 Relation between relative valve/damper position H/H_{100} and sensor output signal (see text)

The use of this flow corrector component as the actual actuator of a flow control mechanism, necessitates that there is also some input signal (originating from some sensor) and some control law which translates the sensor output into actuator input. The actuator control law available with this flow component type is schematically drawn in Figure 4.13; note that the actual flow control behaviour (ie. mass flow rate versus signal) also depends on the valve/damper characteristic, ie. linear or logarithmic.

Within this flow component type there are a number of control parameters on offer, through which a vast range of sensory input devices may be simulated. These parameters which define input signal and actuator behaviour (ie. relative valve/damper position H/H_{100} (valve stem displacement or damper blade angle)) are:
day type index indicating during which days the signal will be processed:

1	weekdays only;	2	Saturday only;	3	Sunday only
4	Saturday + Sunday;	5	weekdays + Saturday;	6	weekdays + Sunday
7	every day				

start hour of day period during which the signal will be processed
finish hour of day period during which the signal will be processed
position outside period indicating which value (%) will be assigned to the relative valve/damper position H/H_{100} during times outside the period defined above; ie. if set to 100% then the valve/damper will be fully-open outside the control period

sensed property index indicating the origin and dimension of the controlling signal:

0	sensor type and sensor location will be defined through *bps*'s building and plant configuration control file. In this way it is for example possible to simulate simultaneously the thermal and hydraulic behaviour of a thermostatic valve. This option is only available with *bps*'s incorporated version of *mfs*
1**	nodal temperature (perhaps outside temperature) T_{n1} ($^{\circ}C$)
2***	signed nodal temperature difference $T_{n1} - T_{n2}$ (K)
3***	absolute nodal temperature difference $\lvert T_{n1} - T_{n2} \rvert$ (K)
4**	nodal pressure P_{n1} (Pa)
5***	signed nodal pressure difference $P_{n1} - P_{n2}$ (Pa)
6***	absolute nodal pressure difference $\lvert P_{n1} - P_{n2} \rvert$ (Pa)
7***	signed mass flow rate in the connection from node $n1$ to $n2$ (kg/s)
8***	absolute mass flow rate in the connection from node $n1$ to $n2$ (kg/s)
9	wind speed (m/s)
10	wind direction (degrees clockwise from North)
11	diffuse horizontal solar radiation (W/m^2)
12	direct normal solar radiation (W/m^2)
13	relative humidity of outdoor air ($\%$)
*	the sequence number of the corresponding plant control loop is input as the first supplementary item to the linkage data of the connection incorporating the valve/damper
**	node name $n1$ is input as the first supplementary item to the linkage data of the connection incorporating the valve/damper
***	node names $n1$ and $n2$ are the 1st and 2nd supplementary items to the linkage data of the connection incorporating the valve/damper

signal lower limit S_l (SU ie Sensor Units) when the signal is less than this value, the relative valve/damper position will be fixed at:

relative valve/damper position "lower" value H_l (%)†

signal upper limit S_u (SU) ($S_u \geq S_l$); when the signal is above this value, the relative valve/damper position will be fixed at:

relative valve/damper position "upper" value H_u (%).† Note that $H_u \leq H_l$ is allowed

hysteresis ΔS_{hy} (SU); signal difference necessary to overcome the controller's hysteresis (see Figure 4.13)

Note that the flow corrector itself does not have inertia properties. The inertia properties of a complete flow control mechanism originate primarily from the sensor (eg. the time constant of a thermostatic valve depends primarily on the thermal resistances and heat capacities of the sensing element and its casing). Inertia related phenomena may be studied by simultaneous simulation of mass and heat flow. This can be achieved by invoking *mfs* from within *bps*.

† Note: (1) by assigning appropriate values to H_l and H_u a valve/damper either opens or closes when the signal value increases; (2) if H_l and H_u are not set to 0% and 100% (or the other way around) the valve/damper will never be fully closed and/or opened during the control period.

The general flow corrector solution algorithm now functions as follows:

(1) it is checked whether the current time step lies inside the defined control period; if not then H/H_{100} is set to the *position outside period* and the algorithm proceeds with step (5)

(2) depending on the sensed property index, the current signal value S is established

(3) suppose the previous value of H/H_{100} is denoted H^*, and the intersection of H^* with the ascending path of the relationship $H/H_{100} = fie(S)$ is called S^*_{asc} (see Figure 4.13) then:
if $(S^*_{asc} - \Delta S_{hy}) < S < S^*_{asc}$ then H/H_{100} is set to H^* else
if $S < (S^*_{asc} - \Delta S_{hy})$ then H/H_{100} is found from intersection of S with the descending path of $H/H_{100} = fie(S)$, else
$S > S^*_{asc}$ and H/H_{100} is found from intersection of S with the ascending path.

(4) H^* is reset to current H/H_{100} and if there was a change in H/H_{100}, S^*_{asc} is recalculated

(5) H/H_{100} is now known and is used to calculate k_v and subsequently the mass flow rate $\dot{m}$

4.4.11. Flow Corrector with Polynomial Local Loss Factor (type 420)

A special case of a valve/damper is one which may be described in terms of a variable dynamic local loss factor C; ie. the valve/damper is approached as if it were a conduit with local dynamic losses dependent on the correctors relative position (eg. valve stem displacement or damper blade angle). The mass flow rate through such a flow corrector is calculated from:

$$\dot{m} = A\left(\frac{2\rho\Delta P}{C}\right)^{1/2} \quad (kg/s) \tag{4.61}$$

with

$$C = a_0 + a_1 H/H_{100} + a_2(H/H_{100})^2 + a_3(H/H_{100})^3 \quad (-) \tag{4.61a}$$

where A is the area of the section containing the corrector (m^2), C is a factor representing local dynamic losses (-), H/H_{100} is the relative valve/damper position (-), and a_i are fit coefficients (-).

The value of the fluid density ρ, depends on the type of fluid and on the temperature of the originating node. The partial derivative for this fluid flow component is calculated from equation (4.36) unless ΔP is too small, in which case *mfs* switches to the numerical approximation of equation (4.28).

It is obvious that the use of this flow corrector component as the actual actuator of a flow control mechanism, necessitates that there is also some input signal (originating from some sensor) and some control law which translates the sensor output into actuator input. Therefor, this component offers the same features and follows the same solution strategy, with respect to signal handling and actuator behaviour (ie. relative valve/damper position), as the general flow corrector component (type 410) described in the previous section.

4.4.12. Ideal (Frictionless) Open/Shut Flow Controller (type 450)

To be able to exert logical control over some individual component or over a part of a flow network, *mfs* offers an ideal (ie. frictionless) open/shut flow controller. Its behaviour in terms of mass flow rate and pressure difference is described by:

$$\dot{m} = 0 \quad (kg/s) \qquad \text{or} \qquad \Delta P = 0 \quad (Pa) \tag{4.62}$$

Due to the calculation algorithms (which are based on calculation of the flow for a given pressure difference) the latter expression cannot be employed directly. So internally, and hidden from the user, $\Delta P = 0$ is actually achieved by assuming a power law relationship describing a very low flow resistance.

The actual behaviour of this flow controller type (ie. when it is open or shut), is described by a number of user-definable parameters, through which a vast range of either real or imaginary sensory input devices may be simulated:

day type index indicating during which days the signal will be processed; see previous section for index definition

start hour of day period during which the signal will be processed

finish hour of day period during which the signal will be processed

position outside period defines whether the controller is open(1) or shut(0) outside the period defined above

sensed property index defining the origin and units of the controlling signal S; see previous section for index definition

signal set point S_{sp} (?);

position inside period defines whether the controller is open(1) or shut(0) when $S \geq S_{sp}$ inside the control period defined above

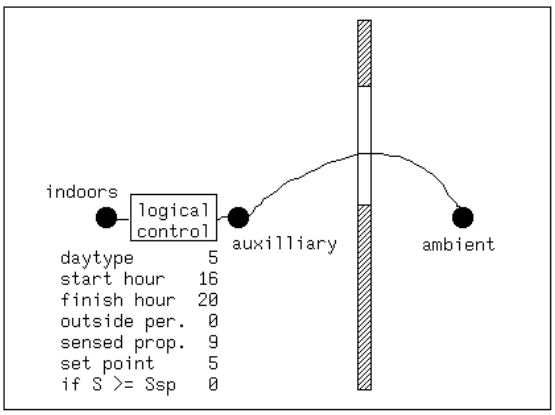

Figure 4.14 Diagrammatic arrangement of logical control over a window

As an example, suppose we want to simulate air flow between a building zone and outside through a window which is only opened during weekdays and Saturdays, after 15:00 and until 20:00 provided that the wind speed is less than 5 (m/s). This may be achieved by introducing three nodes and two components (representing the *open* window and the controller) as schematically drawn in Figure 4.14. By introducing an additional logical controller and linking this parallel to the first logical controller, *alternative* control laws are

achieved (ie. controller opens if either first law is true *or* the second one is true). By linking an extra logical controller in series, an *additive* control law is achieved (ie. opens if first law is true *and* second one is true).

4.5. COUPLING OF FLUID FLOW SIMULATION AND ESP^{R}

As indicated in Section 4.3., the fluid flow simulation module *mfs* may be used in stand-alone mode (which assumes that flows are predominantly pressure driven) or as an integral part of *bps* (for simulation of coupled heat and mass flow). To achieve the latter, copies of a major part of the *mfs* software are also incorporated in two main modules of the *ESP^{R}* system:†

imp

imp, *ESP^{R}*'s main *input management program*, allows interactive definition of the building and/or plant configuration which is to be subjected to indoor and outdoor boundary conditions and simulated over time.
To comply with the *imp* philosophy of handling all data preparation, *imp* was extended with a subroutine which drives *mfs*'s problem description subroutines. This driver fills the valid fluid flow component type arrays, assigns the problem description file and initiates the fluid flow network description process.

bps

bps, *ESP^{R}*'s main *building and plant simulation* engine, predicts building and/or plant heat and mass flows. The building/plant configuration is divided into a large number of finite volumes. Then, at each time step as a simulation proceeds, an energy and mass balance is applied for all volumes, giving rise to a differential matrix for the entire system. This is then solved by custom matrix processing software in terms of any user-imposed control objectives.

mfs's counterpart in *bps* may be invoked, through appropriate entries in the system configuration file, to handle the fluid flow simulation for the building and/or plant. For this, *bps* was extended with some driver subroutines:
- fluid mass flow network set up routine which: (1) opens and reads fluid flow related data files: wind pressure coefficients file and flow network problem description file; (2) checks fluid flow network problem description; (3) assigns flow results file; (4) sets iteration, stack calculation model, matrix solver and trace default values; and (5) initialises flow, derivative and pressure history variables
- fluid mass flow calculation control routine which for each simulation time step: (1) sets temperatures for nodes corresponding to building energy zones; (2) sets temperatures for nodes corresponding to plant energy components; (3) sets boundary nodes temperature and pressure; (4) solves the fluid flow network mass balances; (5) transfers flow simulation results to results file; and (6) invokes one or both of the following subroutines
- results conversion routine which transfers building side air flow results to the main energy simulation modules by calculating building zone infiltration and ventilation conductances,

† to ease the burden of re-creating the corresponding subroutines each time something changes in *mfs*, *imp* and *bps* each have a utility script which automates this updating task

and adjusting the building zones moisture balance information array. The latter array holds essentially fluid flow rates and moisture content of the air being transported. To be able to fill the zonal air flow moisture balance information array it is necessary to know the air moisture content x_j at each fluid flow network node (ie. including those nodes which do not correspond to a building zone). For this, it is assumed that the water vapour is distributed through the network proportional to the air mass flow (ie. disregarding any moisture storage effects for the time being). Then for each node j, a linear equation can be set up:

$$x_j = \sum_{i=1}^{n} \dot{m}_i{}^{+} x_i \,/\, \sum_{i=1}^{n} \dot{m}_i{}^{+} \quad (kg/kg) \tag{4.63}$$

where n denotes the number of nodes connected to node j, and $\dot{m}_i{}^{+}$ is the mass flow rate from node i to node j (only 'positive' air flow is taken into account; ie. only receiving nodes). In case node j represents outdoor air or a building zone, the moisture content is obviously known. The relations above can be combined into the matrix equation:

$$\mathbf{A}\,\mathbf{x} = \mathbf{b} \tag{4.64}$$

where $\mathbf{A}$ is a matrix holding the mass flow 'weight' coefficients, $\mathbf{x}$ is the unknown nodal moisture content vector, and $\mathbf{b}$ is a vector holding the known nodal moisture contents. This matrix equation is solved by the LU decomposition method as described in Section 4.3.3.

- results conversion routine which transfers plant side fluid flow results to the main energy simulation modules by assigning fluid mass flows to plant component inter-connections. This will be elaborated in Section 5.2

Kohonen and Virtanen (1987) pointed out that when air flows through cracks in the building structure, there is some sort of "heat recovery effect". This results in heating of the infiltration air and reducing the heat loss by conduction through the building structure. This thermal coupling of leakage flow and building heat loss was not considered in the present work. Perhaps it might be recommendation for future work.

References

ASHRAE 1975. *Procedures for simulating the performance of components and systems for energy calculations*, American Society of Heating, Refrigerating and Air-Conditioning Engineers, New York. W.F. Stoecker (Ed.)

ASHRAE 1985. *Handbook of Fundamentals*, American Society of Heating, Refrigerating and Air-Conditioning Engineers, Atlanta, GA.

J.W. Axley 1990. Massachusetts Institute of Technology, Cambridge, MA. Private communication

P.H. Baker, S. Sharples, and I.C. Ward 1987. ''A study of domestic background leakage paths through the development of a portable pressurisation rig,'' Final report SERC Grant No. GR/C/51363, University of Sheffield.

Q. Chen 1988. ''Indoor airflow, air quality and energy consumption,'' Doctoral dissertation Delft University of Technology.

J.A. Clarke 1985. *Energy simulation in building design*, Adam Hilger Ltd, Bristol (UK). (ISBN 0-85274-797-7)

J.A. Clarke and D.J. McLean 1986. ‘‘ESP: A building and plant energy simulation system,’’ ESP Manual version 5 / release 3, University of Strathclyde, Glasgow.

J.A. Clarke and J.L.M. Hensen 1988. ‘‘Implementation of a new air flow equation solver in ESP,’’ University of Strathclyde, Energy Simulation Research Unit, ESRU report, Glasgow.

J.P. Cockroft 1979. ‘‘Heat transfer and air flow in buildings,’’ PhD thesis University of Glasgow.

S.D. Conte and C. de Boor 1972. *Elementary numerical analysis: an algorithmic approach*, McGraw-Hill, New York.

K. Häggkvist, U. Svensson, and R. Taesler 1989. ‘‘Numerical simulations of pressure fields around buildings,’’ *Building and Environment*, vol. 24, no. 1, pp. 65-72.

J.L.M. Hensen 1989. ‘‘Outcome of 1988 work-stay at the University of Strathclyde in Glasgow, Scotland,’’ collaborative FAGO/ESRU report 89.08.K, Eindhoven University of Technology.

I.E. Idelchick 1986. *Handbook of hydraulic resistance*, Springer Verlag, Berlin. E. Fried (Ed.), 2nd ed., rev. and augmented

ISSO 1986. ‘‘Luchtkanaalberekening,’’ ISSO-publikatie 17, Rotterdam.

R. Kohonen and M. Virtanen 1987. ‘‘Thermal coupling of leakage flows and heating load of buildings,’’ in *ASHRAE Transactions*, vol. 93:2, pp. 2303-2318, Atlanta, GA.

M.W. Liddament 1986. *Air infiltration calculation techniques - an applications guide*, IEA Air Infiltration And Ventilation Centre (AIVC), Bracknell (UK).

N.C. Markatos 1984. ‘‘Computer analysis of building ventilation and heating problems,’’ CHAM report, Concentration Heat and Momentum Ltd, London.

D.S. Miller 1971. *Internal flow: a guide to losses in pipe and duct systems*, British Hydromechanics Research Association, Fluid Engineering Centre, London.

D.S. Miller 1978. *Internal flow systems*, British Hydromechanics Research Association, Fluid Engineering Centre, London.

C.E.E. Pernot and J.L.M. Hensen 1990. ‘‘Adviezen inzake de kwaliteit van het binnenmilieu van de HeuvelGalerie te Eindhoven,’’ TPD-FAGO-RPT-90-42, p. 41, Eindhoven.

W.H. Press, B.P. Flannery, S.A. Teukolsky, and W.T. Vetterling 1986. *Numerical recipes : the art of scientific computing*, Cambridge University Press, Cambridge, MA.

E. Simiu and R.H. Scanlan 1986. *Wind effects on structures: an introduction to wind engineering*, Wiley-Interscience, Chichester (UK).

D.B. Spalding 1981. ‘‘A general purpose computer program for multi-dimensional one- and two-phase flow,’’ in *Mathematics and Computers in Simulation XXIII*, pp. 267-276, London.

G.N. Walton 1989. ‘‘Airflow network models forelement-based building airflow modelling,’’ in *ASHRAE Transactions 95:2*, pp. 613-620, American Society of Heating, Refrigerating and Air-Conditioning Engineers, Atlanta, GA.

G.N. Walton 1989. ‘‘AIRNET - A computer program for building airflow network modeling,’’ NISTIR 89-4072, National Institute of Standards and Technology,

Gaithersburg, MD.

G.N. Walton 1990. National Institute of Standards and Technology, Gaithersburg, MD. Private communication

J.A. Wisse and C.E.E. Pernot 1990. ‘‘Wind en thermisch comfort rondom en in de Heuvelgalerie te Eindhoven,’’ TNO-TPD rapport 15.002, Eindhoven.

J.A. Wright and V.I. Hanby 1988. ‘‘HVAC component specification: fans,’’ Energy conservation in buildings & community systems programme. Annex X : system simulation (S12), International Energy Agency. Operating agent: University of Liège

CHAPTER FIVE

PLANT SIMULATION

5.1. INTRODUCTION

As indicated in Chapter 3, energy simulation in the building context has until recently been focussed primarily on either the building side or on the plant side of the overall problem domain. In the former approach the influence of the plant system is more or less neglected by over-simplification of the plant. In that approach it is common practice to base the estimation of energy consumption on some presumed, imposed indoor air temperature profile. In the latter approach the complex building energy flow paths are usually grossly simplified, and the building (or each building zone) is commonly regarded as just another component which in this case imposes a thermal load on the plant.
This thesis starts from the principle that neither approach is preferable for the majority of problems associated with the thermal interaction of building structure and auxiliary system; both building and plant have to be approached on equal levels of detailedness or complexity.

As the building modelling part of the overall problem is already quite established (see Chapter 3), one of the the main focus points of the current research is plant simulation. An ASHRAE Task Group (ASHRAE 1975) formulated a definition of system (or plant) simulation applicable to "Energy Requirements for Heating and Cooling of Buildings" as:

> *"... predicting the operating quantities within a system (pressures, temperatures, energy- and fluid flow rates) at the condition where all energy and material balances, all equations of state of working substances, and all performance characteristics of individual components are satisfied."*

They also state that:

> *"It is essential that the dynamic characteristics of the building be considered in the calculation of the thermal loads, but the dynamic response of most systems is much more rapid than that of the building. For this reason a steady-state simulation of the system is adequate for most energy calculations."*

It should be noted that they implicitly assumed a time step of one hour. The ASHRAE Task Group further acknowledged that a future goal would require analysis of dynamic plant performance. The future has already arrived, judging from the consensus of opinion among the modelling community that dynamic modelling is necessary. Numerous evidence supporting this may be found in proceedings of related conferences (eg. CEC 1983, CEC 1987, CEC 1991, IBPSA 1989).
With respect to dynamic plant simulation techniques, two main approaches can be distinguished:

- the sequential modelling technique, in which each separate part of the system (building zone, single component, sub-system etc.) is represented by an equivalent input-output

relationship. These are connected to comprise the whole system in such a way that the output from one component is fed into the next as an input. For each simulation time step, computation then starts at a known boundary condition, followed by calculation of each subsequent (according to some prescribed path) component until the whole system is dealt with. Advantages of this method are: a mixture of modelling methods (analytical, numerical, internal look-up table, etc.) may be used for the different configuration components thus enabling piecemeal component model development from simple to more complex descriptions; and because of the highly modular structure it is relatively easy to add or change certain component models. There are however also a number of serious drawbacks. A sequential approach will cause problems when control dynamics are to be incorporated; when the evaluation of one component needs information of a component further down the calculation stream; and usually also when there are recirculating loops in the system. Different component linking protocols and iterative solution techniques are used to minimize this kind of problems.

- the simultaneous modelling technique, which involves representation of plant parts (a part of a component, a component, a sub-system, etc.) by discrete nodal schemes and by the derivation of energy and mass flow equation sets which represent whole-system, inter-node exchanges over time and space dimensions. These equations are essentially time-averaged heat and mass conservation statements. The resulting plant matrix is then solved simultaneously for each simulation time step. The plant system matrix *is* the system linking protocol and so a number of the problems associated with the sequential approach are overcome.

Most contemporary system simulation models fall into the sequential modelling category. A well known example is TRNSYS (SEL 1988). It should be noted that - unless the networks are really simple - the sequential modelling technique is unable to cope with the kind of fluid flow problems as described in Chapter 4.
As described by Clarke (1985), it is the simultaneous modelling technique which is used by *ESP*^{R}. The present work is also based on this rather new development field, because the simultaneous technique has important advantages over the sequential technique. This will be elaborated in this chapter.

With respect to plant simulation, several modules of *ESP*^{R} are of importance: *plt* the plant only simulation module, *mfs* the fluid flow simulation module as described in Chapter 4, *sim* the building side energy simulation module, and *bps* the integrated building and plant simulation module with its encapsulated version of *mfs*. Furthermore there is *pdb* which allows a user to update a project's plant models database. Each of these modules were extended or enhanced in the present work.
What follows is a general description of how plant simulation is handled within *ESP*^{R}, and no distinction is made between the various plant simulation related modules. For more detailed information regarding the specifics of each, the reader is referred to (Clarke et al. 1991).

Figure 5.1 is a sketch of a combined building and plant configuration, consisting of two rooms, a hydronic heating system connected to one building zone, and an air heating system connected to the other building zone. These are the basic kind of systems on which the current research focuses. One possible solution with respect to the translation of the plant system into a nodal scheme for simultaneous plant modelling, is indicated by the dots. It is apparent that this scheme is quite different from the one in Figure 4.1., basically because

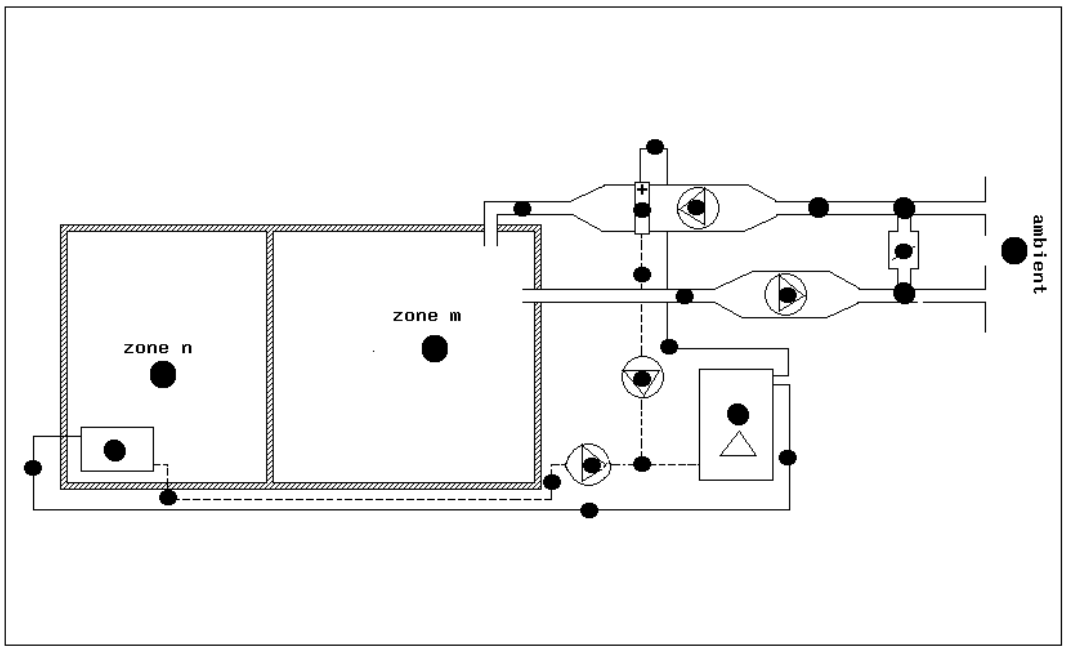

Figure 5.1 Diagrammatic example of a building and plant configuration; the dots indicate a possible nodal scheme for plant system network solution

here the nodes represent components while in the fluid flow network the connections represent components.
Section 5.2. describes how a plant system network may be defined from a user point of view. Section 5.3. describes the modular-simultaneous approach to plant simulation as adopted in the present work. Section 5.3. also indicates how the interaction with the mass flow solver of Chapter 4. is dealt with, and how the eventual plant simulation results may become available to the user.
At present, a number of numerical models are available for usage with this simultaneous plant modelling technique. These are elaborated in Section 5.4. The currently available features with respect to plant control are described in Section 5.5. Finally Section 5.6. describes how the plant matrix is then integrated with the multi-zone building matrix, subjected to any control function based on nodal condition statements, and the combined configuration matrix solved simultaneously and repeatedly as the model steps through its finite time increments.

5.2. PROBLEM DESCRIPTION

To apply the problem to be considered to the simulation system, the user has to define the building and/or plant configuration. Readers who are not yet interested in how this problem description is achieved, might want to skip the current section and continue with the next. How the problem may be described is best explained by elaborating the items in the so-called system configuration input file. Table 5.1 describes these items as far as the plant system is concerned.

Table 5.1 Plant simulation related items of the building and/or plant configuration description file

Item Description
- Configuration type defining a building only, plant only or building & plant simulation - Site description - Name of project related plant components' database - Plant configuration title - Number of plant components, and required plant matrix type - For each component: configuration code number, database entry number, number of controlled variables and associated data array for each - Number of plant component inter-connections - For each inter-connection: component number and node number of receiving node, connection type, component number and node number of connected or referenced node, mass diversion ratio, and up to 2 supplementary data items - Number of plant component containments - For each containment: component number, containment type, and up to 3 supplementary data items - Plant fluid flow simulation index, and if fluid flow simulation required: name of file holding mass flow network description for the current building and/or plant configuration, name of file holding wind pressure coefficients, name of file to which mass flow results will be transferred, and finally for each plant component inter-connection receiving node, a mass flow network *connection* must be referenced

Most items will be self-explanatory, some might need some extra explanation. For instance the configuration type index, is a convenient feature to be able to use the same file for different purposes (eg simply changing the type would allow study of the performance of several plant system alternatives prior to the combined simulation of building & plant).

Site descriptive information could be necessary for calculation of solar radiation. Although it was not done in the present work, it is quite possible to incorporate components of active and passive solar systems, as has been demonstrated by McLean (1982)

When describing a plant network, it is necessary to decide on the number of different plant components. For example, a simple air heating system may be comprised of an inlet duct, supply fan, and heater. Or it may be considered necessary to append a return fan and various ducts to represent the distribution system. Once a decision has been made *pdb* must be used to examine and/or update the plant components database for the current plant configuration.

The plant matrix type indicates that energy only, energy plus one phase fluid, or energy plus two phase† fluid simulation is required. Energy only would be an appropriate option for plant simulations where there are no inter-component mass flows; for instance in case of de-centralized local heating appliances or in case of electric heating.
Energy plus one phase fluid simulation, would be appropriate for a simulation in which the plant system's working fluid is a single phase fluid (eg water or dry air). In this case two matrices are established for the plant network; one to represent the energy balance, the other to represent the fluid mass balance. This option might also be appropriate for a two phase

† Note that in the present context, two phase mass flow refers to a mixture of two fluids (ie dry air and water vapour), and **not** to a phase **changing** fluid

working fluid, in case there is no need for knowledge regarding the second phase fluid; for instance when in a particular application the water vapour distribution is not of interest and the second phase mass flow does not influence the energy balance nor the first phase mass balance.
Energy plus two phase fluid simulation is an appropriate choice in the case where moist air is (one of) the system working fluid(s). In this case three matrices will be established for the plant network; one for the energy balance, and one for each of the two phase mass balances
It should be noted that it is allowed to define a plant network which consists of several sub-networks, say for example one sub-network with water as the working fluid and one with moist air as the working fluid. The simulation type required then obviously needs to correspond to the most demanding sub-network; ie. the one for moist air in the previous example.
Of course, the installed mathematical models must be capable of generating the information required by the requested matrix type (see also Section 5.4). For example, it is possible to install an energy only plant component model in *bps* and then to request a mass balance for that component. Such a mis-match would be detected and disallowed

When a component model is formulated, it is defined which variables *may* be subjected to control action. For example, in a gas-fired water boiler model, the heat flux injected to the combustion chamber may be a selected control variable. When the configuration control file is established (see Section 5.5), a control loop may then be assigned to determine this variable on the basis of some sensed condition and active control law. In the event that such a loop is not established, each control variable associated with a component must be assigned a realistic value. Consider the case of an air heating coil. In a simple component model, the heat flux transferred to the air stream by the coil may be treated as a control variable. A control loop is then established, which in terms of some control system behaviour, acts to determine the required flux exchange to achieve some stable off-coil condition. If such a control loop is not set up, then the flux exchange will remain constant at the value assigned in the system configuration file as the default

Obviously the plant components have to be inter-connected. Section 5.4 will elaborate why connections are only defined for *receiving* nodes, and why the concept of mass diversion ratio was introduced. Note that in case of mass flow network simulation the mass diversion ratio will be obsolete.
Obviously, a node representing water may only be connected to another water node, and nodes representing air may only be connected to other air nodes. The supplementary data items depend on the connection type which defines that the receiving node is connected to: a component which is not participating in the configuration but which is - in terms of temperature and humidity ratio - identical to the current node, a component which is not participating in the configuration but whose conditions - in terms of temperature and humidity ratio - are known and constant, another participating component/node, or a building zone air point or the outdoor air.

The containment information defines the immediate boundary condition of a plant component. From this the component’s parasitic heat loss or heat gain will be established. For many components, the exchange of heat with the surroundings is negligible relative to the internal energy processes. For these components probably no containment information is required and no environmental interaction will take place. With other components a containment may be defined as: outdoor air temperature plus or minus some fixed difference, the temperature of a specified plant node adjusted by some fixed difference, a constant

temperature, or the temperature of a specified building zone air point or construction node. Only in the latter case heat loss from the plant is injected into the building or vice versa. For all other containment types the heat loss or gain to the environment is not balanced by a heat gain or loss for the "containing system".
Note that the connection between plant components and building zones - in terms of delivered plant energy - may be specified more comprehensive as part of the building zone control function as explained in Section 5.6.

The mass flow simulation index indicates whether or not mass flow simulation will be performed by the incorporated version of *mfs*. If not, the mass flow balance will be based on the previously mentioned mass diversion ratios.

5.3. CALCULATION PROCESS

5.3.1. Modular-Simultaneous Approach to Plant Simulation

The integration of building and plant matrices (representing building and plant node capacities and inter-node exchanges) for simultaneous processing, is greatly simplified if both employ a similar numerical technique. The simulation of building side energy flows is based on the finite difference method. For detailed information about this method and the specifics of applying the technique in *ESP*^{R}, the reader is referred to (Clarke 1985). In his thesis, Tang (1985) investigated different modelling techniques for plant side heat and mass flow. He concluded that the "control volume conservation, state-space approach" offers very good prospectives for simultaneous plant simulation. As this method blends well with the finite difference technique, the "control volume conservation, state-space approach" was also adopted for the present work.

Here, plant system modelling is achieved by a modular, component-wise approach. Each plant component model consists of one or more finite volume, state-space† equations, representing the conservation of heat and mass. The plant system is a combination of component models forming a complete set of state-equations for the whole system. At run time, each component has a corresponding subroutine whose mission is to generate the coefficients of these equations. This process is elaborated in Section 5.3.1 for the so-called basic plant component model. The plant matrices to result, the interaction with the mass flow network solver, the solution process, and the final results, are the subjects of the sections thereafter.

5.3.2. Basic Plant Component Model

Consider Figure 5.2 which shows a part of an imaginary plant consisting of three component/nodes which are linked by plant connections. Although each nodal region might only represent part of a component instead of a complete plant component, here they are called components for ease of argument. Following the control volume state-space approach, each node represents volume, mass and heat capacity of some plant component i.
Component i is linked to one or more other components j, $j+1$, etc. from which it *receives*

† in the current context, the *state* of a dynamic system is usually defined as "the minimum set of variables specified at initial time, $t = t_0$, which together with a given input, determine the state of the system at future time, $t > t_0$".

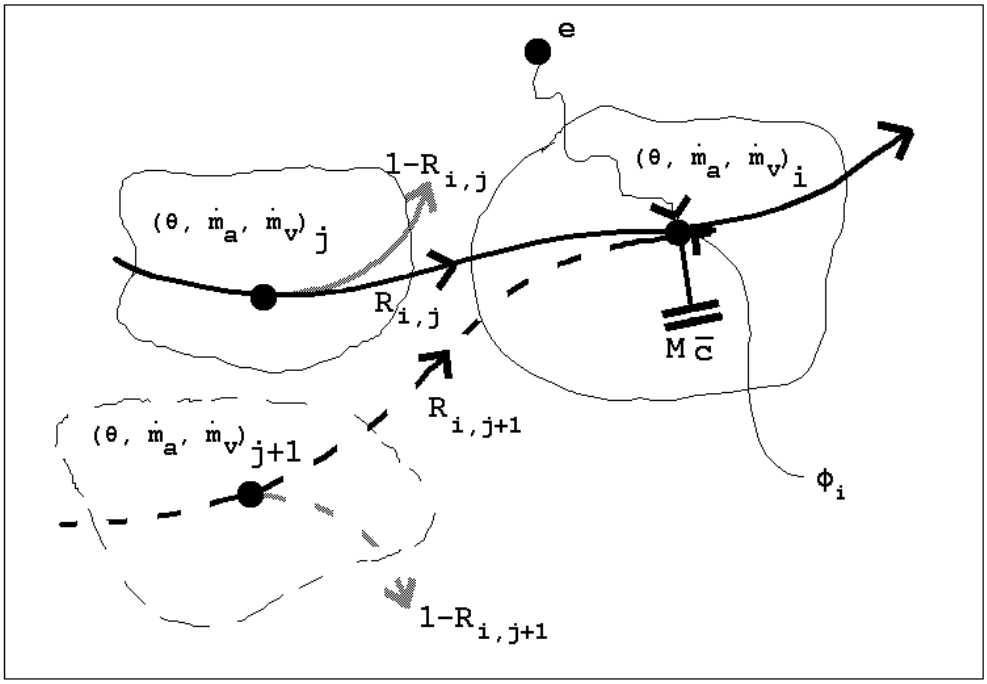

Figure 5.2 Diagrammatic state-space representation of an imaginary plant part or plant component with two external inlet connections to other plant components, internal heat generation and heat exchange with the environment

a mass flow, which is either a single phase fluid (in the present context water or dry air) or a fluid mixture incorporating two phases simultaneously (in the present context dry air and water vapour mixture). Component i might also be linked to an imaginary plant component with known state variable conditions, a building zone or to outdoor conditions. The details of these type of connections will be explained later. For now, only linkages to other plant components are assumed.

The states represented by the model nodes are: temperature θ, first phase mass flow rate $\dot{m}_a$ and second phase mass flow rate $\dot{m}_v$. Component i exchanges heat with the environment e, and there might be generation of heat ϕ.

The energy balance, at any point in time, for node i then yields:

$$\begin{aligned} & R_{i,j}\dot{m}_{a,j}c_{pa}(\theta_j - \theta_i) + R_{i,j}\dot{m}_{v,j}c_{pv}(\theta_j - \theta_i) \\ & + R_{i,j+1}\dot{m}_{a,j+1}c_{pa}(\theta_{j+1} - \theta_i) + R_{i,j+1}\dot{m}_{v,j+1}c_{pv}(\theta_{j+1} - \theta_i) \\ & + UA(\theta_e - \theta_i) + \phi_i + = \frac{\overline{c}_i M_i \partial\theta_i}{\partial t} \qquad (W) \end{aligned} \tag{5.1}$$

where $\dot{m}$ is the mass flow rate (kg/s), $R_{i,j}$ (≤ 1) denotes the ratio between the mass flow rate received by node i and the mass flow rate through node j[†], c_p is the fluid specific heat

[†] thus $R_{i,j}\dot{m}_j$ is the mass flow rate through connection i,j. The concept of (actual or desired) mass diversion ratios $R_{i,j}$ is introduced to enable calculation of mass flows via the various paths through the plant system network in those cases were we are unable or were it is not feasible to specify an actual mass flow

capacity ($J/kg\ K$), θ is the nodal temperature ($^{\circ}C$), U is the component's total heat loss coefficient (W/m^2K) (from node i to the environment) and A the corresponding area (m^2), ϕ_i represents any heat generated and released at node i, $\overline{c}$ is the component's mass weighted average specific heat capacity ($J/kg\ K$), and M is the component's total mass (kg). The subscripts refer to: a for air, e for environment, i, j and $j+1$ for the respective components, and v for water vapour.
In the present example, the component is represented by a single node. Therefore the component thermal capacity has to be expressed as a function of the average component state which is represented by the nodal temperature and - in case of two phase fluid flow - the ratio between second and first mass flow rate (ie. the humidity ratio) for that node. In case of a multi-node component representation, the heat capacity of each separate component region can be treated according to the nodal division of the total component. Such a refinement is demonstrated in the Section 5.4.4. For the current one-node model the average specific heat capacity $\overline{c}$ is the mass weighted average of the specific heat capacities of the N component (imaginary) parts such that:

$$\overline{c} = \sum_{j=1}^{N}(c_j M_j) / \sum_{j=1}^{N} M_j \quad (J/kgK) \tag{5.2}$$

It is assumed that the mass flow diversion ratio R is identical for both mass flow phases. In case of a two phase working fluid like moist air, this implies that the ratio between the two phases (ie. humidity ratio) is equal in each branch after a diversion. In case the working fluid is a single phase fluid (like for instance - in the present context - water), obviously all the above terms related to the second phase mass flow may be dropped. Likewise, the $j+1$ terms related to the second connection may be dropped in case component i receives mass flow from one other component only. In case there are more then two inlet connections, $j+2$, $j+3$ etc. terms will have to be introduced which will be similar to the $j+1$ terms. For ease of argument, the following assumes two phase mass flow and a plant component incorporating two "receiving" connections.

One of the possible methods to solve the partial differential heat equation (5.1) is by numerical approximation. In the present context we want to use the finite difference method for this because the same method is also used to solve the building side energy equations. An approximation for the unknown future time step temperature θ_i can be found from the fully implicit, finite difference formulation:

$$C_{i,j}(\theta_j - \theta_i) + C_{i,j+1}(\theta_{j+1} - \theta_i) + UA(\theta_e - \theta_i)$$
$$+ \phi_i \approx \frac{\overline{c}_i M_i(\theta_i - \theta_i^*)}{\Delta t} \quad (W) \tag{5.3a}$$

where

$$C_{i,j} = R_{i,j}\dot{m}_{a,j}c_{pa} + R_{i,j}\dot{m}_{v,j}c_{pv} \quad (W/K)$$

and where * denotes the current (known) time step. In its fully explicit formulation, and using the same symbols, equation (5.1) becomes:

---

network as discussed in Chapter 4.

$$C^*_{i,j}(\theta^*_j - \theta^*_i) + C^*_{i,j+1}(\theta^*_{j+1} - \theta^*_i) + UA^*(\theta^*_e - \theta^*_i)$$
$$+ \phi^*_i \approx \frac{\overline{c}_i M_i(\theta_i - \theta^*_i)}{\Delta t} \qquad (W) \tag{5.3b}$$

Weighted summation (with weight factor $\alpha \leq 1$) of equations (5.3a) and (5.3b) and rearrangement of the various terms into temperature related coefficients leads to:

$$\left[\alpha\,(-C_{i,j} - C_{i,j+1} - UA) - \frac{\overline{c}_i M_i}{\Delta t}\right]\theta_i$$
$$+ [\alpha\, C_{i,j}]\,\theta_j$$
$$+ [\alpha\, C_{i,j+1}]\,\theta_{j+1}$$
$$= \left[(1-\alpha)(C^*_{i,j} + C^*_{i,j+1} + UA^*) - \frac{\overline{c}_i M_i}{\Delta t}\right]\theta^*_i$$
$$+ [(1-\alpha)(-C^*_{i,j})]\,\theta^*_j$$
$$+ [(1-\alpha)(-C^*_{i,j+1})]\,\theta^*_{j+1}$$
$$+ [-\alpha\, UA\,\theta_e - (1-\alpha)UA^*\theta^*_e - \alpha\,\phi_i - (1-\alpha)\phi^*_i] \qquad (W) \tag{5.4}$$

The bracketed term in front of θ_i is called the self-coupling coefficient. The terms in front of θ_j and θ_{j+1} are called cross-coupling coefficients.

It is assumed here that both the component environment temperature θ_e and the generated heat ϕ_i can be evaluated independently. This allows these terms to be moved to the equation right-hand (ie. known) side. If θ_e or ϕ_i should relate to (other) component conditions, one way to handle this might be to make a first estimate based on previous time step values. Iteration might then be necessary to arrive at the final solution.

Depending on the value of α, equation (5.4) will be identical to the fully implicit formulation ($\alpha = 1$), the fully explicit formulation ($\alpha = 0$), or for instance the Crank-Nicolson formulation ($\alpha = 0.5$). Depending on the component time constant, the explicit formulation will only give a stable solution when the simulation time step is within certain limits. The implicit formulation gives an unconditionally stable solution for all time discretisation schemes. However, large time steps may lead to excessive discretisation errors. In the current program α is a user definable parameter. The default treatment is however, to switch dynamically - and for each component individually - between mixed implicit/explicit and fully implicit formulation depending on the simulation time step and on the component time constant (which both may change during the simulation period). This switching makes that if the simulation time step exceeds 63% of the time constant the fully implicit formulation is used ($\alpha \rightarrow 1$) for that component, otherwise the user specified mixed scheme will be enabled.
Another option for the user is to specify that the plant component state-space equations should be processed as in the steady-state case. This is simply achieved in the program by setting α - in equation (5.4) - equal to unity and M_i equal to zero.

When evaluating the time constant, the component is regarded as a first order resistance/capacitance model for which the time constant equals the product of "thermal resistance" (K/W) and "heat capacity" ($\overline{c}M$ in J/K). The "thermal resistance" is here defined as the ratio of temperature difference over heat transfer rate (which yields either $1/\dot{m}\,c_p$ or $1/UA$ depending on the nature of heat transfer). In case there is more than one heat flow path to the capacitance, one overall "thermal resistance" is found by combining the separate resistances as if they were parallel to each other. This approach yields the following expression for the time constant of component i:

$$\tau = \frac{\overline{c}_i M_i}{C_{i,j} + C_{i,j+1} + UA} \qquad (s) \tag{5.5}$$

It should be noted that evaluation of the time constant serves no other purpose than providing a criterion for the assessment of whether or not to enable the usage of the fully implicit versus the mixed implicit/explicit formulation.

Similar to the energy balance, a mass balance for component i can be derived. For the first and second phase mass flow separately, this yields:

$$\dot{m}_{a,i} - R_{i,j}\dot{m}_{a,j} - R_{i,j+1}\dot{m}_{a,j+1} = 0 \qquad (kg/s) \tag{5.6a}$$

$$\dot{m}_{v,i} - R_{i,j}\dot{m}_{v,j} - R_{i,j+1}\dot{m}_{v,j+1} = 0 \qquad (kg/s) \tag{5.6b}$$

In these equations, the so-called self-coupling coefficient is 1, and the cross-coupling coefficients are $-R_{i,j}$ and $-R_{i,j+1}$ respectively.

Since there is no mass inertia in the component these equations are - in contrast to the energy equation (5.1) - ordinary linear equations which are readily solvable by linear numerical methods. There is no need for mixed explicit/implicit formulation in order to find a good approximation for the future time step mass flow values, essentially because equations (5.6a) and (5.6b) are true for any point in time.

5.3.3. Establishing the Plant Matrices

To illustrate how simultaneous plant simulation is actually achieved, the process will now be elaborated starting from an imaginary example problem. This very simple plant system is schematically drawn in Figure 5.3 and consists of four inter-connected single-node components with mass diversion ratios as indicated. As can be seen, component 3 receives only 80% of the mass flow through component 2. The other 20% is "lost". The reason might be that the system leaks or that we are only interested in a certain part of a larger system. For ease of argument, only one component (no. 1) exchanges heat with the environment, and generation of heat is also limited to a single component (no. 3). This example system forms a closed loop and is not linked to say a room in a building. That these qualities are not essential will be explained later on in Section 5.6.

Using the generalized nodal energy balance equation (5.4), it is relatively easy to establish the overall system energy balance matrix equation for the system shown in Figure 5.3.

$$\mathbf{A} \cdot \theta = \mathbf{b} \tag{5.7}$$

The structure of this overall system energy balance matrix equation is schematically drawn in Figure 5.4.† With reference to this figure, the system energy balance equation for

† Note that in *ESP*^{R} the coefficients matrix **A** is actually not established and held as a two-dimensional

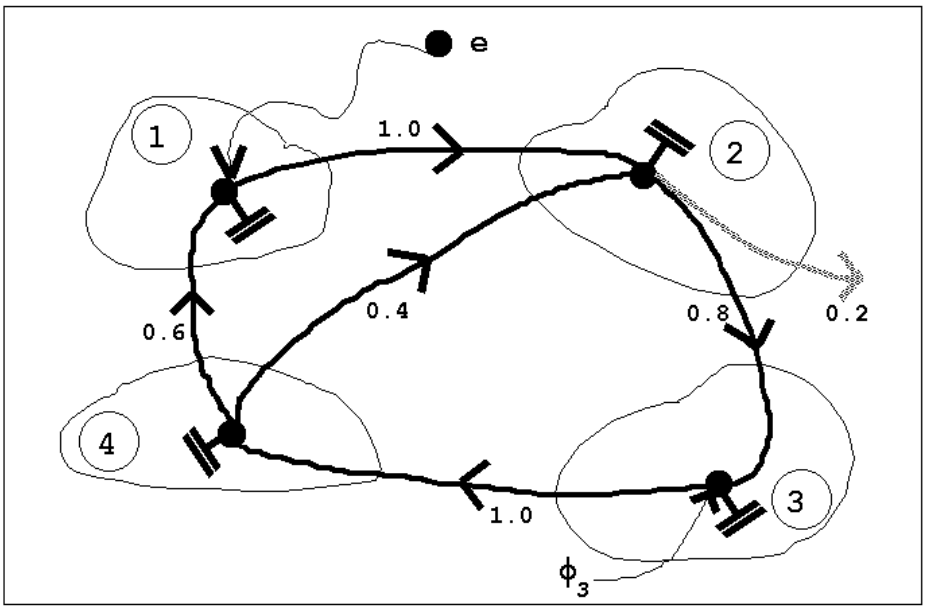

Figure 5.3 Diagrammatic imaginary plant system consisting of interconnected components with mass diversion ratios as indicated

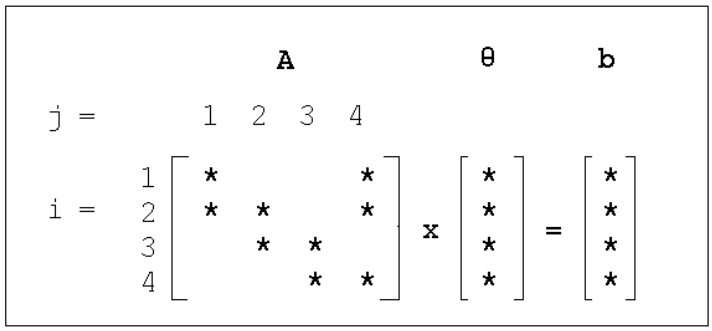

Figure 5.4 Plant system energy balance matrix equation $\mathbf{A} \cdot \theta = \mathbf{b}$

component 1 can be written as:

$$A_{11}\theta_1 + A_{14}\theta_4 = b_1 \qquad (W) \tag{5.7a}$$

where

$$A_{11} = \alpha\,(-C_{1,4} - UA_1) - \frac{\overline{c}_1 M_1}{\Delta t} \qquad (W/K)$$

$$A_{14} = \alpha\, C_{1,4} \qquad (W/K)$$

---

array since this may become very large depending on the application. Instead, two pointer vectors are created holding the addresses of each individual coefficient as they are stored in a one-dimensional array.

$$b_1 = [(1-\alpha)(C^*_{1,4} + UA^*_1) - \frac{\overline{c}_1 M_1}{\Delta t}]\ \theta^*_1 + [(1-\alpha)(-C^*_{1,4})]\ \theta^*_4 + [-\alpha\ UA_1\theta_e - (1-\alpha)UA^*_1\theta^*_e] \quad (W)$$

The system energy balance equation for component 2 becomes:

$$A_{21}\theta_1 + A_{22}\theta_2 + A_{24}\theta_4 = b_2 \quad (W) \tag{5.7b}$$

where

$$A_{21} = \alpha\ C_{2,1} \quad (W/K)$$

$$A_{22} = \alpha\ (-C_{2,1} - C_{2,4}) - \frac{\overline{c}_2 M_2}{\Delta t} \quad (W/K)$$

$$A_{24} = \alpha\ C_{2,4} \quad (W/K)$$

$$b_2 = [(1-\alpha)(C^*_{2,1} + C^*_{2,4}) - \frac{\overline{c}_2 M_2}{\Delta t}]\ \theta^*_2 + [(1-\alpha)(-C^*_{2,1})]\ \theta^*_1 + [(1-\alpha)(-C^*_{2,4})]\ \theta^*_4 \quad (W)$$

For component 3 the system energy balance equation is:

$$A_{32}\theta_2 + A_{33}\theta_3 = b_3 \quad (W) \tag{5.7c}$$

where

$$A_{32} = \alpha\ C_{3,2} \quad (W/K)$$

$$A_{33} = \alpha\ (-C_{3,2}) - \frac{\overline{c}_3 M_3}{\Delta t} \quad (W/K)$$

$$b_3 = [(1-\alpha)(C^*_{3,2}) - \frac{\overline{c}_3 M_3}{\Delta t}]\ \theta^*_3 + [(1-\alpha)(-C^*_{3,2})]\ \theta^*_2 + [-\alpha\ \phi_3 - (1-\alpha)\phi^*_3] \quad (W)$$

And finally for component 4 the system energy balance equation becomes:

$$A_{43}\theta_2 + A_{44}\theta_4 = b_4 \quad (W) \tag{5.7d}$$

where

$$A_{43} = \alpha\ C_{4,3} \quad (W/K)$$

$$A_{44} = \alpha\ (-C_{4,3}) - \frac{\overline{c}_4 M_4}{\Delta t} \quad (W/K)$$

$$b_4 = [(1-\alpha)(C^*_{4,3}) - \frac{\overline{c}_4 M_4}{\Delta t}]\ \theta^*_4 + [(1-\alpha)(-C^*_{4,3})]\ \theta^*_3 \qquad (W)$$

In case one of the components is not linked to another participating plant component, but to some imaginary plant part, a building zone, or to outdoor conditions, the temperature of the connected "node" can be assumed to be known. The terms - in the nodal energy balance equations - related to these known temperatures, may then be moved to the matrix equation known right hand side.

It is obvious that more complex plant systems will result in more complex matrix structures than the one indicated in Figure 5.4. Having mentioned this, for any system two possibilities exist for energy balance matrix solution:

- terms like ϕ_3 (ie. in general all internal component heat transfer quantities) in the "known" $\mathbf{b}$ vector may be assessed by independent component models on the basis of anticipated system performance requirement. An example of this approach can be found in Section 5.4.3.
- terms like ϕ_3 could be "removed" to the future time step side of the equation - $\mathbf{A} \cdot \theta$ - by expanding the single-node model into a multi-node model and introducing ϕ as a state-space variable. In the present context there are multi-node models available (see eg. Section 5.4.4), but introducing additional (ie. non θ, or $\dot{m}$) state-space variables is left for the future.

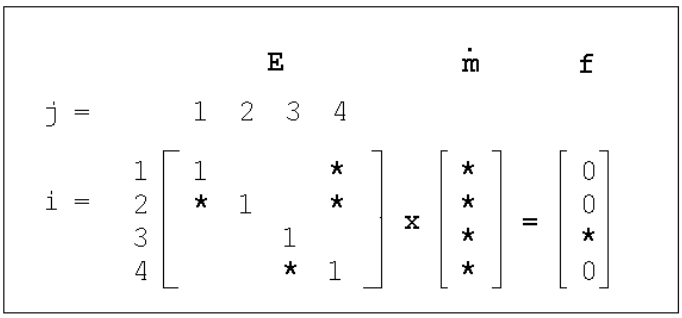

Figure 5.5 Plant system mass balance matrix equation $\mathbf{E} \cdot \dot{\mathbf{m}} = \mathbf{f}$

Similar to the formulation of the energy balance matrix, an overall system mass balance matrix can be derived. As first and second phase mass balance are both based on the same concept, the following description does not discriminate between the two phases. Again for the plant system shown in Figure 5.3, the general formulation of equations (5.6a) and (5.6b) form the basis for the overall system mass balance matrix equation:

$$\mathbf{E} \cdot \dot{\mathbf{m}} = \mathbf{f} \qquad (5.8)$$

This matrix equation is schematically drawn in Figure 5.5. In the present context, it is assumed that component 3 is a "source of mass" (ie. fan, humidifier, pump, etc. depending on the state variable of interest) which sets the mass flow rate through component 3 equal to $\dot{m}_{source}$ (kg/s), or - stated differently - which adjusts the incoming mass flow rate in a way

such that the nodal mass flow rate equals $\dot{m}_{source}$ (kg/s). Given the user specified "source of mass" and mass diversion ratios, solving the matrix equation (5.8) yields the mass flow through each component/node of the plant system. With reference to the general nodal mass balance equations (5.6a) and (5.6b) and to Figure 5.5, the system mass balance equation for component 1 becomes:

$$E_{11}\dot{m}_1 + E_{14}\dot{m}_4 = f_1 \qquad (kg/s) \tag{5.8a}$$

where

$$E_{11} = 1 \qquad (-)$$
$$E_{14} = -R_{1,4} \qquad (-)$$
$$f_1 = 0 \qquad (kg/s)$$

The system mass balance equation for component 2 can be written as:

$$E_{21}\dot{m}_1 + E_{22}\dot{m}_2 + E_{24} = f_2 \qquad (kg/s) \tag{5.8b}$$

where

$$E_{21} = -R_{2,1} \qquad (-)$$
$$E_{22} = 1 \qquad (-)$$
$$E_{24} = -R_{2,4} \qquad (-)$$
$$f_2 = 0 \qquad (kg/s)$$

For component 3 the system mass balance equation is:

$$E_{33}\dot{m}_3 = f_3 \qquad (kg/s) \tag{5.8c}$$

where

$$E_{33} = 1 \qquad (-)$$
$$f_3 = \dot{m}_{source} \qquad (kg/s)$$

Finally, for component 4 the system mass balance equation becomes:

$$E_{43}\dot{m}_3 + E_{44}\dot{m}_4 = f_4 \qquad (kg/s) \tag{5.8d}$$

where

$$E_{43} = -R_{4,3} \qquad (-)$$
$$E_{44} = 1 \qquad (-)$$
$$f_4 = 0 \qquad (kg/s)$$

It should be noted that by definition, a "source of mass" only affects the mass flow rate of itself and of plant components downstream of itself†. In case of a closed loop system (eg.

† The actual reason for this is, that also in case of a "source of mass" node, we only want to employ **one** balance equation. With two equations (ie. one for setting the source of mass, and one to couple the mass flow

the one in Figure 5.3) this effectively involves all other components in the system. However, when the system network incorporates an "open loop" (for example an air exhaust only system) or when it is "incomplete" (eg. when regarding only part of a larger system), the mass flow rate through the first component's inlet connection has to be available when this component is not a "source of mass" itself. To be able to handle these cases, the program has an option with which the first component - in the direction of flow - can be linked symbolically to some other component downstream from a "source of mass". This information link defines the first phase mass flow rate for the first component's inlet connection. The second phase mass flow rate for the first component's inlet connection is then calculated based on the ratio between second and first phase mass flow rate as given for that connection in question. In the present context this ratio is defined by the humidity ratio of some imaginary plant air node, of air in a building zone, or of outdoor air. For the second phase mass balance these connection's $\dot{m}_v$ is thus a known condition and may be moved to the matrix equation's right hand side.

5.3.4. Interaction with *mfs*

In case the user has specified that the plant system network corresponds to (part of) a mass flow network as described in Chapter 4., the *mfs* version incorporated version in *bps* (see Section 4.4.) is activated at each plant simulation time step. When the mass flow network has been solved for a certain plant time step, the mass flow results are transferred to the main energy simulation modules by assigning 1st phase fluid mass flows to plant component interconnections (ie. over-writing of the appropriate data array). The routine which does this, also checks whether flows are directed as expected (ie. the matrix coefficient generators implicitly assume mass flow rates ≥ 0). Then, in case of a two phase mass flow system, the second phase mass flow rate is adjusted so that the ratio between second and first phase mass flow rate (ie. humidity ratio) remains as it was.
As mentioned before, user mapping of plant system and mass flow network is based on plant component inter-connections versus mass flow network connections. This implies that after transferring the results, there might still be plant component nodes for which the mass flow rate is still unknown (eg. nodes in multi-node components which are not directly coupled to inter-component connections). For this reason the plant system mass balance matrix equation (5.8) is processed regardless whether the mass flow network solver is active or not.

5.3.5. Simultaneous Solution of the Plant Matrices

In principle it is possible to combine the plant energy balance matrix equation (5.7) with one or two mass balance matrix equations (5.8) into one overall matrix, which can then be solved simultaneously. In the current program this is not done. Instead the two or three matrix equations are solved one after the other. This approach has distinct advantages. The most noticeable are the considerable reduction of both memory requirement (ie. plant matrix dimension) and of matrix sparsity, and that - in terms of program coding - it is much easier to "administrate" three functionally different matrices. It should be recognised however that there might be a strong thermodynamic coupling between the different matrix equations. If a variable in one balance (say heat transfer due to condensation of water vapour) depends on a state variable solved from one of the other matrix equations (say the actual amount of

---

rate of the next node upstream), the "source of mass" node would indeed affect all other nodes in the plant system, but this would disrupt the matrix structure which is based on one equation per state-space variable and per node.

condensated water vapour), we have to ensure that both values match in order to find a true simultaneous solution of the plant matrices. This is achieved by enabling an iteration process in which each plant model variable which might be involved in inter-matrix-equation coupling is "marked" and its current value is stored. This is done by the appropriate matrix coefficient generator (see next section) for that specific plant model. After solving all plant matrix equations, the new value of each marked variable is compared with its stored value, and if either the absolute or the relative difference is smaller than some user-specified value (in units of temperature, heat flux or mass flow), the new values are accepted as future time step values otherwise the process restarts with the most recent calculated values for the marked variables.

The whole process of plant system matrix processing is schematically shown in Figure 5.6, the entries of which are briefly described in Table 5.2. It can be seen that the core tasks of the MZPMRX subroutine are performed repeatedly for each state-space variable type in the order: $\dot{m}_a$, $\dot{m}_v$, and θ respectively. The mass balances are solved prior to the energy balance because this usually gives a faster overall solution. The reason for this is that in general the dependency of energy balance on mass flow rates in the system is much stronger, than the other way around (ie. dependency of mass balance on system temperatures). As a connection is defined by temperature as well as by mass flow rate, the MZPADJ subroutine has to be called in each state variable loop.

As indicated in the diagram of Figure 5.6, the CONTRL subroutine - which handles the plant control - is by-passed in case the mass flow network solver is active and the first phase mass balance is being processed (ie. controls acting on the energy balance or on the second phase mass balance are not by-passed). By this mechanism it is assured that any mass flow control action which is defined and activated in the mass flow network is preserved in the plant system mass balance. For reasons already indicated above, the plant system mass balance matrix equation is set up (by MZPMSU) and solved (by MZPMSV; which offers the same matrix solvers as indicated in Section 4.2.3.) regardless whether the mass flow network solver is active or not.
After thus processing the mass and energy matrix equations, it is checked whether iteration is necessary by evaluating the difference between assumed value and final value of marked variables. If this difference for any marked variable exceeds the user specified tolerance, iteration is necessary. If so, the process restarts, else the results for the future time-row of the current plant simulation time step are stored (by MZNASS) as the present time-row values for the following plant time step and the program proceeds with the next time increment.

5.3.6. Results Handling

When the whole process of plant system matrix processing is completed for a certain simulation time step, all plant nodal states (ie. temperature, and first and second mass flow rate) are transferred to a user-specified plant results library. Besides all nodal states, this library will also receive for each plant simulation time step and for each plant component if applicable: the control data for that component, the overall heat loss of the component to the environment (ie. $\alpha\, UA(\theta_i - \theta_e) + (1-\alpha)\, UA^*(\theta_i^* - \theta_e^*)$, and any additional output variables for that component. The following sections indicate for each available plant component type whether that component type has any user-specifiable control parameters, and if that component has any additional output variables. The additional output variables are usually variables necessary for calculating the heat transfer inside the component, and may be of interest for the user when evaluating the performance of the plant system.

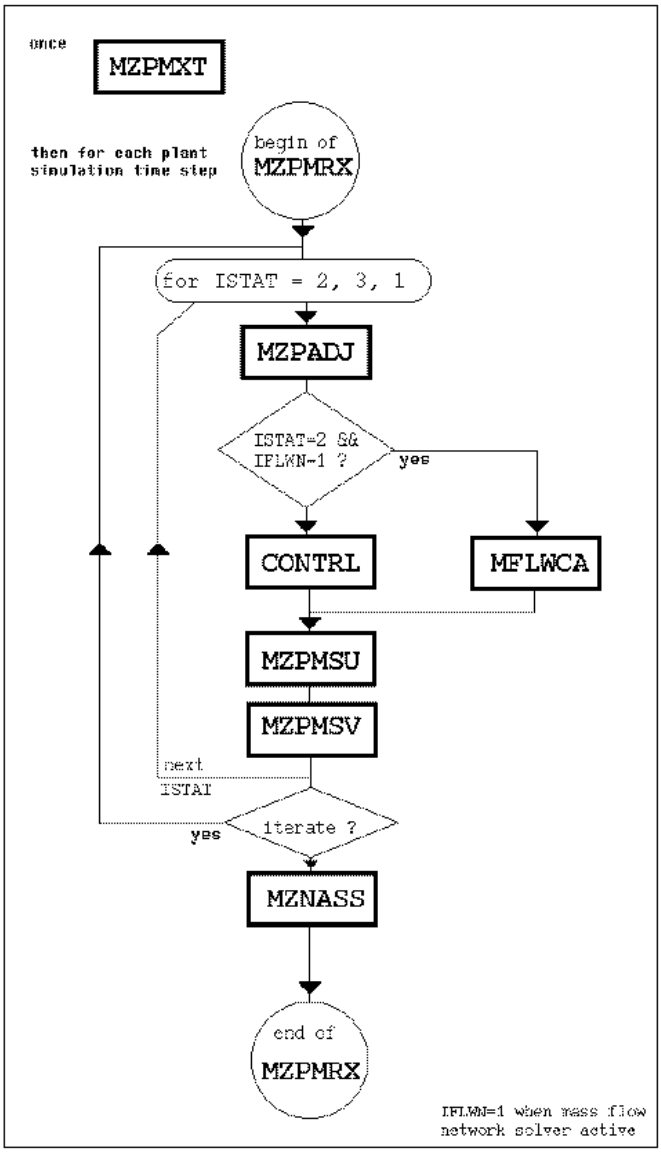

Figure 5.6 Diagrammatic representation of solving the plant system matrix for energy balance (ISTAT = 1), 1st phase mass balance (ISTAT = 2), and 2nd phase mass balance (ISTAT = 3); see Table 5.2 for brief explanation of various subroutines; IFLWN indicates whether *mfs* is active

5.4. AVAILABLE PLANT COMPONENT MODELS

A number of numerical plant component models are made available for usage with the simultaneous plant modelling technique as described in the previous section. The primary task of such a model, is to generate the energy and mass balance equation coefficients during run-time. In case of the basic component model described in Section 5.3 these coefficients are: self-coupling coefficient, cross-coupling coefficient(s), and right hand side of equations (5.4), (5.6a) and (5.6b) respectively.
Each component type model is accompanied by a subroutine for data input management

Table 5.2 Main subroutines involved in solving plant system matrix

Subroutine	Description
MZPMXT	accesses the plant components database and extracts the data needed to establish the templates for the plant network energy, 1st phase mass, and 2nd phase mass balance. Checks that component connections are legally defined, initialises data arrays, and in case the encapsulated version of *mfs* is active: resets the mass diversion ratios to unity, and checks plant/mfs connection mapping regarding fluid types
MZPMRX	controls setting up, solution and results assignment of the plant energy (ISTAT = 1), 1st phase mass (ISTAT = 2), and 2nd phase mass (ISTAT = 3) matrix equation at each plant simulation time step
MZPADJ	organises the information which defines each inter-component coupling. This data is required by the component nodal equation coefficient generators in order to calculate the inter-component connection coefficients. Checks whether mass flows are in the assumed direction (ie. the coefficient generators implicitly assume each connection's mass flow rate ≥ 0. Establishes plant component containment temperatures, if defined to exist
CONTRL	determines plant control status based on most recent available results, by invoking appropriate control routine for each active plant control loop for current time step
MFLWCA	controls the fluid flows calculation for each simulation time step: sets climate variables, temperatures for nodes corresponding to plant components or building zones, sets boundary nodes temperature and/or wind pressure. Calculates fluid densities and connections stack pressure difference. Solves the fluid flow network mass balances; transfers fluid flow simulation results to results file. Establishes and transfers building side air flow and plant side fluid flows
MZPMSU	sets up the plant matrix equations by calling the appropriate matrix coefficient generators, and locating generated equation coefficients in the network matrix
MZPMSV	solves the plant matrix equation. A sparse matrix solver is invoked to solve the matrix equation $\mathbf{A} \cdot \theta = \mathbf{b}$ or $\mathbf{E} \cdot \dot{\mathbf{m}} = \mathbf{f}$ for the solution vector θ or $\dot{\mathbf{m}}$ in terms of the known vector $\mathbf{b}$ or $\mathbf{f}$. The solution vector is then relocated in the future time-row state-space variable array.
MZNASS	adjusts all plant related history variables

(used by *pdb*) and by a subroutine which checks the validity of user specified parameters prior to the actual simulation. These subroutines are very important both from a user point of view and for aiding in ensuring the integrity of the plant system description. However, these subroutines will not be described any further here.
This applies also to a number of generic subroutines which perform tasks such as computing temperature dependent specific heat, density, viscosity, or heat of vaporization for the working fluids of interest, ie. dry air, water vapour, and water.

Important literature sources with respect to plant component modelling are by Stoecker (1975), Hanby and Clarke (1988), Lebrun and Liebecq (1988), a compilation by various researchers (IEA 1988), in proceedings of specific conferences (CEC 1983, CEC 1987, CEC 1991), and documentation related to other simulation systems like for instance TRNSYS (SEL 1988), and HVACSIM$^+$ (Clark 1985). It has to be mentioned that although it may appear that there are many plant component models readily available from literature, this is deceptive to say the least. The reasons for this are:
- most models encountered are described in an analytical fashion. Only in a few cases there is also a numerical formulation, but in these cases the interface is not suitable in the present context
- almost all numerical models encountered are geared at the sequential modelling technique as described in Section 5.1
- most models encountered are steady-state approaches
- (almost) same model descriptions keep on re-occurring

No model was found in literature which could readily be used as it was. Most model

descriptions encountered needed serious reformulation into the control volume state-space representation.
Developing or adjusting models is often difficult and time-consuming. Only recently incentives are taken place to facilitate this process by for instance establishment of a data-base of component models (Lebrun & Liebecq 1988), development of a "neutral format model" which should be usable for various simulation environments (Sahlin & Sowell 1989), or development of other concepts which are aimed at making reuse of models easier (Mattsson 1989).

Given the problem domain context as described in Chapter 1., the attention was focussed on models for plant components relating to domestic heating and ventilating systems. Although already available for usage with *bps*, plant component models of for example cooling coils and humidifiers are not presented here. Another selection criterion for plant component models is, that they need to be as comprehensive as deemed necessary to guarantee thermodynamic integrity. Given this constraint, on the other hand the component models will have to be as simple as possible (especially with regard to usage of descriptive parameters) to enable the user to extract the necessary data from available sources (ie. literature, manufacturers data, etc.).
As the primary scope of the current research is the thermal interaction of building structure and plant system, as opposed to for instance plant component transient behaviour due to fast responding local loop control, the time scales of interest are in the order of say a few minutes and more. This is in no way a constraint related to the methodology. It merely serves to narrow down the huge overall problem domain into a surveyable piece.
It should also be noted that the flow/pressure aspects of the plant component behaviour are supposed to be handled by the mass flow network solver as described in Chapter 4.

Table 5.3 summarizes the currently supported plant component types. The indicated sections elaborate the corresponding models. Were there is a strong resemblance between two or more different component types, these are collected into one section. Note that as explained in Section 5.3, there is no need for diverging junction component models, primarily because for the energy balance only *receiving* inter-connections are of interest.

The model type description includes an index ISV. This index indicates the functionality of a plant component model in terms of supported state variable types and is also in use in the program to define the nature of a node. Figure 5.7 holds the definition of ISV. To exemplify the usage of ISV: imagine a three node water fed air heating coil model, where node i represents the solid materials, node j represents the air, and node k represents water. Then it is easy to check by each node's ISV value that node i has no fluid connections at all, that node j is only connected to other air node(s), and that node k is linked to water node(s) only.

The shaded values in Figure 5.7 might appear to be redundant. However, to be able to establish one, two or three equally structured matrix equations incorporating **all** nodes of a plant system network consisting of different (with respect to working fluid) sub-networks, each node within the system must either be at least of ISV type 0, 1, 9, to be able to perform an energy only balance, or be at least of type 10, 11, 19, to perform an energy + one phase mass balance, or of type 20, 21, 29, to be able to establish all three balances. This is the reason why it might be useful that for instance a coefficient generator for a water node can also generate coefficients for the second phase mass balance. Therefor, all models presented in the following sections are capable of generating matrix coefficients for all three balances.

Table 5.3 Currently supported plant component model types
ISV : functionality (see Figure 5.7); AH = Air Heating; WCH = Wet Central Heating

Code	Nodes	ISV	Model type		Section
10	1	21	AH	converging 2 leg junction	5.4.1.
30	1	21	AH	fan	5.4.2.
50	1	21	AH	heating coil & heat flux control	5.4.3.
60	1	21	AH	duct	5.4.5.
110	1	21	AH	counterflow heating coil with water mass flow control	5.4.3.
120	2	21	AH	plate heat exchanger	5.4.10.
200	1	20	WCH	boiler & heat flux control	5.4.6.
210	2	20	WCH	radiator	5.4.9.
220	1	20	WCH	pipe	5.4.5.
230	1	20	WCH	converging 2 leg junction	5.4.1.
240	1	20	WCH	pump	5.4.2.
250	2	20	WCH	boiler & on/off control	5.4.7.
260	2	20	WCH	boiler & aquastat control	5.4.8.
270	8	20	WCH	radiator	5.4.9.
410	3	> 19	AH	counterflow heating coil fed by WCH system	5.4.4.
500	1	29	WCH	sensor thermostatic radiator valve	5.4.11.
510	1	29		sensor mechanical room thermostat	5.4.12.
900	2	> 19		imaginary mass-less temperature source	5.4.13.

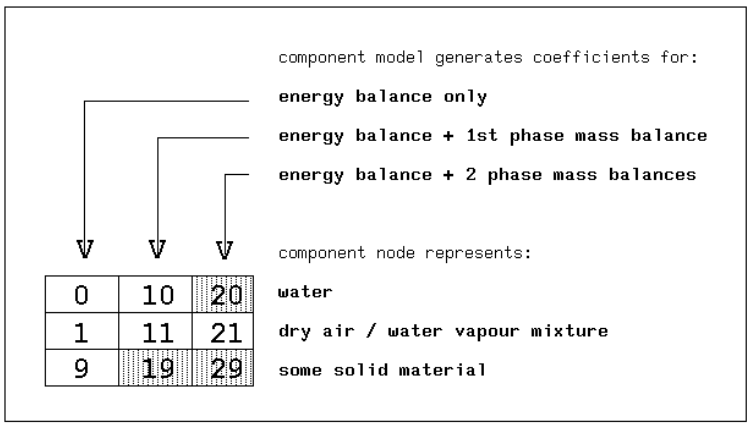

Figure 5.7 Definition of state variable index ISV

5.4.1. Flow Merge (component type 10, 230)

These are matrix coefficient generators for a single node component which models the merging of two flow streams. The model might represent for instance a converging air duct junction or air mixing box in case of plant component type 10, and for instance a converging WCH (wet central heating) pipe junction in case of plant component type 230. The model is essentially the same as the basic component model described in Section 5.3. In this case there will be two external inlet connections and there is no internal heat generation. All the mass involved (ie. wall material and enclosed fluid) is assumed to be concentrated in the one node. Model type 10 and model type 230 are both able to provide the matrix coefficients for all three balance types. In case of model type 230 and second phase mass balance, the self-

coupling coefficient will be set to unity, while the cross-coupling coefficients and right hand side coefficient will be zero, thus enforcing $\dot{m}_v = 0$.

The user-definable parameters for this component are:

1	M	component total mass	kg
2	$\overline{c}$	mass weighted average specific heat	J/kgK
3	UA	component overall heat loss coefficient	W/K

5.4.2. Flow Inducer (component type 30, 240)

A flow inducer might be represented by these single node component matrix coefficient generators. The model can be used to simulate a flow controlled fan (type 30) or WCH pump (type 240). The model has a close resemblance to the the basic component model described in Section 5.3. The difference is that the current model has only one external inlet connection. All the mass involved (ie. wall material and enclosed fluid) is assumed to be concentrated in the one node. Model type 30 and model type 240 are both able to provide the matrix coefficients for all three balance types. In case of model type 240 and second phase mass balance, the self-coupling coefficient will be set to unity, while the cross-coupling coefficients and right hand side coefficient will be zero, thus enforcing $\dot{m}_v = 0$.

In order to simulate the flow/pressure behaviour of a fan or pump, this component should be symbolically linked to a type 310 mass flow network connection type (see Section 4.3.9). In that case the control of fan or pump will be handled too by the mass flow network solver. This is described in Section 5.3.

The user-definable parameters for this component are:

1	M	component total mass	kg
2	$\overline{c}$	mass weighted average specific heat	J/kgK
3	UA	component overall heat loss coefficient	W/K
4	E_r	rated total (electric) power consumption at $\dot{q}_r$	W
5	$\dot{q}_r$	rated volume flow rate	m^3/s
6	η	overall efficiency	$-$

The variable which may be controlled by a so-called plant control loop (as described in Section 5.5) for this component is:

1	$\dot{q}$	volume flow rate	m^3/s

Additional output variables (as meant in Section 5.3.5) for this component are:

1	E	(electric) power consumption	W
2	ϕ	internal heat generation	W

When the incorporated version of *mfs* is active, the (electric) power consumption is calculated from:

$$E = \frac{\dot{m}\,\Delta P}{\eta\,\rho} \quad (W) \tag{5.9}$$

where $\dot{m}$, ΔP, and ρ are respectively actual mass flow, pressure rise, and fluid density for the referenced mass flow network connection. In case the mass flow network solver is not active, the power consumption is computed on the basis of the fan/pump affinity laws (see eg. ASHRAE 1985), from which it follows that:

$$E = \left(\frac{\dot{q}}{\dot{q}_r} \right)^3 E_r \quad (W) \tag{5.9a}$$

where it is assumed implicitly that $\dot{q}_r$ and E_r apply to the current plant system network, and that η is a constant.
When generating the energy balance coefficients, the internal heat generation ϕ for node i is computed from the power consumption, according to:

$$\phi_i = (1 - \eta)\, E \quad (W) \tag{5.10a}$$

which is based on the assumption that losses due to inefficiency will be converted into internal heat generation. This is the usual assumption for incompressible fluids, ie for the pump (see eg Brozza and Mazza 1988). For fans, it is more usual (see eg Wright and Hanby 1988) to evaluate the internal heat generation from:

$$\phi_i = E \quad (W) \tag{5.10b}$$

which is based on the assumption of adiabatic compression and expansion of the air implying that all losses will appear as heat.

In contrast to equation (5.6a) for the basic component model of Section 5.3., the first phase mass balance for the current component type is:

$$\dot{m}_a = \dot{q} \cdot \rho_a \quad (kg/s) \tag{5.11}$$

from which it can be seen that the cross-coupling coefficient for the mass flow balances will be equal zero.

5.4.3. Air Heating Coil; single node (component type 50, 110)

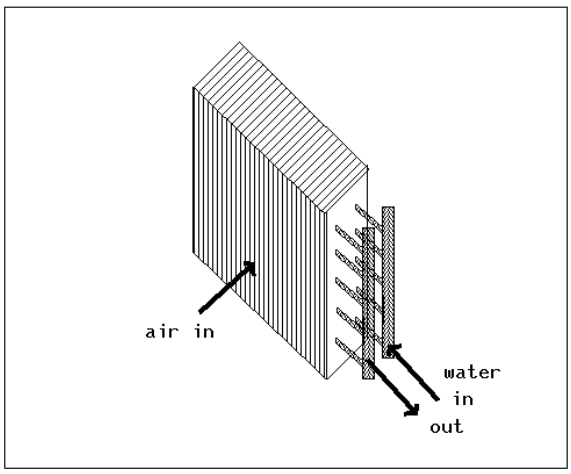

Figure 5.8 Schematic graph of a finned tube air heating coil

Figure 5.8 is a schematic graph of a finned tube heat exchanger which is often used for water-to-air applications. For these kind of air heating coils, there are presently three matrix coefficient generators available representing component models of increasing complexity. The first two are described in this section. These are single node models where all the mass involved (ie. solid material and enclosed fluids) is assumed to be concentrated in the one node. The main difference when compared to the basic component model of Section 5.3., is that these models have only one external inlet connection. The models of type 50 and 110, differ with respect to the controlled variable, and the way in which the heat transfer to the air stream is calculated. In case of type 50, the (controllable) heat transfer to the air is supplied by the user. For a type 110 component, the user has to supply some additional coil parameters from which the heat transfer is calculated. With the latter component type, a variable water supply flow rate with a fixed inlet temperature is assumed.

The user-definable parameters for this component are:

1	M	component total mass	kg
2	$\overline{c}$	mass weighted average specific heat	J/kgK
3	UA	component overall heat loss coefficient	W/K
and in case of plant component type 110 only			
4	A_o	total outside (air side) heat transfer area	m^2
5	A_i	total inside (water side) heat transfer area	m^2
6	A_f	coil face area	m^2
7	R_m	coil metal thermal resistance (relative to A_o)	m^2K/W
8	D_i	internal tube diameter	m
9	$\theta_{w,i}$	inlet water temperature	$°C$

The variables which may be controlled by so-called plant control loops (see Section 5.5) for these component types are:

50:	1	ϕ	coil heat input	W
110:	1	$\dot{m}_w$	water mass flow rate	kg/s

Additional output variables (as meant in Section 5.3.5) for the component type 110 are:

1	ϕ	heat transfer from water to air	W
2	ε	coil effectiveness	$-$
3	$C_{\min}/C_{\max}$	ratio of fluid capacity rates	$-$
4	h_a	air film heat transfer coefficient	W/m^2K
5	h_w	water film heat transfer coefficient	W/m^2K

It is obvious that in case of component type 50, ϕ can be imported directly into the matrix coefficients for the energy balance equation (5.4). For a component type 110, ϕ has to be evaluated first. Here it is assumed that the heat transfer from water to air may be approached as if the coil was operating under steady-state conditions. From this follows the heat transfer which would take place from water to air. Then part of this heat transfer is involved in heating the component's mass and the remainder is used to actually heat the air. This process was already described in Section 5.3. Depending on the transient behaviour of the boundary (ie. coil inlet) conditions, this approach is probably justifiable especially when the simulation

time step is relatively small. Thus assuming steady-state conditions, here we follow an approach as described by for instance Holmes (1988) which can also be found in various textbooks like for example by Kays and London (1984) or by McQuiston and Parker (1988). This approach, which is also known as the N_{TU}-method (Number of Transfer Units), uses the concept of coil effectiveness ε, which is the ratio between actual heat transfer rate and maximum possible heat transfer rate. The actual heat transfer from water to air then becomes:

$$\phi_i = C_{\min}\varepsilon(\theta_{w,i} - \theta_j) \quad (W) \tag{5.12}$$

where $C_{\min}$ is the smaller fluid capacity rate (for definition see equation (5.2a)) of that for the two fluid flows air and water, and θ_j is the temperature of the fluid entering through the component's external connection (ie. inlet air temperature)[†]. A heating coil might have various flow arrangements. Here we assume it is a counterflow coil, which is commonly used for heating air and for that case the effectiveness is given by:

$$\varepsilon = \frac{1 - \exp[-N_{TU}\,(1 - C)]}{1 - C \cdot \exp[-N_{TU}\,(1 - C)]} \quad (-) \tag{5.13}$$

where

$$N_{TU} = A_o/\,[C_{\min}(R_a + R_m + R_w)] \quad (-)$$

$$C = C_{\min}/\,C_{\max} \quad (-)$$

$$R_a = \text{air side thermal resistance} = 1/\,h_a \quad (m^2K/W)$$

$$R_w = \text{water side thermal resistance} = A_o/\,(A_i h_w) \quad (m^2K/W)$$

in which h_a, and h_w are air film heat transfer coefficient and water film heat transfer coefficient, respectively. It should be noted that the input parameter R_m represents not only the thermal resistance of the tube wall (which is often negligible) but also of the fins if any, and may also include external and internal fouling resistances.

The air film heat transfer coefficient depends on: velocity and state of the air when entering the coil, design of the extended coil surface (ie. the fins), size and spacing of the tubes, and depth of the coil. For the general case, where there are no detailed information and/or experimental results available, it is very difficult to give a good relationship for the air film heat transfer coefficient. According to Holmes (1988), when no data is available a working approximation is:

$$h_a = 38 \cdot \overline{v}_a \quad (W/m^2K) \tag{5.14}$$

where $\overline{v}_a$ is the average face velocity (ie. $\dot{m}_a/(\rho_a A_f)$ m/s).

With respect to the water film heat transfer coefficient, the suggestion by Holmes (1988) is followed, that the flow can usually be taken as fully turbulent (even at low Reynolds numbers) and that then the following relationship is appropriate:

$$h_w = 1400\,(1 + 0.015\,\overline{\theta}_w)\,\overline{v}_w^{0.8}\,D_i^{-0.2} \quad (W/m^2K) \tag{5.15}$$

---

† The above assumes that $\theta_{w,i} \geq \theta_j$. When the situation occurs that this constraint is not met, the program will issue a non-fatal warning stating that the air stream is being cooled, based on a heating coil model.

where $\overline{\theta}_w$ is the mean water temperature ($^\circ C$), and $\overline{v}_w$ is the average water velocity (ie. $\dot{m}_w/(\rho_w \pi D_i^2/4)\ m/s$).

In the above, the calculation of the heat transfer from water to air ϕ starts from the current values for temperature θ and first phase mass flow rate $\dot{m}$. These values will not necessarily be identical to the eventual future time-row values. Therefore, temperature and first phase mass flow rate are marked for iteration, as explained in Section 5.3 under *Simultaneous solution of the plant matrices*.

The time constant for this component is calculated with an expression similar to equation (5.5) but with the denominator expanded with the term $+\ \dot{m}_w c_{p,w}$.

5.4.4. Air Heating Coil; multi node (component type 410)

At present, the most comprehensive model available for air heating coils, is the three node model type 410. This is a matrix coefficient generator for an air heating coil which is fed by (part of) a WCH system. It is the same device as schematically drawn in Figure 5.8, but is modelled as shown in Figure 5.9.

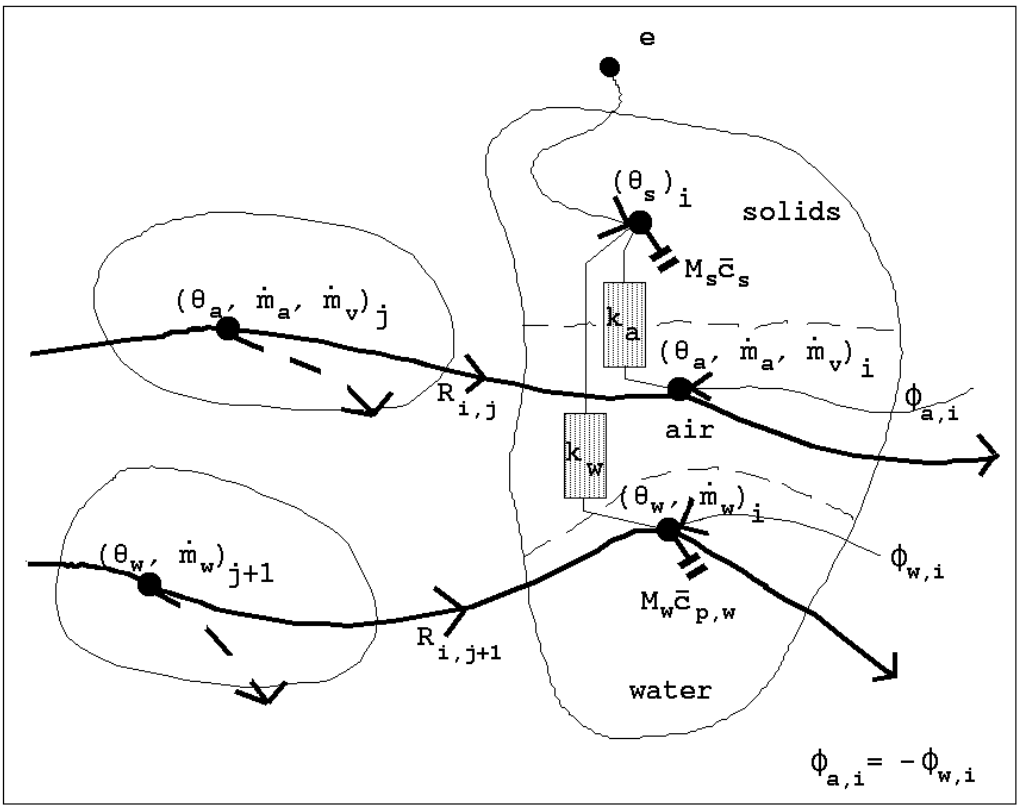

Figure 5.9 Diagrammatic state-space representation of a three node air heating coil model with two external inlet connections to an air and to a water component node

All the mass related to solid materials is assumed to be concentrated in the first node. The second node represents the air inside the coil. The mass related to the water inside the tubes

is assumed to be concentrated in the third node. This model is meant to have two external inlet connections: one were air is the working fluid to the air node, and a water flow connection to the water node. With this component it is thus possible to link two plant system sub-networks with different working fluids.

The user-definable parameters for this component are:

1	M_s	component total mass of solids	kg
2	$\overline{c}_s$	mass weighted average specific heat of solids	J/kgK
3	UA	component overall heat loss coefficient to environment	W/K
4	M_w	mass of encapsulated water	kg
5	A_o	total outside (air side) heat transfer area	m^2
6	A_i	total inside (water side) heat transfer area	m^2
7	A_f	coil face area	m^2
8	R_m	coil metal thermal resistance (relative to A_o)	m^2K/W
9	D_i	internal tube diameter	m

Additional output variables (as meant in Section 5.3.5) for this component type are:

1	ϕ_a	heat transfer from water to air	W
2	ε	coil effectiveness	$-$
3	$C_{\min}/C_{\max}$	ratio of fluid capacity rates	$-$
4	h_a	air film heat transfer coefficient	W/m^2K
5	h_w	water film heat transfer coefficient	W/m^2K
6	k_a	solids to air thermal conductance	W/K
7	k_w	solids to water thermal conductance	W/K

There are no directly controllable variables. All coil boundary conditions (ie. inlet temperatures and mass flow rates) are available from network conditions.
The calculation of the heat transfer between water and air ($\phi_{a,i} = -\phi_{w,i}$) is based on the same assumptions and follows the same approach as adopted for the component model type 110 which is described in the previous section. The solids node is coupled to the air node and water node respectively by the thermal conductances k_a and k_w, which are defined by:

$$k_a = \frac{A_o}{R_a + R_m/2} \quad (W/K) \tag{5.16a}$$

$$k_w = \frac{A_o}{R_w + R_m/2} \quad (W/K) \tag{5.16b}$$

where R_a and R_w are respectively the air and water side thermal resistances as described in the previous section on plant component type 110. Because for a component type 410, the calculation of the heat transfer from water to air ϕ starts from the current values of temperature and first mass flow rate for both air and water, there are four state variables which are marked for iteration: θ_a, θ_w, $\dot{m}_a$, and $\dot{m}_w$.

The energy balance for the solids node yields:

$$k_a(\theta_a - \theta_s) + k_w(\theta_w - \theta_s) + UA(\theta_e - \theta_s) = \frac{\overline{c}_s M_s \partial\theta_s}{\partial t} \quad (W) \tag{5.17a}$$

The energy balance for the (zero mass) air node yields:

$$C_{ij}(\theta_j - \theta_a) + k_a(\theta_s - \theta_a) + \phi_a = 0 \qquad (W) \tag{5.17b}$$

where C_{ij} is defined as in equation (5.3a). Finally, the energy balance for the water node yields:

$$C_{ij+1}(\theta_{j+1} - \theta_w) + k_w(\theta_s - \theta_w) + \phi_w = \frac{\overline{c}_w M_w \partial\theta_w}{\partial t} \qquad (W) \tag{5.17c}$$

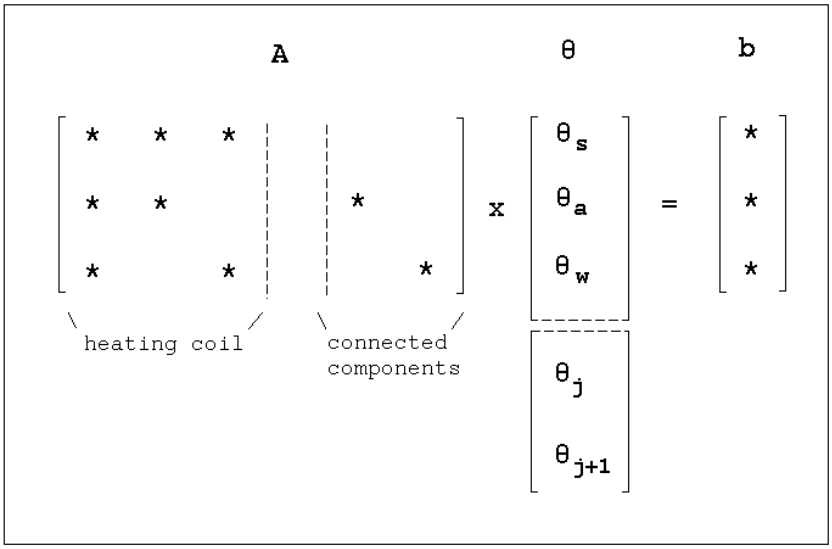

Figure 5.10 Schematic representation of energy balance matrix equation for a three node air heating coil model with two external inlet connections

To solve these partial differential equations, the same numerical approximation technique is used as described in Section 5.3; ie. by weighted summation of explicit and implicit formulation of equation (5.17a) and (5.17c). Obviously, the linear equation (5.17b) does not need a numerical approximation. The process of establishing the self-coupling, cross-coupling and right hand side matrix coefficients for these equations will yield a matrix topology as schematically indicated in Figure 5.10. The particulars of this process will not be repeated here.

The time constant for this component is based on separate formulations for the solids node:

$$\tau_s = \frac{\overline{c}_s M_s}{k_a + k_w + UA} \qquad (s) \tag{5.18a}$$

and for the water node:

$$\tau_w = \frac{\overline{c}_w M_w}{k_w + C_{ij+1}} \qquad (s) \tag{5.18b}$$

For component i as a whole, the larger value of τ_s and τ_w is taken.

The first phase mass balance for the air node yields:

$$\dot{m}_{a,i} - R_{i,j}\dot{m}_{a,j} = 0 \qquad (kg/s) \tag{5.19a}$$

and for the water node

$$\dot{m}_{w,i} - R_{i,j+1}\dot{m}_{w,j+1} = 0 \qquad (kg/s) \tag{5.19b}$$

These equations will yield a matrix structure similar to Figure 5.10, except of course for the off-diagonal entries related to the solids node which will disappear. All diagonal elements - ie. the self-coupling coefficients - will be unity. The off-diagonal entries or cross-coupling coefficients will be $-R_{i,j}$ and $-R_{i,j+1}$ for the air and water node, respectively. All right hand side entries will become zero.

The second phase mass balance for the air node yields:

$$\dot{m}_{v,i} - R_{i,j}\dot{m}_{v,j} = 0 \qquad (kg/s) \tag{5.20}$$

The second phase mass balance matrix coefficients for both the solids and the water node will be such that the second phase mass flow rate will remain zero.

5.4.5. Flow Conduit (component type 60, 220)

There are two matrix coefficient generators available for a single node model of a flow conduit. The model can be used to represent a section of an air duct (type 60) or for simulating a WCH pipe section (type 220). The difference between this flow conduit model and the basic component model of Section 5.3 is that the current model has only one entering external connection. All the mass involved (conduit wall material and enclosed fluid) is assumed to be concentrated in the one node. Both model type 60 and type 220 are capable of generating the matrix coefficients for all three balance types. In case of model 220 and second phase mass balance the generated matrix coefficients will be such that $\dot{m}_v = 0$ will result.

The user-definable parameters for this component are:

1	M	component total mass	kg
2	$\overline{c}$	mass weighted average specific heat	J/kgK
3	UA_e	component overall heat loss coefficient from conduit wall to environment	W/K
4	D_h	hydraulic diameter of duct/pipe	m
5	L	length of duct/pipe section	m
6	A_f	cross sectional face area	m^2

Additional output variables (as meant in Section 5.3.5) for this component type are:

1	v	mean fluid velocity	m/s
2	h_i	inside heat transfer coefficient	W/m^2K
3	UA_x	adjusted heat loss coefficient	W/K

With this component model it is assumed that the nodal temperature θ_i represents the temperature of the fluid leaving the conduit. For the energy balance calculations we start from expressions as described by Malmstrom (1988), and Malmstrom & Olsson (1988).

These are based on the fact that when the environment temperature θ_e is uniform and when steady-state conditions are assumed, the temperature θ of the fluid in a conduit is described by the ordinary differential equation:

$$\dot{m}\, c_p\, L\, \frac{d\theta}{dx} = -UA\,(\theta - \theta_e) \quad (W) \tag{5.21}$$

From this follows that the temperature θ_i of the fluid leaving a duct/pipe section (ie. at $x = L$) may be calculated from:

$$\theta_i = \frac{\theta_j - \theta_e(1 - \exp(UA/\dot{m}\, c_p))}{\exp(UA/\dot{m}\, c_p)} \quad (°C) \tag{5.22}$$

where:

$$\frac{1}{UA} = \frac{1}{h_i A_i} + \frac{1}{UA_e} \quad (K/W) \tag{5.22a}$$

where θj is the temperature of the entering fluid as before, h_i is the inside heat transfer coefficient (W/m^2K), A_i is the inner surface area (= $\pi\, D_h L$ (m^2)), and UA_e incorporates heat conduction through conduit wall and perhaps insulation and convective and radiative heat transfer on the outer surface. The flow is taken to be fully turbulent†, and in case of a pipe (type 220) the relationship of equation (5.15) is employed to calculate h_i. In case of a duct (type 60) the following relation (as described by Malmstrom & Olsson (1988)) is used:

$$h_i = 0.02\left[1 + \left(\frac{D_h}{L}\right)^{2/3}\right]\frac{v_a^{0.78}}{D_h^{0.22}}\,(153 - 0.25\,\theta_a) \quad (W/m^2K) \tag{5.23}$$

where v_a is the mean air velocity in the duct (ie. $\dot{m}_i/(\rho\, A_f)$ m/s), and θ_a is the air temperature ($°C$). The last bracketed term is actually based on $0 < \theta_a < 40°C$, which is a reasonable assumption for the systems intended in this thesis.

The heat loss to the environment depends on UA and on the difference between average fluid temperature θ_m and environment temperature θ_e. If the heat loss to the environment will be based on the conduit exit temperature instead of on θ_m, an adjusted heat loss coefficient UA_x has to be defined:

$$UA_x = UA\,\frac{(\theta_m - \theta_e)}{(\theta_i - \theta_e)} \quad (W/K) \tag{5.24}$$

It may be derived that:

$$\theta_m - \theta_e = \frac{(\theta_j - \theta_e)(-\dot{m}\, c_p/\, UA)(1 - \exp(UA/\dot{m}\, c_p))}{\exp(UA/\dot{m}\, c_p)} \quad (K) \tag{5.25a}$$

From equation (5.22) follows:

$$\theta_i - \theta_e = \frac{\theta_j - \theta_e}{\exp(UA/\dot{m}\, c_p)} \quad (K) \tag{5.25b}$$

† in case Re < 2300 (-), a non-fatal message is issued, warning the user that the flow is possibly laminar

Combining equations (5.24), (5.25a), and (5.25b) leads to:

$$UA_x = \dot{m}\, c_p(\exp(UA/\dot{m}\, c_p) - 1) \quad (W/K) \tag{5.26}$$

To incorporate dynamic thermal behaviour, it is assumed that all mass is concentrated at the duct/pipe exit. If the transport time within this single duct/pipe section is neglected†, and it is assumed that fluid and conduit material have the same temperature, the energy balance for node i yields:

$$C_{ij}(\theta_j - \theta_i) + UA_x(\theta_e - \theta_{i)} = \frac{\overline{c}_i M_i \partial\theta_i}{\partial t} \quad (W) \tag{5.27}$$

where C_{ij} is defined as in equation (5.3a). The energy balance equation (5.27) is then solved as described in Section 5.3.

The first and second phase mass balance matrix coefficients are also generated as indicated in Section 5.3. With respect to the second phase mass balance, the suggestion by Malmstrom & Olsson (1988) is followed to assume that no condensation will occur inside the duct (type 60). During run time, the model compares θ_i with the dew-point temperature θ_{dew} corresponding to the prevailing moist air conditions. If during some simulation time step θ_i becomes less or equal θ_{dew} a warning is issued signaling this event, but the program continues as if no condensation occurs.

5.4.6. Boiler; single node & heat flux control (component type 200)

For domestic hot water boilers to be used in WCH applications or for feeding an air heating coil, there are presently three matrix coefficient generators available representing component models of increasing complexity. Only the first one is described in this section. This involves a single node model where all the mass involved (ie. solids and enclosed water) is assumed to be concentrated in the one node. The main difference when compared to the basic component model of Section 5.3., is that this boiler model has only one external inlet connection. The type 200 hot water boiler is a very simple model in that it does not take into account any efficiency (ie. the results will only incorporate the net heat input into the water flow) and it assumes a linear heat loss relationship between the boiler and the environment.

The user-definable parameters for this component are:

1	M	component total mass	kg
2	$\overline{c}$	mass weighted average specific heat	J/kgK
3	UA	component overall heat loss coefficient	W/K

The variable which may be controlled by a user-definable plant control loop (see Section 5.5) for this component type is:

1	ϕ	net boiler heat input	W

† The transport times for the system as a whole on the contrary, are not neglected. They are implicitly incorporated in the solution process through the nodal thermal capacitances.

It will be obvious that ϕ can be imported directly into the matrix coefficients for the energy balance equation (5.4).
The model is capable of generating matrix coefficients for all three balance types, in order to be able to be incorporated in a plant system which uses both water and moist air as working fluids. In case of second phase mass balance, the generated matrix coefficients will be such that $m_v = 0$ will result.

5.4.7. Boiler; two node & on/off control (component type 250)

This is the second matrix coefficient generator which is available for simulating domestic hot water boilers to be used in WCH applications or for feeding an air heating coil. This model simulates the behaviour of a gas fired conventional or condensing boiler. This is the type of boiler which is commonly encountered in domestic applications in The Netherlands. The model is based on a two node representation of the boiler which is schematically indicated in Figure 5.11. This boiler model was initially developed by Triepels (1984), later modified by Croes (1988), and is further expanded here.

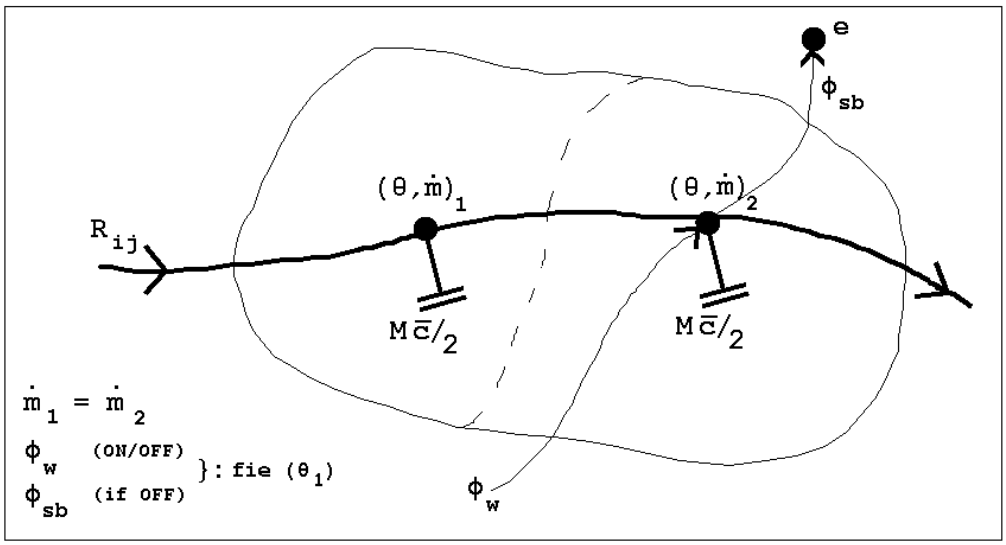

Figure 5.11 Schematic representation of two node boiler model

The total thermal capacitance of boiler structure and encapsulated water is assumed to be evenly distributed over the two nodes. One node is connected to the boiler inlet and the other node is connected to the boiler outlet. The net heat input into the water flow ϕ_w and the heat loss to the environment during stand-by mode ϕ_{sb} are assumed to be effectuated between the two nodes.[†] However, both ϕ_w and ϕ_{sb} will be evaluated at the temperature of the node connected to the inlet, ie. θ_1. In case of steady-state conditions this temperature θ_1 will be equal to the temperature of the incoming water θ_j, which is usually referred to as the system return temperature. In case of a condensing boiler, the water vapour in the flue gases will condensate when the return water temperature is below a certain threshold value ie. θ_c. Here

[†] As pointed out by Lebrun (1991) the fact that the first node does not loose any heat to the environment, imposes a problem when the water flow rate approaches zero. In that case the first node becomes a heat storage without losses. Clearly the model needs further developments to overcome this problem.

we assume $\theta_c \approx 50°C$.

The user-definable parameters for this plant component model are:

1	M	component total mass	kg
2	$\overline{c}$	mass weighted average specific heat	J/kgK
3	F_{ON}	full load gas firing rate when boiler ON	m_0^3/s
4	F_{sb}	stand-by mode gas consumption relative to F_{ON}	$-$
5	H	gas heating value at standard temperature and pressure	J/m_0^3
6	η_c	full load water sided efficiency at θ_c	$-$
7	$tg(\alpha_1)$	tangent of efficiency curve for $\theta_j < \theta_c$	$1/K$
8	$tg(\alpha_2)$	tangent of efficiency curve for $\theta_j > \theta_c$	$1/K$
9	$L_{sb,0}$	stand-by loss at $\theta_j = \theta_e$ relative to F_{ON}	$-$
10	$tg(\beta)$	tangent of stand-by loss curve	$1/K$
11	t_0	normalized start-stop loss	s
12	$\theta_{\max}$	upper boiler temperature limit	$°C$

The "variable" which may be controlled by a user-definable plant control loop (see Section 5.5) for this plant component type is:

1	*ON/OFF*	boiler ON / OFF input control signal	0 or 1

Additional output variables (as meant in Section 5.3.5) for this component type are:

1	*ON/OFF*	boiler was actually ON / OFF	0 or 1
2	F	actual gas consumption	m_0^3/s
3	η	actual water sided efficiency	$-$
4	ϕ_w	heat input into the water	W
5	ϕ_{sb}	stand-by heat loss	W

It is assumed that during a simulation time step - depending on the control signal - the boiler is either ON with a gas consumption of $F_{ON}\ m^3/s$ or is in stand-by mode. In stand-by mode the gas consumption equals $F_{sb}F_{ON}\ m^3/s$ which might be due to the pilot flame (if present). It is assumed that both F_{ON} and the gas caloric value H are expressed in normalized units of volume m_0^3, ie. at standard temperature and pressure (STP). It is also assumed that H and the efficiency η_c correspond, ie. both should be based on either gross caloric value (usually) or on net caloric value. η_c, α, $L_{sb,0}$ and β are used to describe the relationships between respectively the full load water sided efficiency and stand-by losses, and the system return water temperature. α, respectively β is the angle between this curve and the x-axis. If during some simulation time step the boiler temperature should exceed an upper limit $\theta_{\max}$, the temperature for that time step is recalculated with the boiler turned off irrespective of the current value of the ON/OFF control signal.

The calculation of the heat flows ϕ_w and ϕ_{sb} is developed starting from modelling and measurement results for domestic hot water boilers by Van Rij & Overman (1986). Some of their measurement results are shown in Figure 5.12. These involve nine different boilers, of which three are condensing and the remainder are of conventional construction.
From Figure 5.12a, it is quite easy to establish the full load efficiency curve parameters η_c,

Figure 5.12 Full load water sided efficiency and heat losses in stand-by condition as a function of the return water temperature, for nine domestic hot water boilers (source: Van Rij & Overman 1986)

$tg(\alpha_1)$, and $tg(\alpha_2)$. For instance for the boiler denoted $A2$: $\eta_c \approx 0.865$, $tg(\alpha_1) \approx -0.0025\ 1/K$, and $tg(\alpha_2) \approx -0.00025\ 1/K$. From Figure 5.12b the parameters $L_{sb,0}$ and $tg(\beta)$ which describe the stand-by losses curve may be established; for example for the boiler denoted C: $L_{sb,0} \approx 0.008$, and $tg(\beta) \approx 0.00041\ 1/K$.

To predict the heat flows in the boiler, it is assumed that while the boiler is in operation, the heat input into the water flow equals the heat flow at full load under stationary conditions, but using θ_1 instead of the return water temperature θ_j for evaluating the water sided efficiency. Thus:

$$\phi_w = \eta\, F_{ON}\, H \quad (W) \tag{5.28}$$

where

$$\eta = [\eta_c - tg(\alpha)(50 - \theta_1)] \cdot \left[\frac{\Delta t - t_0}{\Delta t}\right]_{1st_ON} \quad (-) \tag{5.29}$$

where α is either α_1 or α_2 depending on whether $\theta_1 < 50°C$ or $\theta_1 \geq 50°C$.
The last bracketed term of equation (5.29) represents the start-stop losses. This term is only applied if the boiler was off during the previous time step. The normalized start-stop losses t_0 have the dimension of time, and can be seen as the time during which the burner is on but no heat is yet delivered to the water flow. The start-stop losses may be caused by instable

flames after the burner starts (some gas may pass unburned), and additional losses just after the burner stops (in that condition the heat exchanger will be much warmer than in steady-state stand-by condition). For the boilers in Figure 5.12, Van Rij & Overman (1988) report start-stop losses in the range $.0 < t_0 < .8\ s$.
As the calculation of the heat input into the water is based on the full load water sided efficiency which already accounts for flue gas losses and losses to the boiler environment, it is not necessary to employ ϕ_{sb} (ie. a thermal loss term) when the boiler in in operation.

Also when the boiler is off, the energy flows are assumed to equal those during stationary stand-by mode. The heat input into the water flow is then calculated from:

$$\phi_w = \eta\, F_{sb} F_{ON}\, H \quad (W) \tag{5.30}$$

where η is computed as in equation (5.29). However, in stand-by mode the heat input ϕ_w is counteracted by the stand-by heat losses:

$$\phi_{sb} = [L_{sb,0} + tg(\beta)(\theta_1 - \theta_e)]\, F_{ON}\, H \quad (W) \tag{5.31}$$

In this equation θ_e is incorporated instead of eg. $20°C$ as implied by Figure 5.12b, to be able to adjust the stand-by losses for other values than $\theta_e = 20°C$.
When the boiler temperatures θ_1 and θ_2 equal the environment temperature θ_e the pilot flame heat input (if present) should approximately counterbalance the stand-by losses (if any); ie. $\phi_w \approx \phi_{sb}$.

The energy balance for node 1 of this component i now becomes:

$$R_{ij}\dot{m}_{w,j} c_{pw}(\theta_j - \theta_{i,1}) = \frac{\overline{c}_i M_i \partial\theta_{i,1}}{2\,\partial t} \quad (W) \tag{5.32a}$$

where R_{ij} is the mass diversion ratio for component node j towards component i. The energy balance for node 2 of the boiler component i becomes:

$$\dot{m}_{w,i} c_{pw}(\theta_{i,1} - \theta_{i,2}) + \phi_w - \phi_{sb} = \frac{\overline{c}_i M_i \partial\theta_{i,2}}{2\,\partial t} \quad (W) \tag{5.32b}$$

Because heat loss to the environment is already incorporated in ϕ_w and/or ϕ_{sb}, the terms in equation (5.4) involving UA do not appear.
The energy balance equations (5.32a) and (5.32b) are incorporated in the overall plant system matrix and solved as indicated in Section 5.3. Because for a component type 250, the calculation of the heat transfer to or from the water starts from the current value of the temperature of the first node, θ_1 is a state variable which is marked for iteration.

As the previous models, this model is also capable of generating matrix coefficients for all two mass balances. This enables incorporation of this model in for example an air heating system fed by a hot water boiler.
The first and second phase mass balance matrix coefficients are generated as indicated in Section 5.3. The first phase mass balance coefficients for node 2 will obviously reflect that $\dot{m}_{w,i,1} = \dot{m}_{w,i,2}$. And the matrix coefficients for the second phase mass balance will evaluate to $\dot{m}_{v,i,1} = \dot{m}_{v,i,2} = 0$.

5.4.8. Boiler; two node & aquastat control (component type 260)

The third matrix coefficient generator which is available for simulating domestic hot water boilers to be used in WCH applications or for feeding an air heating coil is this plant component type 260. This model is based on a plant component model specification described by Dachelet et al. (1988), and Laret (1988, 1989), and is made available in *bps* for two reasons: (1) the model represents a boiler type which although not very common in The Netherlands is in widespread use in the other CEC countries, and (2) to demonstrate how a TRNSYS-type model can be incorporated employing only slight modifications.
The model simulates the thermal behaviour of a fuel oil or gas fired conventional boiler with aquastat control. There is a main control which dictates whether the boiler is on or off. When the main control is on, the current system return water temperature θ_j is checked against the aquastat set point and if
the boiler is controlled such that the average boiler outlet temperature θ_x equals supplied by three fluids: (1) the combustion gas, (2) the heat distributing water, and (3) the environment. The reader is referred to the very thorough description by Dachelet et al. (1988) for further information. Although the model is basically a static model, Dachelet et al. do propose a way to modify the model such that dynamic effects may be studied. This is done by introducing two fictitious thermal masses on the water system. One capacity is coupled to the system return water side, and the other to the boiler exit. When no other information is available, they suggest to distribute the water and boiler thermal capacitances evenly.

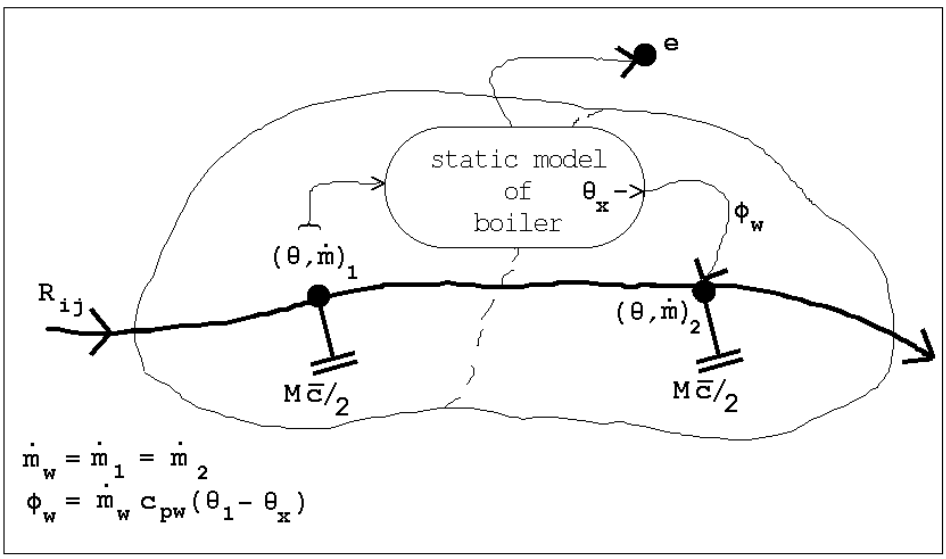

Figure 5.13 Schematic representation of two node dynamic boiler model which uses internally a static boiler model as described by Dachelet et al. (1988)

Here we follow a slightly different approach in that the two nodes are directly coupled, and that the boiler net heat output is represented by a heat flow into the water ϕ_w which is applied to the second node. As will be seen later, the reason for this is that in this way the overall plant system matrix structure is preserved. This approach leads to a model as schematically shown in Figure 5.13. Obviously this model needs future work because it suffers from a similar problem as the previous boiler model: ie no heat loss at zero water

flow rate.

In a TRNSYS-type model distinction is made between PARAMETERS, INPUTS, and OUTPUTS. PARAMETERS are dimensional values which are constant and specific to the equipment considered. The user-definable parameters for the boiler model type 260 are identical to the TRNSYS-type model PARAMETERS:

1	M	component total mass	kg
2	$\overline{c}$	mass weighted average specific heat	J/kgK
3	$\dot{m}_f$	fuel mass flow rate	kg/s
4	CO_2	volumetric ratio of CO_2 in flue gases during operation	$-$
5	$(AU)_0$	heat exchange coefficient water / flue gases in nominal conditions	W/K
6	K_1	sensitivity coefficient for AU	$-$
7	K_2	sensitivity coefficient for AU	$-$
8	Y_w	heat loss coefficient to the environment if OFF	W/K
9	DY_w	heat loss increase to the environment if ON	W/K
10	K_w	weighting factor for defining mean water temperature	$-$
11	$\dot{m}_{f,0}$	fuel nominal mass flow rate	kg/s
12	$\dot{m}_{w,0}$	water nominal mass flow rate	kg/s
13	$(CO_2)_0$	nominal ratio of CO_2 in flue gases	$-$
14	C_1	coefficient for defining specific heat of flue gases	J/kgK
15	C_2	coefficient for defining specific heat of flue gases	J/kgK
16	c_{pf}	fuel specific heat	J/kgK
17	H	fuel heating value	J/kg

In contrast to the TRNSYS-model description, here the specific heat of water c_{pw} is not a parameter, because in *bps* c_{pw} is computed as a function of the water temperature.

INPUTS are variables which are computed in other areas of the program and which may vary with time. In this case the INPUTS for the model are: system water return temperature (here θ_1), water mass flow rate through the boiler ($\dot{m}_{w,1}$), temperature of the environment (θ_e), air temperature (assumed equal to θ_e), and two control variables. Variables which may be selected to be controlled by a user-definable plant control loop (see Section 5.5) for this plant component type are:

1		aquastat set point	$°C$
2	*ON/OFF*	boiler ON / OFF control signal	1 or 0

OUTPUTS are variables computed by the component model which may be printed out or can be transmitted to other areas of the program. Here they are regarded as additional output variables (as meant in Section 5.3.5):

1	θ_x	water exhaust temperature static model	$°C$
2	$\dot{m}_w$	water mass flow rate	kg/s
3		mean useful power	W
4		mean consumed power	W
5		mean fuel mass flow rate consumed	kg/s
6		rate of burner operation time	$-$
7		rate of burner operation time in stand-by mode	$-$

8		global efficiency of the boiler	–
9		efficiency during operation	–
10		effectiveness of equivalent heat exchanger	–
11		heat transfer coefficient of heat exchanger	W/K
12	ϕ_w	net heat input into the water	W

Only two of these OUTPUTS are actually used here to calculate the net heat input into the water:

$$\phi_w = \dot{m}_w c_{pw}(\theta_x - \theta_1) \quad (W) \tag{5.33}$$

which is then applied to the second boiler model node as indicated in Figure 5.13.

This yields the energy balance for node 1 of this component i:

$$R_{ij}\dot{m}_{w,j}c_{pw}(\theta_j - \theta_{i,1}) = \frac{\overline{c}_i M_i \partial\theta_{i,1}}{2\,\partial t} \quad (W) \tag{5.34a}$$

where R_{ij} is the mass diversion ratio for component node j towards component i. The energy balance for node 2 of the boiler component i can be written as:

$$\dot{m}_{w,i}c_{pw}(\theta_{i,1} - \theta_{i,2}) + \phi_w = \frac{\overline{c}_i M_i \partial\theta_{i,2}}{2\,\partial t} \quad (W) \tag{5.34b}$$

Because heat loss to the environment is already incorporated in ϕ_w by the static boiler model, the terms in equation (5.4) involving UA do not appear in these energy balance equations.
The equations (5.34a) and (5.34b) are incorporated in the overall plant system matrix and solved as indicated in Section 5.3. Because for a component type 260, the calculation of the heat transfer to or from the water starts from the current value of the temperature of the first node, θ_1 is a state variable which is marked for iteration.

As the previous models, this model is also capable of generating matrix coefficients for all two mass balances for already mentioned reasons.
The first and second phase mass balance matrix coefficients are generated as indicated in Section 5.3. The first phase mass balance coefficients for node 2 will obviously reflect that $\dot{m}_{w,i,1} = \dot{m}_{w,i,2}$. And the matrix coefficients for the second phase mass balance will evaluate to $\dot{m}_{v,i,1} = \dot{m}_{v,i,2} = 0$.

5.4.9. Radiator (component type 210, 270)

Currently there are two matrix coefficient generators available for simulating a WCH radiator. The type 210 component model is based on a two node representation of a radiator, and the type 270 model uses an eight node model. Both models are presented here in order to be able to perform accuracy versus discretization comparisons (see Chapter 6). In both models, the total thermal capacitances of radiator material and encapsulated water is assumed to be evenly distributed over the nodes.
In broad terms, the same approach as described by Stephan (1988) is followed for modelling the radiator thermal behaviour. However, for incorporating dynamic effects here we start from a two node model instead of from a one node model. This is supported by results from Ham (1988), who concluded after successive simplifications of a 12 node dynamic radiator

model, that a second order model still gave accurate results when compared to measurements.
As pointed out by Triepels (1984), a dynamic two node model with the capacitance nodes coupled to respectively inlet and outlet connection, and heat emission in between the two nodes, yields far better results than a single node coupled to either the average or outlet radiator conditions. A schematic drawing of the current radiator component model is given in Figure 5.14.

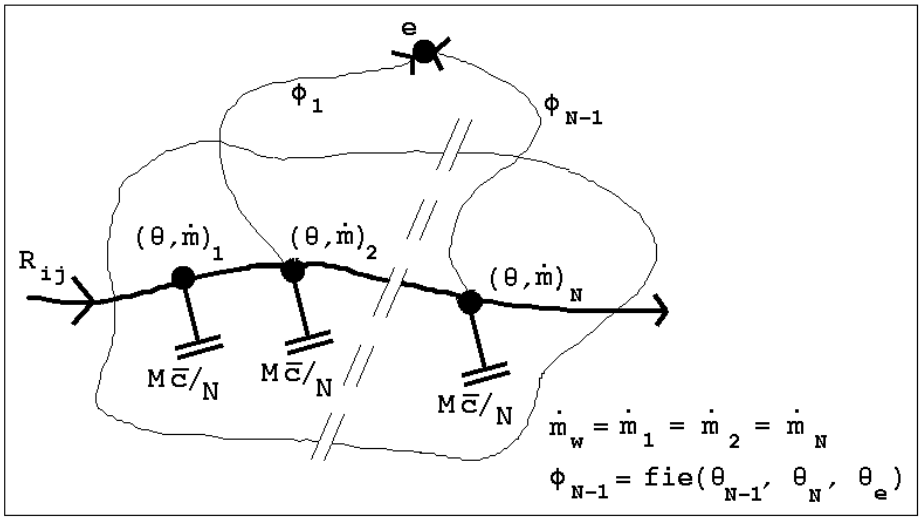

Figure 5.14 Schematic representation of multi node dynamic radiator model

As can be seen, in case of steady-state conditions the temperature of the first node θ_1 will equal the temperature of the incoming water θ_j. The heat transfer from the radiator to the environment ϕ, is assumed to take place between the two nodes, and will therefore appear only in the energy balance of the second node (hence, this model still needs refinements because it suffers from the same problem as indicated before for the boiler models: ie no heat loss from the first node when the water flow rate approaches zero). However, the actual amount of heat transfer which will take place, is evaluated on the basis of both nodal temperatures θ_1 and θ_2, as will be seen below. In case there are more than two nodes the above applies for each pair of successive nodes.

Both models start from commonly available catalogue data. Corrections to account for the influence of the mass flow rate or for the mixing processes within the radiator, may be incorporated in a rudimentary fashion through the usage of nominal output correction factors as can be found in eg. (ISSO 1986). If deemed necessary, correction functions will be incorporated in future, more comprehensive, radiator models.

The user-definable parameters for plant component type 210 and 270 are:

1	M	component total mass	kg
2	$\bar{c}$	mass weighted average specific heat	J/kgK
3	n	radiator exponent	$-$
4	ϕ_0	nominal heat emission of radiator	W
5	$\theta_{s,0}$	nominal supply temperature	$°C$

6	$\theta_{x,0}$	nominal exit temperature	$°C$
7	$\theta_{e,0}$	nominal environment temperature	$°C$
8	I_Z	index of coupled building zone	$-$
9	N_W	number of walls used for defining θ_e	$-$
10	$I_{W,1}$	index of 1st wall for defining θ_e	$-$
11	$a_{W,1}$	weighting factor for 1st wall when defining θ_e	$-$
12	$I_{W,2}$	index of 2nd wall for defining θ_e	$-$
13	$a_{W,2}$	weighting factor for 2nd wall when defining θ_e	$-$
		etc.	

Additional output variables (as meant in Section 5.3.5) for the component type 210 and 270 are:†

1	θ_e	environment temperature	$°C$
2	$\Delta\theta$	logarithmic mean temperature difference	K
3	ϕ_1	heat emission between nodes 1 and 2	W
		in case of type 270 for $k = 3, 4, 5, 6, 7, 8$:	
$k+1$	ϕ_{k-1}	heat emission between nodes $k-1$ and k	W

It is common practice to assume an exponential relationship between the heat emission of a radiator ϕ and the mean temperature difference between the radiator and its environment $\Delta\theta$:

$$\frac{\phi}{\phi_0} = \left(\frac{\Delta\theta}{\Delta\theta_0}\right)^n \quad (-) \tag{5.35}$$

where ϕ_0 is the radiator heat emission under nominal temperature difference conditions $\Delta\theta_0$ which may be found in manufacturers data or handbooks. In this equation the exponent n depends on type and dimensions of the radiator, the way in which the radiator is connected, and on characteristics of the room; in general $1.25 \le n \le 1.6$, for radiators usually $n = 1.3$ and for convectors $n =$ up to 1.6.
It is assumed that equation (5.35) is valid for the radiator as a whole (for a model type 210), as well as for each separate region of the radiator in case of a model type 270.

The (logarithmic) mean temperature difference $\Delta\theta$ is calculated from:

$$\Delta\theta = \frac{\theta_s - \theta_x}{\ln\left(\dfrac{\theta_s - \theta_e}{\theta_x - \theta_e}\right)} \quad (K) \tag{5.36}$$

where θ_s is the supply temperature, θ_x is the exit temperature, and θ_e is the environment temperature. As described by Stephan (1988) it is sometimes advantageous to employ the arithmetic mean temperature difference‡, but this is only valid when the water mass flow

† Note that the time step averaged net total heat output of the radiator is also transferred to the plant results library (see Section 5.3.5)

‡ Note that the arithmetic mean temperature difference (ie. $(\theta_s + \theta_x)/2 - \theta_e$) is commonly used to calculate the exponent n from standardized radiator tests (eg. DIN 4704 and NEN 5065)

rate and the temperature differences are relatively close to the nominal conditions. As, under those conditions the logarithmic mean temperature difference approximates the arithmetic mean temperature difference, it was decided to always use the former, ie. equation (5.36), unless $\theta_s \approx \theta_e$ or $\theta_x \approx \theta_e$ in which case the arithmetic mean temperature difference is used to avoid numerical problems.
It should be noted that this approach implies that the heat transfer coefficient for the radiator approaches zero when the temperature difference with the environment becomes small. An alternative approach might incorporate a lower limit for the heat transfer coefficient, signals that in reality the heat transfer coefficient does not approach zero either. This is a subject for further work.

It is assumed that under non-nominal conditions the environmental temperature θ_e for calculating the actual heat emission of the radiator may be approximated by:

$$\theta_e \approx \frac{\theta_{a,Z} + \sum_{k=1}^{N_W} a_{W,k}\theta_{W,k}}{1 + \sum_{k=1}^{N_W} a_{W,k}} \quad (°C) \tag{5.37}$$

where $\theta_{a,Z}$ is the air temperature of the building zone in which the radiator is located, $\theta_{W,k}$ is the inside surface temperature of a wall k in that building zone, and $a_{W,k}$ is a weighting factor representing the relative influence of $\theta_{W,k}$ in evaluating θ_e (might involve radiation exchange factor, obstruction by furniture, etc.). In case of a plant only simulation or when the user chooses to set $I_Z = 0$, the radiator environment temperature is set to its nominal value, or to the containment temperature if defined to exist.
It should be noted that distinction between heat emission by radiation and by convection (fraction by radiation varies from $0.1 \cdots 0.5$ (–); see eg. ISSO 1986) may be accounted for by defining an appropriate control function actuator as will be explained in Sections 5.5. and 5.6.

The energy balance for the first node of the radiator component i as indicated in Figure 5.14. yields:

$$R_{ij}\dot{m}_{w,j}c_{pw}(\theta_j - \theta_{i,1}) = \frac{\overline{c}_i M_i \partial\theta_{i,1}}{N\,\partial t} \quad (W) \tag{5.38}$$

where R_{ij} is the mass diversion ratio for component node j towards component i, and N denotes the number of nodes in which the radiator is divided (ie. $N = 2$ or $N = 8$ for model type 210 and 270 respectively). The energy balance for the other node(s) of the radiator component i can be written as:

$$\dot{m}_{w,i}c_{pw}(\theta_{i,k-1} - \theta_{i,k}) - \phi_{k-1} = \frac{\overline{c}_i M_i \partial\theta_{i,k}}{N\,\partial t} \quad (W) \quad k = 2 \text{ or } k = 2, 3, \ldots, N \tag{5.39}$$

where

$$\phi_{k-1} = \frac{\phi_0}{\Delta\theta_0^n}\left[\frac{\theta_{i,k-1} - \theta_{i,k}}{\ln\left(\frac{\theta_{i,k-1} - \theta_e}{\theta_{i,k} - \theta_e}\right)}\right]^n \quad (W) \tag{5.39a}$$

As described in Section 5.3, equation (5.39) may be approximated either by an explicit formulation for $\theta_{i,k}$, or by an implicit formulation, or by a mixed scheme. Unless the fully explicit formulation is employed, in which case the present time-row value of ϕ_{k-1} depends solely on already known temperatures, the ϕ_{k-1} term as defined by equation (5.39a) presents us with a problem in that it can not yet be evaluated because of the still unknown future time-row temperatures $\theta_{i,k-1}$ and $\theta_{i,k}$. This problem is solved by first solving equation (5.38) for $\theta_{i,k}$ under the assumption that $\theta_{i,k-1}$ and θ_e are known conditions. Similar to the approach as suggested by Stephan (1988) for a sequential model, the Newton-Raphson technique for solving non-linear equations is used, but in this case only for determining ϕ_{k-1}. With the Newton-Raphson technique a new estimate for $\theta_{i,k}$ is found from the previous iteration step estimate $\theta^*_{i,k}$ estimate† by:

$$\theta_{i,k} = \theta^*_{i,k} \frac{\mathrm{fie}(\theta_{i,k})}{\mathrm{fie}'(\theta_{i,k})} \quad (^\circ C) \tag{5.40}$$

where $\mathrm{fie}(\theta_{i,k})$ is the imbalance of equation (5.39) for which we want to locate the root for $\theta_{i,k}$, and $\mathrm{fie}'(\theta_{i,k})$ is the derivative of this function:

$$\mathrm{fie}'(\theta_{i,k}) = -\dot{m}_{w,i} c_{pw} - \frac{\overline{c}_i M_i}{N \Delta t} - n \frac{\phi_0}{\Delta \phi_0^n} \left[\frac{\theta_{i,k-1} - \theta_{i,k}}{\ln\left(\frac{\theta_{i,k-1} - \theta_e}{\theta_{i,k} - \theta_e}\right)} \right]^{n-1} \frac{\frac{\theta_{i,k-1} - \theta_{i,k}}{\theta_{i,k} - \theta_e} - \ln\left(\frac{\theta_{i,k-1} - \theta_e}{\theta_{i,k} - \theta_e}\right)}{\left(\ln\left(\frac{\theta_{i,k-1} - \theta_e}{\theta_{i,k} - \theta_e}\right)\right)^2} \quad (W) \tag{5.40a}$$

With the plant component type 210 we only have to do this for the second node. In case of plant component type 270 this process is repeated for each successive nodal temperature $\theta_{i,k}$ each time assuming that $\theta_{i,k-1}$ is a known condition. The equations (5.38) and (5.39) are then incorporated in the overall plant system energy matrix and solved as described in Section 5.3. Because the calculation of the radiator heat emission starts from the current temperature of the first node, $\theta_{i,1}$ is marked for iteration.

As the previous models, this model can also generate matrix coefficients for two mass balances. The first and second phase mass balance matrix coefficients are generated as indicated in Section 5.3. The first phase mass balance coefficients will obviously reflect that $\dot{m}_{w,i,1} = \dot{m}_{w,i,2} = \cdots = \dot{m}_{w,i,N}$. The matrix coefficients for the second phase mass balance will evaluate to $\dot{m}_{v,i,1} = \dot{m}_{v,i,2} = \cdots = \dot{m}_{w,i,N} = 0$.

5.4.10. Plate Heat Exchanger (component type 120)

The matrix coefficient generator described in this section, is meant to represent a plate heat exchanger which may be used as an air-to-air heat recovery device in ventilating and/or warm air heating systems. The type 120 component model is based on a two node

† note that here * denotes the previous iteration step estimate which is **not** necessarily the previous time step value

representation of a cross flow plate heat exchanger, and is schematically drawn in Figure 5.15.

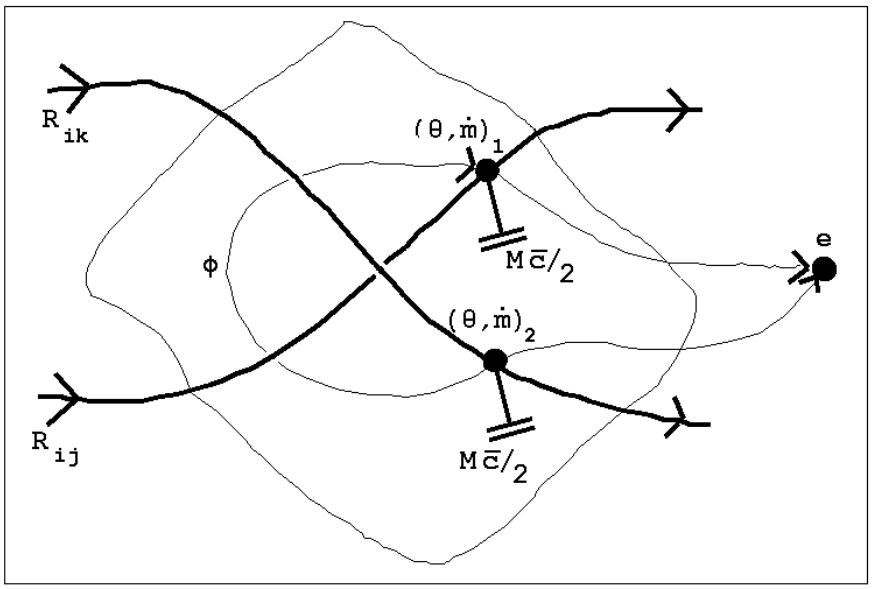

Figure 5.15 Schematic representation of a two node model for a cross flow plate heat exchanger

All the mass involved is assumed to be evenly distributed over the two nodes which are coupled to the exits of the component. The component overall heat loss coefficient - to the environment - is also assumed to be evenly distributed over the two nodes. Both nodes are linked to air nodes somewhere else in the plant system. In case of a ventilation heat recovery device, the flow path via node j and node 1 could represent the fresh air supply to the building, while the flow via node k and node 2 could represent the exhaust air from the building.
This type 120 model, is a simple model with obviously limited dynamic possibilities. It would be possible to incorporate more comprehensive models of heat recovery devices as described by for instance Kohonen et al. (1988), but this is left for the future. Having mentioned this, the current model only uses readily available catalogue data and is therefore presented here as a model which may be employed in combined large-scale building and plant simulation.

The user-definable parameters for this plate heat exchanger are:

1	M	component total mass	kg
2	$\overline{c}$	mass weighted average specific heat	J/kgK
3	UA	component overall (environment) heat loss coefficient	W/K
4	A_o	total plate heat transfer area	m^2
5	A_f	heat exchanger net face area	m^2

Additional output variables (as meant in Section 5.3.5) for this component type are:

1	ϕ	heat exchange from flow via node 2 to other flow	W
2	ε	coil effectiveness	–
3	$C_{\min}/C_{\max}$	ratio of fluid capacity rates	–
4	h_1	air film heat transfer coefficient flow 1	W/m^2K
5	h_2	air film heat transfer coefficient flow 2	W/m^2K

It is assumed that the heat transfer (ie. exchange) ϕ between the two air streams, may be evaluated as if the component was operating under steady-state conditions. Then part of this heat transfer is involved in changing the temperature of the component's thermal mass and the remaining heat actually heats or cools the air streams. This approach is quite similar to the technique described in Section 5.4.3. Thus assuming steady-state conditions, the exchange of heat may be calculated with the N_{TU}-method which uses the concept of thermal effectiveness ε. The N_{TU}-method is described in various textbooks like for example by Kays and London (1984) or by McQuiston and Parker (1988). The thermal effectiveness ε, is defined as the ratio between actual heat transfer rate and maximum possible heat transfer rate. The exchange of heat between the two air streams then becomes:

$$\phi = C_{\min}\varepsilon(\theta_k - \theta_j) \quad (W) \tag{5.41}$$

where $C_{\min}$ is the smaller fluid capacity rate (for definition see equation (5.3a)) of that for the two air streams, and θ_j and θ_k are the temperatures of the air entering through the component's external connections.† A heat exchanger might have various flow arrangements. Here we assume it is a cross flow arrangement, which is commonly used for plate heat exchangers. For a cross flow heat exchanger with both streams unmixed, the effectiveness may be approximated by:

$$\varepsilon \approx 1 - \exp\left\{\frac{1}{\eta\, C}\,[\exp(-N_{TU}\,\eta\, C) - 1]\right\} \quad (-) \tag{5.42}$$

where

$$N_{TU} = A_o/[C_{\min}(1/h_1 + 1/h_2)] \quad (-)$$

$$\eta = N_{TU}^{-0.22} \quad (-)$$

$$C = C_{\min}/C_{\max} \quad (-)$$

in which A_o is the total heat transfer area (ie. approximately the number of plates times the area per plate), and h_1, and h_2 are the air film heat transfer coefficients for the two air streams. In contrast to the component types 110 and 410, the thermal resistance of the (metal) plate itself is neglected. If deemed necessary, fouling can be accounted for by adjusting the plate heat transfer area.

The main factors influencing the air film heat transfer coefficient are: velocity and state of the air when entering the heat exchanger, and the design of the heat exchanger ie. aspect ratio, size and spacing of the plates. For the general case, where there are no detailed information and/or experimental results available, it is very difficult to give a good

† Equation (5.41) defines the sign convention for ϕ which will only be positive when $\theta_k \geq \theta_j$. If this condition is not met, this merely indicates that the air stream through node 2 will cool instead of heat the other air stream.

relationship for the air film heat transfer coefficient. Within the framework of a previous study (Hensen & De Wit 1986), a literature review was conducted regarding heat transfer due to forced convection between two flat plates. One of the results of this study was that for $\mathrm{Re} > 2300$ the various expressions which can be encountered in literature are quite consistent. One of the easiest expressions to work with, originates from Duffie and Beckman (1980), and states that for fully developed turbulent flow between two flat plates with one side heated and the other side insulated[‡]:

$$\mathrm{N} = 0.0158\,\mathrm{Re}^{0.8} \quad (-) \tag{5.43}$$

Assuming dry air with $0 \leq \theta_a \leq 25°C$, and a plate spacing in the range $0.5 \cdots 2\ mm$, this yields the following approximation:

$$h_a \approx 10 \cdot \overline{v}_a \quad (W/m^2K) \tag{5.44}$$

where $\overline{v}_a$ is the average air velocity between the plates (ie. $\dot{m}_a/(\rho_a A_f)\ m/s$). It should be noted that although equation (5.44) is only an approximation, by calculating the effectiveness ε on the basis of physical correlations for the heat transfer, the model 120 heat exchanger will most likely yield the right trend in results whenever the air flow rates change in an absolute sense or relative to each other.
Because the calculation of the heat exchange ϕ starts from the current values of temperature and first mass flow rate for both air streams, there are four state variables which are marked for iteration: θ_1, θ_2, $\dot{m}_{a,1}$, and $\dot{m}_{a,2}$.

The energy balances for the two nodes can now be written as:

$$C_{ij}(\theta_j - \theta_{i,1}) - \frac{UA}{2}(\theta_{i,1} - \theta_e) + \phi = \frac{\overline{c}_i M_i \partial\theta_{i,1}}{2\,\partial t} \quad (W) \tag{5.45a}$$

$$C_{ik}(\theta_k - \theta_{i,2}) - \frac{UA}{2}(\theta_{i,2} - \theta_e) - \phi = \frac{\overline{c}_i M_i \partial\theta_{i,2}}{2\,\partial t} \quad (W) \tag{5.45b}$$

where C_{ij} is defined as in equation (5.3a). The above energy balance equations are then incorporated into the overall system matrix and solved as described in Section 5.3.

The first and second phase mass balance matrix coefficients are also generated as described in Section 5.3.. In case of the second phase mass balance, the model compares θ_i with the dew-point temperature θ_{dew} corresponding to the prevailing moist air conditions. If during some simulation time step θ_i falls below θ_{dew}, a warning message is issued but the program continues as if no condensation occurs.

5.4.11. Thermostatic Radiator Valve (component type 500)

The matrix coefficient generator described in this section, is meant to represent the thermal behaviour of a thermostatic radiator valve. The hydraulic behaviour (including hysteresis etc.) may be represented by a (flow component type 410) general flow corrector component

‡ Which is close to the actual conditions in any channel through the plate heat exchanger if only one half of this channel is taken into account. The centre plane through the channel may be regarded adiabatic, because the channel wall temperatures will be symmetrical when viewed perpendicular to the direction of flow.

as described in Section 4.3.10. Thus this plant component type 500 is actually only the sensor part of a thermostatic radiator valve. The type 500 component model is based on a single node representation of a thermostatic valve as described by Ast (1988). The model is schematically drawn in Figure 5.16.

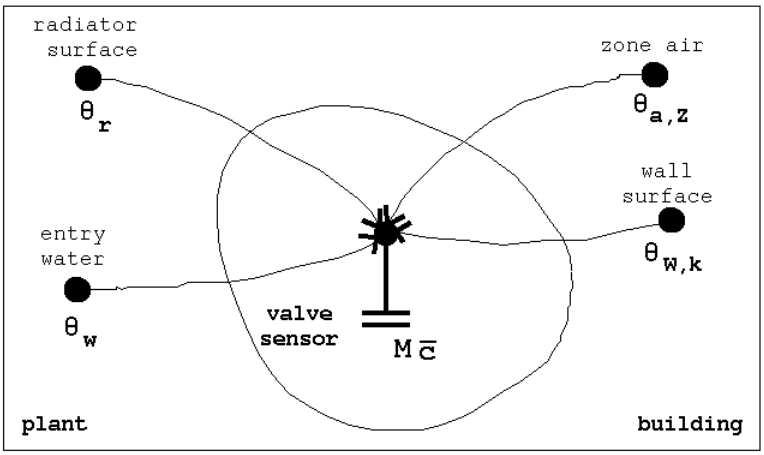

Figure 5.16 Schematic of a single node model for representing the thermal behaviour of a thermostatic radiator valve (after: Ast 1988)

As Ast (1988) points out, if it is assumed that the heat transfer between casing and sensor proceeds fast compared to the dynamic behaviour of sensor and casing, the total mass may be thought concentrated in a joint mass point. This node is coupled to the radiator entry water temperature θ_w, the mean radiator temperature θ_r, the air temperature of the building zone $\theta_{a,Z}$, and to the surface temperature of a wall $\theta_{W,k}$ in that zone, with appropriate equivalent heat transfer conductances.
The user-definable parameters for this plant component type 500 are:

1	M	component total mass	kg
2	$\overline{c}$	mass weighted average specific heat	J/kgK
3	I_Z	index of coupled building zone	–
4	I_W	index of coupled wall in that zone	–
5	k_w	thermal conductance between water and sensor	W/K
6	k_a	equivalent convective heat transfer conductance	W/K
7	k_W	equivalent radiative heat transfer conductance to wall	W/K
8	k_r	equivalent radiative heat transfer conductance to radiator	W/K

Additional output variables (as meant in Section 5.3.5) for this component type are:

1	$\theta_{a,Z}$	air temperature of the building zone	$°C$
2	$\theta_{W,k}$	surface temperature of wall	$°C$

As described by Ast (1988), the thermal conductance between water and sensor k_w may be estimated from measurement results of standardized tests. The equivalent convective heat

transfer conductance k_a may be estimated from the product of valve outer surface area and convective heat transfer coefficient. The equivalent radiative heat transfer conductances k_W and k_r may be estimated from the product of valve outer surface area and radiation heat transfer coefficients. It should be noted that these conductances may be regarded as weighting factors amongst each other with respect to the temperatures involved. Without going into details on how to achieve these, here it suffices to present some commonly encountered parameter values as derived from Ast (1988):

0.05	≤	M	≤	0.15	kg
900	≤	$\bar{c}$	≤	1200	J/kgK
0.002	≤	k_w	≤	0.007	W/K
0.03	≤	k_a	≤	0.12	W/K
0.03	≤	k_W	≤	0.06	W/K
0	≤	k_r	≤	0.006	W/K

The energy balance for this thermostatic valve component i yields:

$$k_w(\theta_w - \theta_i) + k_a(\theta_a - \theta_i) + k_W(\theta_W - \theta_i) + k_r(\theta_r - \theta_i) = \frac{\bar{c}_i M_i \partial\theta_i}{\partial t} \qquad (W) \quad (5.46)$$

In terms of the basic plant model of Section 5.3., the current model has two user-definable external connections: one to the radiator entry water temperature (which defines θ_w), and the second to some other radiator temperature (defining θ_r). Obviously both connections do not involve any mass flow. The terms k_w and k_r are the so-called cross-coupling matrix coefficients.
In case of a plant only simulation or when the user chooses to set $I_Z = 0$, the building zone air temperature and wall surface temperature will be set to default values: $\theta_{a,Z} = \theta_{W,k} = 20°C$ or to the containment temperature if defined to exist. All terms related to the building zone and wall will be moved to the matrix equation right hand side. Thus the partial differential equation (5.46) can be incorporated in the overall plant system matrix as described in Section 5.3.

This model is also capable of generating matrix coefficients for the two mass balances. This enables incorporation of this model in for example a configuration which incorporates both a WCH system and a ventilating system.
Both the first and second phase mass balance matrix coefficients are generated as indicated in Section 5.3., and will obviously reflect that $\dot{m}_{a,i} = \dot{m}_{v,i} = 0$.

5.4.12. Mechanical Room Thermostat (component type 510)

The plant component type 510 is a matrix coefficient generator for a model which represents the thermal behaviour of a mechanical room thermostat.† The mechanical room thermostat is a device which is used as the sensor part for so-called reference room control of a heating

† The plant component type 510 may also be employed as part of a plant control loop (see Section 5.5.) representing a electronic room thermostat. Although the availability and number of installed electronic room thermostats is rapidly increasing, they are still - at least in The Netherlands - far outnumbered by mechanical room thermostats.

system. Usually the room thermostat also functions as a control switch for the boiler and is as such incorporated in a electric circuit together with the fuel valve and boiler safety thermostat. However, the current model represents only the thermal part of a mechanical room thermostat. The corresponding actuator part and control law (describing set point, set differential, etc.), are described in the following Section 5.5.
The type 510 component model is based on a single node representation of a mechanical room thermostat, which is schematically drawn in Figure 5.17.

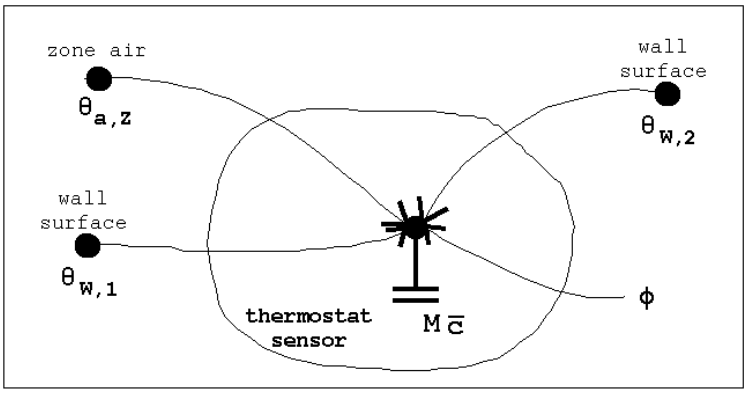

Figure 5.17 Schematic of a single node model for representing the thermal behaviour of a mechanical room thermostat

A typical feature of this type of device is the so-called acceleration heating of the room thermostat, which is represented here by ϕ. This acceleration heating is enabled whenever the sensor temperature falls below the thermostat set point and the fuel gas flow to the boiler is activated. The objective of the acceleration heating is to prevent overshoot of indoor temperature. This is achieved by increasing the sensor temperature relative to the actually sensed temperature, in order to disable the burner operation before the actually desired room temperature is reached.

The total mass of the room thermostat (which is usually fairly small), is assumed to be concentrated in the one node. This node is coupled via appropriate heat transfer conductances to the air temperature of the building zone $\theta_{a,Z}$, to the surface temperature of a wall $\theta_{W,1}$ in that zone, and to the surface temperature of the wall $\theta_{W,2}$ on which the room thermostat is mounted.
The user-definable parameters for this plant component type 510 are:

1	M	component total mass	kg
2	$\overline{c}$	mass weighted average specific heat	J/kgK
3	I_Z	index of coupled building zone	–
4	$I_{W,1}$	index of coupled wall in that zone	–
5	$I_{W,2}$	index of wall on which device is mounted	–
6	k_a	equivalent convective heat transfer conductance	W/K
7	$k_{W,1}$	equivalent radiative heat transfer conductance to wall $W,1$	W/K
8	$k_{W,1}$	equivalent thermal conductance to wall $W,2$	W/K

The variable which may be selected to be controlled by a user-definable plant control loop (see Section 5.5) for the mechanical room thermostat model is:

1	ϕ	acceleration heating	W

Additional output variables (as meant in Section 5.3.5) for this component type are:

1	$\theta_{a,Z}$	air temperature of the building zone	$°C$
2	$\theta_{W,1}$	surface temperature of wall 1	$°C$
3	$\theta_{W,2}$	surface temperature of wall 2	$°C$

As with the previous component model, the equivalent convective heat transfer conductance k_a may be estimated from the product of casing outer surface area and convective heat transfer coefficient. The equivalent radiative heat transfer conductance $k_{W,1}$ may be estimated from the product of outer surface area and radiation heat transfer coefficient. The equivalent thermal conductance $k_{W,2}$ may be estimated from ratio of contact area and thermal resistance between the sensor and wall surface. These conductances may be regarded as weighting factors amongst each other with respect to the various temperatures involved. Without going into details on how these values are arrived at, estimates for the various parameter values are:

0.05	$\leq$	M	$\leq$	0.15	kg
900	$\leq$	$\overline{c}$	$\leq$	1200	J/kgK
0.03	$\leq$	k_a	$\leq$	0.2	W/K
0.01	$\leq$	$k_{W,1}$	$\leq$	0.1	W/K
0.01	$\leq$	$k_{W,2}$	$\leq$	0.5	W/K

The energy balance for this room thermostat component i yields:

$$k_a(\theta_a - \theta_i) + k_{W,1}(\theta_{W,1} - \theta_i) + k_{W,2}(\theta_{W,2} - \theta_i) + \phi = \frac{\overline{c}_i M_i \partial\theta_i}{\partial t} \quad (W) \tag{5.47}$$

When compared to the basic plant model of Section 5.3., the current model has no user-definable external connections, thus there will be no so-called cross-coupling matrix coefficients.
In case of a plant only simulation or when the user chooses to set $I_Z = 0$, the building zone air temperature and wall surface temperatures will be set to default values: $\theta_{a,Z} = \theta_{W,1} = \theta_{W,2} = 20°C$ or to the containment temperature if defined to exist. All terms related to the building zone and walls will be moved to the matrix equation right hand side. Then the partial differential equation (5.47) can be incorporated in the overall plant system matrix as described in Section 5.3.

This model is also capable of generating matrix coefficients for the two mass balances. This enables incorporation of this model in for example a configuration which incorporates both a WCH system and a ventilating system. Both the first and second phase mass balance matrix coefficients are generated as indicated in Section 5.3., and will obviously reflect that $\dot{m}_{a,i} = \dot{m}_{v,i} = 0$.

5.4.13. Imaginary Mass-less Temperature Source (component type 900)

The plant component type 900 is a matrix coefficient generator for a two node imaginary mass-less temperature source. The first node represents air and the second node represent water. Each node has one external inlet connection. The model is capable of generating matrix coefficient for all three balance types. In case of a second phase mass balance, the generated coefficients for the water node will be such that $\dot{m}_v = 0$.
There are no user-definable parameters for this component.

The variables which may be controlled by a user-definable plant control loop (see Section 5.5) are:

1	θ_a	air temperature	$^\circ C$
2	θ_w	water temperature	$^\circ C$

This model is specifically suited for setting up small plant networks for verification and validation purposes as will be seen in Chapter 6.

5.5. AVAILABLE PLANT CONTROL FEATURES

As indicated in the previous sections, when formulating a plant component model, it is defined which variables *may* be subjected to some plant control strategy. In the event a control strategy is not necessary, the control variable will be assigned some default value as defined in the system configuration file described by Table 5.1., otherwise a plant control strategy has to be defined.
In *bps* and *plt* a plant control strategy is comprised of one or more *control loops*.[†‡] Each control loop is defined by: sensor location, actuator location, controller type, and control law. A control loop is not static but has a temporal dimension so that it can change as a function of time.

A sensor exists to measure some control variable for transmission to the control law representing the active controller. The control variable may be any nodal state variable active within a simulation, an outdoor condition, one of the plant component additional variables, or may be a derived combination of the previous. The sensor location is defined by three data items I_1, I_2, and I_3 which are assigned the meanings as indicated in Table 5.4. The nature of the signal which is actually sensed, will be defined by the controller type.

Table 5.4 Sensor location definition for plant control loops

I_1 Value & Meaning	I_2 Value & Meaning	I_3 Value & Meaning
>0 building zone	**=0** zone air point	**=0** ie not used

† To differentiate, for building control strategies the term *control function* is employed.

‡ Note that in case of mass flow simulation, the fluid mass flow network may also incorporate flow controllers. These flow control devices are not necessarily controlled by plant *control loops*, but may be activated independently (see Sections 4.3.10 to 4.3.12).

I_1 Value & Meaning		I_2 Value & Meaning		I_3 Value & Meaning	
>0	building zone	**>0**	construction in zone	**=0**	inside surface
>0	building zone	**>0**	construction in zone	**>0**	position within construction
=0	sensor in whichever zone control function is associated with	**=0**	zone air point	**=0**	ie not used
-1	sensor in plant component	**>0**	plant component	**>0**	node within component
-2	sensor measures mix of zone air and mean radiant temperature	**>0**	building zone	**>0**	convective weighting factor C (%). Sensed temperature θ_s: $\theta_s = \theta_a\, C/100 + \theta_r\, (1 - C/100)$
-3	sensor measures outdoor conditions	**≥0**	index identifies which variable to use	**=0**	ie not used
-4	sensor measures additional plant component output	**>0**	plant component	**>0**	index of additional output variable for corresponding component type

Thus 0,0,0 would indicate sensing of the air condition of whichever zone was assigned the corresponding control; 5,0,0 would sense zone 5 air conditions; 3,5,0 would sense zone 3, construction 5 surface conditions; 2,6,1 would sense zone 2, construction 6, outermost surface conditions; -1,15,3 would sense plant component 15, node 3 conditions; -2,7,65 would sense zone 7 mixed temperature with a 65% air temperature weighting and 35% mean radiant temperature weighting; -4,10,1 would sense plant component 10, first additional output (eg. in case of type 250 boiler this would indicate whether the boiler was actual on or off).

Actuators exist to transmit the output of a controller to some building zone or plant component, usually to reduce the deviation of the sensed control variable from some user-specified set point. Actuator locations can be set to any building side node (air, surface, mixed, intra-construction) or plant component participating in a simulation. Like the sensor, actuator location is defined by three data items (say J_1, J_2 and J_3) which are assigned the meanings as indicated in Table 5.5. The property which is actually regulated (ie. temperature, heat flux, mass flow rate, etc) will also be defined by the controller type.

Table 5.5 Actuator location definition for plant control loops

J_1 Value & Meaning		J_2 Value & Meaning		J_3 Value & Meaning	
>0	building zone	**=0**	zone air point	**=0**	ie not used
>0	building zone	**>0**	construction in zone	**=0**	inside surface
>0	building zone	**>0**	construction in zone	**>0**	position within construction as for sensor

J_1 Value & Meaning		J_2 Value & Meaning		J_3 Value & Meaning	
=0	actuator in whichever zone the control function is associated with	**=0**	zone air point	**=0**	ie not used
-1	actuator in plant component	**>0**	plant component	**>0**	control variable for corresponding component type
-2	actuator inputs mix of convective and radiant heat flux to a zone	**>0**	building zone	**>0**	convective weighting factor C (%). Injected convective heat flux to air point ϕ_c from: $\phi_c = \phi_t\, C/100$ and radiant heat flux ϕ_r to surfaces from: $\phi_r = \phi_t\,(1 - C/100)$;

The actual property sensed by the sensor and actuated at the actuator is controlled by the *controller type*. Table 5.6 lists the currently supported options. Obviously, not every combination of sensor location, actuator location, and controller type would make sense (eg. when the sensor is located in a building zone air point, only those controller types which measure dry bulb temperature or enthalpy would be sensible). Invalid combinations will be disallowed by the program.
The "*variable expecting numerical value*" implies a wide range of control variables which may best be exemplified by for instance the control signals for a type 260 boiler: aquastat set point which usually is a value in the range $60 \cdots 90°C$, an boiler ON / OFF signal which must either be 0 or 1.

Table 5.6 Currently supported plant controller types

Index	Sensed property	Actuated property
0	temperature	heat flux
1	temperature	flow rate
2	enthalpy	heat flux
3	enthalpy	flow rate
4	1st phase mass flow rate	heat flux
5	1st phase mass flow rate	flow rate
6	2nd phase mass flow rate	heat flux
7	2nd phase mass flow rate	flow rate
8	additional plant output	heat flux
9	additional plant output	flow rate
10	temperature	variable expecting numerical value
11	enthalpy	variable expecting numerical value
12	1st phase mass flow rate	variable expecting numerical value
13	2nd phase mass flow rate	variable expecting numerical value
14	additional plant output†	variable expecting numerical value

A control law is an algorithm which represents the logic of some controller (real or imaginary). Its purpose is to translate (algorithmically) the sensed condition to the actuated

† Type 14 is also the appropriate choice in case of a sensor type -3 and sensed variable other than temperature or enthalpy

state in terms of the control system characteristics. Table 5.7. gives an overview of the control law subroutines presently available for plant control.

Table 5.7 Currently supported plant control laws

Index	Control law description
0	All plant component control variables set to zero. This would also be the appropriate choice in case of a control loop which is set up to define sensor location and sensor type for a mass flow corrector component (see eg. Sections 4.3.10 to 4.3.12). No required data items.
1	Basic proportional action for use with a type of controller which actuates heat flux 8 required data items: 1: maximum heating flux (W)/ 2: minimum heating flux (W)/ 3: maximum cooling flux (W)/ 4: minimum cooling flux (W)/ 5: heating set point for control variable (SU)/ 6: cooling set point for control variable (SU)/ 7: throttling range for heating (SU)/ 8: throttling range for cooling (SU)
2	Basic proportional action for use with a type of controller which actuates flow rate 4 required data items: 1: maximum flow rate (m^3/s *or* kg/s)/ 2: minimum flow rate (m^3/s *or* kg/s)/ 3: set point for control variable (SU)/ 4: throttling range for control variable (SU)
3	Basic proportional numerical value generator for use with a type of controller acting on a variable which expects such a signal 5 required data items: 1: output O_u when $S \geq S_u$ (-)/ 2: output O_l when $S \leq S_l$ (-)/ 3: upper set point for control variable S_u (SU)/ 4: lower set point for control variable S_l (SU)/ 5: ΔS to overcome controller's hysteresis (SU)
4	Optimum start controller generating either ON (ie. 1) signal or heating flux, when time is past the optimum start time necessary to reach desired temperature level at a specified time† 5 required data items: 1: output, ie. either "1" or heating flux (W)/ 2: time when desired temperature should be reached ($hour$)/ 3: desired temperature level θ_0 ($°C$)/ 4: coefficient a_0 (s)/ 5: coefficient a_1 (s/K)/
*	For control laws 1. and 2. the upper set point equals the set point plus half the throttling range, and the lower set point equals the set point minus half the throttling range
*	SU stands for *Sensor Units* indicating that the units are assumed to correspond to the sensor
*	Behaviour of control law 3. is similar to relationship sketched in Figure 4.13

Given the framework and the resources available to the present research project, the currently available control laws are restricted to the ones indicated in Table 5.7. It must be clear that it is quite feasible to set up control laws which represent the control behaviour of a self adaptive optimum start control algorithm or the control behaviour of a proportional-integrating (PI), a proportional-integrating-differentiating (PID), or some logic controller. However, this is left for the future.

With the ingredients described above it is possible to simulate all controllers commonly encountered in domestic and (small) commercial buildings. This is best illustrated by some examples:
• Most widespread - at least in The Netherlands - is centralized ON/OFF boiler control with a

† The expression used to calculate the time Δt necessary to reach the desired temperature level θ_0 based on some sensed temperature θ, originates from Birtles and John (1983, 1985): $\Delta t = \exp[\, a_0 + a_1(\theta - \theta_0)]$ (s). In a study by Van der Laan (1987), and Van der Laan et al. (1987), this was found to be one of most practical expressions available from literature at the time.

mechanical room thermostat in a reference room. To simulate such a control, a room thermostat model needs to be coupled to the reference room. Then a control loop is set up which senses the thermostat temperature (a plant node) and actuates the boiler ON/OFF (ie. 1 or 0) signal. A second control loop might be set up which senses whether the boiler is actually - due to action of the boiler maximum thermostat - ON/OFF (this is an additional plant model output), and which actuates the acceleration heating of the room thermostat. This may then be expanded with a third control loop which task could be to regulate the water flow through the system by controlling the pump.

- To investigate the performance of an optimum start controller, a control loop using control law 4 could be employed. This control loop would have to incorporate a sensor measuring zone side air temperature or a mix of zone side air and mean radiant temperature, and would have to actuate the boiler. In case of boiler type 200, the controller's type would be 0, and in case of boiler type 250 or 260, the controller type would be 10.
- Boiler aquastat set point control based on outdoor temperature can be achieved by setting up a control loop which senses the outdoor temperature and actuates the aquastat set point. When using control law three and setting for example the five required data items to 20, 90, 20, -10, and 0 respectively, will linearly decrease the aquastat set point from 90 to 20 for outdoor temperatures increasing from -10 to $20°C$. For even lower or higher outdoor temperatures, the aquastat set point will be remain at the limiting values 90 and 20 respectively. No hysteresis is taken into account.
- In order to achieve decentralized room temperature control, the previous example might be supplemented with thermostatic radiator valves. This may be realized by setting up a mass flow network representing the hydronic system and incorporating flow corrector components (eg. flow component type 410). The plant system network would have to incorporate one or more radiators "equipped" with a thermostatic radiator valve (plant model type 500). For each controlled radiator a plant control loop would be set up which senses the temperature of the corresponding thermostatic radiator valve. Control law 0 would be appropriate for such a control loop. When defining the mass flow network, the sensed property index of a flow corrector component would then point to the plant control loop which actually senses the temperature of the corresponding thermostatic valve.

5.6. COUPLING OF BUILDING AND PLANT

Coupling of building and plant in a mathematical numerical sense, effectively means combining the building side energy balance matrix equation (see Clarke 1985), the plant energy balance matrix equation (5.7), one or two plant mass balance matrix equations (5.8), and preferably also some matrix equation representing the flow through a combined building and plant mass flow network. In principle, it is possible to combine all five matrix equations into one overall super-matrix, which can then be solved simultaneously. This super-matrix would probably be very difficult to administrate and would have a complicated, and highly sparse structure. Besides this, some sort of iteration would still be necessary because of all the non-linear relationships for which some form of linearization was needed in order to incorporate them into the respective matrix equations as explained in Chapter 4. and the previous sections of the current chapter.
Division of the overall simulation problem into separate functional sub-systems - as described before - is therefor almost unavoidable from a practical point of view. This approach has distinct advantages. The most noticeable are the strong reduction of both memory requirement (ie. matrix dimensions) and of matrix sparsity, and that - in terms of computer coding - it is much easier to "administrate" up to five functionally different matrices. Other advantages are that mixed-frequency and variable time stepping schemes are

possible, and that it becomes very easy to leave out of consideration one or more matrices, depending on the problem at hand; for example when the problem incorporates a building only, plant only, plant + flow, etc.
It should be recognised however that there might be strong thermodynamic and/or hydraulic couplings between the different matrix equations. If a variable in one balance (say air temperature of a zone) depends on a state variable solved from one of the other matrix equations (say the temperature of a radiator), we have to ensure that both values match in order to find a true (ie. in terms of thermodynamic integrity) simultaneous solution of the overall problem.

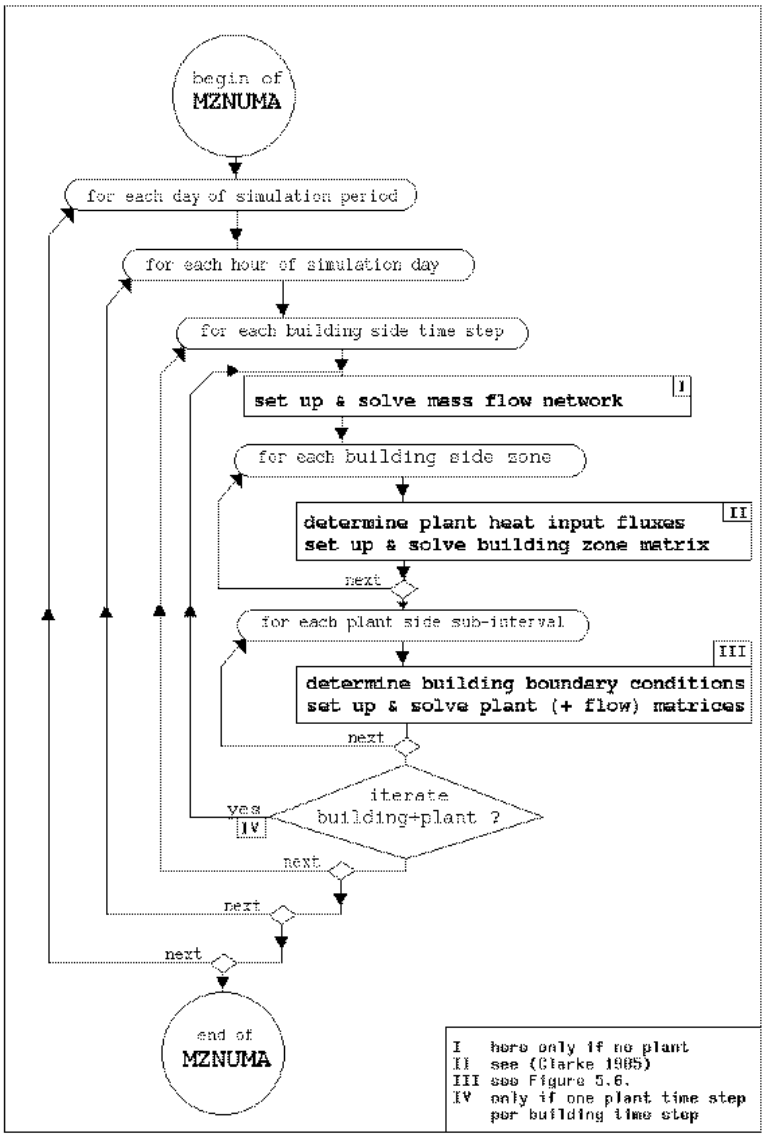

Figure 5.18 Indicative flow chart showing the main loops in the simulation process for a combined building and plant configuration

The current status with respect to the general lay-out of *bps*'s main numerical controller MZNUMA is visualized in Figure 5.18. As indicated in this diagram, the overall configuration simulation time increments may be smaller than one hour.† A complete configuration time step involves the evaluation of all building-side zones followed by the processing of the plant system equations. If a mass flow network is defined to exist, this is processed together with the plant system network as described in Section 5.3.3. In case the user defined a building-only configuration, the mass flow network is processed prior to building zones.
At each overall configuration simulation time step the building- and plant-side state-space equations, and the mass flow network equations are generated and solved from up to five separate matrix equations. The building-side solution process is invoked once per user-specified time step. This process uses a matrix partitioning technique (ie. one partition for each building zone) as described by Clarke (1985). For the building, heat input or extraction by the plant are regarded as as known boundary conditions.
Since it is practice to process the plant equations at a greater frequency than building matrices (because of the different time constants), the plant matrix may be established at some sub-interval of the building time step. For the plant, the connections with the building are treated as excitations. Then the plant matrix is solved by a sparse matrix method as described in Section 5.3.4.

Division of the overall simulation problem in a building-side and a plant-side may leed to certain difficulties. When processing the building-side energy balance, heat input or heat extraction by the plant for the time step under consideration should be known. It is common practice to use plant side temperatures and mass flow rates from the previous time step in evaluating this heat exchange. When building-side control is based on a plant-side originating signal a similar time shift occurs. When processing the plant-side energy balance, the component losses are calculated with containment (perhaps building-side) temperatures which were calculated with plant-side state variable values from the previous plant time step. A similar effect may occur when plant-side control is based on a signal originating from the building-side.
One way to deal with this kind of problems, is to make use of a mechanism such as indicated in Figure 5.18. which could be labeled as a mixed direct/iterative solution scheme. At the indicated point in the calculation process, the plant heat input as assumed in processing the building side is compared with the plant heat emission as calculated when processing the plant side. If the difference exceeds some user specified value, the whole building and plant solution process is repeated based on the newly calculated values. If either the absolute or the relative difference between assumed and newly calculated building/plant heat exchange satisfies the user specified tolerances, the model proceeds with the next time step. In order to prohibit excessive number of iterations, the iteration process may only be enabled when the user specifies one plant time step per building time step.

The total heat exchange of a plant component with its environment is comprised of component losses or parasitic heat exchange, and a "deliberate part" (which in a real system is usually zero for the majority of components). This distinction is reflected in the two ways in which - from a user point of view - the heat flux exchange between a plant component and a building zone may be defined:

- when a plant component containment is defined as being a building zone (see Section 5.2),

† Note that by choosing a time step the user implicitly decides to ignore the process dynamics within the time step

all heat exchange with the environment will be effectuated at the air node of the corresponding building zone. This option is assumed in Figure 5.18.

- the user may also opt to enable a special building control function (ie. BCL06) which during run time will determine the heat flux exchange between the building zone and a user specified plant component node. Note that there may only be one heat flux coupling like this per building zone. Two possibilities then exist:

  1: the plant node in question (say node i) is assumed to impose a thermal load on the zone's air point (say node Z) through air flow. The heat transfer may then be calculated directly by simultaneous solution of the equations:

$$\phi = \dot{m}_a \, c_{pa} \, (\theta_i - \theta_{a,Z}) \quad (W) \tag{5.48a}$$

  and

$$\phi = \frac{D - B\,\theta_{a,Z}}{C} \quad (W) \tag{5.48b}$$

  where equation (5.48b) is the so-called CE (ie. characteristic equation) which emerges when the building zone energy balance matrix is processed as far as possible for an as yet unknown plant heat input ϕ (see Clarke 1985, pp. 141).

  2: the plant component model in question is able to compute a heat exchange flux ϕ based on prevailing zone conditions. This heat flux is then incorporated in the building side energy balance via a CE similar to equation (5.48b). In this case the heat is transferred to the building zone via any actuator type (see Table 5.5.) to: the zone air point, mix of zone air plus all surfaces (eg. a radiator), some wall surface (eg. some directed radiator), inside a construction (eg. floor heating), etc.

  With this option the scheme in Figure 5.18 changes a little in that the building side plant input heat flux is not determined until after the building zone matrix has been solved.

References

ASHRAE 1975. *Procedures for simulating the performance of components and systems for energy calculations*, American Society of Heating, Refrigerating and Air-Conditioning Engineers, New York. W.F. Stoecker (Ed.)

ASHRAE 1985. *Handbook of Fundamentals*, American Society of Heating, Refrigerating and Air-Conditioning Engineers, Atlanta, GA.

H. Ast 1988. ''HVAC component specification: thermostatic valve,'' Energy conservation in buildings & community systems programme. Annex X : system simulation (S15), International Energy Agency. Operating agent: University of Liège

A.B. Birtles and R.W. John 1983. ''Performance of heating systems under optimum start control,'' in *Proc. CIB Symposium on Heating Systems in Practice*, Stockholm.

A.B. Birtles and R.W. John 1985. ''A new optimum start control algorithm,'' in *Proc. Int. Symp. on Control and Operation of Building HVAC Systems*, Trondheim (SINTEF).

M. Brossa and A. Mazza 1988. ''HVAC component specification: pump,'' Energy conservation in buildings & community systems programme. Annex X : system simulation (S11), International Energy Agency. Operating agent: University of Liège

CEC 1983. *System Simulation in Buildings. Proceedings of the International Conference held in Liège (Belgium) on 6-8 December 1982*, Commission of the European Communities, Brussels. J. Lebrun (Ed.), CEC report XII/425/83-EN

CEC 1987. *System Simulation in Buildings. Proceedings of the International Conference held in Liège (Belgium) on 1-3 December 1986,* Commission of the European Communities, Brussels. J. Lebrun (Ed.), CEC report XII-469-87-EN

CEC 1991. *System Simulation in Buildings. Proceedings of the International Conference held in Liège (Belgium) on 3-5 December 1990,* Commission of the European Communities, Brussels. J. Lebrun (Ed.), CEC report in print

D.R. Clark 1985. ''HVACSIM+ Building systems and equipment simulation program: reference manual,'' NBS report NBSIR 84-2996, U.S. Dept. of Commerce, Gaithersburg, MD.

J.A. Clarke 1985. *Energy simulation in building design,* Adam Hilger Ltd, Bristol (UK). (ISBN 0-85274-797-7)

J.A. Clarke, J.W. Hand, P. Strachan, J.L.M. Hensen, and C.E.E. Pernot 1991. ''ESP^{R} A building and plant energy simulation research environment,'' Energy Simulation Research Unit, ESRU Manual U91/2, University of Strathclyde, Glasgow.

M.E.J. Croes 1988. ''De invloed van het regelgedrag van een cv-installatie op energieverbruik en luchttemperatuurvariaties,'' FAGO afstudeerrapport, Eindhoven University of Technology, Eindhoven.

M. Dachelet, J.P. Eppe, J. Hannay, L. Laret, J. Lebrun, G. Liebecq, and B. Lorea 1988. ''HVAC component specification: fuel oil boiler,'' Energy conservation in buildings & community systems programme. Annex X : system simulation (S1), International Energy Agency. Operating agent: University of Liège

DIN 1984. ''Prüfung von Raumheizkörpern,'' DIN 4704 Teil 4, Deutsches Institut für Normung e.V..

J.A. Duffie and W.A. Beckman 1980. *Solar engineering of thermal processes,* John Wiley & Sons, New York.

Ph.J. Ham 1988. ''Dynamisch warmtegedrag van radiatoren en convectoren. Metingen en modelvorming,'' *Verwarming en Ventilatie,* vol. 45, no. 5, pp. 315-334.

V.I. Hanby and J.A. Clarke 1988. ''SERC Plant component model catalogue,'' Final report SERC Grant GR/D/07459 Coordination of HVAC component models, Glasgow.

J.L.M. Hensen and M.H. de Wit 1986. ''Ontwerphulpmiddelen en overwegingen met betrekking tot eenvoudige bouwkundige luchtcollectoren voor verwarming van verse ventilatielucht,'' TNO-TPD rapport 1825, Eindhoven.

M.J. Holmes 1988. ''HVAC component specification: heating and cooling coils,'' Energy conservation in buildings & community systems programme. Annex X : system simulation (S6), International Energy Agency. Operating agent: University of Liège

IBPSA 1989. *Proceedings of Building Simulation '89,* International Building Performance Simulation Association, Vancouver.

IEA 1988. ''HVAC component specification booklets,'' Energy conservation in buildings & community systems programme; Final report Annex X, International Energy Agency. Operating agent: University of Liège, J. Lebrun

ISSO 1986. ''Vermogen van radiatoren en convectoren bij niet-genormeerde opstelling,'' ISSO-publikatie 1 (inclusief ontwerp NEN 5065), Stichting ISSO, Rotterdam.

W.H. Kays and A.L. London 1984. *Compact heat exchangers*, McGraw-Hill, London. 3rd ed.

R. Kohonen, M. Nyman, and P. Marjamäki 1988. ''HVAC component specification: heat recovery devices,'' Energy conservation in buildings & community systems programme. Annex X : system simulation (S7), International Energy Agency. Operating agent: University of Liège

M.J. van der Laan 1987. ''Het opwarmen van woningen en optimaliseringsregeling,'' FAGO afstudeerrapport, Technische Universiteit Eindhoven.

M.J. van der Laan, J.L.M. Hensen, and P.J.J. Hoen 1987. ''Optimaliseringsregeling en nachtverlaging in woningen,'' *Verwarming en Ventilatie*, vol. 44, no. 11.

L. Laret 1988. ''Boiler physical model for use in large scale building simulation,'' in *Proc. USER 1 working conference at Ostend*, pp. 23-28, Society for Computer Simulation International, Ghent (B).

L. Laret 1989. ''Accurate boiler models for large scale simulation,'' in *Proc. Building Simulation '89*, pp. 375-380, International Building Performance Simulation Association IBPSA, Vancouver.

J. Lebrun and G. Liebecq 1988. ''System simulation in buildings; models of HVAC components,'' in *Proc. USER 1 working conference at Ostend*, pp. 17-22, Society for Computer Simulation International, Ghent (B).

J. Lebrun and G. Liebecq 1988. ''System Simulation Synthesis Report,'' Energy conservation in buildings & community systems programme; Final report Annex X, International Energy Agency. Operating agent: University of Liège, J. Lebrun, report AN10 881020-RF

J. Lebrun 1991. Private communication.

T.G. Malmstrom and L.G. Olsson 1988. ''HVAC component specification: ducts,'' Energy conservation in buildings & community systems programme. Annex X : system simulation (S14), International Energy Agency. Operating agent: University of Liège

T.G. Malmstrom 1988. ''HVAC component specification: piping,'' Energy conservation in buildings & community systems programme. Annex X : system simulation (S13), International Energy Agency. Operating agent: University of Liège

S.E. Mattsson 1989. ''Concepts supporting reuse of models,'' in *Proc. Building Simulation '89*, pp. 175-180, International Building Performance Simulation Association IBPSA, Vancouver.

D.J. McLean 1982. ''The simulation of solar energy systems,'' PhD thesis University of Strathclyde, Glasgow.

F.C. McQuiston and J.D. Parker 1988. *Heating, ventilating, and air conditioning. Analysis and design*, John Wiley & Sons, New York. 3rd ed.

NNI 1986. *CV-radiatoren en -convectoren. Bepaling van het vermogen*, Nederlands Normalisatie-instituut, Delft. NEN 5065

M.L.D. van Rij and P.Th.J. Overman 1986. ''Efficiency of CH boilers under laboratory and practical conditions,'' in *Proc. Int. Gas Research Conf.*, pp. 284-294, Toronto.

P. Sahlin and E.F. Sowell 1989. ‘‘A neutral format for building simulation models,’’ in *Proc. Building Simulation ’89*, pp. 147-154, International Building Performance Simulation Association IBPSA, Vancouver.

SEL 1988. ‘‘TRNSYS, a transient system simulation program,’’ Engineering Experiment Station Report 38-12, University of Wisconsin-Madison, Solar Energy Laboratory, Madison, WI. Manual for version 12.2 and later

W. Stephan 1988. ‘‘HVAC component specification: radiator,’’ Energy conservation in buildings & community systems programme. Annex X : system simulation (S4), International Energy Agency. Operating agent: University of Liège

D. Tang 1985. ‘‘Modelling of heating and air-conditioning system,’’ PhD thesis University of Strathclyde, Glasgow.

P.P.N. Triepels 1984. ‘‘De invloed van warmteopslag in wanden op het regelgedrag van verwarmingssystemen: een ontwikkeld rekenmodel,’’ FAGO afstudeerrapport, Technische Universiteit Eindhoven.

J.A. Wright and V.I. Hanby 1988. ‘‘HVAC component specification: fans,’’ Energy conservation in buildings & community systems programme. Annex X : system simulation (S12), International Energy Agency. Operating agent: University of Liège

CHAPTER SIX

VERIFICATION AND VALIDATION

6.1. INTRODUCTION

Computer simulation of heat and mass transfer in building and plant configurations may be thought of as a two step process: (1) modelling of the real physical processes at play, allowing the problem to be solved more easily within practical constraints, and (2) numerical solution of the resulting models. Both steps involve simplifications, assumptions, and are likely to introduce errors in the resulting computer code. Verification and validation is necessary, in order to be able to use the program with confidence.

Verification and validation is thus essential when developing computer simulation programs. It should be noted however, that inaccurate prediction results are not always due to program errors. In their report on validation of building energy analysis simulations, Judkoff et al. (1983) identify seven main sources of error, which - given the context of heat and mass transfer in building and plant configurations - translate into:

1. differences between the actual weather conditions surrounding the building and plant and the weather assumed in the simulation;
2. differences between the actual effect of occupant behaviour and those effects assumed by the user;
3. user error in deriving building and plant input files;
4. differences between the actual thermal and physical properties of the building and plant and those input by the user;
5. differences between the actual heat and mass transfer mechanisms operative in individual components and the algorithmic representation of those mechanisms in the program;
6. differences between the actual interactions of heat and mass transfer mechanisms and the representation of those in the program; and
7. coding errors.

The error sources 1 through 4 are called external since they are independent of the internal workings of the method of calculation. External errors are not under the control of the developer of the computer program. Error sources 5 through 7 are called internal and are directly linked to the internal workings of a prediction technique. Internal errors are contained within the coding of the program.

This chapter will concentrate on internal errors; ie the ability of the simulation program to predict real building and plant performance when given perfect input data. The following sections elaborate the origins of a validation methodology, and - by means of specific case studies - how this may be applied to the program described in this thesis. Although it is recognized that validation is extremely important, the validation activities within the current project, had to be restricted to these examples due to lack of available resources. Two factors may be brought to attention in order to further justify this: (1) a number of the presented plant component models stem from research projects which incorporated verification and validation of those models (see eg IEA (1984) or Lebrun and Liebecq (1988)), and (2) ESP

is already the subject of an extensive validation project. This project is briefly indicated in the following section. Finally, the last section of this chapter, identifies possible directions for future validation activities.

6.2. METHODOLOGY

Ever since the emerging of building energy simulation models, their developers have been involved in verification and validation studies. Usually this involved comparison of measured data with predictions from some specific model by an individual research team (eg. as reported by Lammers 1978). There have also been at least three studies which attempted to establish a more general validation methodology applicable to building energy simulation programs. The first (IEA 1980) and second, reported by Judkoff et al. (1983), resulted in a three part methodology involving inter-model comparisons, analytical tests, and the use of empirical data. The advantages and disadvantages - as summarized by the authors - of each of these three parts are indicated in Table 6.1

Table 6.1 Validation techniques (from: Judkoff et al. 1983)

Techniques	Advantages	Disadvantages
COMPARATIVE: Relative test of model and solution process	No input uncertainty Any level of complexity Inexpensive Quick: many comparisons possible	No truth standard
ANALYTICAL: Test of numerical solution	No input uncertainty Exact truth standard given the simplicity of the model Inexpensive	No test of model Limited to cases for which analytical solutions can be derived
EMPIRICAL: Test of model and solution process	Approximate truth standard within accuracy of data acquisition system Any level of complexity	Measurement involves some degree of input uncertainty Detailed measurements of high quality are expensive and time consuming A limited number of data sites are economically practical

This methodology was further refined and extended in the third study as reported in (BRE/SERC 1988), by Irving (1988) and by Bloomfield (1989). The authors state that:

> *"The word ´validation´ is much misunderstood. It is not feasible to verify the correctness of every path through detailed dynamic thermal simulation programs, to investigate every assumption and approximation, or to take account of every situation in which a program might be used in practice. A working definition of validation was adopted: the testing of the theoretical (physical) correctness of a program and of the mathematical and numerical solution procedures used."*

and they propose a five stage validation methodology, comprising:

1. an initial examination of a model's theory and a thorough inspection of the corresponding source code
2. analytical verification involving a comparison of predictions with analytical solutions

which apply to some well defined, usually simplified case
3. inter-model comparison involving a comparison of the target model with several other models which are usually better known to the validators and may have been subjected to a greater or lesser degree of previous testing
4. empirical validation involving a comparison of predictions with measured data for the same problem domain
5. a parametric sensitivity analysis to ascertain whether or not the model predictions lie within the uncertainty band associated with the input data

This approach was also adopted by the 'model validation and development sub-group' (MVDS) of a collaborative European Community research project in the field of Passive Solar Architecture known as PASSYS. The principal objective of the MVDS, which involves research consortia from ten EC countries, is to approve/define a European validation methodology and to test this by applying it to a common model, ESP. A complete description of the MVDS work may be found in (CEC 1989). As described by Clarke (1990), some eight climate and building side sub-systems were identified as candidates for validation studies in this way. In addition, and principally by the mechanism of empirical validation and sensitivity analysis, an attempt has been made to evaluate ESP^R's performance at the whole model level.

Although none of the validated sub-systems nor the version of ESP^R that was researched by the MVDS incorporates plant simulation features, the above is mentioned here to indicate that the current research starts from a sound basis and from notably the most stringently verified and validated building energy simulation model available today.

To indicate how the above mentioned methodology may be applied to the current extensions of the ESP energy simulation environment, this section now continues with some case studies exemplifying the various verification and validation stages. Due to the nature of the available data, most case studies incorporate inter-model comparison to some extent.

6.2.1. Theory and Code Examination

Theory and code examination is perhaps the most important step of the verification and validation methodology. However, this step is often underestimated. Good examples of theory examination may be found in the IEA Annex X (Lebrun and Liebecq 1988) and the PASSYS (CEC 1989) reports. Both cases involved cross-referencing of each other work by different research groups.
Regarding examination of the underlying theory of fluid flow and plant simulation in the present work, the reader is referred to the previous chapters. Inspection of the corresponding source code is difficult to exemplify. Suffices to remark that all code has been thoroughly checked with computer aided software engineering (CASE) tools (Kruyt 1989) for any syntax errors. The code is very modular structured and heavily commented in order to be more or less self-documentary. The inbuilt trace facilities may be enabled by the user to track the simulation process at a detailed level during run-time. Were possible, the user supplied input data is checked prior to the actual simulation (for example whether or not the user has defined a valid plant network). As indicated in the previous chapters, a number of parameters is checked during run-time (for instance whether or not the flow is actually laminar in a component expecting such).

6.2.2. Analytical Verification

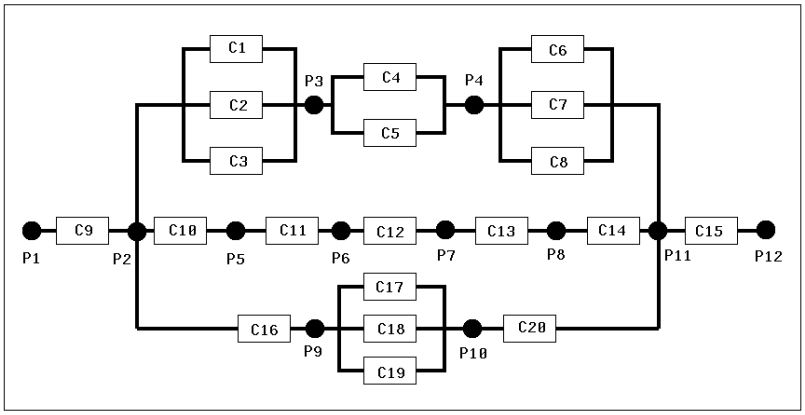

Figure 6.1 Network of fluid flow components arranged in series and parallel

As an example of analytical verification, consider the network of fluid flow components which is schematically drawn in Figure 6.1. This problem was introduced by Walton (1989) to test his AIRNET air flow network simulator. It is a relatively complex network of 'common orifice flow' components (type 40). The problem involves 12 nodes and 20 fluid flow components arranged in series and parallel. The pressure-flow relationship for this type of components (see Section 4.4.4.) can be written as:

$$\dot{m} = C\sqrt{\Delta P} \quad (kg/s) \tag{6.1}$$

where $C = C_d\, A\sqrt{2\rho}$, in which C_d is the discharge factor (-), A is the opening area (m^2), and ρ is the fluid density (kg/m^3). Starting from equation (6.1), it is easy to combine parallel flow components into a single replacement component. For example the combination say C_a of the components C_1, C_2, and C_3 is given by:

$$C_a = C_1 + C_2 + C_3 \quad (kg/s \cdot Pa^{½}) \tag{6.2}$$

It is also possible to convert components in series into a single replacement component. For instance the combination say C_b of C_{10} through C_{14}, is given by:

$$C_b = [\ 1/C_{10}^2 + 1/C_{11}^2 + 1/C_{12}^2 + 1/C_{13}^2 + 1/C_{14}^2\ ]^{-1/2} \quad (kg/s \cdot Pa^{½}) \tag{6.3}$$

In this way it is feasible to derive one single replacement component C_{tot} for the whole network, for which it is then easy to analytically compute the fluid mass flow rate given some pressure difference between the two outermost nodes. Starting from the parameter values as indicated in Table 6.2., it may be deduced that for this network the mass flow rate evaluates to $\dot{m} = 0.0611024$ (kg/s) for $P_1 - P_2 = 100$ (Pa) and $\rho = 1.20415$ (kg/m^3). Actually, by choosing the parameters to represent a combination of large and small flow resistances, a network results which is known to be difficult to solve. When setting the relative and absolute convergence criteria parameters to $1.\,10^{-4}$ $(-)$ and $1.\,10^{-6}$ (kg/s) respectively, *mfs* computes the 'true' mass flow rate $\dot{m} = 0.06110$ (kg/s) in 32 iterations. Walton's AIRNET needs 12 iterations for the same result. It should be noted however that AIRNET needs additional input parameters, in order to enable its linear initalization process. It is also worth mentioning here that when the Steffensen convergence acceleration

Table 6.2 Discharge factor C_D and area A of fluid flow components (type 40: common orifice flow) in Figure 6.1

Component	C_D	A (m^2)	Component	C_D	A (m^2)
C1	.6	0.01	C11	.6	0.01
C2	.6	1.0	C12	.6	1.0
C3	.6	2.0	C13	.6	0.02
C4	.6	0.05	C14	.6	2.0
C5	.6	0.06	C15	.6	1.0
C6	.6	1.0	C16	.6	0.02
C7	.6	1.0	C17	.6	2.0
C8	.6	1.0	C18	.6	0.01
C9	.6	1.0	C19	.6	1.0
C10	.6	1.0	C20	.6	0.03

mechanism (see Section 4.3.3.) would be disabled, *mfs* would not converge to a solution. Probably due to its previously mentioned linear initalization process, AIRNET will converge without the convergence accelerator, but would need 157 iterations under these circumstances.

6.2.3. Inter-model Comparison

As an example of inter-model comparison, simulation results for the boiler model with aquastat control (type 260; see Section 5.4.8.) were compared with results as reported by Dachelet et al. (1988). They compared experimental data with results calculated with the (original) TRNSYS (SEL 1988) version of the boiler model. Here, results calculated with the *bps* implementation of the same boiler model are compared to both the experimental data and to the results as computed with TRNSYS.

The boiler under consideration is a relatively small unit of 27 (kW) nominal heat output. The parameters describing the boiler are collected in Table 6.3.

Table 6.3 Parameters describing the boiler under consideration (ie of type 260: 2 node model & aquastat control)

M	component total mass	225	kg
$\bar{c}$	mass weighted average specific heat	950	J/kgK
$\dot{m}_{f}$ *	fuel mass flow rate	6.303	$10^{-4}\ kg/s$
CO_2 *	volumetric ratio of CO_2 in flue gases during operation	.136	–
$(AU)_0$	heat exchange coefficient water / flue gases in nominal conditions	34.28	W/K
K_1	sensitivity coefficient for AU	.5	–
K_2	sensitivity coefficient for AU	.005	–
Y_w	heat loss coefficient to the environment if OFF	4.208	W/K
DY_w	heat loss increase to the environment if ON	9.792	W/K
K_w	weighting factor for defining mean water temperature	.5	–
$\dot{m}_{f,0}$	fuel nominal mass flow rate	6.303	$10^{-4}\ kg/s$
$\dot{m}_{w,0}$	water nominal mass flow rate	1.624	kg/s
$(CO_2)_0$	nominal ratio of CO_2 in flue gases	.136	–
C_1	coefficient for defining specific heat of flue gases	3.294	$10^3\ J/kgK$
C_2	coefficient for defining specific heat of flue gases	2.105	$10^3\ J/kgK$
c_{pf}	fuel specific heat	1880	J/kgK

H	fuel heating value	42.875	10^6 J/kg
*	test dependent		

This boiler was subjected to a series of tests in a laboratory facility, covering full as well as part load and stand-by conditions. Table 6.4. comprises all test conditions which are necessary as inputs to the model as well as some of the results.

Table 6.4 Inputs to the boiler model and some results; experimental data (derived from: Dachelet et al. 1988)

	inputs				outputs	
test	θ_e	θ_1	$\dot{m}_w$		η	ON
-	$°C$	$°C$	kg/s	$°C$	-	-
1	16.9	75.0	1.259	75.8	.847	.183
2	23.4	86.1	1.505	99.9	.868	1.00
3	20.9	82.2	1.333	84.2	.871	.483
4	16.8	58.3	1.322	59.1	.873	.183
5	14.4	76.3	1.318	79.2	.881	.683
6	17.8	67.5	1.380	69.5	.890	.483
7	24.3	86.9	1.490	99.9	.891	1.00
8	21.5	71.8	0.3405	99.9	.897	1.00
9	20.8	54.3	1.411	56.3	.905	.483
10	21.6	39.9	0.1143	99.9	.906	1.00
11	23.6	67.4	1.544	99.9	.908	1.00
12	14.5	56.8	1.259	59.7	.916	.683
13	20.8	54.3	1.411	56.3	.922	.483
14	24.4	46.3	1.624	99.9	.924	1.00

θ_e	temperature of the environment
θ_1	boiler water inlet temperature
$\dot{m}_w$	water mass flow rate
	aquastat set point temperature
	99.9 indicates continuous operation
η	global efficiency of the boiler
ON	rate of burner operation time

In *bps* the boiler model was incorporated in a small plant network consisting of a temperature source component model (type 900), the boiler, and a pump (type 240). The water node of the temperature source was controlled to set the supply temperature for the boiler (θ_1), and the pump was controlled to deliver the water mass flow rate ($\dot{m}_w$); both are inputs as defined in Table 6.4. This plant network was then simulated during a number of time steps so as to achieve steady-state conditions. The final results with respect to computed global boiler efficiency and burner operation rate are collected in respectively Figure 6.2 and Figure 6.3. These figures also show the results as predicted by the TRNSYS version of the boiler model, and enable comparison of predictions with measurements results.

From Figure 6.2 and 6.3, it is apparent that the TRNSYS version of the boiler model and the *bps* implementation give almost identical results. Some discrepancy may be observed for the results for test 13 of Table 6.4. Given that the inputs for test 13 seem to be exactly the same as for test 9, it was concluded that there is probably a typing error in the data as presented by Dachelet et al. (1988). This is indeed the case, as was found out after communication with the authors. The boiler inlet temperature for test 13 should read 45.2 instead of 54.3 $°C$.

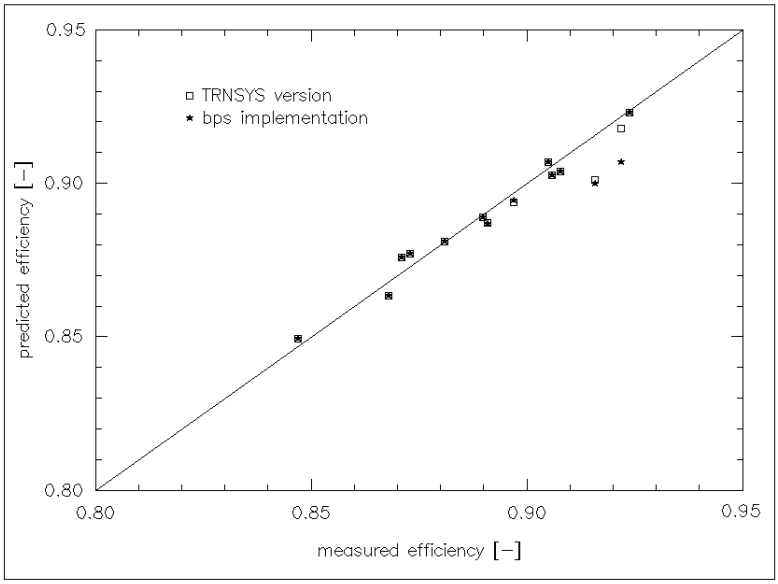

Figure 6.2 Inter-model comparison of boiler component predicted versus measured global efficiency

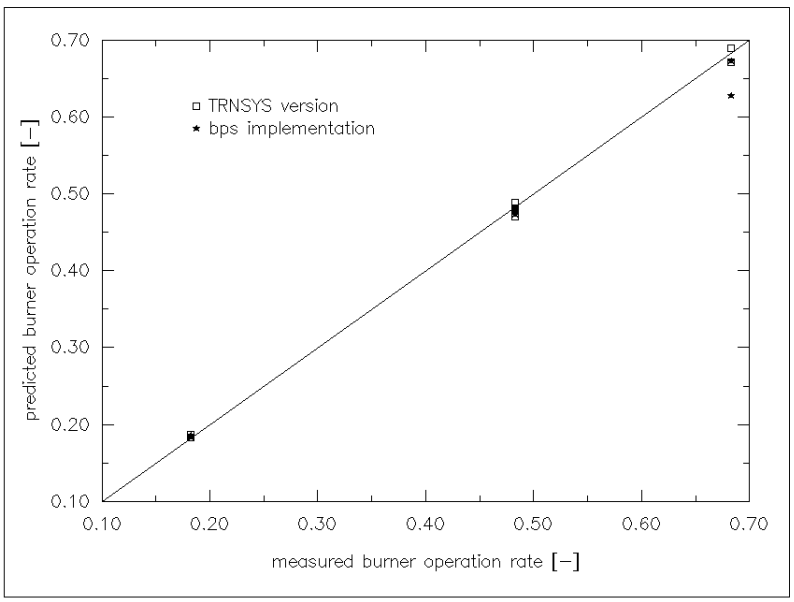

Figure 6.3 Inter-model comparison of boiler component predicted versus measured burner operation rate

With the new inlet temperature, the results for the two models were almost identical.

6.2.4. Empirical Validation

Although it would perhaps be preferable to conduct a whole model validation exercise, this was not done in the present research due to lack of available resources. Also the full scale measurements as mentioned in Chapter 2. are not suitable for this purpose.
Instead, the radiator plant component models (type 210 (2 node) and 270 (8 node)), as described in Section 5.4.9., were selected as subjects in an example of empirical validation. In their publications, Crommelin and Ham (1982), and Ham (1988) report extensive measurements and modelling theory regarding dynamic thermal behaviour of different radiators and convectors. One of the tests they performed concerned a step change in radiator inlet water temperature at a constant water mass flow rate. It should be noted that step change experiments constitute one of the most rigorous experimental methods to investigate the dynamic behaviour of some system. The radiator under investigation was a 1-plate radiator of 800 mm height and 960 mm length. The parameters describing this radiator are collected in Table 6.5.

Table 6.5 Parameters describing the radiator (ie of type 210 or 270) subjected to a step change in inlet water temperature

M	component total mass	20.6	kg
$\bar{c}$	mass weighted average specific heat	1275	J/kgK
n	radiator exponent	1.3	–
ϕ_0	nominal heat emission of radiator	925	W
$\theta_{s,0}$	nominal supply temperature	91.0	$°C$
$\theta_{x,0}$	nominal exit temperature	70.4	$°C$
$\theta_{e,0}$	nominal environment temperature	28.2	$°C$

The nominal values as presented in Table 6.5 were derived from the measurement results as presented in the above mentioned publications. Transformed to the commonly used nominal temperatures 90/70/20 for $\theta_{s,0}/\,\theta_{x,0}/\,\theta_{e,0}$, the nominal heat emission would evaluate to $\phi_0 = 1100\ (W)$ when using the logarithmic mean temperature difference (see Section 5.4.9.) and to $\phi_0 = 1105\ (W)$ when using the arithmetic mean temperature difference. These values differ markedly from the manufacturers data which states $\phi_0 = 1005\ (W)$. The above merely serves to exemplify one of the error sources as indicated in the introduction to this chapter.

The radiator model was incorporated in a small plant network consisting of a temperature source component model (type 900), the radiator, and a pump (type 240). The water node of the temperature source was controlled to set the supply temperature for the radiator, and the pump was controlled to deliver the constant water flow rate ($q_w = 1.092 \cdot 10^{-5}\ m^3/s$). This plant network was then simulated during a number of time steps so as to achieve steady-state conditions. At a certain point in time, say $t = 0$, the temperature of radiator supply water was suddenly changed from 91.0 to $70.4°C$ after which the simulation was carried on long enough to achieve steady-state conditions again. The *bps* simulation results and the measurement and simulation results as reported by Crommelin and Ham (1982) are shown in Figure 6.4 for the radiator heat emission and in Figure 6.5 for the radiator outlet water temperature. The *bps* simulation results comprise those for the two different radiator models when using different simulation time-steps.
It should be noted that the graphs are arrived at by connecting the centre-points of the

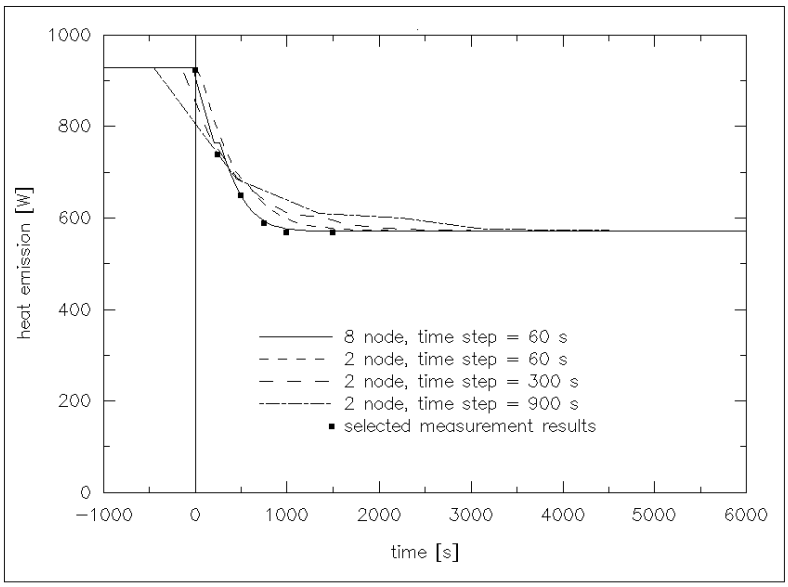

Figure 6.4 Radiator heat emission following a step change in inlet water temperature (91.0 -> $70.4°C$), as computed by *bps* with the two radiator models using different simulation time-steps. To the right are measured (dots) and computed (+) results as presented by Crommelin and Ham (1982). Some measurement results were copied to the left graph.

successive time step; eg in the case of the 900 (s) time steps, the result at $t = -450(s)$ is connected with the result at $t = +450(s)$, etc. Graphs using stair step display of the results turned out to be very confusing, ie it is then very difficult to distinguish the differences between the investigated cases.

From Figure 6.4, it may be concluded that the 8 node radiator model, accurately describes the heat emission dynamics given the time step which was used. From the 2 node model results, it is apparent that the time step length plays an important role. It may be concluded that the error in computed heat emission increases with the time step length. The time constant of this radiator, given the current mass flow rate, is in the order of 300 (s). It can be seen that the error does not increase excessively for time steps much larger than the components time constant. This is probably due to the fact that the solution method switches from a Crank-Nicholson scheme to fully implicit for those conditions. Whether or not the errors introduced by increasing the time step length are acceptable, depends on the problem at hand. When for instance the primary interest is the total heat output during a certain period, the errors as shown in Figure 6.4 may be quite acceptable. The error in total radiator heat emission for the period shown when compared to the 8 node / 60 s time step case, is largest for the 2 node / 900 s time step case but is still only 3%.

From Figure 6.5, it may be concluded too that the 8 node radiator model - given the time step used - gives the most accurate outlet water temperature predictions. For the 2 node model the same remarks as above apply. Again, whether errors introduced by employing a less rigorous model or larger simulation time steps will be acceptable or not, depends on the problem at hand.

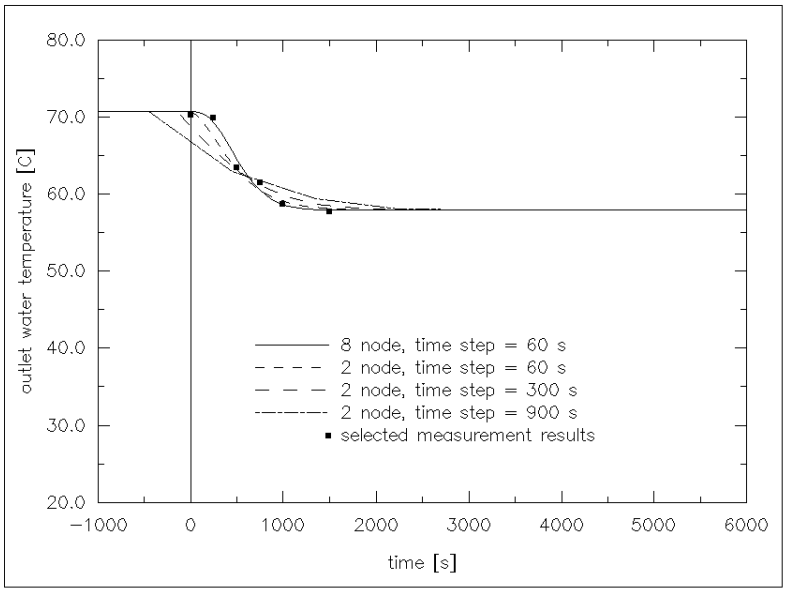

Figure 6.5 Radiator outlet water temperature following a step change in inlet water temperature (91.0 -> $70.4°C$), as computed by *bps* with the two radiator models using different simulation time-steps. To the right are measured (dots) and computed (+) results as presented by Crommelin and Ham (1982). Some measurement results were copied to the left graph.

Another experiment reported by Crommelin and Ham (1982) and Ham (1988), concerned a step change in radiator water flow rate with (almost) constant inlet water temperature. One of the radiators they experimented on, was a 1-plate radiator of 400 mm height and 1920 mm length. The parameters describing this radiator are collected in Table 6.6.

Table 6.6 Parameters describing the radiator (ie of type 210 or 270) subjected to a step change in water flow rate

M	component total mass	20.9	kg
$\bar{c}$	mass weighted average specific heat	1350	J/kgK
n	radiator exponent	1.3	–
ϕ_0	nominal heat emission of radiator	1030	W
$\theta_{s,0}$	nominal supply temperature	89.7	$°C$
$\theta_{x,0}$	nominal exit temperature	68.5	$°C$
$\theta_{e,0}$	nominal environment temperature	22.2	$°C$

As with the previous radiator, the nominal values as presented in Table 6.6 were derived from measurements. Transformed to the commonly used nominal temperatures 90/70/20 for $\theta_{s,0}/\,\theta_{x,0}/\,\theta_{e,0}$, the nominal heat emission would evaluate to $\phi_0 \approx 1105\ (W)$. This values too differs markedly from the manufacturers data which states $\phi_0 = 1041\ (W)$.

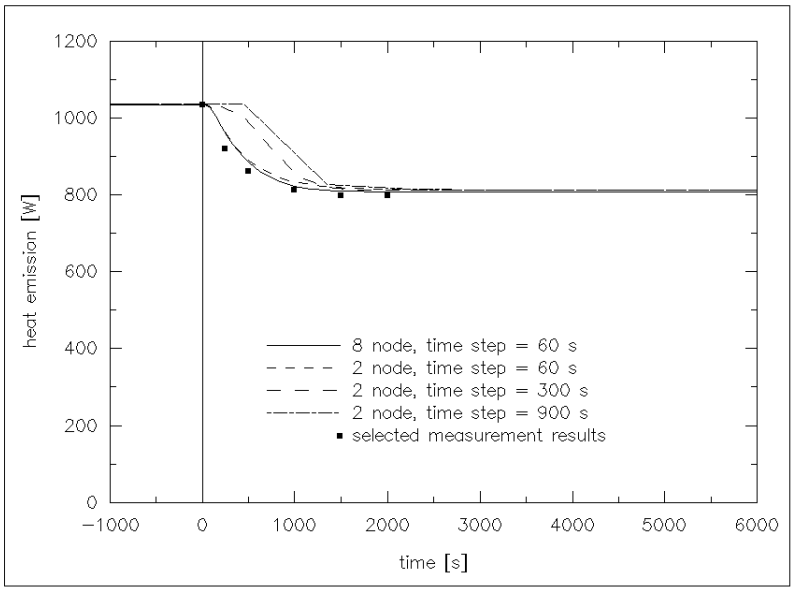

Figure 6.6 Radiator heat emission following a step change in water flow rate ($1.193 \cdot 10^{-5}$ -> $5.524 \cdot 10^{-6}$ m^3/s), as computed by *bps* with the two radiator models using different simulation time-steps. To the right are measured (dots) and computed (+) results as presented by Crommelin and Ham (1982). Some measurement results were copied to the left graph.

For the simulations, the small plant network as described above was used. The water node of the temperature source was controlled to set the supply temperature for the radiator (89.7, $88.6°C$ before, respectively after the step change), and the pump was controlled to deliver the water flow rates. The plant network was then simulated. At a certain point in time, say $t = 0$, the water flow rate through the network was suddenly decreased from $q_w = 1.193 \cdot 10^{-5}$ m^3/s to $q_w = 5.524 \cdot 10^{-6}$ m^3/s, after which the simulation continued long enough to achieve steady-state conditions again. The *bps* simulation results and the measurement and simulation results as reported by Crommelin and Ham (1982) are shown in Figure 6.6 for the radiator heat emission and in Figure 6.7 for the radiator outlet water temperature.

From Figure 6.6, it is apparent that both the 8 node model and the 2 node model describe the dynamic behaviour of the radiator heat emission very well provided that the simulation time step is small enough. At larger time steps the errors increase. The differences between the various time step lengths are larger than in the case of the inlet temperature step change. This is due to the fact that the radiator model uses the first node's temperature to decide whether iteration is necessary (see also Section 5.4.9.). This results in a too high heat emission immediately after the flow rate step change, which is most apparent for the larger time steps. As mentioned before, whether the errors introduced by increasing the time step length are acceptable, depends on the problem at hand. For the simulation period as shown in Figure 6.6, the error in total radiator heat emission when compared to the 8 node / 60 s time step case, is largest for the 2 node / 900 s time step case but is still only 4%.

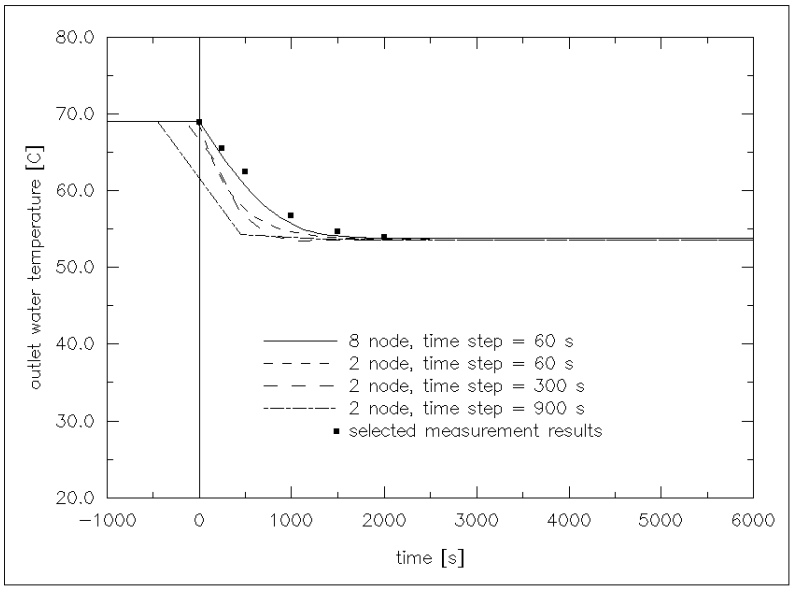

Figure 6.7 Radiator radiator outlet water temperature following a step change in water flow rate ($1.193 \cdot 10^{-5}$ -> $5.524 \cdot 10^{-6}$ m^3/s), as computed by *bps* with the two radiator models using different simulation time-steps. To the right are measured (dots) and computed (+) results as presented by Crommelin and Ham (1982). Some measurement results were copied to the left graph.

From Figure 6.7, it may be concluded that the 8 node radiator model - given the time step used - gives the most accurate outlet water temperature predictions. For the 2 node model the same remarks as above apply. Because for the larger time steps the initial heat emission after the step change is too large, it is evident that the return water temperatures will be too low. Again, whether errors introduced by employing a less rigorous model or larger simulation time steps will be acceptable or not, will depend on the problem at hand.

From the above follows that when larger time steps are to be allowed, it is probably better to not only use the first node's temperature but also it's mass flow rate as an indication of iteration necessity. Finally, and in support of similar remarks in Section 5.3.4., it may also be concluded from the above that it is probably worthwhile to investigate whether a combination of simulation time step control and iteration procedures would be beneficial for the accuracy and CPU resources.

6.2.5. Parametric Sensitivity Analysis

Parametric sensitivity analysis can be used to establish the model predictions uncertainty band associated with the input data. As an example of this technique, one of the previous step change experiments was repeated with small changes in some of the input parameters. For this the radiator described by Table 6.5 and the experiments involving a step change in inlet water temperature were chosen. As described above, the difference between the

measured nominal heat emission and manufacturers data was approximately 6% for this radiator. For the radiator described by Table 6.6, this difference was approximately 9%. It was decided to repeat the simulations with changes in the nominal heat emission of +/- 8%.

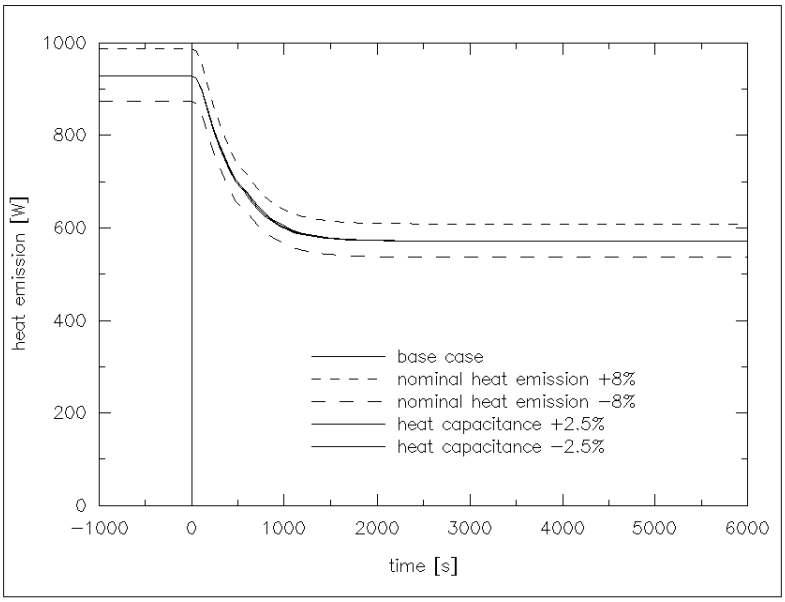

Figure 6.8 Uncertainty band for *bps* predicted radiator heat emission associated with input parameters. The simulation (with 2 node radiator model using 60 s time steps) involved a step change in inlet water temperature (91.0 -> $70.4°C$).

Another input parameter which was subjected to small changes, is the radiator's total heat capacitance (ie. product of total mass and mass weighted average specific heat). It was assumed that the uncertainty associated with this parameter is in the order of say 2.5%.

The inlet water temperature step changes described in the previous section, were repeated using the 2 node radiator model and with simulation time steps of 60 s. The results with respect to predicted heat emission are shown in Figure 6.8. From this, it is clear that the nominal heat emission is an important parameter, and any uncertainty in this parameter causes an almost equal relative uncertainty in the heat emission predictions (in fact: $\phi_1/\phi_2 = (\phi_{0,1}/\phi_{0,2})^n$). From the results it is also apparent that the uncertainty in nominal heat emission only affects the absolute value of the heat output and not the dynamic behaviour.
The effects of changes in total heat capacitance on the other hand, are negligible, both in an absolute sense and with respect to dynamic behaviour.

The results with respect to the uncertainty band for predicted outlet water temperature are shown in Figure 6.9. As may be expected from the above, any uncertainty in nominal heat emission has a much stronger influence on the predictions uncertainty, than a uncertainty in total radiator heat capacitance. Again, this only affects the temperatures in an absolute sense.

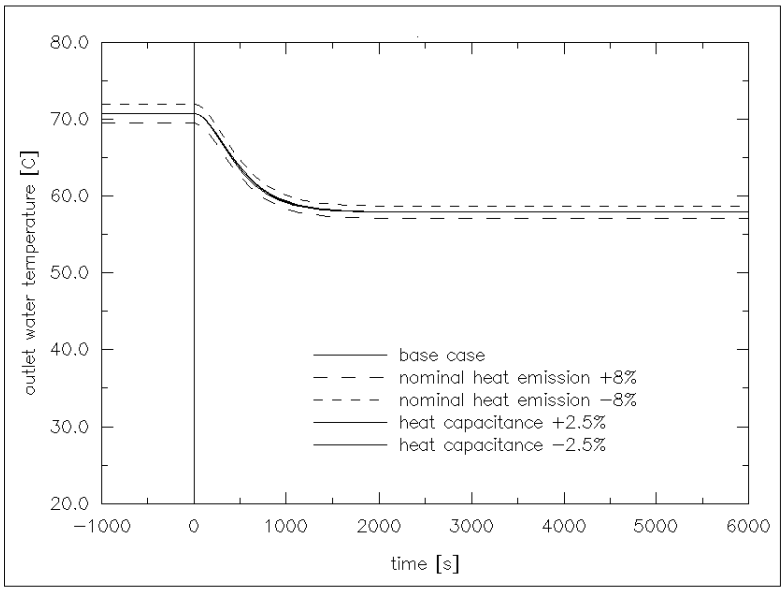

Figure 6.9 Uncertainty band for *bps* predicted radiator outlet water temperature associated with input parameters. The simulation (with 2 node radiator model using 60 s time steps) involved a step change in inlet water temperature (91.0 -> $70.4°C$).

Neither uncertainty will affect the dynamic behaviour of the predicted outlet water temperatures.

6.3. FUTURE WORK

As explained before, the verification and validation efforts in the current project have been mostly directed towards the first phases or steps of the validation methodology: development/examination of theory respectively production/inspection of source code, and analytical verification. Because the other methodology steps have been applied selectively only, there is still a lot of work to be done in those areas. This does not only apply to plant and fluid flow component models as such, but also to the interaction of those models with the building model and to the overall building/plant configuration model as a whole.

This chapter focussed on internal errors. There remains however the issue of external errors which often cause much larger uncertainties than internal errors. Evidence suggesting this may be found in the previous sections. In terms of plant simulation, the necessary input parameters are often difficult to extract from published data. Manufacturers data is usually related to specific test conditions under steady full load operation; part load steady state data is scarce and dynamic performance test results are even more scarce. It is necessary - for all parties which are involved in or benefit from system simulation - to agree that this sort of data is crucial and to act accordingly; ie to persuade the industry to publish appropriate data, and to develop standardized procedures and reporting formats for dynamic performance tests.

Another way of trying to prevent external errors, is by user guidance via a so-called 'intelligent front-end'. This issue will be discussed further in Chapter 8.

References

D.P. Bloomfield 1989. ''Evaluation procedures for building thermal simulation programs,'' in *Proc. Building Simulation '89*, pp. 217-222, International Building Performance Simulation Association IBPSA, Vancouver.

BRE/SERC 1988. *An investigation into analytical and empirical validation techniques for dynamic thermal models of buildings*, Building Research Establishment / Science and Engineering Research Council, Watford (UK).

CEC 1989. ''The PASSYS Project Phase 1. Subgroup Model Validation and Development Final Report 1986-1989,'' 033-89-PASSYS-MVD-FP-017, Commission of the European Communities, DG XII of Science, Research and Development, Brussels. S. Østergaard Jensen (Ed.)

J.A. Clarke 1990. ''The model validation activities of project PASSYS,'' in *Proc. 2nd European Conf. on Architecture held at Paris, Dec. 1989*, ed. T.C. Steemers and W. Palz, pp. 403-406, Kluwer Academic Publishers, Dordrecht (NL).

R.D. Crommelin and Ph.J. Ham 1982. ''Onderzoek naar de warmteafgifte van radiatoren en convectoren onder niet-stationaire condities,'' TNO-IMG rapport C 503, Delft.

M. Dachelet, J.P. Eppe, J. Hannay, L. Laret, J. Lebrun, G. Liebecq, and B. Lorea 1988. ''HVAC component specification: fuel oil boiler,'' Energy conservation in buildings & community systems programme. Annex X : system simulation (S1), International Energy Agency. Operating agent: University of Liège

Ph.J. Ham 1988. ''Dynamisch warmtegedrag van radiatoren en convectoren. Metingen en modelvorming,'' *Verwarming en Ventilatie*, vol. 45, no. 5, pp. 315-334.

IEA 1980. ''Comparison of load determination methodologies for building analysis programmes,'' Energy conservation in buildings & community systems programme; Annex I, International Energy Agency. Distribution: Air Infiltration and Ventilation Centre, Coventry (UK)

IEA 1984. ''Glasgow commercial building monitoring project; final report,'' Energy conservation in buildings & community systems programme; Annex IV, International Energy Agency. Operating agent: Building Research Establishment, Garston (UK)

A.D. Irving 1988. ''Validation of dynamic thermal models,'' *Energy and Buildings*, vol. 10, no. 3, pp. 213-220.

R. Judkoff, D. Wortman, B. O'Doherty, and J. Burch 1983. ''A methodology for validating building energy analysis simulations,'' SERI/TR-254-1508, Solar Energy Research Institute, Golden, CO.

E.W. Kruyt 1989. *FORCHECK A FORTRAN verifier and programming aid*, Leiden University. User manual

J.T.H. Lammers 1978. ''Human factors, energy conservation and design practice,'' Doctoral dissertation Eindhoven University of Technology (FAGO).

J. Lebrun and G. Liebecq 1988. ''System Simulation Synthesis Report,'' Energy conservation in buildings & community systems programme; Final report Annex X,

International Energy Agency. Operating agent: University of Liège, J. Lebrun, report AN10 881020-RF

SEL 1988. ‘‘TRNSYS, a transient system simulation program,’’ Engineering Experiment Station Report 38-12, University of Wisconsin-Madison, Solar Energy Laboratory, Madison, WI. Manual for version 12.2 and later

G.N. Walton 1989. ‘‘AIRNET - A computer program for building airflow network modeling,’’ NISTIR 89-4072, National Institute of Standards and Technology, Gaithersburg, MD.

CHAPTER SEVEN

APPLICATION

7.1. INTRODUCTION

In addition to the primary objective of developing tools for the research of the thermal interaction of building and heating and ventilating system, *mfs*, *plt*, and *bps* have been used extensively on the application level. Apart from anything else, this probably best exemplifies the need for these kind of models.

A very important requirement for any successful application is easy access to, and an efficient mechanism for retrieval of previously generated simulation results. Therefore this chapter starts with describing the available options with respect to simulation results recovery. The nature of the generated results itself, has already been elaborated in Chapter 4 and Chapter 5.

Then this chapter continues with the description of a number of case studies which are divided into two groups. The first one is concerned with case studies in a modelling orientated context. In that section, calculations and results with "long term value" are presented. In this respect one has to think of results which are primarily aimed at the modelling community and which may be of use in intelligent knowledge based systems and the like. The main purpose of this section is to enlarge the application scope of the present research, both with respect to user target group and with respect to time.

The second group of case studies is concerned with application in a building engineering context. In that section calculations and results with "immediate value" will be presented. These will be results, intended for and aimed at the professional community (ie consultants, architects, plant system designers etc). The intention is to give feasible solutions to some "real world" problems. The main purpose of this section is to give a flavour of the possibilities and the problems which may be addressed and solved by means of simultaneous building and plant heat and mass transfer simulation.

7.2. RESULTS RECOVERY

An efficient way of results recovery is an absolute necessity for model application and utilization in practice. The following sections elaborate how results recovery may be achieved in case of fluid flow and plant simulation results, respectively. Because the current system is developed for usage in a UNIX environment, all UNIX tools become immediately available to the user ’for free’. The final section on results recovery exemplifies usage of some of these tools.
For information regarding results recovery with respect to building side simulation, the user is referred to Clarke et al. (1991)

7.2.1. Fluid Flow Simulation Results

Fluid flow results (ie. pressures, flow rates, boundary conditions, and solution process information) are stored for each simulation time step in an ASCII format file. A small piece of such a file has been shown in Table 4.6. For a user, these kind of results are rather difficult to evaluate. Therefore, *mfs* offers the following features with respect to results recovery:†

Tabular output of results; "pretty print" mode

In this tabular output mode, the user is able to create - interactively - a table with the pressure and mass flow results for one or more nodes. The current table lay-out is based on a maximum of 2 node result sets per table. The mass flow results are presented in total flow entering and total flow leaving the node. For internal nodes entering mass flow should be equal to leaving mass flow, at least within the boundaries set by the error tolerance criteria. For boundary nodes however, entering and leaving mass flows are unlikely to be equal.

Table 7.1 *mfs* tabular "pretty print" output for 2 nodes

Node pressure and fluid flow entering (+ve) or leaving (-ve), resp. Day 9 of month 1 (1967)						
Hour	living			south		
	Pa	m^3/hr	m^3/hr	Pa	m^3/hr	m^3/hr
1.00	-23.93	640.4	-652.5	-20.00	0.7024	-126.0
2.00	-23.93	640.4	-652.5	-20.00	0.6906	-126.0
3.00	-23.60	638.7	-650.7	-19.75	0.	-129.0
4.00	-23.50	638.4	-650.6	-19.66	0.	-128.4
5.00	-23.45	639.2	-651.7	-19.52	0.	-131.6
6.00	-23.28	638.9	-651.4	-19.33	0.	-135.8
7.00	-23.62	640.8	-653.8	-19.59	0.	-132.9
8.00	-23.45	636.7	-648.4	-19.70	0.	-130.6
9.00	-23.18	634.9	-646.2	-19.51	0.	-132.2
10.00	-23.07	633.6	-644.6	-19.47	0.	-132.6
11.00	-22.91	632.3	-642.8	-19.40	0.	-133.3
12.00	-23.15	630.0	-639.8	-19.84	0.	-126.9
13.00	-23.42	629.4	-638.7	-20.20	0.	-122.8
14.00	-22.83	627.5	-636.6	-19.64	0.	-129.5
15.00	-22.59	627.4	-636.5	-19.38	0.	-133.1
16.00	-22.59	627.4	-636.5	-19.38	0.	-133.1
17.00	-22.93	627.4	-636.5	-19.76	0.	-126.8
18.00	-23.11	627.7	-636.8	-19.95	0.	-125.4
19.00	-22.59	627.4	-636.5	-19.38	0.	-133.0
20.00	-22.08	626.6	-635.6	-18.86	0.	-142.0
21.00	-22.12	627.8	-637.1	-18.82	0.	-143.2
22.00	-22.12	628.1	-637.5	-18.80	0.	-145.6
23.00	-22.12	630.4	-640.3	-18.64	0.	-154.3
24.00	-22.02	629.4	-639.0	-18.60	0.	-154.6

To allow output for less than the entire simulation period, the user may set the start and stop date. For ease of interpretation, the user may choose to have the mass flow rates expressed in either kg/s or m^3/h or relative to some volume (eg expressed as an Air Change Rate). In the latter two cases the density of the fluid which is taken into account, is based on the temperature of the originating node. Note that if the flows originate from nodes with different temperatures then it is likely that there will be a nodal *volume* flow imbalance.

† For this it does not matter whether the results stem from simulation by *mfs* or originate from incorporated mass flow simulation by *plt* or by *bps*.

As an example of tabular output, Table 7.1 shows pressure and volume flow rate results for the nodes **living** (of type internal) and **south** (a boundary node) of Table 4.3. The results for the 12th hour, correspond to the data in Table 4.6. It should be noted that the flow rates are accumulated over four connections in the case of node **living** and over three connections in the case of node **south**.

Tabular output of results; "raw table" mode

This tabular output mode allows the user to define/create a "raw" table of data. This kind of output is actually meant for preparing simulation results to be transferred to some other (graphical) data analysis package. The table starts with some comment lines, with "#" in column 1. Each subsequent line of the table holds the simulation results for one time step. The first item on a line is the date and time expressed as Julian date, where 1.0 is equivalent to January 1st 1:00 hours. Up to 20 more user-definable columns are available to hold nodal pressures or net linkage flow rates. For convenience, the flow rate output units may be set to either *kg*/*s* or m^3/h, and the output period may be restricted to comprise only part of the simulation period. To be able to separate this table from other output when *mfs* is used from within a UNIX-script, the results are flushed through the standard error channel. As an example of "raw table" output, Table 7.2 shows pressure results for nodes **living**, **kitchen** and **bed**, and the net volume flow rates between these nodes.

Table 7.2 *mfs* "raw table" pressure and flow rate output for 3 nodes

```
# Problem : house.mfn
# Cp-wind : pressc.db1
# Climate : clm67
# Results : house.mfn.res
# Table contents (pressure in Pa; flow rate in mˆ3/hr) :
```

# Julian date	living	kitche	living-kitche	bed	living-bed
9.0417	-23.93	-23.93	77.15	-58.78	61.01
9.0833	-23.93	-23.93	77.15	-58.78	61.01
9.1250	-23.60	-23.60	78.15	-58.45	58.67
9.1667	-23.50	-23.51	78.76	-58.35	58.19
9.2083	-23.45	-23.45	80.10	-58.30	58.65
9.2500	-23.28	-23.28	81.41	-58.12	57.69
9.2917	-23.62	-23.62	79.95	-58.47	60.80
9.3333	-23.45	-23.46	79.52	-58.30	55.66
9.3750	-23.18	-23.18	80.52	-58.03	52.89
9.4167	-23.07	-23.07	80.77	-57.92	51.18
9.4583	-22.91	-22.91	80.83	-57.76	49.42
9.5000	-23.15	-23.15	78.27	-58.00	47.68
9.5417	-23.42	-23.42	76.24	-58.26	47.63
9.5833	-22.83	-22.83	79.34	-57.68	43.97
9.6250	-22.59	-22.60	80.83	-57.44	43.12
9.6667	-22.59	-22.60	80.83	-57.44	43.12
9.7083	-22.93	-22.93	78.70	-57.78	44.13
9.7500	-23.11	-23.12	77.61	-57.96	45.03
9.7917	-22.59	-22.60	80.83	-57.44	43.12
9.8333	-22.08	-22.09	84.32	-56.93	40.34
9.8750	-22.12	-22.13	84.60	-56.97	41.76
9.9167	-22.12	-22.12	85.23	-56.97	41.78
9.9583	-22.12	-22.12	87.39	-56.97	43.49
10.0000	-22.02	-22.03	87.58	-56.87	42.13

Graphical output of results

Obviously, the graphical output mode is only available when *mfs* is run on a device with graphical capabilities (eg a workstation). In this mode, the user is able to draw a time based graph of flow rate results. The user must first define the node for output, and then the coupled node to indicate the connection of interest. Alternatively, the keyword "all" may be used for the coupled node to indicate that all connections with the node in question must be taken into account. As was the case with tabular output, the user may redefine start and stop dates and may choose to present the results - instead of in *kg*/*s* - in m^3/h or relative to some volume.

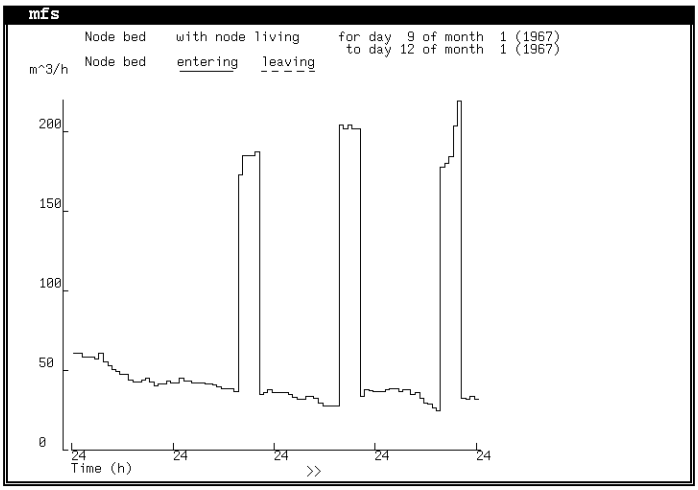

Figure 7.1 Example of *mfs* graphical output for a single node

As an example of graphical output, Figure 7.1 shows the volume flow rates for connections between the nodes **bed** and **living** of Table 4.3. The results for the 12th hour of the first day correspond to the data in Table 4.6. From the graph the influence of the open kitchen window is apparent; due to the defined control strategy, this window is not opened on the first day of the simulation period.

7.2.2. Plant Simulation Results

After a *bps* run, the user may subsequently use *res* (see Clarke et al. 1991)) to recover previously generated building and/or plant simulation results. With respect to the plant results, *res* is capable of generating time series graphs similar to Figure 7.1 for the stored results: all plant nodal states (ie. temperature, and first and second mass flow rate), and for each plant component - if appropriate- control data, heat loss to the environment, and additional output variables. It is also possible to generate "raw table" output as described in Section 7.2.1. This kind of output may then be transferred to - and manipulated by - any general (graphical) data analysis package.

7.2.3. Using UNIX Tools

One more mode of results recovery should be mentioned here because they are available to the user: the UNIX way. Although not very easy at first glance, this is probably the most powerful and versatile method. UNIX includes various text filters and text file scanners with which for instance an *mfs* results file but also "raw table" output may be processed. These software tools offer a very flexible and individual way to retrieve, modify and present simulation results. This is best demonstrated through a few examples.

Table 7.3 Result of some UNIX commands (see text) used to extract specific data from an *mfs* results file; ie. whole data file reduced to output results specific to node **kitchen** and restricted to the hours between 18:00 and 21:00 (one simulation day only)

Date: 9/ 1/1967 18.00 Dryb= 0.0 Wdir= 340. Wvel= 1.6 It= 7 OK=1								
Node	**Fld**	**Type**	**Temp**	**Hght**	**Pressure**	**Residual**	**Sabs(Flw)**	
kitche	1	0	20.8	1.5	-23.116	-0.67956E-07	0.40540	
From	**To**	**Comp**	**Typ**	**Fld**	**Pi-Pj**	**Pstack**	**Flw 1**	**Flw 2**
living	kitche	door	130	1.	0.39976E-02	0.	0.19464	-0.16923
kitche	north	crack	120	1.	-4.9478	1.0621	-0.80631E-02	0.
kitche	w_ctl	w_ctl	450	1.	-4.5052	0.	0.	0.
kitche	t_junc	duct_1	220	1.	101.42	-40.682	0.33473E-01	0.
Date: 9/ 1/1967 19.00 Dryb= 0.0 Wdir= 335. Wvel= 1.1 It= 5 OK=1								
Node	**Fld**	**Type**	**Temp**	**Hght**	**Pressure**	**Residual**	**Sabs(Flw)**	
kitche	1	0	20.8	1.5	-22.596	-0.94244E-08	0.40436	
From	**To**	**Comp**	**Typ**	**Fld**	**Pi-Pj**	**Pstack**	**Flw 1**	**Flw 2**
living	kitche	door	130	1.	0.40141E-02	0.	0.19518	-0.16871
kitche	north	crack	120	1.	-4.1430	1.0621	-0.69963E-02	0.
kitche	w_ctl	w_ctl	450	1.	-3.7005	0.	0.	0.
kitche	t_junc	duct_1	220	1.	101.42	-40.682	0.33471E-01	0.
Date: 9/ 1/1967 20.00 Dryb= 0.5 Wdir= 290. Wvel= 0.6 It= 5 OK=1								
Node	**Fld**	**Type**	**Temp**	**Hght**	**Pressure**	**Residual**	**Sabs(Flw)**	
kitche	1	0	20.8	1.5	-22.086	-0.60627E-07	0.40322	
From	**To**	**Comp**	**Typ**	**Fld**	**Pi-Pj**	**Pstack**	**Flw 1**	**Flw 2**
living	kitche	door	130	1.	0.40319E-02	0.	0.19577	-0.16815
kitche	north	crack	120	1.	-3.3310	1.0347	-0.58345E-02	0.
kitche	w_ctl	w_ctl	450	1.	-2.8999	0.	0.	0.
kitche	t_junc	duct_1	220	1.	101.38	-40.682	0.33462E-01	0.
Date: 9/ 1/1967 21.00 Dryb= 0.0 Wdir= 260. Wvel= 0.4 It= 5 OK=1								

Suppose for some reason, one is only interested in results related to a specific node, say **kitche**, and only for the hours between 18:00 and 20:00. Then one way to extract these specific data from the overall results file (say **house.mfn.res**) is through the UNIX commands:

awk ’/1967 18/,/1967 21/’ house.mfn.res | egrep -i "(date | node | from | kitche)"

The first part of this command (**awk**) is used to select only those parts of **house.mfn.res** which comprise each line between an occurrence of the search pattern "1967 18" and a line with the next occurrence of "1967 21" inclusive. The results of this are "piped" into a second UNIX command, ie. **egrep**. This command is used to copy all the lines containing one of the key words **date, node, from** or **kitche** (in upper or lower case) to the standard output. The results will look similar to Table 7.3. This is a convenient way of data reduction, which is useful especially in cases with a large number of nodes and/or components.

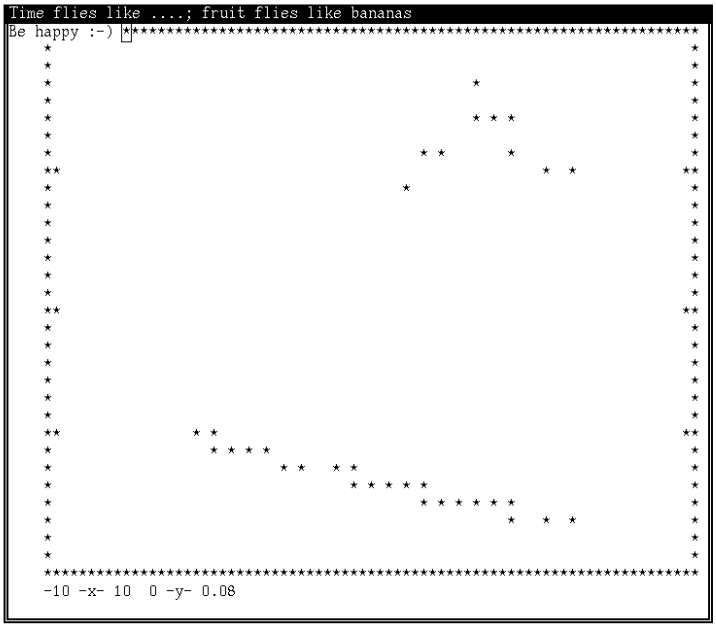

Figure 7.2 Result of some UNIX commands (see text) used to extract specific data from an *mfs* results file; ie. a "graphical" impression of the relation between outside air temperature (X-axis) and mass flow rate through the connection between nodes **living** and **bed**

As another example, suppose that one would like to get an insight into the relation - if any - between outside air temperature and the mass flow rate through a certain connection, say between node **living** and node **bed**. This is best achieved by presenting this specific data in a 2-D graphical fashion; ie. make a plot of flow rate (Y-axis) against outside air temperature (X-axis). Then one way to realise this is through the UNIX command sequence:

grep Dryb house.mfn.res | awk '{print $6}' > /tmp/xxx
grep living house.mfn.res | grep bed | cut -c54-68 | paste /tmp/xxx - | graph -g 1 -m 0 | plot
rm /tmp/xxx

The first line of this command sequence, uses **grep** and **awk** to find the outside air temperature for each time step and to write these values to a temporary file **/tmp/xxx**. The second line uses **grep** two times to first find all lines containing **living** which are then scanned for occurrence of the search key **bed**. This gives for each time step the flow rate results for the **living - bed** connection. From these the actual flow rate value is selected through usage of **cut**. We now have the Y-values of our plot points. The X-values of our plot-points are already in **/tmp/xxx**, so we can use **paste** to join the abscissaes and ordinates of the plot points. To actually create a graphical display, we here use **graph** and **plot**. This will give a "picture" on any terminal, similar to Figure 7.2. A much nicer picture can be made on a terminal with graphical capabilities; eg. by usage of **grtool** (instead of **graph** and **plot**) in a workstation window environment. Finally the third command line removes the temporary file **/tmp/xxx**.

7.3. CASE STUDIES: MODELLING ORIENTATED CONTEXT

In a modelling orientated context, the models presented in this thesis may be used as a virtual laboratory for numerical experiments in the field of simultaneous building/plant heat and mass transfer simulation. Exemplifying this kind of application, the following two sections describe experiments related to the numerical solution strategy of some plant component ie. the radiator model. The first experiment is concerned with the type of numerical approximation to the governing partial differential energy balance equation, while the second experiment concerns the simulation strategy issue of iteration versus smaller time steps.

It should be noted that with respect to combined building and plant simulation a number of interesting "interaction issues" could not yet be addressed due to lack of available time and resources. They could however be researched quite easily with the tools as they are right now. Examples of such issues are: should the building side be processed before the plant side or the other way around; is it justifiable to use a smaller time step for the plant simulation when the control is based on a building side sensor; should the plant heat losses (either parasitic or deliberate) be time averaged (both with respect to driving temperature difference and amount of energy), when the plant simulation time step is smaller then the building simulation time step; etc.

7.3.1. Numerical Approximation of Energy Balance Equation

As explained in Section 5.3.1., the basic plant components energy balance is described by equation (5.1). There are different numerical approximation schemes to solve this partial differential equation: explicit, implicit, or mixed. The user may choose to investigate different schemes by changing the user definable parameter α. This parameter is the weighting factor between the fully explicit and the fully implicit formulation.

Say we want to see the influence of α on the solution of the problem described in the first part of Section 6.2.4.; ie a radiator (defined by the parameters in Table 6.5) in a stationary environment, with a constant water flow rate, and experiencing a step change in inlet water temperature from 91.0 to $70.4°C$. In addition to this, for now, we are only interested in the two node radiator model, and we want to know the results for a simulation time step which is either much smaller than the component's time constant (which is approximately 300 s), or which is of the same order as the component's time constant.

Figure 7.3 shows the simulation results for the different numerical approximation schemes when using simulation time steps of 60 s. Also shown are the results in case the radiator model would be operated in steady-state mode (ie neglecting any heat capacitance). For comparison reasons, Figure 7.3 incorporates the same selection of measurement results which are shown in Figure 6.4. From the simulation and measurement results it is apparent that for these 60 s time steps, there is not much difference between the Crank-Nicolson approximation (default for time steps less than 63% of the plant component's time constant) and the fully implicit formulation, although the fully implicit formulation appears to give somewhat better results especially immediately after the step change. Using the fully explicit formulation and 60 s time steps is less accurate than the two previously mentioned numerical approximation schemes. As could be expected, the steady-state approach introduces the largest errors. When compared to the fully implicit scheme, the total heat emission between 0 and 2000 s is 0.9% higher for the Crank-Nicolson approximation, 3.3% higher for the

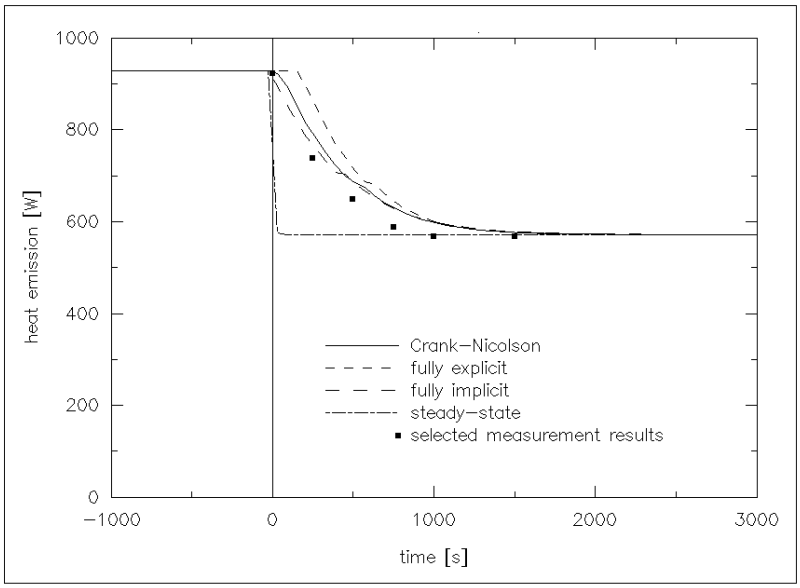

Figure 7.3 Radiator heat emission following a step change in inlet water temperature (91.0 -> 70.4°*C*), as computed by *bps* with the two node radiator model using a simulation time step of 60 *s* and employing different numerical approximation schemes; (for measurement results, see Figure 6.4).

explicit formulation, and 11.2% lower for the steady-state approach.

Figure 7.4 shows the simulation results when using simulation time steps of 300 *s*. In this case the fully explicit formulation is numerically instable; ie does not give a solution. From the simulation and measurement results it is apparent that for these larger simulation time steps, the fully implicit formulation gives much better results than the Crank-Nicolson approximation, especially immediately after the step change. The fully implicit formulation is the default whenever the simulation time step exceeds 63% of the plant component's time constant, which is true for the present case.

Two conclusions may be drawn from this case study: (1) the default choice of numerical approximation scheme is supported by the results, and (2) for time steps which are small relative to the plant components time step, there seems to be very little difference between a Crank-Nicolson approximation and a fully implicit formulation, suggesting that the latter is applicable to a much wider range of time step length than is sometimes suggested.

7.3.2. Iteration vs Time Step Reduction

As a second case study in a modelling orientated context, suppose we want to investigate whether it is more beneficial to enable the iteration scheme as elaborated in Section 5.3.4. or to disable iteration and decrease the simulation time step length. For this we consider the same problem as in the previous section, ie a radiator (defined by the parameters in Table 6.5) in a stationary environment, with a constant water flow rate, which experiences a step change in inlet water temperature from 91.0 to 70.4°*C*. We only want to investigate the two node radiator model, but for simulation time step lengths ranging from say 30 *s* (ie

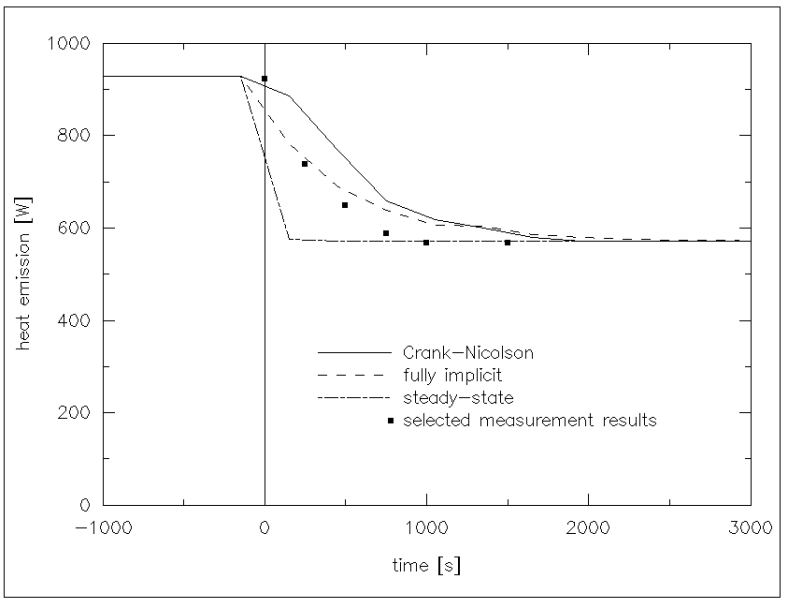

Figure 7.4 Radiator heat emission following a step change in inlet water temperature (91.0 -> 70.4°*C*), as computed by *bps* with the two node radiator model using a simulation time step of 300 *s* and employing different numerical approximation schemes; (for measurement results, see Figure 6.4).

approximately 10% of the components time constant) to 900 *s* (≈ 3 times the components time constant).

Figure 7.5 shows the simulation results for the various time steps and with or without the iteration mechanism enabled. The iteration threshold values were set at 0.001 for the relative error and to 0.2*K* for the absolute error in terms of temperature. Figure 7.5 also shows some measurement results which were also incorporated in Figure 6.4. From the simulation and measurement results it is apparent that when the iteration mechanism is disabled, the prediction accuracy decreases with increasing simulation time step length. With the iteration mechanism enabled, the results for time steps of 120 *s* and less (not shown) are almost identical to those for the "no iterations - time step = 30 *s*" case. When iteration is enabled and the time steps are chosen larger than 120 *s*, the accuracy of prediction decreases but only due to the large time steps. This means that the predicted average heat emission per time step is computed correctly in the sense that the overall energy balance over the entire simulation period is correct, but that due to the larger time steps detailed information is lost. As can be seen from Figure 7.5, if the iteration mechanism is disabled the computed heat emission shifts in time when the time step size increases. This does lead to errors in the overall energy balance over the entire simulation period.

Enabling the iteration mechanism may obviously increase the number of computational steps within a certain simulation time step. When comparing iteration versus time step reduction, we should therefore compare the total number of computational steps which are needed to simulate a certain period. Table 7.4. summarizes the results for the problem sketched above, for the simulation period $0 \leq time \leq 3000$ *s*.

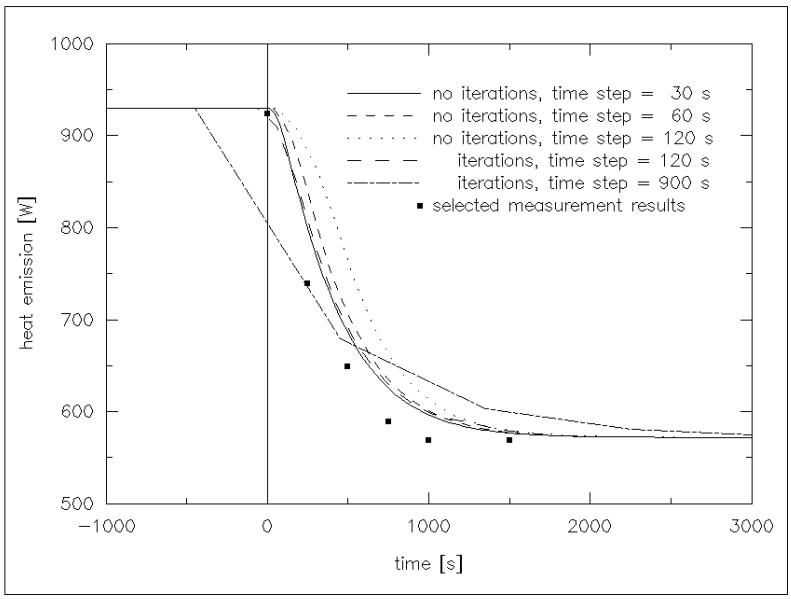

Figure 7.5 Radiator heat emission following a step change in inlet water temperature (91.0 -> 70.4°*C*), as computed by *bps* with the two node radiator model using various simulation time steps and with or without the iteration mechanism enabled; (for measurement results, see Figure 6.4).

Table 7.4 Number of computational steps corresponding to the results in Figure 7.5, for the simulation period $0 \leq time \leq 3000$ *s*

iteration mechanism	time steps			
	length *s*	number	additional	total
disabled	30	100	0	100
disabled	60	50	0	50
disabled	120	25	0	25
enabled	120	25	31	56
enabled	240	12.5	24	36.5
enabled	450	6.7	18	24.7
enabled	900	3.3	16	19.3

Since the actual simulation results for the "no iteration, 30 *s* steps" were almost identical to the "iteration, 120 *s* steps" case, it can be concluded that the iteration mechanism outperforms the time step reduction strategy by at least a factor 1.8 for the given problem. This factor will even become larger, if we are satisfied with the reduced information results for larger time steps and iteration enabled as indicated above.

It should be noted that the above is restricted to an isolated problem; ie the conclusions should not be generalized. Iteration versus time step reduction, is an interesting issue which needs much more research. In the end it might well be, that instead of one or the other approach a mixture proves to be most beneficial.

7.4. CASE STUDIES: BUILDING ENGINEERING CONTEXT

The use of the system in a building performance evaluation context, and the design benefits to accrue, will be demonstrated in the following sections. This is achieved by elaborating three case studies showing the system's real world application, and the results of this with respect to building design improvement. The first case study exemplifies application of the fluid flow simulation model in stand-alone mode. The problem considered, involves comfort aspects of air flow through an extensive shopping mall. The second case study exemplifies coupled heat transfer and air flow in a building. The problem described is an environmental assessment of hospital spaces were air flow rates were judged to be critical in limiting thermal stress in zones with significant solar radiation gain. Both these case studies were actually performed in a real consultancy context. Apart from anything else, this signals the need in practice or the utilization factor of the kind of tools described in this thesis.
Finally the third case study exemplifies simultaneous building and plant simulation. In this case some aspects of a mechanical room thermostat controlling a domestic wet central heating system are investigated.

7.4.1. Air Flow through Shopping Arcades

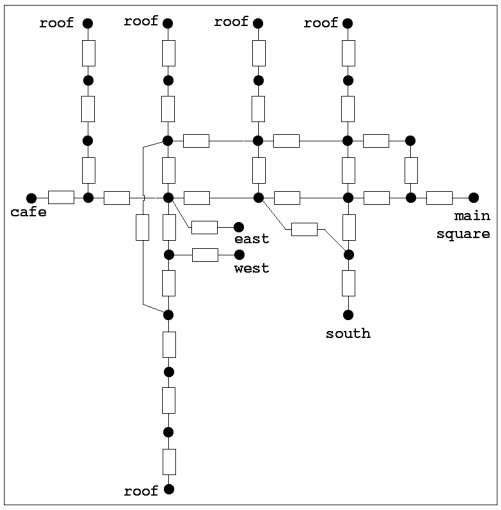

Figure 7.6 Sketch of fluid flow network representing main air flow paths through shopping arcades

In Eindhoven, The Netherlands, a major alteration of the inner-city is in progress. In this context, an extensive shopping mall, the "Heuvel Galerie", is being built. This 4-level complex incorporates a 220 metre long shopping arcade, interspersed with atria and dome-shaped roofs, approximately 20,000 m^2 shops, a 8,600 m^2 concert hall, 3,000 m^2 restaurants, a 1,200 units car park, offices, and appartments.
It should be apparent that such a building is a highly complicated system. The manner in which air will flow depends on the external pressures on entrances and domes, temperature differences inside and with respect to outdoors, and impulses by the ventilation system. For this building *mfs* was used to make predictions with respect to the indoor environment (Wisse and Pernot 1990, Pernot and Hensen 1990).
Although various conditions were investigated, here only results with respect to the winter

will be presented. The question was whether thermally uncomfortable conditions would occur in the shopping arcades due to the combination of relatively cold air and high air velocities.

To give an idea of how part of the building was abstracted for this study, Figure 7.6 shows a sketch of the fluid flow network representing the main air flow paths through the shopping arcades of the mall. In absense of more suitable data, the building was considered as a number of zones (the nodes), connected by air flow opening components (fluid flow component type 110). The flow network was simulated for the winter period of a climate reference year for The Netherlands (Bruggen 1978). The wind speed reduction factor was assumed to be 0.5.

Table 7.5 summarizes some informative statistics (from a user point of view) related to this study. It is apparent that now - unlike with previous air flow simulation models - most effort is related to input preparation and results manipulation, as opposed to the actual simulation time. Also shown in this table are the number of iterations per time step. The fact that the average number of iterations per consecutive time step is almost half of number of iterations for the 1st time step, can be regarded as evidence supporting the statement in Section 4.3.3. that previous time step values are usually equally good or better first iteration guesses than those resulting from the linear initialization technique.

Table 7.5 Some statistics related to the case study on air flow through shopping arcades

number of nodes for the shopping arcades	29
number of flow components	33
typical number of iterations for 1st time step	≈ 27
average number of iterations per consecutive time step	≈ 16
data preparation starting from architectural drawings etc	≈ 1 *day*
number of studied design alternatives; ie *mfs* runs	> 100
typical system time requirement per *mfs* run (1 simulation day)	≈ 1 min
typical system time requirement per design alternative for results manipulation using standard UNIX tools	≈ 5 min

The basic results emerging from the simulation incorporate nodal pressures and flow rates. These may then be transformed to eg average connection air velocities. As an example, consider Figure 7.7 which shows results with respect to the air velocities which may be expected in the pedestrian entrance area. For commercial reasons, the architects and the developers want the entrance areas to be as open as possible. From the first results it was clear however that the original design proposal (incorporating air curtains for the main entrance) would lead to unacceptably high air velocities. One of the main conclusions was that additional air flow restrictions were necessary. For this it was suggested to apply double sets of sliding doors (wind sluices) at the "cafe" and "west" entrances, and to incorporate extra sliding doors + side hung doors at the main entrance. In case of severe wind, it should be possible to further restrict the (open) cross-section of the main entrance to about 6 m^2.

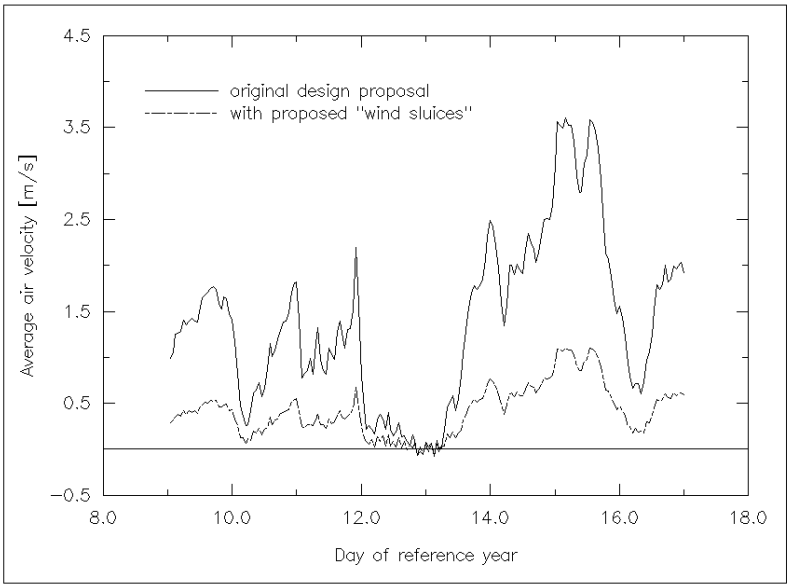

Figure 7.7 Predicted effect of proposed "wind sluice" to decrease the air velocities in the pedestrian entrance area; ie the passage connecting to the main square.

7.4.2. Environmental Assessment of Hospital Spaces

This case study concerns an environmental assessment of hospital spaces located in central Scotland, where air flow rates were judged to be critical in limiting summer overheating in zones with significant solar radiation gain (Hand 1990; Hensen, Hand & Clarke 1991). Figure 7.8 shows the part of the hospital under consideration, which consist of a dayroom and adjoining dining room. As can be seen, the dayroom has very large glazing areas.

It was requested to advise on useful operating strategies and/or possible modifications to the building in order to better control its summertime indoor thermal environment. The actual case study involved a number of building thermal performance simulations regarding several aspects including shading analysis. However, here we concentrate on one issue only, namely infiltration analysis by simulation of coupled heat and mass transfer.

After reduction of solar gain, the primary means of preventing summer overheating is ’free cooling’ by increasing the infiltration of ambient air. This may be achieved by for example opening of windows. Both the resulting cooling load by infiltration air and the indoor temperature, are influenced by the temperature difference between outside and inside, and by the actual air flow rates. In building thermal performance simulations, it has thus far been very problematic and time consuming to realistically incorporate the air flow rates. The main reason for this is that the rate of air flow depends on pressure differences which may be caused by wind or by stack effects due to temperature differences. Especially with a free floating indoor air temperature problem - like in the present case study - heat removal and air flow are closely coupled.

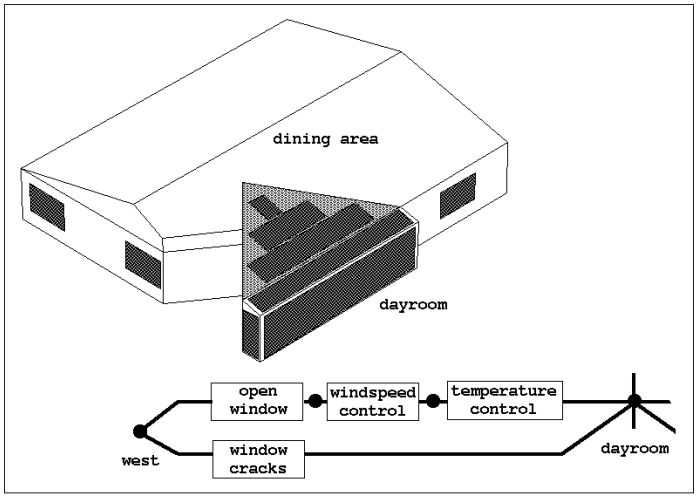

Figure 7.8 Schematic representation of the dayroom and adjoining dining room, when viewed from the south-west. Diagram of a fraction of the fluid flow network representing the west facade dayroom window.

For the dayroom and dining area, a building thermal simulation model had been set up. In addition to this, a flow network was created with nodes representing the dayroom and the dining area on two levels to account for temperature stratification, and with nodes representing the wind induced pressures on the various facades. These nodes are inter-connected by flow components representing internal connections (doors etc), and infiltration openings (cracks etc) in the exterior envelope. The windows are also represented by flow components. In order to investigate the effects of their opening or closing, additional flow components representing logical control (ie type 450 frictionless fluid flow components) are incorporated in series with the window flow components, as indicated in Figure 7.8 for the dayroom west window only. These logical controllers are set up so as to mimic occupant behaviour with respect to opening and closing of windows. It was envisaged that the windows would be opened whenever the air temperature of either the dayroom or the dining exceeds say 24°*C* during the period between 11:00 and 18:00 hours. It was also assumed that the occupants will not open the west and south orientated windows whenever it is very windy. Therefore, for these windows additional logical controllers are incorporated to prevent window opening in case the wind speed exceeds say 6 *m*/*s*. Of course these control strategies are just examples and may be changed at will.

In order to demonstrate the effect on predicted air temperature, of simulation based on coupled or decoupled heat and mass transfer several simulation studies were performed. All these simulations were performed using *bps* and its incorporated version of *mfs*, and are thus based on simultaneous and continuous simulation of heat transfer and air flow. It should be noted that this is already at a higher level than building thermal simulation using infiltration/ventilation rates estimated by independent means which has been common practice up to now.
Figure 7.9 shows predicted dayroom air temperatures for July 7 and 8 of a reference year, and assuming various window control strategies. The first two window control strategies investigated are: (1) windows continuously closed, and (2) window opening controlled by

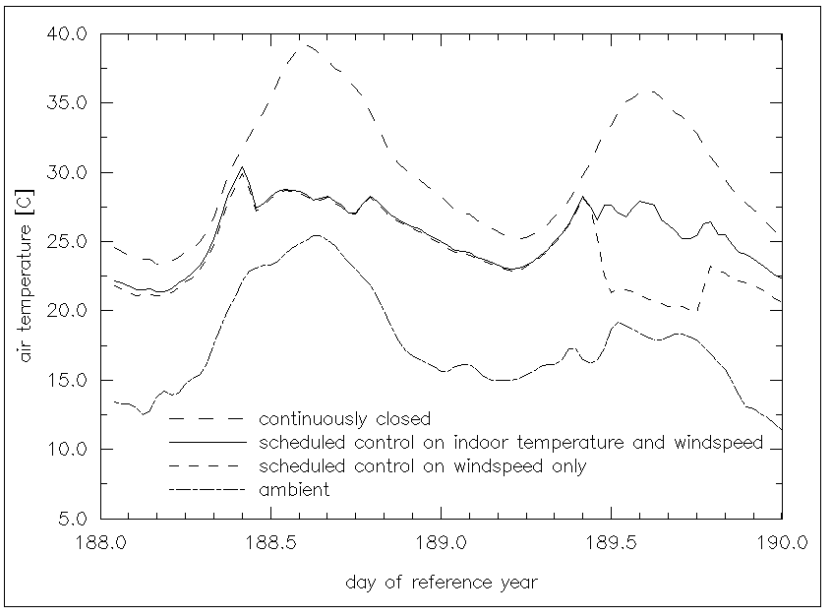

Figure 7.9 Predicted dayroom air temperature for July 7 and 8, assuming various window control strategies.

time of day and wind speed. If coupled heat and mass transfer were not possible these two cases would at least enable the user to predict upper and lower levels for the air temperatures to be expected.
The third window control strategy involved scheduled control both by wind speed and indoor temperature which is deemed to be more realistic than the previous strategies. The results for this control strategy are also shown in Figure 7.9. As can be seen, the results for July 7 are almost identical to the control by wind speed only case because the indoor temperature was above 24°*C* throughout the period between 11:00 and 18:00 hours. For July 8 however, there are marked differences because this is a day where the temperature control was actually activated.

On July 8 the wind speed exceeded 6 *m*/*s* throughout the control period, and so the west and south orientated windows were not opened. The sharp air temperature decrease in case of the scheduled control on wind speed only, is also not due to an increase of infiltration but is caused by air flow from the dining area to the dayroom (because north and east facing windows were opened the air flow through the building changed from predominantly south-west to north-east to predominantly north to east). This is evidenced by Figure 7.10, which shows the predicted infiltration rates for the dayroom. Obviously as with the air temperatures, there are marked differences between the various control strategies. Infiltration is defined here as ambient air which enters the zone directly; ie in case of the dayroom excluding air flow via the dining area. Because the ambient air may enter the dayroom via the roof and the east and west window, infiltration rates may occur which seem to be out of order at first glance. For example the two peaks on July 8 and in case of control by temperature too, are due to the fact that the east window is opened because of high indoor temperature. In that case air enters via this window, while at that point in time the air would leave via this window in the other two control strategy cases due to the prevailing environmental conditions. This example may serve to illustrate the complexity of air flow paths through the building as a function of wind speed, wind direction, indoor temperatures, and control behaviour.

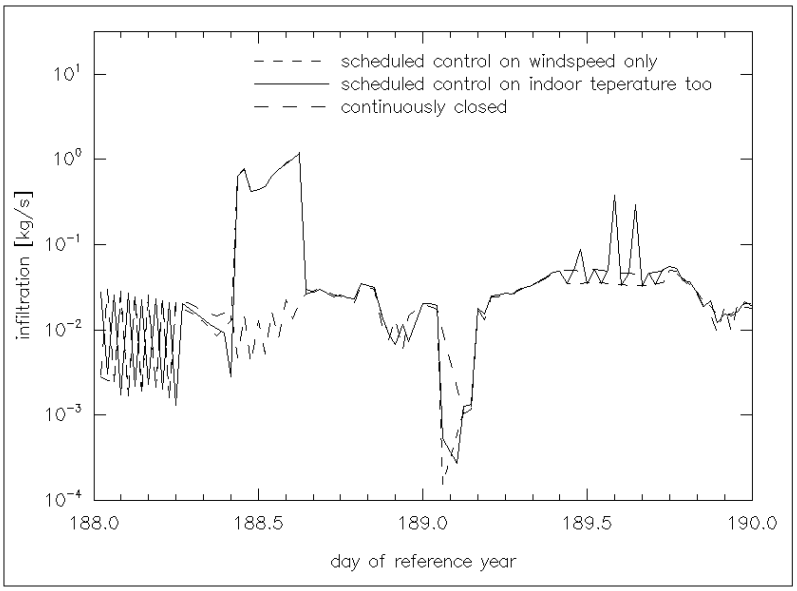

Figure 7.10 Predicted dayroom infiltration rates for July 7 and 8, assuming various window control strategies.

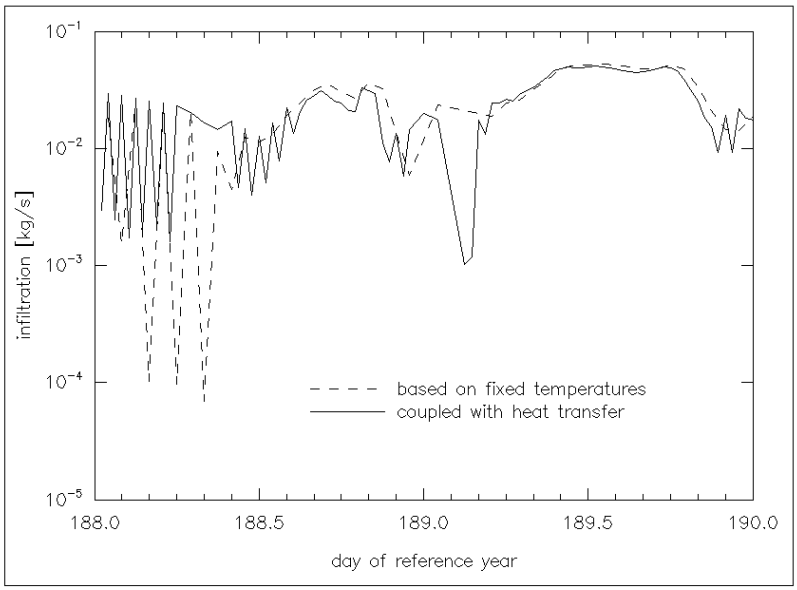

Figure 7.11 Effect of coupled/decoupled heat and mass transfer on predicted dayroom infiltration rates for July 7 and 8, assuming all windows closed.

In the previous cases, the air flow rates were calculated starting from the actual indoor air temperatures thus coupling heat and mass transfer. To illustrate the importance of this, some additional simulations were performed in which two cases were compared: (1) the indoor temperatures are at some fixed value, and (2) the indoor temperatures are as predicted by the thermal building simulation. So the pressure difference due to inside/outside temperature difference are accounted for in both cases, but it is only in the second case that varying indoor temperatures - both with respect to ambient as between the various zones - are taken

into account. The first case exemplifies usage of *mfs* in stand-alone mode, while the second case concerns the version incorporated in *bps*. In both cases it was assumed that the windows are continuously closed. The corresponding indoor and ambient temperatures are shown in Figure 7.9. Figure 7.11 shows the simulation results for the dayroom infiltration rate. The differences are clear, thus stressing the importance of simulation of coupled heat and mass transfer especially when buoyancy effects play an important role or are strongly time varying.

7.4.3. Influence of Acceleration Heating on Room Thermostat Behaviour

This final case study was inspired by experimental findings from the pilot measurements which were mentioned in Chapter 1. These measurements, reported in (Hensen et al. 1987), were carried out in a relatively small flat with ditto heating system (wet central heating system, controlled by a mechanical room thermostat). Technical considerations led to some modifications of the heating system during the measurements, one of which was disabling the thermostat's acceleration heating (which is used to raise the temperature of the sensor more rapidly towards the switch-off temperature in order to decrease the room air temperature differential). The acceleration heating is very important with respect to the boiler switch frequency. In this specific case and given the prevailing environmental conditions, the burner cycle time (burner-on till burner-on) was about 90 times longer when the acceleration heating was disabled. The total burner-on time - for an equal period of time - was approximately 50% shorter, suggesting a strong decrease in fuel consumption. It should be noted however, that in this specific case both the number of cycles per hour (at average heating season conditions ≈ 30) and the boiler stand-by heat losses may be regarded as well above average.
A longer cycle time also has consequences with respect to the fluctuation of the air temperature. Without the acceleration element the fluctuation of the mean room air temperature during one cycle, is much larger. Thermal comfort acceptability criteria for these fluctuating conditions, were discussed in Chapter 2.

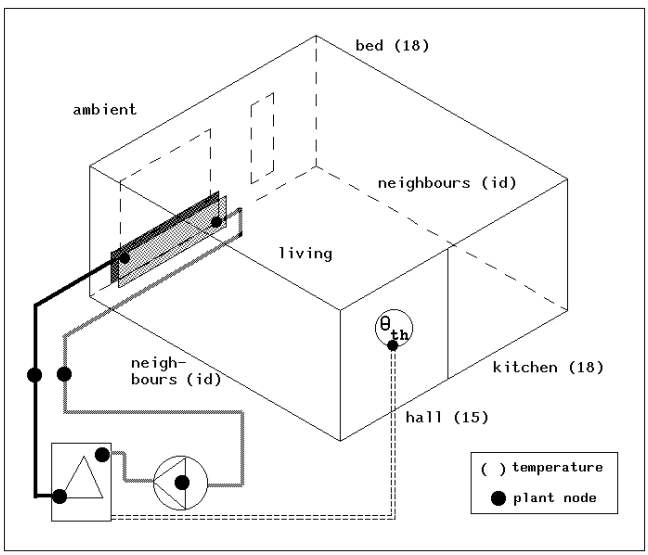

Figure 7.12 Schematic representation of a building and plant configuration comprising a living room serviced by (part of) a wet central heating system.

The objective of the present case study is to see whether the above mentioned observations can be repeated - by computer simulation - for a more general case, and to investigate whether decrease of thermostat acceleration heating might be a potential energy conservation strategy. Due to available resources, the following is a very limited attempt in this respect, but is to be felt useful in demonstrating yet another field of application of the models described in this dissertation.

Imagine a building and plant configuration as schematically shown in Figure 7.12. The room is facing due south, and is located at ground level of a reference house for energy related research as described in (NOVEM 1990), which represents a typical Dutch, garden-orientated, terraced house. The exterior envelope is insulated according to prevailing regulations (walls and roof: thermal resistance $R_c \approx 2.5\ m^2K/W$; ground floor: $R_c \approx 1.3\ m^2K/W$). For the present study, the air temperatures of the spaces adjoining the living room are kept at constant values as indicated in Figure 7.12. The infiltration rate (1.0 air changes per hour) was also kept constant, and for the casual gains a reference profile as suggested by Van der Laan et al. (1988) was used. The living room is serviced by (part of) a wet central heating system, comprising:

- a (two node model) radiator ($M = 25\ kg$; $\overline{c} = 600\ J/kgK$) with a nominal heat emission of 2000 W (at nominal temperatures 90/70/20), and heat emission exponent 1.3. The radiator environment temperature is evaluated (using equation (5.37)) from the living room air temperature and the inside surface temperatures of the facade and the ground floor. The latter two are both assigned a weight factor (see equation (5.37)) of 0.5.
- the (two node model) boiler ($M = 25\ kg$; $\overline{c} = 1000\ J/kgK$) denoted $A2$ in Figure 5.12a, and with respect to stand-by losses, the boiler denoted C in Figure 5.12b. The normalized start-stop losses are set at 1 s, and upper boiler temperature limit is set at 95°C. The gas consumption in stand-by mode is set at 1% of the full load gas consumption. The latter is scaled down to accommodate the current single radiator system: 8.3E-5 m_0^3/s gas with a caloric heating value of 35 MJ/m_0^3, which yields a heat output of approximately 2500 W when the water sided efficiency is 0.86.
- a pump delivering a fixed water flow rate of 2.4E-5 m^3/s
- two connecting lengths (10 m each) of 15 mm in diameter wet central heating pipe
- a mechanical room thermostat ($M = 0.05\ kg$; $\overline{c} = 1000\ J/kgK$) located in the living room, and sensing a mix of air temperature and inside surface temperature of the common dividing wall with the neighbouring house and the wall separating the living from the hall. The equivalent thermal conductances between these temperatures and the sensor were estimated at: 0.04, 0.01, and 0.01 W/K respectively.

With respect to building/plant interaction and control, the following was defined:

- a building side control function (as described in Section 5.6), defining that the heat output of the radiator would be effectuated at the building zone air point. Note that for all other plant components a constant containment temperature of 18°C was assumed
- a first plant control loop to actuate the boiler on the basis of the temperature sensed by the room thermostat. Unless stated otherwise, the set point temperature was 21.5°C, and a hysteresis of 0.5 K was assumed.
- a second plant control loop sensing whether the boiler was actually on or off during a certain simulation time step, and which - in case it was on - inputs a heat flux into the sensing element. This control loop thus simulates the acceleration heating of the room thermostat.

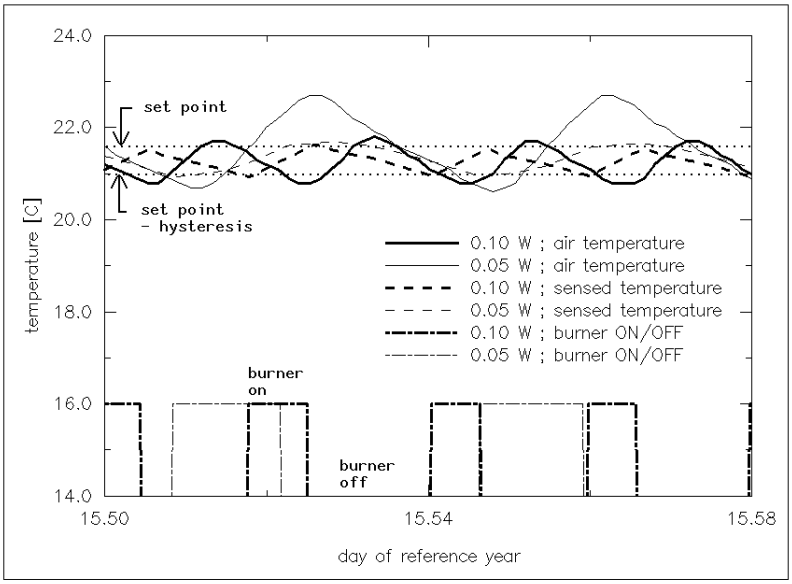

Figure 7.13 Influence of acceleration heating on fluctuation of mean living room air temperature and on temperature as sensed by the room thermostat during a two hour simulation period.

The degree of heat input is the primary parameter to be considered in the following. To illustrate the influence of the degree of acceleration heating, Figure 7.13 shows some simulation results comprising a two hour period of a Dutch climatic reference year for energy research (Bruggen 1978). The simulations were performed for two values of thermostat heat input: 0.05 and 0.10 *W*. For the given conditions, this gives either approximately 1 or 2 cycles per hour, resulting in air temperature differentials of approximately 1 and 2 *K* respectively. Figure 7.13 also indicates the set point differential. It may be seen that in the 0.05 *W* input case, the sensed temperature still rises even after the burner is switched off. This is due to the fact that at those points in time the room air temperature is actually higher than the thermostat set point. Note that there are two transient factors which play a role in the time lag and damping of the sensed temperature when compared to the room air temperature: (1) the sensed temperature depends on both air temperature and building construction temperatures (which lag behind because of thermal inertia of the building materials), and (2) thermal inertia effects of the heating system itself.

As also demonstrated by Figure 7.13, the resulting average room air temperature is affected too by the degree of acceleration heating; ie the average air temperature increases with decreasing acceleration heating. There is however yet another factor which influences the resulting average room air temperature: the thermal load of the system (which affects the length of time the thermostat is switched on). This is clearly demonstrated by Figure 7.14 which shows the room air temperature (and its deviation from the thermostat set point) in relation to the ambient temperature which is obviously a measure for the thermal load imposed on the heating system. When compared to average climatic conditions for The Netherlands, the data for January 13 represent an extremely cold day, while the data for January 15 represent a fairly average day.
For the simulations presented in Figure 7.14, a heat input to the thermostat sensing element

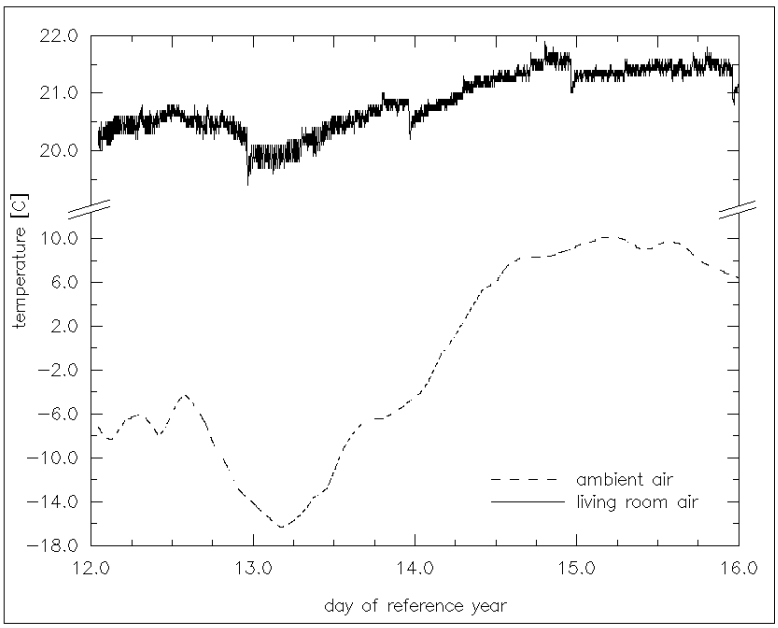

Figure 7.14 Influence of thermal load on sustained deviation between room air temperature and set point ($21.5°C$) of mechanical room thermostat. Note the enlarged top y-axis scaling!

of 0.20 W was assumed, which resulted in burner cycle frequencies of approximately 3, 4, and 5 per hour for the periods around 1:00 and 12:00 on January 13, and around 12:00 on January 15 respectively. This illustrates that the cycle frequency decreases when the thermal load increases. The corresponding relative burner-on periods were approximately 73%, 62%, and 32% respectively.

To investigate whether the overall gas consumption is also affected, several simulations - comprising the period January 12 to January 15 inclusive - were performed for various degrees of acceleration heating. From the results presented above it may be clear that when the simulations would start from a constant thermostat set point, this would lead to different average room air temperatures. Obviously the results would then be incomparable. Therefore some of the thermostat set points where chosen (by trial and error) such that the resulting average room air temperature (for January 15) would be equal. The most important simulation results - with respect to the investigated problem - are collected in Table 7.6.

When the cycle frequencies and the corresponding air temperature differentials are compared with the thermal comfort criteria as described in Chapter 2, all cases presented in Table 7.6 fall within the comfort limits for transient conditions. Only the cases with the smallest degree of heating acceleration seem to be critical during the extremly cold day; ie air temperature differential (= peak-to-peak amplitude) approximately 3.3 K. It should be noted however that the criteria as described in Chapter 2 should be applied to the operative temperature, the fluctuation of which is much smaller than the air temperature fluctuation. This is evidenced by Figure 7.15 which shows simulation results for the "0.01 W and $\theta_{=} 21.5°C$" case during January 15. From this figure it may also be concluded that in order to create thermally comfortable conditions, the thermostat set point would have to be higher

Table 7.6 Results of simulations - comprising the period January 12 to January 15 inclusive - for various degrees of acceleration heating applied to the mechanical room thermostat

description		parameter value or result				
acceleration heating	W	0.20	0.10	0.05	0.01	0.01
set point	$°C$	22.4	21.5	21.5	21.5	20.8
overall average air temperature	$°C$	20.6	20.7	21.1	21.5	20.8
idem but Jan 13 only	$°C$	20.4	20.7	21.1	21.3	20.4
idem but Jan 15 only	$°C$	21.3	21.3	21.6	22.0	21.3
average cycle freq. Jan 13 only	h^{-1}	4.0	1.8	1.0	0.8	0.8
average cycle freq. Jan 15 only	h^{-1}	4.5	2.0	1.1	0.9	0.9
air temp. differential Jan 13 only	K	0.3	1.3	2.3	3.3	3.3
air temp. differential Jan 15 only	K	0.3	1.0	2.1	3.0	3.0
total gas consumption	m_0^3	16.1	16.0	16.6	17.1	16.0
idem but Jan 13 only	m_0^3	4.9	5.0	5.2	5.4	5.1
idem but Jan 15 only	m_0^3	2.9	2.7	2.9	3.0	2.7

than $21.5°C$, because the operative temperature falls below the thermal comfort zone if we assume normal indoor clothing and nearly sedentary activity.

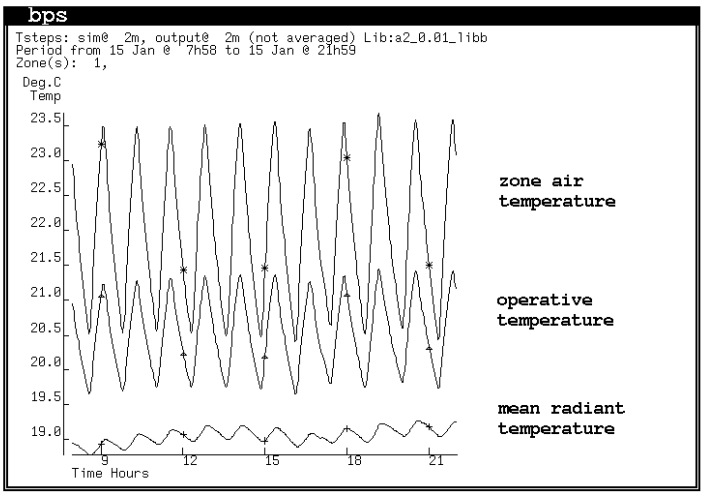

Figure 7.15 Air, mean radiant, and operative temperature during January 15 of the reference year, for $\phi_{th} = 0.01\ W$ and $\theta_{=}\ 21.5°C$

When comparing the gas consumption results for the cases with equal average air temperature, Table 7.6 indeed evidences that it is possible to conserve energy - while maintaining thermally comfortable conditions - by decreasing the burner cycle frequency. Lowering the cycle frequency from 4.5 to 2.0 h^{-1}, results in a gas consumption reduction of only 1% when the whole period is taken into account, but in a 7% reduction when just the "average heating season day" (ie January 15) is taken into account. This suggests that the optimal strategy is to apply the "cycle frequency control" strategy selectively; ie weather

dependent.

Obviously the above has to be investigated further with respect to what is the optimal strategy (ie development of rules for intelligent controllers), and for which type of systems is it applicable. In the present context, this case study should be regarded as a demonstration of applying the models presented in this thesis.

References

R.J.A. van der Bruggen 1978. ‘‘Energy consumption for heating and cooling in relation to building design,’’ Doctoral dissertation Eindhoven University of Technology (FAGO).

J.A. Clarke, J.W. Hand, P. Strachan, J.L.M. Hensen, and C.E.E. Pernot 1991. ‘‘ESP^{R} A building and plant energy simulation research environment,’’ Energy Simulation Research Unit, ESRU Manual U91/2, University of Strathclyde, Glasgow.

J.W. Hand 1990. ‘‘Erskine Hospital Environmental Report,’’ ESRU project report, University of Strathclyde, Energy Simulation Research Unit, Glasgow.

J.L.M. Hensen, L.C.H. Dings, and W.J.A. van de Ven 1987. ‘‘Meetproject Someren,’’ rapport FAGO 87.08.K., Technische Universiteit Eindhoven, Eindhoven.

J.L.M. Hensen, J.W. Hand, and J.A. Clarke 1991. ‘‘Building design assessment through coupled heat and airflow simulation: two case studies,’’ in *Proc. 12th AIVC Conf. "Air Movement and Ventilation Control within Buildings", Ottawa, Sep 1991*, pp. 239-249, IEA Air Infiltration and Ventilation Centre, Coventry (UK).

M.J. van der Laan, M. Dubbeld, and J.E.F. van Dongen 1988. ‘‘Ontwerp van een standaard referentiegedrag voor energieverbruiksberekeningen,’’ TNO-MT rapport R 88/080, Delft.

NOVEM 1990. *Referentie Tuinkamerwoning,* Nederlandse Maatschappij voor Energie en Milieu, Sittard.

C.E.E. Pernot and J.L.M. Hensen 1990. ‘‘Adviezen inzake de kwaliteit van het binnenmilieu van de HeuvelGalerie te Eindhoven,’’ TPD-FAGO-RPT-90-42, p. 41, Eindhoven.

J.A. Wisse and C.E.E. Pernot 1990. ‘‘Wind en thermisch comfort rondom en in de Heuvelgalerie te Eindhoven,’’ TNO-TPD rapport 15.002, Eindhoven.

CHAPTER EIGHT

CONCLUSIONS AND FUTURE WORK

8.1. INTRODUCTION

The need for an integral approach of the integrated, dynamic system consisting of a building and its heating and ventilating system, has been demonstrated. After having defined the practical objectives (thermal comfort and optimum fuel consumption), the main goal of the work described in this dissertation was then to develop / enhance building performance evaluation tools to enable this integral approach.
In the following, the general conclusions of the present work are summarized. These are followed by some recommendations towards possible future work.

8.2. CONCLUSIONS

With respect to assessment of the practical objectives, it is concluded that our theoretical knowledge regarding thermal comfort in transient conditions is still limited. Experimental results for fluctuating temperatures confirm the prevailing ASHRAE standard (1981). Care must be taken when employing ASHRAE's acceptability criteria regarding temperature drift or ramp outside the comfort zone.

With respect to developing building performance evaluation tools, it is advisable to build on what already exists. For the present work it was arguably decided to start from the *ESP*^{R} energy simulation environment. In the present context, the main development areas were identified as: fluid flow simulation, plant simulation, and integration with the building side of the overall problem domain.

For fluid flow simulation, a mass flow network solver has been developed. The employed simultaneous network solution technique proved to be very efficient. The module may be operated either in stand-alone mode or from within an integrated building and plant energy simulation module. The program is capable of handling any user-defined fluid flow network - representing building side air flow, and flow of the working fluid (including air) through the heating or ventilating system - when subjected to time varying flow control and / or to transient boundary conditions.

While the foundation was already present, the capabilities and the robustness of the plant simulation side of the existing simulation environment has been greatly increased. The employed modular-simultaneous plant simulation technique proved to be very promising. A number of plant simulation features and numerical models representing controllers and components of domestic heating and ventilating systems have been added. It was recognised that although these models represent the current state-of-the-art, there is still a lot of theoretical work to be done. Simulation of combined heat and fluid flow through both building and plant has been achieved. For a simultaneous approach, division of the overall problem description into a small number of functional matrix equations representing the main heat and fluid transfer mechanisms is profitable. Obedience of first thermodynamic

law principles, can be ensured by employing iteration mechanisms. From a limited number of tests, iteration seemed to be preferable to time step control in this context.

A five stage validation methodology was adopted, and its applicability has been demonstrated by a number of examples addressing each successive step of the methodology. Apart from their demonstrative purpose, the results of these studies increased our confidence in the program.
By means of a number of imaginary and real world case studies, the described energy simulation environment was shown to be applicable in both a modelling orientated context and in a building engineering context. In the former case it is used for generating modelling knowledge which may then be transferred to the building simulation research community for future work. In the latter case the system is used for solving practical problems. Two of the presented case studies are actually based on professional consultancy projects, which may serve to indicate the commercial potentials of the work presented.

In conclusion, this dissertation describes a "modular-simultaneous" technique for the simulation of combined heat and fluid flow in a building / plant context. The present performance of the system indicates that it is practical to solve the building / plant heat and mass flow network in detail. Moreover, the solution of complex building / plant / fluid flow networks in the transient state is now feasible on inexpensive computers. This enables an integral approach of the thermal interaction of building structure and heating and ventilating systems.

8.3. FUTURE WORK

It will be obvious that the present work is merely a step towards an envisaged future "intelligent, integrated, building design system". A lot of work remains to be done. Various lines of future research can be identified or supported by the results and conclusions of the present work. Although some topics could be categorized under more than one heading, the main areas are:

8.3.1. Theory

While the system described in this dissertation is robust and well adapted for its task, the present work revealed the need for certain future developments, some of which are already in progress.
In the field of fluid flow simulation these include the development of additional fluid flow component models (especially improved large opening models), incorporation of Computational Fluid Dynamics (CFD) techniques (as an intermediate step one could imagine simplified network models generated with a CFD approach), expansion of the system’s wind pressure database (or alternatively prediction of surface wind pressures by CFD techniques) and theoretical / experimental verification and validation of the simplifying assumptions in the fluid flow component models.
With respect to plant simulation future work is necessary regarding the development of additional plant component models in the required ‘state-space’ format, expansion of the plant control facilities, research of the iteration vs time step control issue, incorporation of better solvers, work in the field of plant simulation results analysis, and theoretical / experimental verification and validation of the assumptions in the present and future plant component models.
Regarding the interaction of building and plant there are also a number of development

areas, including imbedded plant components, zone air temperature gradients as caused by the plant, additional (2/3 dimensional) heat and mass transfer mechanism, combination with moisture transport, and of course again, theoretical / experimental verification and validation of the simplifying assumptions.

8.3.2. User Interface

It may be apparent that while development of building performance evaluation tools as described in this dissertation will comprise a valuable addition to the building engineer's toolkit, they also create new problems deriving from the conflict between the necessity for the tools to be powerful, comprehensive and according to first thermodynamic law principles to adequately represent the real world complexity while also being simple, straightforward and intuitive to facilitate user interaction. Such problems are not restricted to novice users but they apply to experienced users as well (Van Nes 1991). These problems are one of the factors which may cause the external errors as identified in Chapter 6.
As Clarke (1991) points out, the conflict between power and ease of use is further exagerated by the divergence of the conceptual outlook of the design orientated program users and the technically orientated program developers. And to complete the confusion, there is the subtly different terminology of the various engineering professions. One - very promising - way to tackle these problems, is by utilisation of Knowledge Based System (KBS) and Human-Computer Interaction (HCI) techniques to create an Intelligent Front End (IFE). One of the projects underway in this area is described by Clarke et al. (1989).

8.3.3. Software Structure

The software underlying the building performance evaluation tools which are described in this dissertation is self-documentary, highly modular, and well structured compared to any current standard. However the sheer size and the complexity of the complete system, gives rise to problems with respect to software construction, testing and maintenance. Future work is certainly necessary to be able to cope with such problems which will become larger and larger unless some drastic changes will take place. In this respect, the reader could be referred to major developments which are underway in the area of sophisticated, object-orientated, (energy simulation) model development environments, currently finding support in the UK (Clarke et al. 1990), in Europe generally, and in North America (Buhl et al. 1991).

8.3.4. Application

Due to available resources the present work had to be restricted to development of the tools. The actual application of the tools was limited to a number of case studies. As indicated in Chapter 1 and without repeating them here, there are numerous problems related to buildings and the HVAC systems which service them, for which an integral approach (ie with tools as described in this dissertation) is essential if we want to find a satisfactory solution. It is not only for such problems that an integral approach is necessary. Also in optimisation studies, one has to approach the overall system integrally, because optimisation of part(s) of the system will only yield the optimum for the overall system by pure coincidence.

8.3.5. Technology Transfer

Last but not least there is the issue of technology transfer. Although their impact on technology transfer has already been proven on numerous occasions, it is worth mentioning

again that units like for instance the Energy Design Advisory Service (EDAS) at the University of Strathclyde, and the Working group FAGO-TNO-TUE (collaboration between the Netherlands Organisation for Applied Scientific Research and Eindhoven University of Technology) play an essential role with respect to the transfer of technology generated in projects such as the present work. Their primary instrument for technology transfer is through application of the work such as described in this dissertation. This is demonstrated in Section 7.4.1. and Section 7.4.2.
Another way of technology transfer which is perhaps more indirect but potentially equally powerful, is via developments towards intelligent, knowledge based, systems as indicated above. Work in this area has only recently been started, but seems to be very promising. An example of work in this area which is directly linked to the present work is described by Hensen (1991).

References

ASHRAE 1981. ''Thermal environmental conditions for human occupancy,'' ANSI/ASHRAE Standard 55-1981, American Society of Heating, Refrigerating and Air-Conditioning Engineers, Atlanta, GA.

F. Buhl, E. Erdem, J-M. Nataf, F.C. Winkelmann, M.A. Moshier, and E.F. Sowell 1991. ''The U.S. EKS: advances in the SPANK-based Energy Kernel System,'' in *Proc. 3rd Int. Conf. on System Simulation in Buildings, Dec 1990*, pp. 107-150, University of Liege. Lawrence Berkeley Laboratory report LBL-29419

J.A. Clarke, J.H. Rutherford, and D. MacRandal 1989. ''An intelligent front-end for computer-aided building design,'' in *Proc. 3rd European Simulation Congress, Edinburgh*, pp. 362-368, Society for Computer Simulation International, Ghent.

J.A. Clarke, G.P. Hammond, A. Irving, K. James, S. Lockley, D. MacRandal, D. Tang, T.J. Wiltshire, and A. Wright 1990. *Energy Kernel System. Presentation to the Steering Committee*, University of Strathclyde, Energy Simulation Research Unit, Glasgow. Paper 90-001

J.A. Clarke and D. Mac Randal 1991. ''An intelligent front-end for computer-aided building design,'' *Int. Journal of Artificial Intelligence in Engineering*, vol. 6, no. 1, pp. 36-45.

J.L.M. Hensen 1991. *Development of an intelligent, knowledge based, tool for the integral approach of building design and auxiliary system*, Eindhoven University of Technology. Grant proposal to the Royal Netherlands Academy of Arts and Sciences

F.L. van Nes 1991. ''Boeken, computers en ergonomen. Gemak van gebruik door gebruiksgemak,'' Inaugural speech, Eindhoven University of Technology.

SUMMARY

In this dissertation, developments in the field of building performance evaluation tools are described. The subject of these tools is the thermal interaction of building structure and heating and ventilating system. The employed technique is computer simulation of the integrated, dynamic system comprising the occupants, the building and its heating and ventilating system.

With respect to buildings and the heating and ventilating systems which service them, the practical objective is ensuring thermal comfort while using an optimum amount of fuel. While defining the optimum had to be left for other workers, the issue of thermal comfort is addressed here.
The conventional theory of thermal comfort in conditions characteristic for dwellings and offices assumes steady-state conditions. Yet thermal conditions in buildings are seldom steady, due to the thermal interaction between building structure, climate, occupancy, and auxiliary systems. A literature rewiew is presented regarding work on thermal comfort specifically undertaken to examine what fluctuations in indoor climate may be acceptable. From the results, assessment criteria are defined.

Although its potentials reach beyond the area of Computer Aided Building Design, a description is given of building and plant energy simulation within the context of the CABD field of technology. Following an account of the present state-of-the-art, the choice for starting from an existing energy simulation environment (*ESP*^{R}) is justified. The main development areas of this software platform - within the present context - are identified as: fluid flow simulation, plant simulation, and their integration with the building side of the overall problem domain.

In the field of fluid flow simulation, a fluid flow network simulation module is described. The module is based on the mass balance approach, and may be operated either in stand-alone mode or from within the integrated building and plant energy simulation system. The program is capable of predicting pressures and mass flows in a user-defined building / plant network comprising nodes (ie building zones, plant components, etc) and connections (ie air leakages, fans, pipes, ducts, etc), when subjected to flow control (eg thermostatic valves) and / or to transient boundary conditions (eg due to wind).

The modelling and simulation techniques employed to predict the dynamic behaviour of the heating and ventilating system, are elaborated. The simultaneous approach of the plant and its associated control is described. The present work involved extensions to the *ESP*^{R} energy simulation environment with respect to robustness of the program, and with respect to additional plant simulation features, supported plant component models and control features.

The coupling of fluid flow, plant side energy and mass, and building side energy simulation into one integrated program is described. It is this "modular-simultaneous" technique for the simulation of combined heat and fluid flow in a building / plant context, which enables an integral approach of the thermal interaction of building structure and heating and ventilating system.

A multi stage verification and validation methodology is described, and its applicability to the present work is demonstrated by a number of examples addressing each successive step of the methodology.

A number of imaginary and real world case studies are described to demonstrate application of the present work both in a modelling orientated context and in a building engineering context.

Then the general conclusions of the present work are summarized. Next and finally, there are recommendations towards possible future work in the areas of: theory, user interface, software structure, application, and technology transfer.

SAMENVATTING

In dit proefschrift worden ontwikkelingen beschreven op het gebied van gereedschap voor het evalueren gebouwprestaties. Het werkgebied van dit gereedschap is de thermische wisselwerking tussen gebouw en verwarmings- en ventilatie-installatie. De gebruikte techniek is computer-simulatie van het geïntegreerde, dynamische systeem bestaande uit de gebruikers, het gebouw en de installaties.

Met betrekking tot gebouwen en hun installaties, is het praktische doel om te zorgen voor een thermisch behaaglijk binnenklimaat bij een optimaal brandstofverbruik. Terwijl het definiëren van het optimum voor andere onderzoekers moest blijven liggen, wordt hier wel ingegaan op het aspect van thermische behaaglijkheid.
De gebruikelijke theorie betreffende thermische behaaglijkheid in omstandigheden geldend voor woningen en kantoren, gaat uit van stationaire condities. Toch zijn de thermische omstandigheden in gebouwen vrijwel nooit stationair ten gevolge van de thermische wisselwerking tussen gebouw, buitenklimaat, gebruik en installaties. Er wordt een literatuurstudie beschreven naar onderzoek op het gebied van thermische behaaglijkheid dat zich specifiek richtte op het al dan niet aanvaardbaar zijn van bepaalde binnenklimaat fluctuaties. Uit de resultaten hiervan zijn aanvaarbaarheids-criteria afgeleid.

Alhoewel de potentiële mogelijkheden zich niet beperken tot het gebied van Computer Aided Building Design, wordt gebouw- en installatie-simulatie hier toch geplaatst in de context van CABD ontwikkelingen. Na een beschrijving van de huidige state-of-the-art, wordt de keuze om uit te gaan van een bestaande simulatie-omgeving (*ESP*^{R}) verantwoord. De gebieden waar dit softwarepakket (binnen de huidige context) uitbreiding behoeft, kunnen worden aangeduid als: simulatie van vloeistof- en gasstroming, simulatie van de installatie en integratie hiervan met de gebouwkant van het gehele probleemveld.

Op het gebied van simulatie van vloeistof- en gasstroming, wordt een simulatie-module voor massastroom-netwerken beschreven. Deze module is gebaseerd op de massabalans-methode en kan zowel zelfstandig als vanuit het geïntegreerde gebouw- en installatie-simulatiepakket worden gebruikt. Het programma is in staat om drukken en massastromen te voorspellen in een door de gebruiker gedefinieerd gebouw- en installatie-netwerk van knopen (zoals gebouwzones, installatie-onderdelen, etc) en verbindingen (te weten luchtlekken, ventilatoren, buizen, kanalen, etc) terwijl dat wordt beïnvloed door stromingsregelaars (bijv. thermostatische ventielen) en / of variërende randvoorwaarden (bijv. door winddrukken).

De modellerings- en simulatietechnieken, die worden gebruikt om het dynamische gedrag van de verwarmings- en ventilatie-installatie te voorspellen, worden toegelicht. De simultane benadering van de installatie met bijbehorende regeling, wordt beschreven. Het voorliggende werk omvatte uitbreidingen aan het *ESP*^{R} simulatiepakket op het gebied van de robuustheid van het programma en met betrekking tot extra mogelijkheden voor het simuleren van installaties in het algemeen, het aantal beschikbare modellen van installatie-componenten en regelmogelijkheden.

Er wordt beschreven hoe de simulatie van vloeistof- en gasstroming, massa- en warmte-stroom door de installatie en de simulatie van warmtetransport door het gebouw, is

gekoppeld in een geïntegreerd simulatieprogramma. Door deze "modulair-simultane" techniek voor simulatie van gecombineerd massa- en warmtetransport in de gebouw- en installatie-context, wordt een integrale benadering van de thermische interactie tussen gebouw en verwarmings- en ventilatie-installatie mogelijk.

Er wordt een stapgewijze verificatie- en validatie-methodologie beschreven. De toepasbaarheid daarvan voor het huidige werk, wordt gedemonstreerd door een aantal uitgewerkte voorbeelden gericht op ieder afzonderlijke aspect van deze methodologie.

Er worden een aantal denkbeeldige en praktische voorbeelden behandeld om de toepasbaarheid van het huidige werk te demonstreren voor zowel modellerings- en simulatiegerichte problemen als voor praktijkgerichte problemen.

Vervolgens worden de algemene conclusies uit het voorliggende werk samengevat. Daarna en tot slot, worden er aanbevelingen gedaan voor mogelijk toekomstig onderzoek op het gebied van: theorie, gebruiksgemak, software-structuur, toepassingen en kennisoverdracht.

CURRICULUM VITAE

Jan Hensen was born on 9 April 1953 in Tilburg, The Netherlands. In 1971 he successfully completed the HBS-B examinations at the St.-Pauluslyceum in Tilburg. Due to circumstances, he then fulfilled his compulsory military duties and worked both as a truck driver and as a horse rider / instructor.

In 1975 he started his building engineering study at the Faculty of Architecture and Building Science of Eindhoven University of Technology. He graduated in 1981 under supervision of prof.ir.J. Vorenkamp who is with the FAGO unit (Physical Aspects of the Built Environment). The masters projects were an optimisation study regarding energy consumption in offices, and an experimental study on convective heat transfer in a convective loop system.

From 1981 until 1986 he was a researcher in the Group FAGO-TNO-TUE (collaboration between the Netherlands Organisation of Applied Scientific Research (TNO) and Eindhoven University of Technology) and worked on several projects. One of the larger projects was the "Energieproeftuin Hoofddorp" which involved real scale experiments with 56 low-energy houses.

In 1986 he was offered the opportunity to start the present work at the FAGO unit of Eindhoven University of Technology. This work resulted in 1991 in the dissertation you are now reading.

Statements

going with the dissertation of J.L.M. Hensen

1 In contradiction to what is implied, ASHRAE's statement regarding acceptability of temperature drift or ramp outside the comfort zone, should be restricted to acceptable temperature changes during daytime and in upward direction only.
ASHRAE 1981. "Thermal environmental conditions for human occupancy", American Society of Heating, Refrigerating and Air-Conditioning Engineers, Atlanta GA, ANSI/ASHRAE Standard 55-1981, and this dissertation, Chapter 2.

2 Stolwijk's model of the human thermoregulatory system is often wrongly referred to as if it was a model for thermal comfort prediction.
J.A.J. Stolwijk 1970. "Mathematical model of thermoregulation", in "Physiological and behavioral temperature regulation", eds. Hardy, J.D., A.P. Gagge and J.A.J. Stolwijk, Thomas Books, Springfield IL, and this dissertation, Chapter 2.

3 In view of recent research results regarding ventilation efficiency, a term like "air change rate" is deceptive to say the least.

4 It is surprising that room thermostats and thermostatic radiator valves are still marketed with centigrade scale, while it is common professional knowledge that the sustained difference between set point and actual room temperature is load dependent.
This dissertation, Chapter 7

5 The common advice to tune a domestic heating system such that in average ambient conditions a burner frequency of approximately 6 cycles per hour will result, neither has an apparent origin nor will it always yield optimum results.
This dissertation, Chapter 7

6 Because in many alleged Sick Building cases, the causes are clearly identifiable, the word Syndrome is often appended uncalled-for.

7 Even a 60^{th} edition of a handbook still does not guarantee it is flawless.
Recknagel Sprenger 1979. "Taschenbuch für Heizung und Klimatechnik", E. Sprenger (ed.), Vol. 60, R. Oldenbourg Verlag GmbH, München.

8 Compared to previous generation computer systems, a workstation not only indirectly offers greater potential for the protection of our environment through its increased computing power, but also in a direct sense by reducing the amount of paper consumption for printouts, code listings etc.

9 If an academic unit, in engaging scientific staff, too much emphasizes practical experience instead of scientific quality, this will have adverse effects in the long run.

10 In view of the proven positive results and the readily available sport facilities, one would expect universities to stimulate physical exercise much more than is done at the moment.

Eindhoven, 7 June 1991